

Distribution Agreement:

In presenting this thesis or dissertation as a partial fulfillment of the requirements for an advanced degree from Emory University, I hereby grant to Emory University and its agents the non-exclusive license to archive, make accessible, and display my thesis or dissertation in whole or in part in all forms of media, now or hereafter known, including display on the world wide web. I understand that I may select some access restrictions as part of the online submission of this thesis or dissertation. I retain all ownership rights to the copyright of the thesis or dissertation. I also retain the right to use in future works (such as articles or books) all or part of this thesis or dissertation.

Signature:

Gavin Smith

Date

Radical Chain Reduction and C(sp²/sp³) Carboxylation via Formate Activation

By

Gavin C.J. Smith

Doctor of Philosophy

Chemistry

William Wuest, Ph.D.

Advisor

Huw Davies, Ph.D.

Committee Member

Dennis Liotta, Ph.D.

Committee Member

Kimberly J. Arriola, Ph.D.

Dean of the James T. Laney School of Graduate Studies

Date

Radical Chain Reduction and C(sp²/sp³) Carboxylation via Formate Activation

By Gavin C.J. Smith

B.S., University of California, Santa Cruz, 2018

Advisor: William Wuest, Ph.D.

An abstract of a dissertation submitted to the Faculty of the James T. Laney School of Graduate Studies of Emory University in partial fulfillment of the requirements for the degree of Doctor of Philosophy in Chemistry 2023

Abstract

Radical Chain Reduction and C(sp²/sp³) Carboxylation via Formate Activation

By: Gavin Smith

Over the last several decades, various modes of catalysis in chemical synthesis have emerged at the forefront of synthetic organic chemistry to make carbon-carbon bond formation more efficient and selective. While single electron transformations have maintained synthetic utility for decades, the emergence of photoredox catalysis has reinvigorated the field of single electron processes by introducing mild and catalytic conditions for single electron activation of organic molecules via redox manipulations. While many photoredox methodologies have relied on highly reducing or oxidizing photocatalysts for radical formation, we utilized previous methodologies in our group to access potent reductants via mild hydrogen atom transfer processes. We have demonstrated through a polarity matched hydrogen atom transfer between an electrophilic thiyl radical and abundant formate salts, we are able to mildly generate the radical anion of carbon dioxide (CO₂^{•-}), a potent reductant ($E_{1/2}^{\circ} = -2.2$ V vs SCE). We demonstrate the utility of this reaction in a variety of reductive transformations including hydroarylation, defluoroalkylation, ketyl radical formation, detosylation, and radical deamination of aryl ammonium salts. Furthermore, our research shows CO₂^{•-} as a nucleophilic source of CO₂ as it adds across alpha, beta-unsaturated alkenes in a 1,4-addition. In addition, formate activation with phenyl triflimide is used nickel-catalyzed cross coupling to generate aryl/vinyl carboxylic acids from their corresponding aryl/vinyl bromide precursors. Finally, we utilize computational chemistry to help elucidate the mechanistic features of a protocol for catalytic dearomatization of unactivated arenes via catalytic hydroalkylation.

Radical Chain Reduction and C(sp²/sp³) Carboxylation via Formate Activation

By Gavin C.J. Smith

B.S., University of California, Santa Cruz, 2018

Advisor: William Wuest, Ph.D.

A dissertation submitted to the Faculty of the James T. Laney School of Graduate Studies
of Emory University in partial fulfillment of the requirements for the degree of Doctor of
Philosophy in Chemistry 2023

Acknowledgments

Reflecting on my time at Emory, I really believe that I would not have made it through this PhD without the support of friends, mentors, and peers. I first want to thank my advisors, Dr. Bill Wuest and Dr. Nate Jui. Nate, thank you for introducing me to the world of photoredox and methodology, my time spent working with you shaped me as a scientist and will forever influence how I think about and communicate my science. Bill, thank you for welcoming me into your lab and providing me with a familiar home when I needed it. I know I am incredibly stubborn and hard-headed at times but I appreciate your willingness to work with me, allowing me to pursue research I am passionate about, and encouraging me to seek out opportunities I didn't think I deserved. I'm proud of the science we did and excited to see what comes out of the lab in the future.

Cecie, working with you and developing a friendship with you was the most important thing I did in graduate school. I developed so much as a scientist working with you and I don't think I will ever be a part of a better team. I am so proud of the science we did together and grateful for the friendship we have. It didn't matter how bad of a day I had, five minutes with you and I'm smiling and laughing so hard I can't breathe. There are so many aspects of our relationship that I miss but I know I have a friend for life with you. Kelly, you were the best of us in the Jui lab—an incredible role model, a talented scientist, and reliable friend. Mark, our time was short working together but I will miss being able to geek out with over Star Wars and I am so proud of the incredible scientist you have become and can't wait to see where you go next.

Ana, moving labs was stressful and intimidating but you immediately made the Wuest lab feel like home. I look up to you in so many ways and can't imagine the last few years without you. So many silly memories and thoughtful conversations, I am so lucky to have a friend like

you. Carter, hanging out and goofing around with you in lab the last couple years has been the highlight of my day. Thank you for putting up with my shenanigans and for always being on the same page when it's time to get a sweet treat. Drason, thank you for being a phenomenal project partner and friend (and bantering with me)—I'm proud of you and can't wait to read about the incredible chemistry you do at Scripps. Madeline (Maddie), while I may have given custody of you to Carter, it was always us first! You are hilarious and I can't wait to see where you end up. Andy, I'm proud of the scientist you have become over the past year and will miss talking about chemistry and joking around with you in our office.

Kim, Anna, and Zakiria—you three will always be my first friends in Atlanta and I wouldn't have made it through my first year without you. I miss you all and I am so happy to see you all thriving. To everyone in the Wuest lab and the Jui lab, whether we were close friends or just acquaintances, I appreciate you all and am grateful to have had the opportunity to work with you.

To mom and dad, you have supported and loved me every step of the way in every stage of my life and I am forever grateful for your love, patience, and support. To my big sister Sarah, I would not be in the position I am today had you not carved a path for me to follow. I have and will always look up to you and am so proud of the person you have become. To my brother Sean, I am proud of the work that you have accomplished over the past year and am looking forward to what comes next. My Uncle Paul and Aunt Margaret, my favorite aunt and uncle, thank you for the unconditional support and love you have provided me all my life.

Finally, to my queer family—Rico, Jenna, Jessica, and Joseph. It doesn't matter how much we talk, whether it's every week or every few months. You are friends for life and each of you has been so important to me at different stages of graduate school. Rico, I need to give an

extra shoutout to you because you were such an important person my first couple years of graduate school. You always answered the phone and were there for me through tough times and I will always remember that. I love you all.

Table of Contents

Chapter 1: An overview of Single Electron Transformations, the Emergence of Photoredox Catalysis, and Nickel-Catalyzed Cross-Couplings.....	1
1.1 Single Electron Transformations.....	2
1.1.1 Hydrogen Atom Abstraction.....	2
1.1.2 Halogen Atom Abstraction.....	4
1.1.3 The Emergence of Photoredox Catalysis.....	6
1.2 An Overview of Nickel-Catalyzed Cross Couplings.....	10
1.3 References.....	11
Chapter 2: Radical Chain Reduction via the Carbon Dioxide Radical Anion (CO₂^{•-}).....	15
2.1: An Overview of Photoredox in the Jui Lab.....	17
2.2: An Overview of the Carbon Dioxide Radical Anion.....	19
2.2.1 Mechanistic Investigations into CO ₂ ^{•-} as an Upconverted Reductant.....	20
2.2.2: Investigations into Radical Chain Generation of CO ₂ ^{•-}	25
2.2.3: Generation of CO ₂ ^{•-} with Alternative Initiators.....	26
2.2.4: Reductive Process Enabled by CO ₂ ^{•-}	29
2.3 References.....	36
Chapter 3: Hydrocarboxylation of Electron-Deficient Alkenes via the Carbon Dioxide Radical Anion (CO₂^{•-}).....	42
3.1: Discovery and Optimization of the CO ₂ ^{•-} as a Nucleophilic Source of CO ₂	44
3.2: References.....	52

Chapter 4: Nickel/Visible-Light Catalyzed Carboxylation of C(sp²) Bromides via Formate Activation.....	58
4.1: Incentive and Overview of C(cp ²) Carboxylations.....	60
4.2: Initial Investigations Using Alternative Initiators.....	62
4.3: Reaction Optimization Under Photochemical Conditions.....	64
4.4: Mechanistic Investigations into Phenyl Triflimide.....	67
4.5 References.....	77
Chapter 5: Supporting Information.....	82
S2.4 Supporting Information.....	82
S2.4.1 General Information.....	82
S2.4.2 Optimization of Hydrodehalogenation with CO ₂ ^{•-}	84
S2.4.3: General Procedures.....	87
S2.4.4: Alternative Initiators.....	89
S2.4.5: Preparation of Starting Materials.....	90
S2.4.6: Preparation of Substrates from the Substrate Table.....	102
S2.4.7: Fluorescence Quenching Experiments.....	117
S2.4.8: Transient Absorption Spectroscopy.....	118
S2.4.9: Quantum Yield Experiments.....	123
S2.4.10: Chain Length Approximation.....	125
S2.4.11: Computational Details.....	125
S2.4.12: Electrochemical Measurements.....	141
S2.4.13: References.....	143

S3.3.1 General Information.....	149
S3.3.2: Optimization of Carboxylation of Michael Acceptors.....	152
S3.3.3: Preparation of Substrates.....	153
S3.3.4: Preparation of Products from Figure 3.5.....	155
S3.3.5: Computational Details.....	160
S3.3.6: References.....	161
S4.6.1 General Procedures.....	164
S4.6.2 Electrochemical Measurements.....	165
S4.6.3. Optimization Details.....	166
S4.6.4: Investigations into the Role of Phenyl Triflimide.....	170
S4.6.5: Preparation of Starting Materials.....	173
S4.6.6: Preparation of Products from Substrate Table.....	176
S4.6.7: References.....	189
5.1: Appendix: Spectra.....	193

List of Figures

Figure 1.1: Common Photoredox Catalysts Alongside their Excited State Redox Potentials and λ_{max}	7
Figure 1.2: Graphic representation of oxidative/reductive quenching cycles shared by all photoredox-catalyzed systems alongside common stoichiometric donors and acceptors.....	8

Figure 1.3: Graphic representation of a Jablonski diagram (A) alongside the different energy transfer mechanisms—Forster (B) and Dexter (C).....	9
Figure 2.1: A representative catalytic cycle for thiol/formate catalyzed photoredox systems in the Jui lab.....	19
Figure 2.2: Modified Catalytic Cycle Generating Electrophilic Thiyl Radical via SET.....	21
Figure 2.3: Factors Contributing to the Feasibility of HAT from Formate.....	21
Figure 2.4: Formate Catalyzed Reduction of an Aryl Chloride via Thiol Oxidation.....	23
Figure 2.5: HAT catalyst Screen and Control.....	24
Figure 2.6: A Summary of Mechanistic Evidence for $\text{CO}_2^{\bullet-}$ Generation.....	25
Figure 2.7: The Formation of Electrophilic Radicals under Alternative Conditions.....	27
Figure 2.8: Alternative Initiators Screen.....	27
Figure 2.9: Proposed Mechanistic Scenario for Aryl Chloride Reduction.....	28
Figure 2.10: A Summary of Intermolecular Hydroarylation Protocols via (Hetero)aryl Radical Giese Addition.....	29
Figure 2.11: Modern Examples of Unactivated Alkene Hydroarylation with Unactivated Arenes.....	30
Figure 2.12: Solvent Screen for Hydroarylation.....	31
Figure 2.13: Potential Solvent Factors Impacting Reaction Efficacy.....	32
Figure 2.14: Cosolvent Screening for Hydroarylation.....	33
Figure 3.1: Potential Reaction Mechanism for CO_2 Incorporation via $\text{CO}_2^{\bullet-}$	44
Figure 3.2: Optimization/Controls for Hydrocarboxylation of Michael Acceptors.....	45
Figure 3.3: Optimization of Carboxylation for 1,1-Diphenylethylene.....	46

Figure 3.4: Investigations into Michael Acceptor Single Electron Reduction.....	48
Figure 3.5: Reduction Potential Series Demonstrating the Split Reactivity for Michael Acceptors.....	49
Figure 3.6: Evaluation of Olefin Conjugate Addition with Different Formyl C-H Sources...50	
Figure 3.7: Graphic Representation of the Anomeric Effect in Formyl C-H Systems.....52	
Figure 4.1: Classical Methods of Constructing Carboxylic Acids.....60	
Figure 4.2: Catalytic Strategies for C(sp ²) Carboxylation.....61	
Figure 4.3: Initial Mechanistic Scenario for C(sp ²) Carboxylation.....62	
Figure 4.4: Overview of Reaction Screening for Alternative Initiators.....63	
Figure 4.5: Reduction Pathway and CV of Phenyl Triflimide.....68	
Figure 4.6: Evaluation of Alternative Sulfonylating Agents.....71	
Figure 4.7: Nickel Photocatalyst Dependence.....74	

List of Schemes

Scheme 1.1: General Overview of Radical Philicity and Polar Effects.....	4
Scheme 1.2: Classical Example of XAT-mediated Tin cyclization in the Racemic Total Synthesis of Hirustene.....	5
Scheme 1.3: Generation of alpha-amino radicals under Photocatalytic Conditions for XAT from Aryl/Alkyl Halides.....	6

Scheme 1.4: Standard catalytic cycle for nickel-catalyzed reductive cross-electrophile coupling.....	11
Scheme 2.1: Radical Hydroarylation and Defluoroalkylation of Olefins.....	18
Scheme 2.2: Initial hypothesis regarding the generation of CO ₂ ^{•-} via HAT.....	19
Scheme 4.2: Reaction Pathway for CO Generation.....	69
Scheme 4.3: Carbon Monoxide Recycling System.....	72
Scheme 4.4: Proposed Mechanistic Scenario.....	75

List of Tables

Table 2.1: Hydroarylation Substrate Scope.....	34
Table 2.2: Alternative Reduction Scope.....	35
Table 4.1: Solvent Screen Under Photochemical Conditions.....	64
Table 4.2: Reaction Screening with Electron-Rich/Neutral Arene.....	65
Table 4.3: HAT Catalyst Screen.....	66
Table 4.4: Reaction Controls.....	70
Table 4.5: Phenyl Triflimide Loading.....	73
Table 4.6: Substrate Scope for C(sp ²) Carboxylation.....	47

List of Abbreviations

3DPAFIPN 2,4,6-tris(diphenylamino)-5-fluoroisophthalonitrile

4CzIPN 1,2,3,5-tetrakis(carbazol-9-yl)-4,6-dicyanobenzene

4CzTPN 2,3,5,6-tetrakis(carbazol-9-yl)-1,4-dicyanobenzene

AcOH acetic acid

AIBN azobisisobutyronitrile

APCI atmospheric-pressure chemical ionization

CySH cyclohexanethiol

CV cyclic voltammetry

DABCO 1,4-diazabicyclo[2.2.2]octane

DBU 1,8-diazabicyclo[5.4.0]undec-7-ene

DCM dichloromethane

DFT density functional theory

DMSO dimethyl sulfoxide

DMF dimethylformamide

Et₂O diethyl ether

EtOAc ethyl acetate

GCMS gas chromatography mass spectrometry

HAT hydrogen atom transfer

HMPA hexamethylphosphoramide

HPLC high performance liquid chromatography

HRMS high-resolution mass spectrometry

LCMS liquid chromatography mass spectrometry

MeCN acetonitrile

MeOH methanol

MHz mega hertz

MTBE methyl tert-butyl ether

NMR nuclear magnetic resonance

Oxidative Addition

PC photocatalyst

PCET proton-coupled electron transfer

PhSH thiophenol

PTFE polytetrafluoroethylene

PTH 10-phenylphenothiazine

RE Reductive Elimination

SCE saturated calomel electrode

SET single electron transfer

TAS transient absorption spectroscopy

TBDPS tert-Butyldiphenylsilyl

TEA triethylamine

TFE 2,2,2-trifluoroethanol

THF tetrahydrofuran

TLC thin layer chromatography

**Chapter 1: An overview of Single Electron Transformations, the
Emergence of Photoredox Catalysis, and Nickel-Catalyzed Cross-
Couplings**

1.1 Single Electron Transformations

In most traditional undergraduate chemistry courses, the emphasis on bond forming is typically centered around two-electron chemistry with classical electrophiles and nucleophiles. Single electron, or radical, processes are often considered too complex for undergraduate research courses despite its utility and abundance in both organic chemical transformations in addition to various enzymatic processes. Regardless of their absence in undergraduate research courses, the utility of radical processes has only increased over the last several decades as emerging technologies to generate and use single electron transformations have become increasingly important. Currently at the forefront of synthetic organic chemistry, single electron transformations are often accessed via single electron redox manipulations in addition to hydrogen/halogen atom abstractions (HAT/XAT) protocols.

1.1.1 Hydrogen Atom Abstraction

When considering the movement of hydrogen atoms in organic systems, most chemists will immediately think of heterolytic cleavage of carbon/heteroatom-hydrogen cleavage—in other words Bronsted-Lowry acid-base chemistry.¹ While the heterolytic cleavage of hydrogen-carbon/heteroatom bonds provide useful anionic and cationic species, the homolytic cleavage of the same bonds generates complementary radical species with unique selectivity profiles.² As described by James Meyer, hydrogen atom transfer can be thought of as “the concerted movement of a proton and an electron in a single kinetic step where both the proton and the electron originate from the same reactant and travel to the same product”^{2a} and is described simply in equation 1. In any HAT process, there is an abstractor and a donor, as show in equation 1, X acts as the abstractor thereby generating an X-H bond while simultaneously



generating a new radical that may undergo further HAT processes or engage in other bond forming reactions.

In order to understand the driving force for HAT processes, it is important to highlight the correlation between HAT rate constants and the corresponding bond dissociation energies (BDEs) of the reactive species. This relationship is detailed in equations 2 and 3 (derived from the Bell-Evans-Polanyi principle) where E_a is the activation energy, ΔH is the enthalpic driving force, and α and β represent reaction parameters. When looking closely at ΔH , the importance of BDEs becomes clear as the closer they are to one another the smaller ΔH becomes thereby the smaller the E_a becomes.³ HAT processes have implications in a wide variety of systems

$$E_a = \alpha(\Delta H) + \beta \quad (2)$$

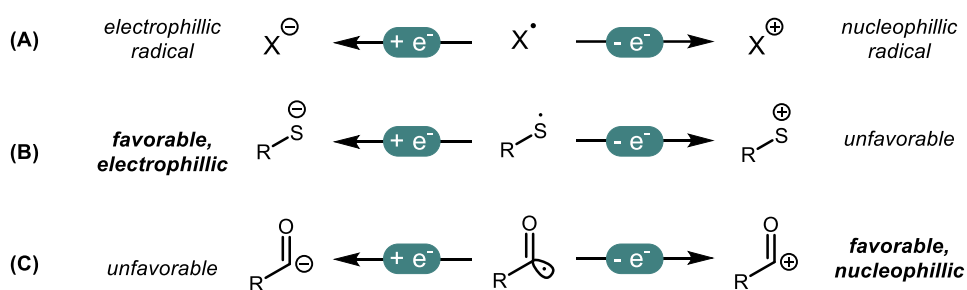
$$\Delta H^\circ = \text{BDE}(\text{AH}) - \text{BDE}(\text{XH}) \quad (3)$$

including metal mediated reactions,⁴ biological systems,⁵ and a wide breadth of chemical reactions. While BDEs are particularly important for HAT processes, so is the concept of ‘radical philicity’ and ‘polar effects’.

Although free radicals are considered electronically neutral, depending on the atom the radical is located on they still experience a polar effect. This polar effect has implications on the activation energy of an HAT event and is directly related to the charge transfer experienced during the HAT process.⁶ To better exemplify this, consider Scheme 1.1. As demonstrated in Scheme 1A, a radical’s polar effect can be best described by its affinity towards single electron oxidation or reduction. If a radical is more inclined to accept an electron (in other words its anionic form is more stable) it is said to be nucleophilic while if a radical is more inclined to give up an electron (its cationic form is more stable) then it is said to be electrophilic. This concept is

further demonstrated in Scheme 2A and Scheme 2B where thiyl radicals are electrophilic due to their affinity towards electrons while the opposite is true for acyl radicals. As such, the rate of HAT between an electrophilic radical such as a tert-butoxy radical and an aldehyde is fast while HAT between a tert-butoxy radical and a thiol is slow as the polar effects are unfavorable. To summarize, HAT processes rely primarily on two components of a reaction system—the BDE of the reactive components as well as their respective philicity.

Scheme 1.1: General Overview of Radical Philicity and Polar Effects.



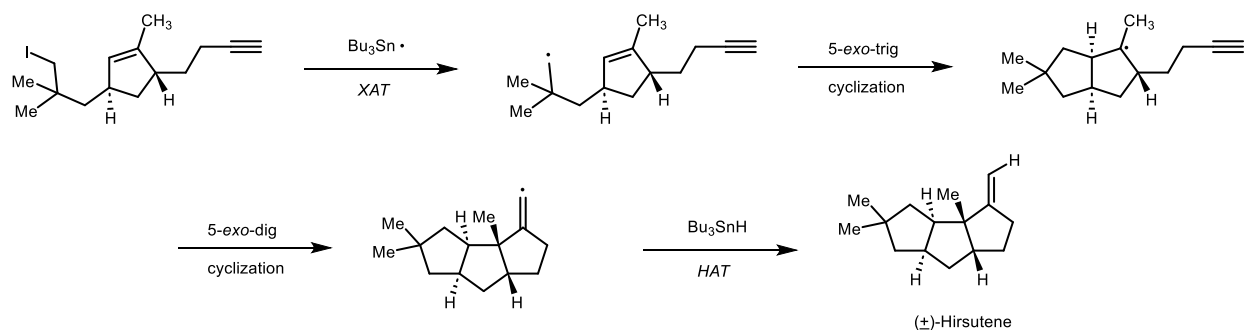
1.1.2 Halogen Atom Abstraction

While hydrogen atom abstraction is a fundamental tool for the generation of various carbon or heteroatom-centered radicals, a complimentary and perhaps more well-known process is that of halogen atom abstraction (XAT).⁷ In a similar fashion to HAT, XAT processes are primarily guided by BDEs and reactivity is generally consistent with the Bell-Evans-Polanyi principle discussed earlier although polar, steric, and hyperconjugative effects also play a role.⁸ An interesting feature of HAT when juxtaposed with HAT is the observed switch in polar effects observed and suggested by Hammett plots. In HAT processes, cationic character is typically observed on the forming carbon-centered radical in the charge-transition state while the opposite is true for XAT processes as the nucleophilic abstractor imparts anionic charge on the forming

carbon-centered radical.⁹ In part, this observed flip in reactivity is thought to be correlated to the difference in electronegativity between carbon-halogen bonds and carbon-hydrogen bonds which is intrinsically related to bond polarizability and therefore charge transfer states. HAT processes have important implications in organic synthesis and XAT also have important implications in a variety of organic methodologies.

Two of the perhaps most well-known examples of XAT in organic synthesis involve the use of tin and alpha amino radicals—notably both are examples of nucleophilic radicals. A classical example a useful tin-mediated XAT reaction is in the total synthesis of Hirsutene which actually relies on both an HAT and XAT event for this radical cascade (Scheme 1.2).¹⁰ In this example, upon initiation with AIBN¹¹, HAT from tributyltin hydride generates the tin-centered radical which upon XAT with the primary alkyl iodide undergoes two sequential cyclizations followed by an HAT event to furnish the racemic product thereby forming two rings and a quaternary carbon center in a single step.

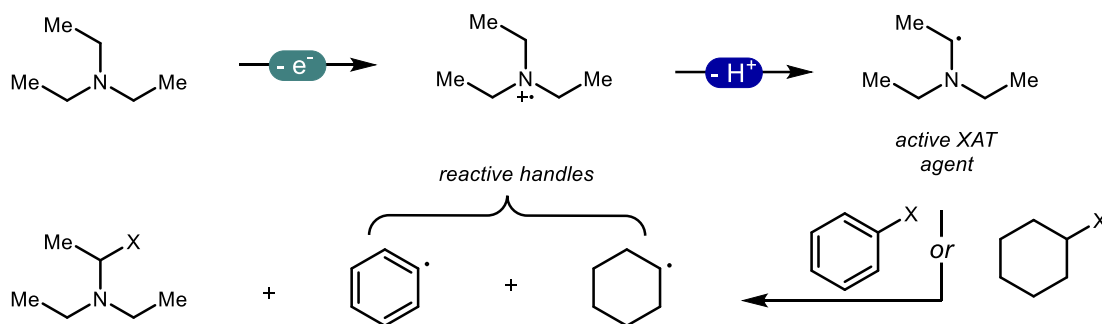
Scheme 1.2: Classical Example of XAT-mediated Tin cyclization in the Racemic Total Synthesis of Hirsutene



Although tin-mediated radical processes demonstrate the utility of XAT processes, the high toxicity of tin alongside the potentially explosive initiators needed to begin the bond-

forming process make these reactions rather hazardous. While there are a large number of modern nucleophilic halogen atom abstractors that have gained attention in recent years, perhaps one of the most notable examples is that of aminoalkyl radicals as XAT agents.¹² In this example pioneered by the Leonori group, amino alkyl radicals are generated under photocatalytic conditions (discussed in the next section) where an oxidation deprotonation sequence generates the active XAT agent *in situ* under mild conditions (Scheme 1.3). Upon abstracting a halogen atom from a C(sp²/sp³) halogen bond, the corresponding alkyl/aryl radicals can then undergo various useful transformations including deuteration, alkylation, allylation, olefination, and arylation.

Scheme 1.3: Generation of alpha-amino radicals under Photocatalytic Conditions for XAT from Aryl/Alkyl Halides

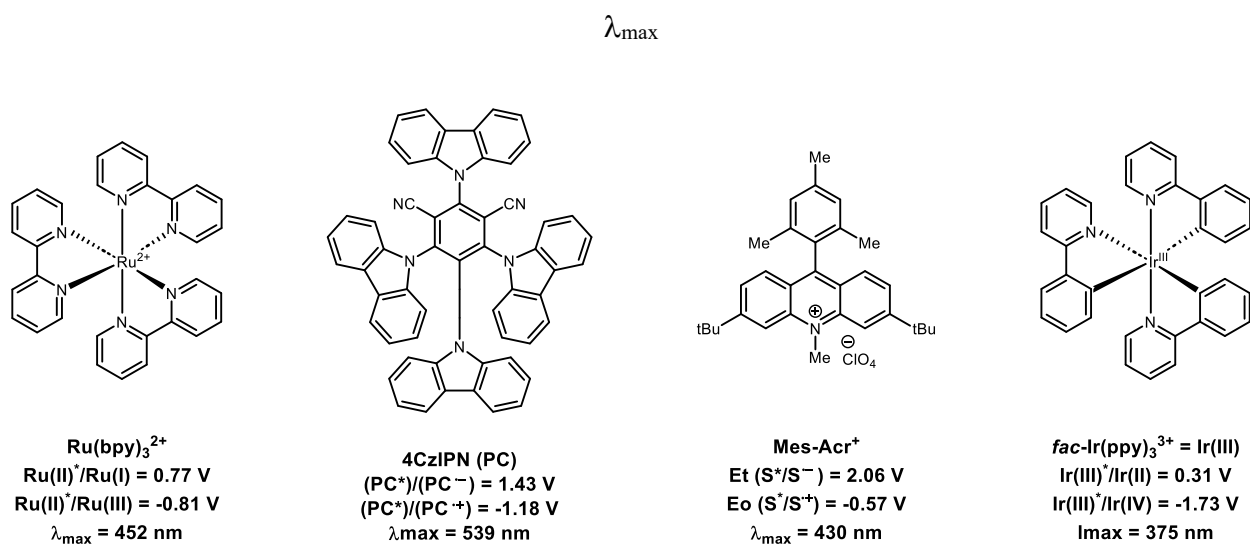


1.1.3 The emergence of Photoredox Catalysis

Although single electron transformations have been well documented as useful reactive intermediates, the often harsh conditions required to generate these reactive species left a hole in the field that was quickly filled in with the emergence of photoredox catalysis. In 2008, the Yoon group and the Macmillan group published¹ reports in tandem regarding the visible-light promoted intramolecular [2+2] cycloaddition of olefins¹³ alongside the enantioselective α -

alkylation of aldehydes¹⁴ using the transition-metal complex $\text{Ru}(\text{bpy})_3^{2+}$. Most photoredox catalysts are either organic dyes or transition-metal complexes that absorb light in the visible region and operate in catalytic amounts (often between 0.5-1 mol%) at room temperature making their use highly attractive. Furthermore, because many organic molecules used in organic synthesis do not absorb light in the visible region making unproductive side reactions unlikely.¹⁵ Shown in Figure 1.1 are some of the most commonly used organic and transition-metal photocatalysts with a large breadth in reactivity with respect to redox potentials with the most modern photocatalysts being acridinium-based dyes (Mes-Acr^+)¹⁶ and donor-acceptor cyanoarenes (4CzIPN)¹⁷.

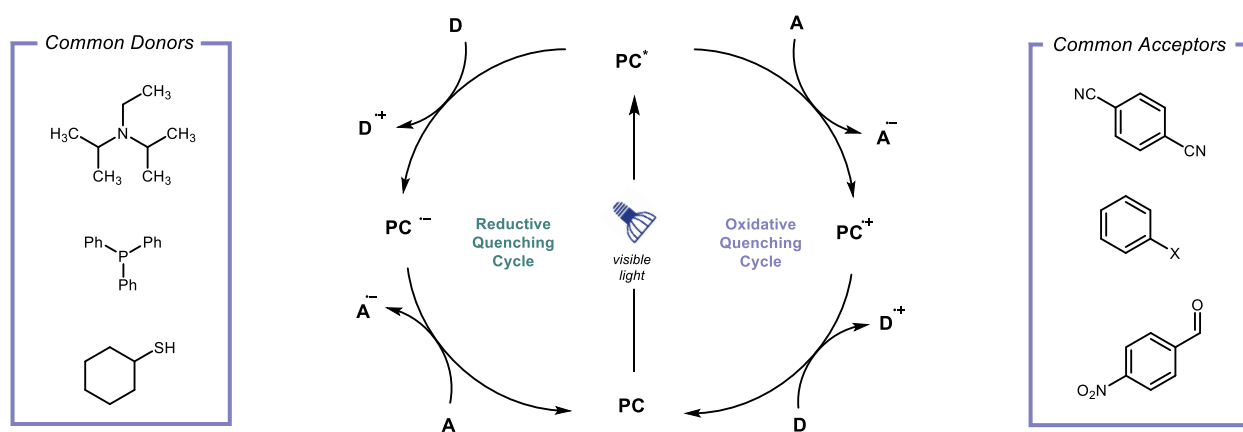
Figure 1.1: Common Photoredox Catalysts Alongside their Excited State Redox Potentials and



Within the realm of photoredox catalysis, there are essentially two modes of action to activate organic molecules—single electron oxidation/reduction and energy transfer. For single electron reduction/oxidation to be active and catalytic, stoichiometric additives are necessary and come in the form of electron acceptors (**A**) and electron donors (**D**). There are essentially two modes of activation within this system that allow access to different redox properties of the

photocatalyst and these modes come in the form of a ‘Reductive Quenching Cycle’ and an ‘Oxidative Quenching Cycle’ (**Figure 1.2**). In a reductive quenching cycle, upon excitation with visible light, the photocatalyst may undergo single electron oxidation of some donor molecule (trialkylamines are the most common) which then delivers the radical anion of the photocatalyst. The radical anion of the photocatalyst may then deliver that electron to another substrate delivering the photocatalyst back to the ground state. Alternatively, the opposite process may also occur in which an excited state reduction of some reducible species (A) delivers the radical cation of the photocatalyst which then oxidizes a substrate delivering the photocatalyst back to the ground state. This conveniently allows the reaction parameters to be tuned in order to access different redox states of the photocatalyst.

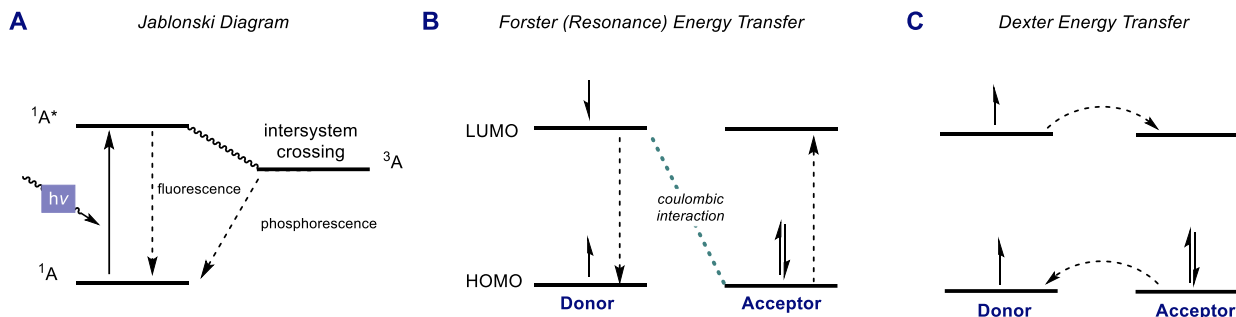
Figure 1.2: Graphic representation of oxidative/reductive quenching cycles shared by all photoredox-catalyzed systems alongside common stoichiometric donors and acceptors.



Another important feature of photocatalysts is their excited states (singlet and triplet excited states) and its inherent relation to energy transfer pathways. While reduction/oxidation potentials are important components in determining whether a redox event will happen, equally

important is their lifetime in either the single or triplet excited state¹⁸. The singlet and triplet excited states can be best summarized by a Jablonski diagram (**Figure 1.3A**).

Figure 1.3: Graphic representation of a Jablonski diagram (**A**) alongside the different energy transfer mechanisms—Forster (**B**) and Dexter (**C**).



Upon excitation with visible light, the photocatalyst may promote an electron to its singlet excited state which then rapidly decays back to its resting state, most often in the form of fluorescence. Alternatively, from the singlet excited state intersystem crossing (ISC) may occur over to its triplet excited state followed by a spin forbidden (which accounts for its longer lifetime) decay in the form of phosphorescence¹⁹. While fluorescence and phosphorescence are both common pathways, both the singlet and triplet excited states may also engage in energy transfer processes.

The first of which, Forster Resonance Energy Transfer, relies on a coulombic interaction between the excited state of the donor molecule and acceptor molecule. This excited state interaction generates a dipole in the acceptor molecule which eventually leads to an electronic transition. Alternatively, Dexter energy transfer could occur in which the donor and acceptor molecule can approach each other in solution and form a caged complex within the solvent system. This complex may result in orbital overlap between the two molecules allowing an energy transfer to occur, in other words this type of energy transfer is guided by proximity of the

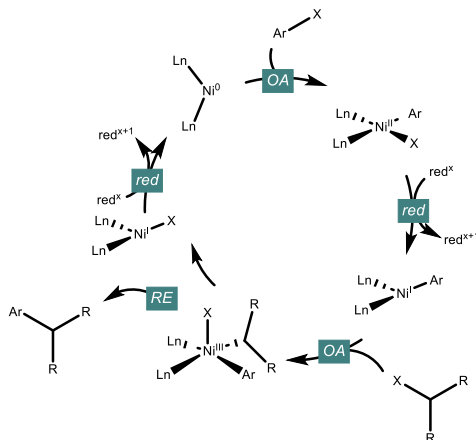
donor and acceptor molecule to one another and may be sensitive to solvent and triplet excited state lifetimes.

1.2 An Overview of Nickel-Catalyzed Cross Couplings

Although palladium-catalyzed reactions have dominated the world of carbon-carbon/carbon-heteroatom bond forming reactions, in recent years nickel-catalyzed cross couplings has emerged as an interesting alternative. Although their reactivities with respect to cross-coupling reactions essentially parallel each other, one of the primary differences between the two metals is the more favorable interactions between nickel and single-electron processes²⁰. This has allowed for the emergence of a subset of nickel-catalyzed cross-couplings in which radicals, formed either through XAT with the metal center of dual photoredox catalysis, may engage the metal center to forge C(sp²)-C(sp³) bonds²¹. Typically, these cross-couplings occur in the manner described in scheme 1.4.

Generally with nitrogen centered ligands, the nickel(0) may undergo oxidative addition with a C(sp²) (pseudo)halide to form a Ni(II) complex which is reduced back to Ni(I) by some stoichiometric metal reductant (often zinc or manganese). This complex may undergo XAT with an alky electrophile followed by radical rebound to generate the activated Ni(III) complex which is poised for reductive elimination to furnish the C(sp²)-C(sp³) product. Another equivalent of reductant may then engage the nickel center and regenerate the catalytic cycle. The primary difference between typical cross-electrophile couplings and metallophotoredox is the role of the photocatalyst which may essentially replace the metal reductants and regulate the nickel catalytic cycle with its own redox manipulations.

Scheme 1.4: Standard catalytic cycle for nickel-catalyzed reductive cross-electrophile coupling.



1.3 References

- (1) Kauffman, G. B., Thomas, L., & Lowry, M. (2023). The Brønsted-Lowry Acid-Base Concept. *J. Chem. Educ.*, **2023**, *14*, 28-31.
- (2a) Mader, E. A., Davidson, E. R., & Mayer, J. M. (2007). Large ground-state entropy changes for hydrogen atom transfer reactions of iron complexes. *J. Am. Chem. Soc.*, **2007**, *129*, 5153-5166.
- (2b) Mayer, J. M. (2011). Understanding hydrogen atom transfer: From bond strengths to marcus theory. *Acc. Chem. Res.*, **2011**, *44*, 36-46.
- (2c) Capaldo, L., & Ravelli, D. (2017). Hydrogen Atom Transfer (HAT): A Versatile Strategy for Substrate Activation in Photocatalyzed Organic Synthesis. *Eur. J. Org. Chem.*, **2017**, *15*, 2056-2071.
- (3) Roberts, B. P., & Steel, A. J. (1994). An Extended Form of the Evans-Polanyi Equation: a Simple Empirical Relationship for the Prediction of Activation Energies for Hydrogen-atom Transfer Reactions. *J. Chem. Soc. Perk.*, **1994**, *2*, 2155-2162.

- (4) Green, S. A., Crossley, S. W. M., Matos, J. L. M., Vásquez-Céspedes, S., Shevick, S. L., & Shenvi, R. A. (2018). The High Chemofidelity of Metal-Catalyzed Hydrogen Atom Transfer. *Acc. Chem. Res.*, **2018**, *51*, 2628-2640.
- (5) Poulos, T. L. (2014). Heme enzyme structure and function. *Chem Rev.*, **2014**, *114*, 3919-3962.
- (6) Roberts, B. P. Polarity-reversal catalysis of hydrogen-atom abstraction reactions: concepts and applications in organic chemistry. *Chem. Soc. Rev.*, **1999**, *28*, 25-35.
- (7) Juliá, F., Constantin, T., & Leonori, D. Applications of Halogen-Atom Transfer (XAT) for the Generation of Carbon Radicals in Synthetic Photochemistry and Photocatalysis.. *Chem. Rev.*, **2022**, *122*, 2292-2352.
- (8) Itsenko, O., Norberg, D., Rasmussen, T., Långström, B., & Chatgililoglu, C. (2007). Radical carbonylation with [11C]carbon monoxide promoted by oxygen-centered radicals: Experimental and DFT studies of the mechanism. *J. Am. Chem. Soc.*, **2007**, *129*, 9020-9031.
- (9a) Brivati, A., R Symons, M. C., A Tinling, D. J., Wardale, H. W., Williams, D. O., Chem Soc, J., Kuivila, H. G., & Walsh, E. J. Halogen Atom Abstraction Reactions: Free-Radical Abstraction of Iodine from Substituted Iodobenzenes. *J. Am. Chem. Soc.*, **1969**, *2*, 5924-5925.
- (9b) Danen, W. C., Winter, R. L., Tanner, D. D., Darwish, D., Mosher, M. W., Bunce, N. J., & Amer, J. Iodine from Aliphatic Iodides. Evidence to Support Anchimeric Assistance by Neighboring Halogen in Homolytic Reactions¹. *J. Am. Chem. Soc.*, **1971**, *93*, 716-719.
- (10) Curran, P.; Rakiewicz, D. Tandem Radical Approach to Linear Condensed Cyclopentanoids. Total Synthesis of (+) – Hirsutene. *J. Am. Chem. Soc.*, **1985**, *107*, 1449-1450.

- (11) Xia, J., Matyjaszewski, K. Controlled/"Living" Radical Polymerization. Homogenous Reverse Atom Transfer Radical Polymerization using AIBN as the Initiator. *Macromolecules*, **1997**, *30*, 7692-7696.
- (12) Constantin, T., Zanini, M., Regni, A., Sheikh, N. S., Juliá, F., & Leonori, D. Aminoalkyl radicals as halogen-atom transfer agents for activation of alkyl and aryl halides. *Science*, **2020**, *367*, 1021-1026.
- (13) Ischay, M. A., Anzovino, M. E., Du, J., & Yoon, T. P. Efficient visible light photocatalysis of [2+2] enone cycloadditions. *J. Am. Chem. Soc.*, **2008**, *130*, 12886-12887.
- (14) Nicewicz, D. A., & MacMillan, D. W. C. Merging photoredox catalysis with organocatalysis: The direct asymmetric alkylation of aldehydes. *Science*, **2008**, *322*, 77–80.
- (15) Prier, C. K., Rankic, D. A., & MacMillan, D. W. C. Visible light photoredox catalysis with transition metal complexes: Applications in organic synthesis. *Chem. Rev.*, **2013**, *1123*, 5322-5363.
- (16) Joshi-Pangu, A., Lévesque, F., Roth, H. G., Oliver, S. F., Campeau, L. C., Nicewicz, D., & DiRocco, D. A. Acridinium-Based Photocatalysts: A Sustainable Option in Photoredox Catalysis. *J. Org. Chem.*, **2016**, *81*, 7244-7249.
- (17) Speckmeier, E., Fischer, T. G., & Zeitler, K. A Toolbox Approach to Construct Broadly Applicable Metal-Free Catalysts for Photoredox Chemistry: Deliberate Tuning of Redox Potentials and Importance of Halogens in Donor-Acceptor Cyanoarenes. *J. Am. Chem. Soc.*, **2018**, *140*, 15353-15365.

- (18) Sartor, S. M., McCarthy, B. G., Pearson, R. M., Miyake, G. M., & Damrauer, N. H. Exploiting Charge-Transfer States for Maximizing Intersystem Crossing Yields in Organic Photoredox Catalysts. *J. Am. Chem. Soc.*, **2018**, *140*, 4778-4781.
- (19) Strieth-Kalthoff, F., James, M. J., Teders, M., Pitzer, L., & Glorius, F. (2018). Energy transfer catalysis mediated by visible light: principles, applications, directions. *Chem. Soc. Rev.*, **2018**, *47*, 7190-7202.
- (20) Ananikov, V. P. Nickel: The “spirited horse” of transition metal catalysis. *ACS Catal.*, **2015**, *5*, 1964-1971.
- (21a) Chan, A. Y., Perry, I. B., Bissonnette, N. B., Buksh, B. F., Edwards, G. A., Frye, L. I., Garry, O. L., Lavagnino, M. N., Li, B. X., Liang, Y., Mao, E., Millet, A., Oakley, J. v., Reed, N. L., Sakai, H. A., Seath, C. P., & MacMillan, D. W. C. Metallaphotoredox: The Merger of Photoredox and Transition Metal Catalysis. *Chem. Rev.*, **2022**, *122*, 1485-1542.
- (21b) Weix, D. J. Methods and Mechanisms for Cross-Electrophile Coupling of Csp² Halides with Alkyl Electrophiles. *Acc. Chem. Res.*, **2015**, *48*, 1767-1775.
- (21c) Poremba, K. E., Dibrell, S. E., & Reisman, S. E. Nickel-Catalyzed Enantioselective Reductive Cross-Coupling Reactions. *ACS Catal.*, **2020**, *10*, 8237-8246.

Chapter 2: Radical Chain Reduction via the Carbon Dioxide Radical Anion ($\text{CO}_2^{\bullet-}$)

Adapted and reprinted in part with permission from Hendy, C. M.; Smith, G.; Xu, Z.; Lian, T.; Jui, N. *J. Am. Chem. Soc.*, **2021**, *143*, 8987-8992.

Copyright 2021 American Chemical Society

<https://pubs.acs.org/doi/10.1021/jacs.1c04427>

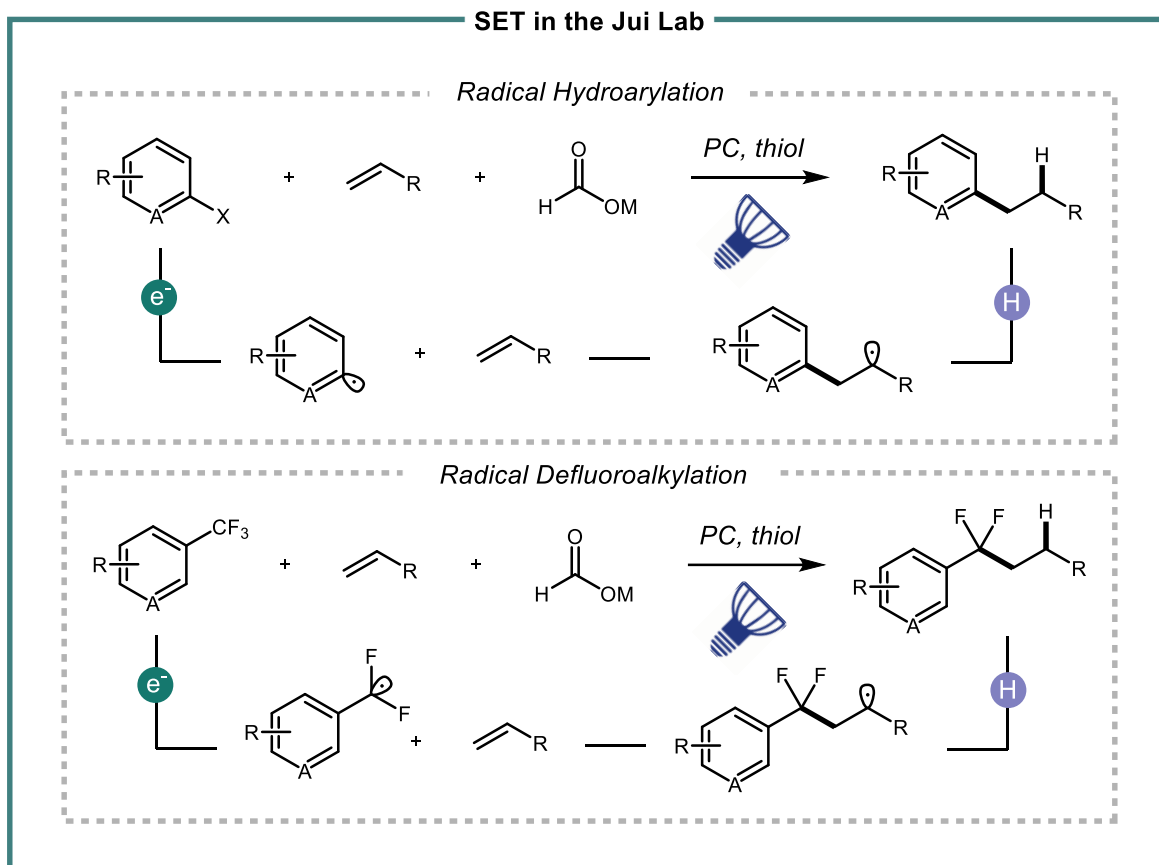
C. M. Hendy contributed to both carboxylation and reduction scope. Z. Xu performed transient absorption spectroscopy and Stern-Volmer quenching experiments.

Abstract: The emergence of photoredox catalysis and electrochemistry has demonstrated both the utility of radical intermediates in synthetic chemistry and their inherent limitations. We have developed a new method for reductive radical formation in which the generation of the carbon dioxide radical anion ($\text{CO}_2^{\bullet-}$) serves as both a powerful reductant and a source of nucleophilic carbon dioxide via a novel radical chain mechanism. Through a polarity matched hydrogen atom transfer (HAT) between an electrophilic radical and a formate salt, the $\text{CO}_2^{\bullet-}$ is generated. We have demonstrated that this intermediate can act as a single electron transfer agent to achieve difficult reductions or it can undergo a Giese type reaction with electron deficient olefins to make synthetically useful 1,4-dicarbonyls where substrate reduction potential may be used to predict reaction outcome. We found an initiation event leading to the formation of a thiyl radical can be achieved through either thiol oxidation, homolytic cleavage of disulfides, or through the thermal initiation of classical radical initiators such as AIBN. Under this novel radical chain mechanism, we are able access the $\text{CO}_2^{\bullet-}$ under mild conditions and demonstrate its ability to serve as either a powerful reducing agent or a source of nucleophilic carbon dioxide.

2.1 An Overview of Photoredox in the Jui Lab

In recent years, radical intermediates have emerged at the forefront of synthetic chemistry. Radicals are highly reactive species with complementary selectivity profiles to ionic intermediates, and many methods for radical generation have been developed with dissolving metals^{1,2} and electrochemistry^{3,4} being among the most abundant. Within this area, single electron reduction of olefins or halogenated substrates allows for reliable formation of radical species from readily available starting materials. Recently, the fields of photoredox catalysis and electrochemistry have offered exciting alternatives to radical generation/reactivity, but significant limitations remain. Electrochemistry allows for precise tuning of potential but over oxidation/over reduction processes make capturing radical species impossible in many cases.⁵ On the other hand, photoredox catalysis readily allows for radical intermediates to be intercepted^{6,7}, but many of the photocatalysts (PC) used in these systems are limited by the energy visible light provides (up to 2.8 eV for visible light⁸), leaving difficult redox events out of reach using traditional methods.

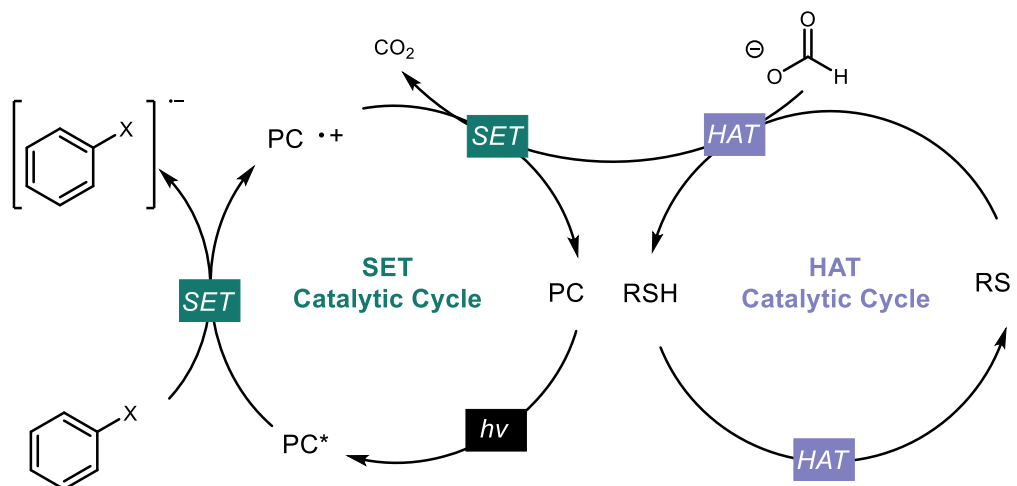
In the Jui lab, we have typically relied on highly reducing photocatalysts to achieve single electron transformations that were previously inaccessible.⁹ The potent reducing power of these photocatalysts has allowed access to valuable radical intermediates for carbon-carbon bond formation including aryl and difluorobenzyl radicals. As shown in Scheme 2.1, the carbon-carbon bond formation occurs in very similar manners. Upon single electron reduction from a highly reducing photocatalyst, the carbon-centered radical is formed which may undergo a Giese type addition to the corresponding alkene generating an alkyl radical which may be capped upon HAT. This methodology has allowed for the rapid construction of traditionally challenging molecules including phenethylamines and compounds bearing difluoroalkyl motifs.

Scheme 2.1: Radical Hydroarylation and Defluoroalkylation of Olefins

Interestingly, within these systems although different photocatalysts are used the catalytic cycles do operate in parallel with one another. Upon excitation with visible light (blue LEDs), the photocatalyst (PC) is excited to its triplet/singlet excited state (PC*) which may then undergo single electron reduction of some organic species. This organic species may then undergo mesolytic fragmentation to generate the carbon centered radical alongside the radical cation of the photocatalyst (PC⁺). Following Giese-type addition to an alkene by the aryl/difluorobenzyl radical another alkyl radical is generated which may then be capped via a polarity matched HAT process between the newly generated alkyl radical and a catalytic thiol (**Figure 2.1**). In order to turn over both catalytic cycles, an interaction between thiol radical and

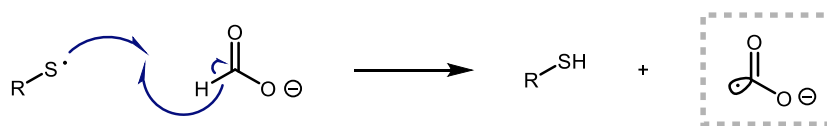
a formate salt delivers an electron to the photocatalytic and a hydrogen atom to the thiol – an interaction that has long been ambiguous in our group.

Figure 2.1: A representative catalytic cycle for thiol/formate catalyzed photoredox systems in the Jui lab.



Implied within the interaction between thiyl radical is the presence of the highly elusive and transient carbon dioxide radical anion via the HAT process shown in **Scheme 2.2**

Scheme 2.2: Initial hypothesis regarding the generation of $\text{CO}_2^{\bullet-}$ via HAT



2.2: An Overview of the Carbon Dioxide Radical Anion

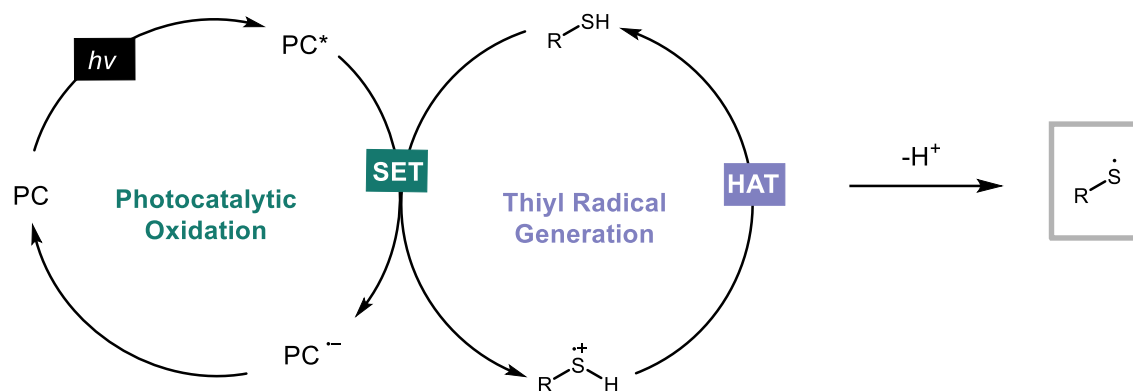
The carbon dioxide radical anion $\text{CO}_2^{\bullet-}$ is known to be a highly reactive and elusive intermediate, typically formed via electrochemical reduction of carbon dioxide.^{10,11} Given its very potent reduction potential ($E_{1/2}^0 = -2.2 \text{ V vs SCE}$)¹² and intrinsic reactivity, $\text{CO}_2^{\bullet-}$ has the potential to be a useful synthetic intermediate. Despite the high value of generating this

intermediate, very few examples exist of its utility in organic synthesis. Previous work carried out by Barba¹³ and Kubiak¹⁴ show that reduction of CO₂ to CO₂^{•-} may be employed in carboxylation reactions under the corresponding photochemical or electrochemical conditions. In 2017, the Jamison group designed an approach that allows for the generation and capture of CO₂^{•-} with UV light in a flow reactor thereby facilitating carbon-carbon bond formation.¹⁵ While these initial reports demonstrate the utility of this useful intermediate, the requirement of harsh conditions (super reductants, UV light, electrochemistry) limit its practicality. As such, its utility is understudied. Given the use of formate and HAT systems in our previous work, we sought to elucidate the details for CO₂^{•-} generation and how we might leverage its formation in organic synthesis.

2.2.1 Mechanistic Investigations into CO₂^{•-} as an Upconverted Reductant

Under our previous conditions, we had relied on an excited state reduction of highly reducing photocatalysts to access reactive radical species via single electron reduction while the corresponding alkyl radical generated formed thiyl radical via HAT. We sought to augment this system bypassing the need for highly reducing catalysts by directly generation of CO₂^{•-} via thiol oxidation. The low oxidation potential of various alkyl/aryl thiols¹⁶ are well-established allowing for the oxidation and subsequent deprotonation (the radical cation of thiols experience enhanced acidity relative to their redox neutral counterpart)¹⁷ of a thiol leading to the generation of thiyl radical—this would set up a catalytic cycle outlined in **Figure 2.2**. By augmenting this system towards thiyl radical generation, the framework for is set for intentional generation of the carbon dioxide radical anion.

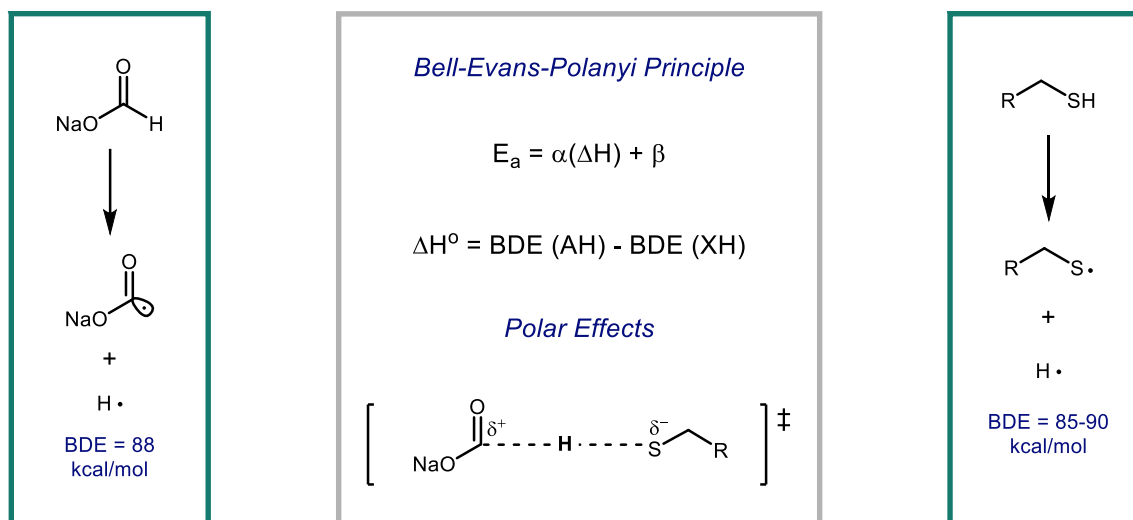
Figure 2.2: Modified Catalytic Cycle Generating Electrophilic Thiyl Radical via SET



Simple thiol oxidation generates potent reductant

One of the first questions that we asked about this system is the energetic feasibility of this system, is HAT from formate via thiyl radical a favorable process? As discussed earlier, for an HAT event to be favorable it is important to have matched polar effects and bond dissociation energies. As shown in Figure 2.3, the polar effects of this interaction are clearly favorable as the carbon dioxide radical anion is likely to expel a radical (to make CO_2 simultaneously) while thiyl radical is favored to form the anion.

Figure 2.3: Factors Contributing to the Feasibility of HAT from Formate

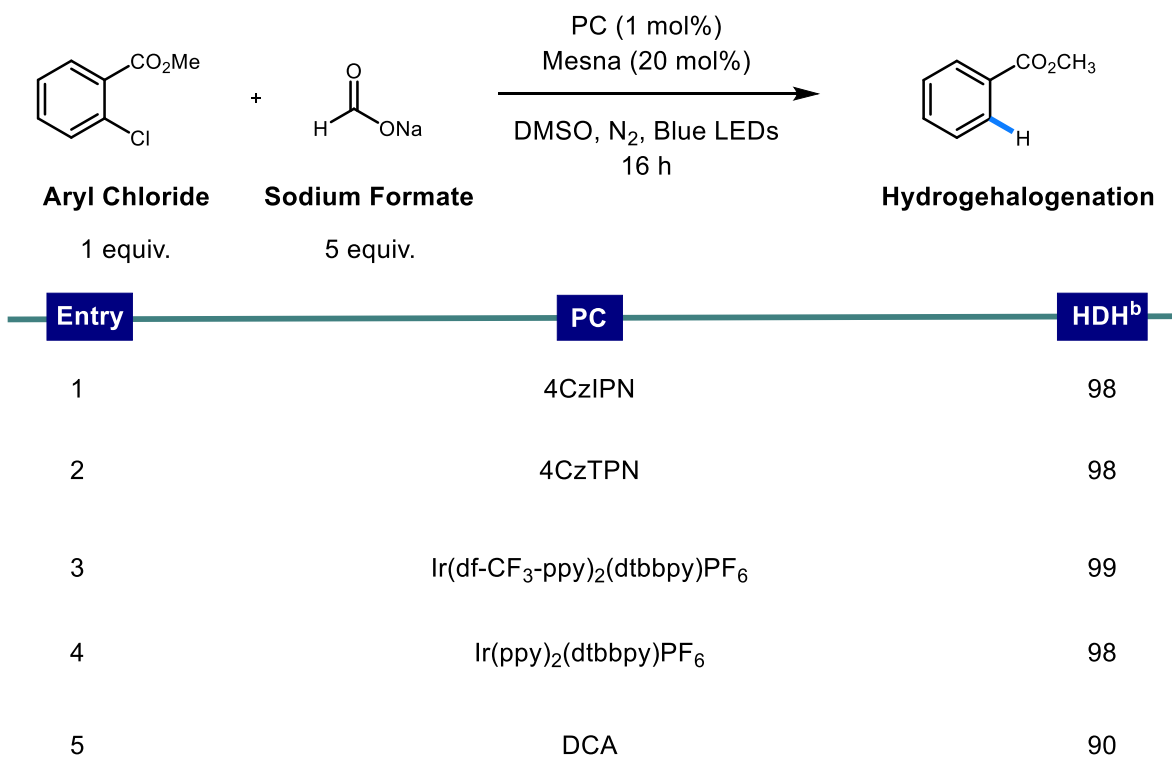


The next question that needed answering is the BDE of the two reactive species. The S-H BDE of a typical alkyl/aryl thiol is well-known to be around 85-90 kcal/mol.¹⁸ What was not known at the time however, is the formyl C-H BDE of formate. In order to quantify the BDE of sodium formate we relied on DFT calculations employed at (U)B3LYP levels of theory with the 6-31+G(d,p) basis set. By performing geometry optimizations and quantifying the energetic minima of the reactive species, we found formyl C-H BDE of formate to be 89.6 kcal/mol. With the energetic feasibility established, we next sought to evaluate this hypothesis on a model system.

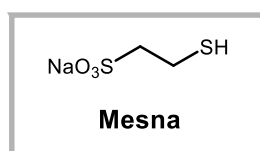
Under standard conditions (developed and modified from conditions optimized in Chapter 3), we first sought to evaluate the hydrodehalogenation of 2-chloromethyl benzoate (a challenging reduction at -2.1 V vs SCE).¹⁹ We were excited to see that under the conditions outlined in Figure 2.4, conversion from the aryl chloride to the HDH product went smoothly in high yield (93-100%). It is important to recognize that SET from any of the photocatalysts is highly disfavored with the most reducing photocatalyst holding a reduction potential more than 600 mV more positive than that of the aryl chloride. This implies that single electron reduction occurs from $\text{CO}_2^{\cdot-}$, the only reactive species in this experiment that is energetically capable of performing this reduction. It is important to note that although none of the photocatalyst screened in this experiment are reducing enough with respect to the aryl chloride, they are oxidizing enough with respect to the thiols present (Figure 2.6B). This feasible oxidation, implies single electron oxidation thiol to make the upconverted reductant. It is important to note that DMSO may contain trace amounts of thiol impurities²⁰⁻²² capable of promoting this reaction, as such mechanistic experiments were conducted with freshly distilled DMSO (solvents from old bottles were capable of promoting this reaction without added thiol cocatalyst).

Interestingly, this reaction was found to tolerate a wide variety of HAT catalysts. As shown in Figure 2.5, all thiol catalysts are efficient in this reaction system (entries 2-6) and the tertiary amine DABCO was also capable of facilitating reduction albeit at a diminished yield

Figure 2.4: Formate Catalyzed Reduction of an Aryl Chloride via Thiol Oxidation^a



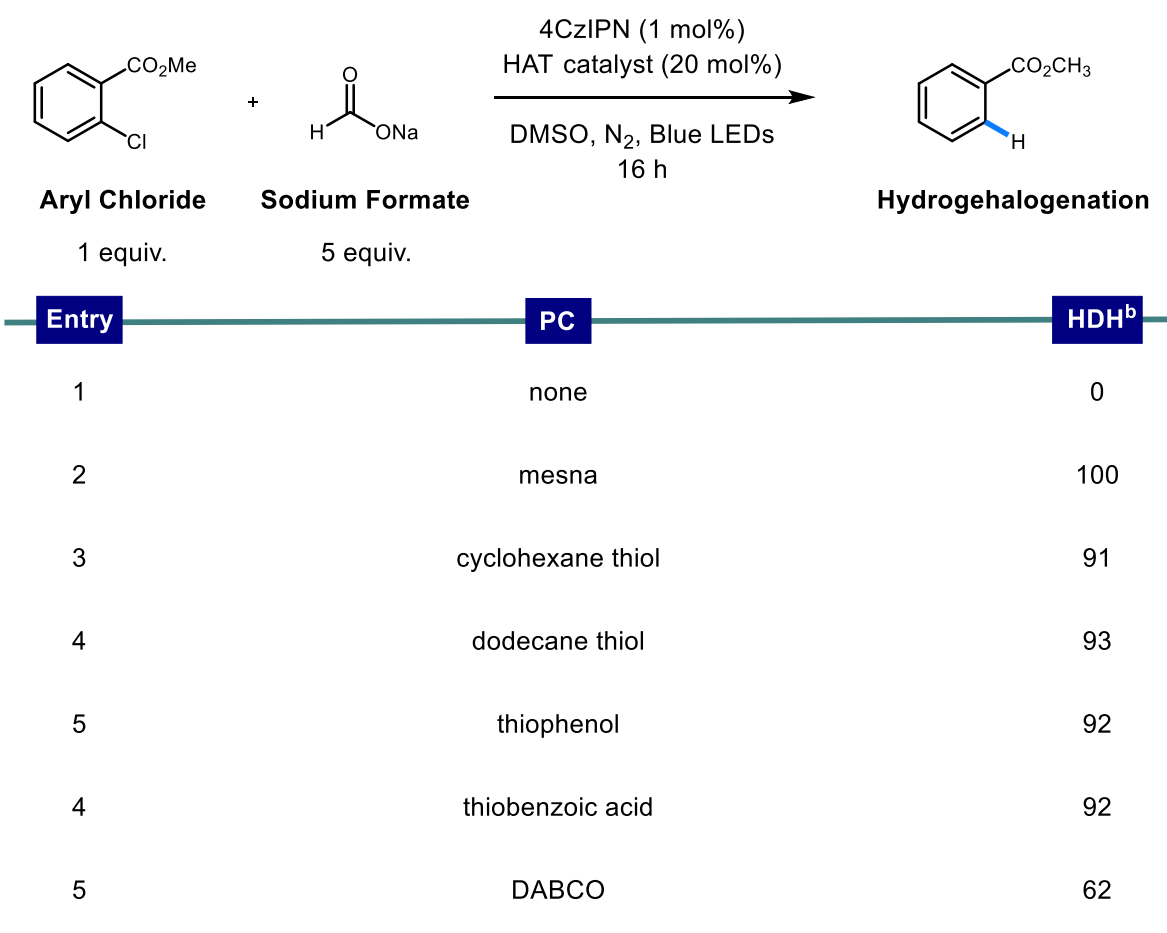
^a Conditions: aryl chloride (1 equiv.), sodium formate (5 equiv.), photocatalyst (PC, 1 mol%), Mesna (20 mol%), DMSO [0.1 M], N₂, Blue LEDs, 16 h. Reactions performed on a 0.1 mmol scale. ^bYield determined via ¹H NMR using CH₂Br₂ as an internal standard.



(entry 7). In the absence of any HAT catalyst, we found zero conversion to the HDH product indicating that formate oxidation to the oxygen centered electrophilic radical (although energetically feasible) is not a viable pathway in this system.

All together, this allows us to summarize are mechanistic data in support of $\text{CO}_2^{\cdot-}$ behaving as an unconverted reductant shown in **Figure 2.6A**. As clearly shown in the reduction potential series, all employed photocatalyst (despite their weak reducing power) are able to convert the aryl chloride to the HDH product via thiol oxidation to make the carbon dioxide

Figure 2.5: HAT catalyst Screen and Control^a

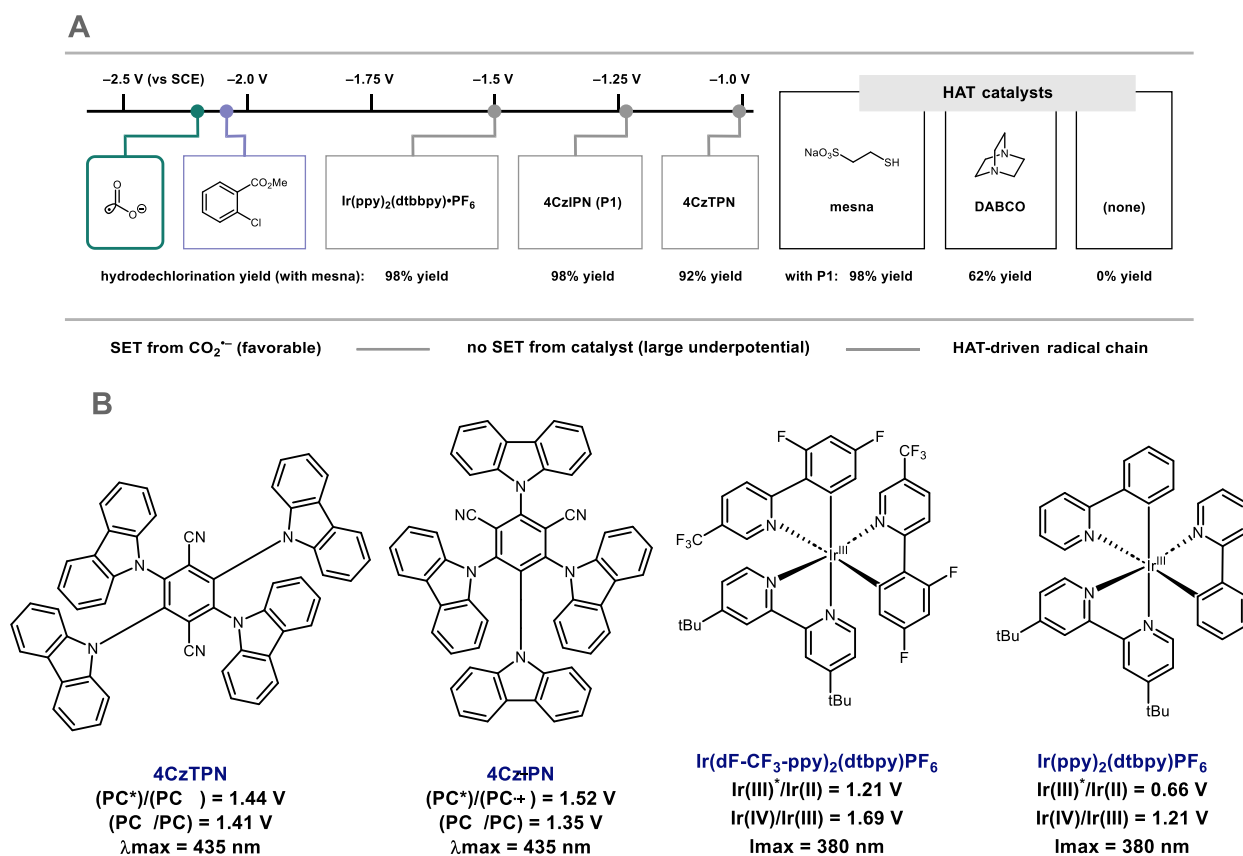


^a Conditions: aryl chloride (1 equiv.), sodium formate (5 equiv.), photocatalyst (PC, 1 mol%), HAT catalyst (20 mol%), DMSO [0.1 M], N_2 , Blue LEDs, 16 h. Reactions performed on a 0.1 mmol scale. ^bYield determined via ^1H NMR using CH_2Br_2 as an internal standard.

radical anion—the only reductant capable of this transformation due to the large underpotential from the catalyst. Various electrophilic HAT catalysts are operative in this system and the reaction does not proceed in their absence. Additional controls demonstrate that the reaction

does not proceed in the absence of blue light, photocatalyst, and formate. Furthermore, we conducted a series of photophysical experiments that demonstrate this reaction is an HAT driven radical chain (discussed further in Chapter 2.2.2).

Figure 2.6: A Summary of Mechanistic Evidence for $\text{CO}_2^{\bullet-}$ Generation



2.2.2: Investigations into Radical Chain Generation of $\text{CO}_2^{\bullet-}$

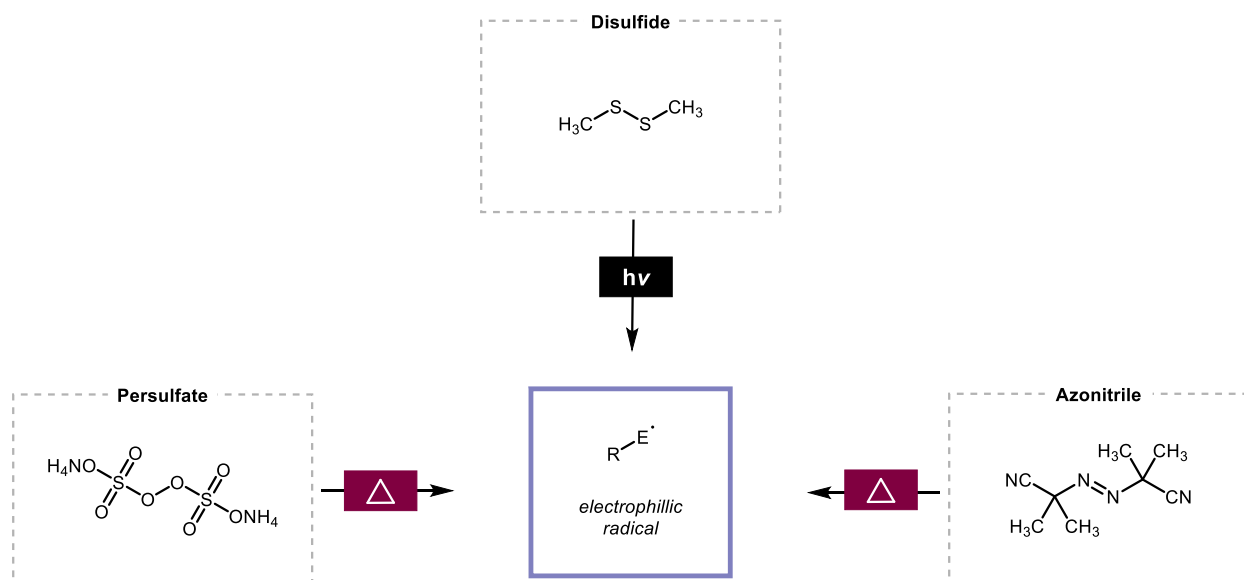
Given the fact that this reaction relies primarily on the shuttling of labile hydrogen atoms around, we hypothesized that it was likely that there may be chain characteristics to this reaction. Using the protocols established by the Yoon group for characterizing chain processes²³ in photoredox catalysis we were able to quantify the quantum yield (Φ) of the reaction under our

standard conditions to be 2.63. Quantum yield is defined as the number of product molecules that are formed per absorbed photon.²³ In other words, it is the ratio of the moles of product formed divided by the einsteins of light absorbed where einstein is the energy in one mole of photons. As such, any value greater than one indicates that a radical chain is occurring and is consistent with our findings.

Consistent with our hypotheses regarding thiol oxidation, we employed transient absorption spectroscopy²⁴ in collaboration with the Lian lab, and quantified the rate of thiyl formation under our standard conditions ($4.0 \times 10^{-3} \text{ M}^{-1}\text{s}^{-1}$) in addition to the quantum yield of the triplet excited state ($\Phi = 0.0072$) and the radical chain length greater than or equal to 365 (see *Supporting information*). Despite our strong mechanistic evidence indicating that $\text{CO}_2^{\bullet-}$ formation is occurring and is the active reductant, given the elusive nature of this intermediate we sought alternative ways of generation this reductant that may eliminate any ambiguity.

2.2.3: Generation of $\text{CO}_2^{\bullet-}$ with Alternative Initiators

Given our understanding that this reaction proceeds as an HAT driven chain reaction, product formation should not be dependent on a closed catalytic cycle. Rather it should be dependent on an initiation event as is consistent with other radical chain mechanisms. We hypothesized that if all that is needed is an electrophilic radical to get the show going, alternative means of initiation should also be operable. The most obvious of which would exploit the weak BDE of disulfides as disulfides absorb visible light and may undergo direct photolysis to generate two equivalence of thiyl radical (Figure 2.7).²⁵ Alternatively, thermal activation of a persulfate or AIBN would generate the corresponding electrophilic radicals also poised for HAT from formate. In order to test this hypothesis, we reexamined the hydrodehalogenation of 2-chloromethyl benzoate—this time in the absence of any photocatalyst.

Figure 2.7: The Formation of Electrophilic Radicals under Alternative Conditions**Figure 2.8:** Alternative Initiators Screen^a

Entry	Initiator	SM	HDH
1	20 mol% methyl disulfide, blue LEDs	0	99
2	20 mol% ammonium persulfate, 20 mol% mesna, 100°C	0	96
3	20 mol% AIBN, 20 mol% mesna, 100°C	50	48

^aConditions: Aryl chloride (1.0 eq.), sodium formate (5 eq.), initiator (20 mol%), DMSO [0.1M], N_2 , Blue LEDs or 100°C, 16 hrs, 0.1 mmol scale. ^bYield determined via 1H NMR using dibromomethane as an internal standard.

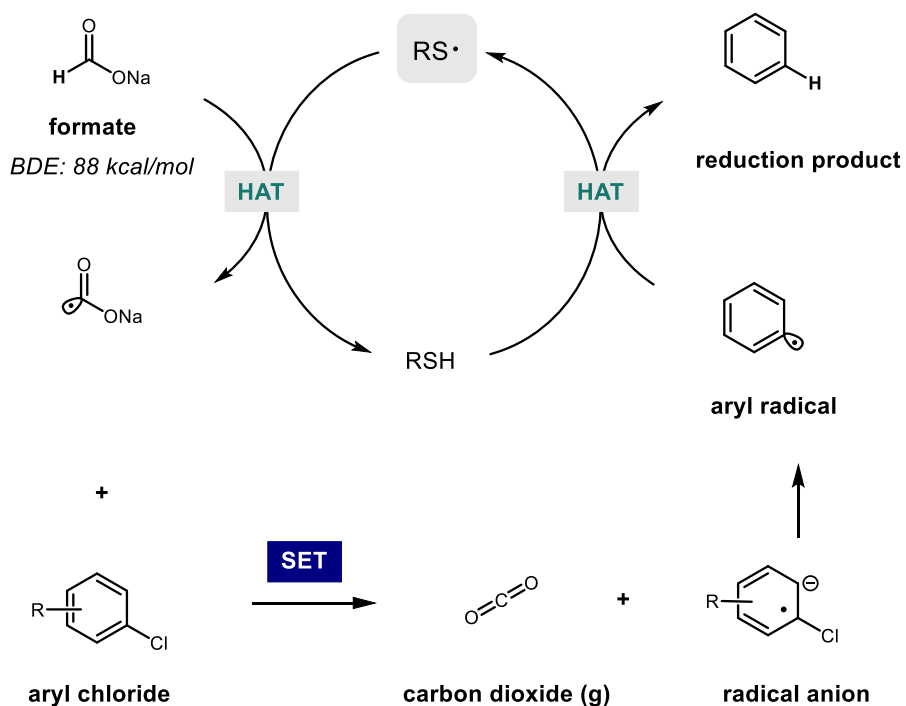
We found that when 4CzIPN was replaced with 20 mol% of an initiator and the corresponding initiation conditions, our hypotheses were confirmed. Using 2-chloromethyl benzoate, sodium formate, 20 mol% dimethyl disulfide, and blue light we were able to see

almost quantitative reduction to the corresponding HDH product (**Figure 2.8**, entry 1).

Furthermore, the use of ammonium persulfate or AIBN at 100°C in combination with 20 mol% Mesna we saw efficient conversion to the corresponding HDH product (entries 2-3). Given the absence of any photocatalyst, we were excited to show for the first time that $\text{CO}_2^{\cdot-}$ is in fact the active reductant in our system.

With our mechanistic data in hand including photophysical interrogations, photochemical generation of $\text{CO}_2^{\cdot-}$, and alternative initiators we were able to put together a proposed mechanistic scenario (Figure 2.9). Upon formation of thiyl radical, either via photocatalytic initiation or alternative initiation, HAT from sodium formate delivers the key reductant. Upon single electron reduction with an aryl chloride CO_2 is released alongside the radical anion of the aryl chloride. Upon mesolytic fragmentation, a chloride anion is expelled after which the corresponding aryl radical may abstract a hydrogen atom from thiol delivering the reduced product alongside another equivalent of thiyl radical thereby propagating the chain.

Figure 2.9: Proposed Mechanistic Scenario for Aryl Chloride Reduction



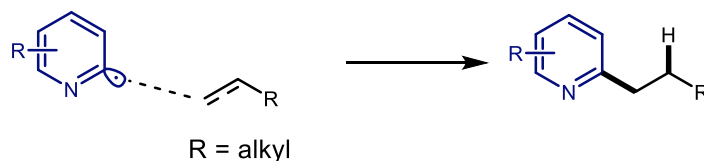
2.2.4: Reductive Process Enabled by $\text{CO}_2^{\bullet-}$

Given our previous work developing catalytic systems for the hydroarylation of olefins with (hetero)aryl radicals, we sought to expand upon that reactivity. Our previous conditions for hydroarylation involved the use of either a heteroaryl radical and an unactivated alkene, or an aryl radical and an activated alkene.⁹ The additional stabilization provided in the transition state of this transformation helps to promote intermolecular carbon-carbon bond formation over (hetero)aryl radical capping with a hydrogen atom. A more challenging transformation, however, is the intermolecular coupling between an *aryl* radical and an *unactivated* alkene—the stabilization present in our previous systems is not activated in this transformation (Figure 2.10).

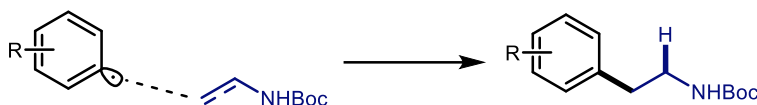
Figure 2.10: A Summary of Intermolecular Hydroarylation Protocols via (Hetero)aryl Radical

Giese Addition

Hydroarylation of Unactivated Alkenes with Heteroaryl Halides



Hydroarylation of Vinyl Amines with Aryl Halides

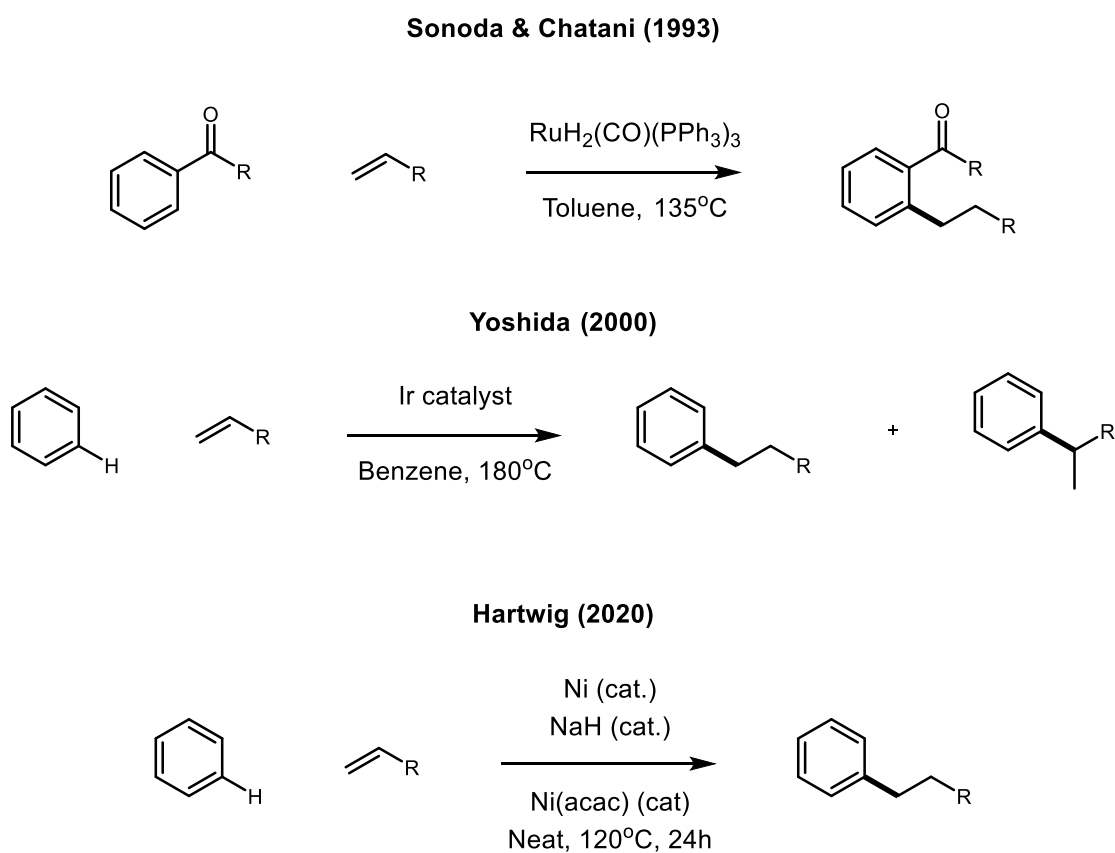


Hydroarylation of Unactivated Alkenes with Aryl Halides



Although the intermolecular hydroarylation of unactivated alkenes was known at the time, the conditions/requirements for this transformation were limiting. Sonoda and Chatani demonstrated the ruthenium catalyzed hydroarylation of alkenes although a directing group was required alongside harsh conditions (Figure 2.11).²⁶ Several years later the Yoshida group developed a protocol for coupling aryl rings with unactivated alkenes via iridium catalysis although poor selectivity between linear and branched products was required in addition to high temperatures.²⁷ More recently, the Hartwig group developed a similar protocol that minimized the formation of branched products but still relied on high temperature and harsh conditions.²⁸

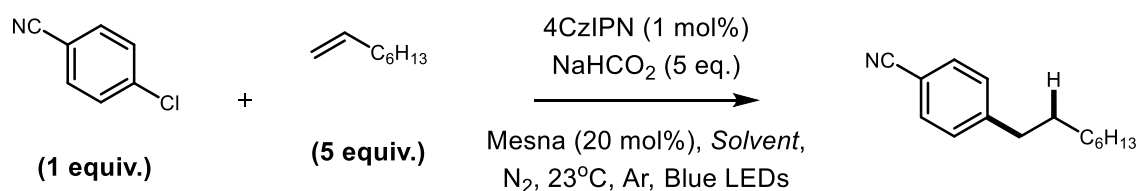
Figure 2.11: Modern Examples of Unactivated Alkene Hydroarylation with Unactivated Arenes



When using our optimized conditions for aryl halide reduction, we encountered an expected issue with most of the mass balance being made up of the HDH product (Figure 2.12,

entry 1). We have previously shown, that DMSO contains a significant amount of decomposition products that may serve as HAT donors thereby providing potentially stoichiometric amounts of HAT donors promoting HAT over intermolecular addition. Distilling DMSO over calcium hydride the same day reduces the amount of these impurities, however blue LEDs catalyze this decomposition as well making the difference in reactivity negligible (entry 2). As such, the net result is a negligible shift in product distribution. Interestingly, when DMF and DMA were employed as solvents in this protocol, similar reactivity to that of DMSO is observed.

Figure 2.12: Solvent Screen for Hydroarylation



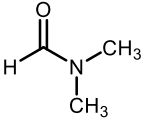
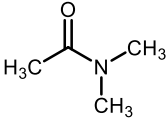
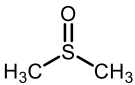
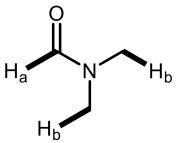
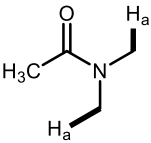
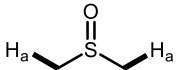
Entry	Solvent	SM	HDH	Product ^b
1	DMSO	0	60%	40%
2	DMSO ^c	0	50%	45%
3	DMF	0	48%	35%
4	DMA	0	50%	32%

^aConditions: Aryl chloride (1.0 eq.), alkene (5 eq.), sodium formate (5 eq.), initiator (20 mol%), Solvent [0.1M], N₂, Blue LEDs or 100°C, 16 hrs, 0.1 mmol scale. ^bYield determined via ¹H NMR using dibromomethane as an internal standard. ^cDMSO distilled the same day

Given the reactivity profile of DMSO, DMF, and DMA are all similar to one another, we decided to examine potential similarities between these solvents. We first considered the

polarity index—DMF, DMA, and DMSO are among the most polar solvents employed in organic chemistry (Figure 2.13).²⁹ Their high polarity may help solubilize the formate salt and help drive the necessary reductant into solution. Secondly, the dielectric constant of the solvent, essentially a value measuring a substances ability to store electrical energy, may also play a role here with all solvents containing high values although DMSO is the highest.²⁹ It is possible that changing the dielectric constant of a system may impact the ability to carry out redox manipulations thereby impacting the reaction. Finally, given the nature of this reaction and issues with aryl radical capping we naturally considered the BDEs of potentially labile sources of hydrogen atoms. Given the intermediacy of a high energy aryl radical, this reactive intermediate is likely able to abstract hydrogen atoms from the solvent³⁰ which has relatively low BDEs compared to the aryl radical (~ 110 kcal/mol).³¹

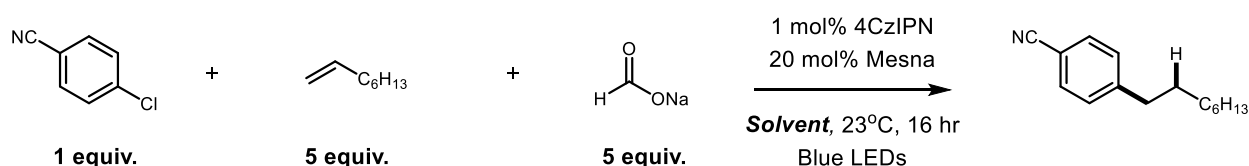
Figure 2.13: Potential Solvent Factors Impacting Reaction Efficiency

	 DMF	 DMA	 DMSO
Polarity Index:	6.4	6.5	7.2
Dielectric Constant:	36.7	37.8	46.7
Potentially labile C-H Bonds:			
BDE*:	^a 95.0; ^b 94.0	^a 92.5-94.1	^a 94.02

*BDE measured in kcal/mol.

Given the reaction proceeds only in DMSO, DMF, and DMA, we hypothesized that a cosolvent system may be useful in order to satiate but also slow down reactivity. Although 1:1 mixtures of hexanes and $\text{CH}_2\text{Cl}_2/\text{DMSO}$ did not enhance reactivity, we were excited to see that a 1:1 acetonitrile/DMSO mixture promoted product formation in 80% yield. Although acetonitrile's polarity index and dielectric constant (5.8 & 37.5) are comparable to DMSO/DMF/DMA, the C-H BDEs are quite higher (~98 kcal/mol).³² Although the difference is not substantial, perhaps the energy barrier is high enough that HAT from the aryl radical is reduced enough to promote intermolecular hydroarylation.

Figure 2.14: Cosolvent Screening for Hydroarylation



Entry	Solvent	Hydroarylation ^a
1	1:1 Hexanes/DMSO	10%
2	1:1 $\text{CH}_2\text{Cl}_2/\text{DMSO}$	40%
3	1:1 ACN/DMSO	80%

^aYields determined via ^1H NMR using dibromomethane as an internal standard; Reduction potentials reported vs SCE.

With our optimized conditions in hand, we first considered the coupling between 4-chlorobenzonitrile ($E_{p/2} = -2.1$ V vs SCE) with 1-octene to afford the alkylation product **1** in 66% yield via photocatalytic initiation conditions. Although slightly less efficient, we found that alternative initiation conditions also promoted the desired reactivity (disulfide: 50%, persulfate: 42% yield). Although we had reported a series of radical hydroarylation systems, these

conditions are unique in that they allow for the direct coupling of benzene-derived radicals with unactivated olefins. Furthermore, this methodology proceeds without the need for directing groups on either reaction component—a common limitation to aryl C-H activation strategies. Monosubstituted alkenes bearing alcohol and alkyl chloride functional groups reacted to give alkylated products **2** and **3** in 46 and 85% yield, respectively, where the remaining material was direct aryl chloride reduction. The more electron-rich olefins 2-methyl-2-butene and isopropenyl acetate also underwent smooth hydroarylation to **4** and **5**, 66% and 81% yield. Evaluation of the aryl radical scope with 1-octene revealed that a number of electron-poor aryl and heteroaryl chlorides can be engaged in this protocol with high functional group tolerance including sulfonamides, phosphonates, and esters (**6-14**, 32-80% yield). The ortho, meta, para effect is seen in entries 8-10 where the ortho substituent inclines the reaction towards HDH presumably due to a steric effect. Moreover, aryl radical coupling reactions employing bromobenzene, 4-chlorobenzonitrile, and 2-bromothiazole all smoothly engaged *tert*-butylvinyl carbamate (**3**

Table 2.1: Hydroarylation Substrate Scope^a

Hydroarylation Substrate Scope					
<p>alternative initiators</p> <p>MeS-SMe/blue LEDs: 50% yield^b</p> <p>(NH₄)₂S₂O₈/100°C: 42% yield^b</p>					
<p>1: 66% yield</p>	<p>2: 46% yield</p>	<p>3: 85% yield</p>	<p>4: 66% yield</p>	<p>5: 81% yield</p>	
<p>6: 51% yield^c</p>	<p>7: 37% yield^c</p>	<p>8: 69% yield</p>	<p>9: 75% yield</p>	<p>10: 75% yield</p>	<p>11: 80% yield^{c,d}</p>
<p>12: 70% yield</p>	<p>13: 43% yield</p>	<p>14: 59% yield</p>	<p>phenethylamines</p> <p>15: 74% yield^{c,e}</p> <p>16: 81% yield^e</p> <p>17: 98% yield^{c,e}</p>		

^aReaction conditions: substrate (1 equiv), olefin (5 equiv), P1 (1 mol %), mesna (20 mol %), sodium formate (5 equiv), MeCN/DMSO (1:1, v/v), blue light, 16 h. ^bYield determined by ¹H NMR with internals standard. ^cReaction conducted with aryl bromide. ^dReaction conducted at 100 °C. ^eDMSO used as solvent.

synthesis. Currently, this methodology is limited to substrates that contain electron-withdrawing groups in the *meta*-position—a drawback that stems from competitive nucleophilic demethylation processes alongside issues associated with trialkylammonium salt formation. Recently, Nicewicz demonstrated a consecutive photoinduced electron transfer process of acridinium salts that effectively cleaves arylsulfonamide N-S bonds.³⁴ Under our conditions, we found that the carbon dioxide radical anion is effective at achieving reduction where radical chain deprotection gave **21-23** in 52-84% yield. We have previously reported the use of highly reducing photocatalysts to carry out radical defluoroalkylation of trifluoromethylaromatics to give difluoroalkyl products and found our much simpler conditions can also accomplish this chemistry, albeit at reduced yield (**24-26**, 30-50% yield). Finally, we found that these conditions effectively reduce aliphatic aldehydes (**27-29**, 80-97% yield). Although the net transformation itself is not necessarily interesting, the intermediacy of the ketyl radical³⁵ is a valuable synthetic intermediate typically accessed via samarium diiodide (a compound known to be extremely unstable).

2.3 References

- (1) Birch, A. J. Reduction by Dissolving Metals. Part I. *J. Chem. Soc.* **1944**, No. 430, 430–436.
- (2) Hook, J. M.; Mander, L. N. Recent Developments in the Birch Reduction of Aromatic Compounds: Applications to the Synthesis of Natural Products. *Nat. Prod. Rep.* **1986**, *3*, 35–85.
- (3) Möhle, S.; Zirbes, M.; Rodrigo, E.; Gieshoff, T.; Wiebe, A.; Waldvogel, S. R. Modern Electrochemical Aspects for the Synthesis of Value-Added Organic Products. *Angew. Chem., Int. Ed.* **2018**, *57*, 6018–6041.

- (4) Peters, B. K.; Rodriguez, K. X.; Reisberg, S. H.; Beil, S. B.; Hickey, D. P.; Kawamata, Y.; Collins, M.; Starr, J.; Chen, L.; Udyavara, S.; et al. Scalable and Safe Synthetic Organic Electroreduction Inspired by Li-Ion Battery Chemistry. *Science*, **2019**, *363*, 838–845.
- (5) Nelleborg, P.; Lund, H.; Eriksen, J. Photochemical Vs. Electrochemical Electron Transfer Reactions. One-Electron Reduction of Aryl Halides by Photoexcited Anion Radicals. *Tetrahedron Lett.* **1985**, *26*, 1773–1776.
- (6) Prier, C. K.; Rankic, D. A.; MacMillan, D. W. C. Visible Light Photoredox Catalysis with Transition Metal Complexes: Applications in Organic Synthesis. *Chem. Rev.* **2013**, *113*, 5322–5363.
- (7) Romero, N. A.; Nicewicz, D. A. Organic Photoredox Catalysis. *Chem. Rev.* **2016**, *116*, 10075–10166.
- (8) Arias-Rotondo, D. M.; McCusker, J. K. The Photophysics of Photoredox Catalysis: A Roadmap for Catalyst Design. *Chem. Soc. Rev.* **2016**, *45*, 5803–5820.
- (9) a. Wang, H., & Jui, N. T. Catalytic Defluoroalkylation of Trifluoromethylaromatics with Unactivated Alkenes. *J. Am. Chem. Soc.*, **2018**, *140*, 163–166.
- b. Vogt, D. B., Seath, C. P., Wang, H., & Jui, N. T. Selective C-F Functionalization of Unactivated Trifluoromethylarenes. *J. Am. Chem. Soc.*, **2019**, *141*, 13203–13211.
- c. Boyington, A. J., Riu, M. L. Y., & Jui, N. T. Anti-Markovnikov Hydroarylation of Unactivated Olefins via Pyridyl Radical Intermediates. *J. Am. Chem. Soc.*, **2017**, *139*, 6582–6585.
- (10) Stevens, G. B.; Reda, T.; Raguse, B. Energy Storage by the Electrochemical Reduction of CO₂ to CO at a Porous Au Film. *J. Electroanal. Chem.* **2002**, *526*, 125–133.

- (11) Franco, F.; Rettenmaier, C.; Jeon, H. S.; Cuenya, B. R. Transition Metal-Based Catalysts for the Electrochemical CO₂ reduction: From Atoms and Molecules to Nanostructured Materials. *Chem. Soc. Rev.* **2020**, *49*, 6884–6946.
- (12) Koppenol, W. H.; Rush, J. D. Reduction Potential Of the Carbon Dioxide/Carbon Dioxide Radical Anion: A Comparison with Other C1 Radicals. *J. Phys. Chem.* **1987**, *91*, 4429–4430.
- (13) Morgenstern, D. A.; Wittrig, R. E.; Fanwick, P. E.; Kubiak, C. P. Photoreduction of Carbon Dioxide to Its Radical Anion by [Ni₃(μ₃-I)₂(dppm)₃]: Formation of Two Carbon-Carbon Bonds via Addition of CO₂ •⁻ to Cyclohexene. *J. Am. Chem. Soc.* **1993**, *115*, 6470–6471.
- (14) Otero, M. D.; Batanero, B.; Barba, F. CO₂ Anion-Radical in Organic Carboxylations. *Tetrahedron Lett.* **2006**, *47*, 2171–2173.
- (15) (a) Seo, H.; Katcher, M. H.; Jamison, T. F. Photoredox Activation of Carbon Dioxide for Amino Acid Synthesis in Continuous Flow. *Nat. Chem.* **2017**, *9*, 453–456.
- (b) Seo, H.; Liu, A.; Jamison, T. F. Direct β-Selected Hydrocarboxylation of Styrenes with CO₂ Enabled by Continuous Flow Photoredox Catalysis. *J. Am. Chem. Soc.* **2017**, *139*, 13969–13972.
- (c) Kang, G.; Romo, D. Photocatalyzed, β-Selective Hydrocarboxylation of α,β-Unsaturated Esters with CO₂ Under flow for β-Lactone Synthesis. *ACS Catal.* **2021**, *11*, 1309–1315.
- (16) Roth, H. G., Romero, N. A., & Nicewicz, D. A. Experimental and Calculated Electrochemical Potentials of Common Organic Molecules for Applications to Single-Electron Redox Chemistry. *Synlett*, **2016**, *27*, 714–723.
- (17) Hager, D., & Macmillan, D. W. C. Activation of C-H bonds via the merger of photoredox and organocatalysis: A coupling of benzylic ethers with schiff bases. *J. Am. Chem. Soc.*, **2014**, *136*, 16986–16989.

- (18) Dénès, F., Pichowicz, M., Povie, G., & Renaud, P. Thiyl radicals in organic synthesis. In *Chem. Rev.*, **2014**, *114*, 2587–2693.
- (19) Enemærke, R. J.; Christensen, T. B.; Jensen, H.; Daasbjerg, K. Application of a New Kinetic Method in the Investigation of Cleavage Reactions of Haloaromatic Radical Anions. *J. Chem. Soc., Perkin Trans.*, **2001**, *2*, 1620–1630.
- (20) Garusinghe, G. S. P.; Bessey, S. M.; Boyd, C.; Aghamoosa, M.; Frederick, B. G.; Bruce, M. R. M.; Bruce, A. E. Identification of Dimethyl Sulfide in Dimethyl Sulfoxide and Implications for MetalThiolate Disulfide Exchange Reactions. *RSC Adv.* **2015**, *5*, 40603–40606.
- (21) Wang, Z.; Liu, J.; Dai, Y.; Dong, W.; Zhang, S.; Chen, J. Dimethyl Sulfide Photocatalytic Degradation in a Light-Emitting Diode Continuous Reactor: Kinetic and Mechanistic Study. *Ind. Eng. Chem. Res.* **2011**, *50*, 7977–7984.
- (22) Deguchi, Y.; Kono, M.; Koizumi, Y.; Izato, Y. I.; Miyake, A. Study on Autocatalytic Decomposition of Dimethyl Sulfoxide (DMSO). *Org. Process Res. Dev.* **2020**, *24*, 1614–1620.
- (23) Cismesia, M. A., & Yoon, T. P. Characterizing chain processes in visible light photoredox catalysis. *Chem. Sci.*, **2015**, *6*, 5426–5434.
- (24) Berera, R., van Grondelle, R., & Kennis, J. T. M. Ultrafast transient absorption spectroscopy: Principles and application to photosynthetic systems. *Photosynth., Res.*, **2009**, *101*, 105–118.
- (25) a. Kilgore, H. R., & Raines, R. T. Disulfide Chromophores Arise from Stereoelectronic Effects. *J. Phys. Chem. B.*, **2020**, *124*, 3931–3935.
- b. Yang, Y. M., Yu, H. Z., Sun, X. H., & Dang, Z. M. Density functional theory calculations on S–S bond dissociation energies of disulfides. *J. Phys. Org. Chem.*, **2016**, *29*, 6–13.

- (26) Murai, S., Kakiuchi, F., Sekine, S., Tanaka, Y., Kamatani, A., Sonoda, M., & Chatani, N. Efficient catalytic addition of aromatic carbon-hydrogen bonds to olefins. *Nature*, **1993**, *366*, 529-531.
- (27) Matsumoto, T., Taube, D. J., Periana, R. A., Taube, H., & Yoshida, H. Anti-Markovnikov olefin arylation catalyzed by an iridium complex. *J. Am. Chem. Soc.*, **2000**, *122*, 7414–7415.
- (28) Saper, N. I., Ohgi, A., Small, D. W., Semba, K., Nakao, Y., & Hartwig, J. F. Nickel-catalysed anti-Markovnikov hydroarylation of unactivated alkenes with unactivated arenes facilitated by non-covalent interactions. *Nat. Chem.*, **2020**, *12*, 276–283.
- (29) Reichardt, C.. Empirical Parameters of the Polarity of Solvents. *Angew. Chem. Int. Ed.*, **1965**, *4*, 29–40.
- (30) a. Salamone, M., Milan, M., Dilabio, G. A., & Bietti, M. Reactions of the cumyloxyl and benzyloxyl radicals with tertiary amides. hydrogen abstraction selectivity and the role of specific substrate-radical hydrogen bonding. *J. Org. Chem.*, **2013**, *78*, 5909–5917.
- b. Salamone, M., Dilabio, G. A., & Bietti, M. Reactions of the cumyloxyl and benzyloxyl radicals with strong hydrogen bond acceptors. Large enhancements in hydrogen abstraction reactivity determined by substrate/radical hydrogen bonding. *J. Org. Chem.*, **2013**, *77*, 10479–10487.
- (31) Davico, G. E., Bierbaum, V. M., Depuy, C. H., Ellison, G. B., & Squires, R. R. The C-H Bond Energy of Benzene. *J. Am. Chem. Soc.*, **1995**, *117*, 2590-2599.
- (32) Gribov, L., Novakov, I., Pavlyuchko, I., Korolkov, V. v, & Orlinson, B. S. Spectroscopic Calculation of CH Bond Dissociation Energies for Aliphatic Nitriles. *J. Struct. Chem.*, **2004**, *45*, 771-777.

- (33) Blakey, S. B. B.; MacMillan, D. W. C. The First Suzuki CrossCouplings of Aryltrimethylammonium Salts. *J. Am. Chem. Soc.* **2003**, *125*, 6046–6047.
- (34) MacKenzie, I. A.; Wang, L.; Onuska, N. P. R.; Williams, O. F.; Begam, K.; Moran, A. M.; Dunietz, B. D.; Nicewicz, D. A. Discovery and Characterization of an Acridine Radical Photoreductant. *Nature*, **2020**, *580*, 76–80.
- (35) Szostak, M., Fazakerley, N. J., Parmar, D., & Procter, D. J. Cross-coupling reactions using samarium(II) iodide. *Chem. Rev.*, **2014**, *114*, 5959–6039.

Chapter 3: Hydrocarboxylation of Electron-Deficient Alkenes via the Carbon Dioxide Radical Anion (CO₂^{•-})

Adapted and reprinted in part with permission from Hendy, C. M.; Smith, G.; Xu, Z.; Lian, T.;

Jui, N. *J. Am. Chem. Soc.*, **2021**, *143*, 8987-8992.

Copyright 2021 American Chemical Society

<https://pubs.acs.org/doi/10.1021/jacs.1c04427>

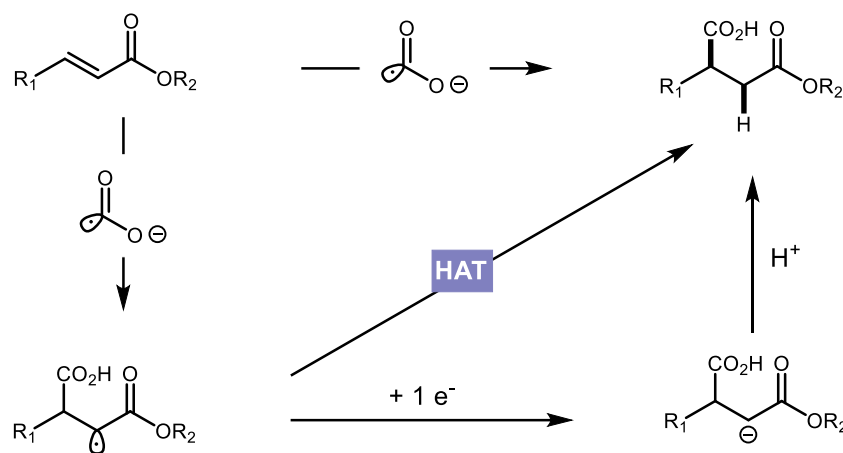
C. M. Hendy contributed to both carboxylation and reduction scope.

Abstract: After demonstrating the reducing capability as the carbon dioxide radical anion ($\text{CO}_2^{\bullet-}$) as a potent single electron reductant, we found that its interaction with electron-deficient alkenes was unique. Instead of undergoing single electron reduction with electron-deficient alkenes, specifically α, β -unsaturated carbonyls, we instead observed radical conjugate addition across the double bond to furnish synthetically valuable 1,4-dicarbonyls. Interestingly, substrate reduction potential could be used to predict reaction outcomes where α, β -unsaturated carbonyls within the reducing potential of $\text{CO}_2^{\bullet-}$ underwent single electron reduction while those outside of the window underwent Giese-type addition. Furthermore, when attempting to access other acyl radicals from formyl C-H bonds we found a direct correlation between the bond dissociation energy of the formyl group and reaction outcome.

3.1: Discovery and Optimization of the $\text{CO}_2^{\cdot-}$ as a Nucleophilic Source of CO_2

When expanding the reaction scope of the carbon dioxide radical anion, we came across a unique byproduct when electron-deficient alkenes—specifically Michael acceptors—were employed in the reaction conditions. Instead of single electron reduction, we instead noticed CO_2 incorporation across the double bond in a Giese type conjugate addition (**Figure 3.1**).¹

Figure 3.1: Potential Reaction Mechanism for CO_2 Incorporation via $\text{CO}_2^{\cdot-}$

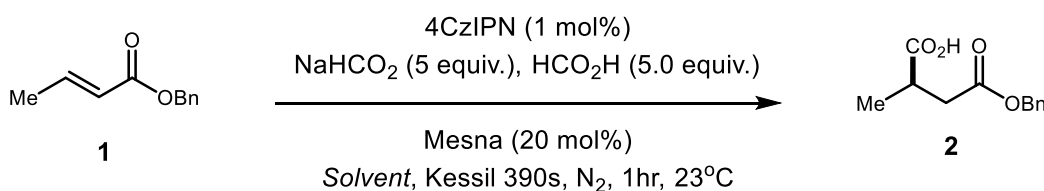


We hypothesized this reaction mechanism could be occurring in two ways. Upon conjugate addition of the carbon dioxide radical anion across the alkene, the resulting alkyl radical could directly pick up a hydrogen atom to furnish the hydrocarboxylated product. Alternatively, following conjugate addition the formed alkyl radical may undergo radical polar crossover² to form the resulting anion after which protonation would deliver the hydrocarboxylated product. Intrigued by this reactivity, we decided to optimize this reaction and investigate the scope of this methodology.

Using alpha, beta-unsaturated ester **1** we optimized the reaction system to form hydrocarboxylated product **2** (**Figure 3.2**). While most formate salts were operative under this

system, we opted to use sodium formate as it is the most affordable of the formate salts. Using the odorless and solid thiol Mesna, we next evaluated the solvents used. Using 1 mol% of commercially available 4CzIPN, 20 mol% Mesna, sodium formate (5.0 equiv.), formic acid (5.0 equiv.), in DMSO [0.1M] under irradiation with blue lights afford **2** in 31% yield. Interestingly, increasing water concentration for the solvent system saw a substantial increase in product formation (entries 2-4) ranging from 47-95% yield with 20% H₂O/DMSO as the optimal solvent. This is likely a result of increasing solvent polarity to help solubilize formate.

Figure 3.2: Optimization/Controls for Hydrocarboxylation of Michael Acceptors



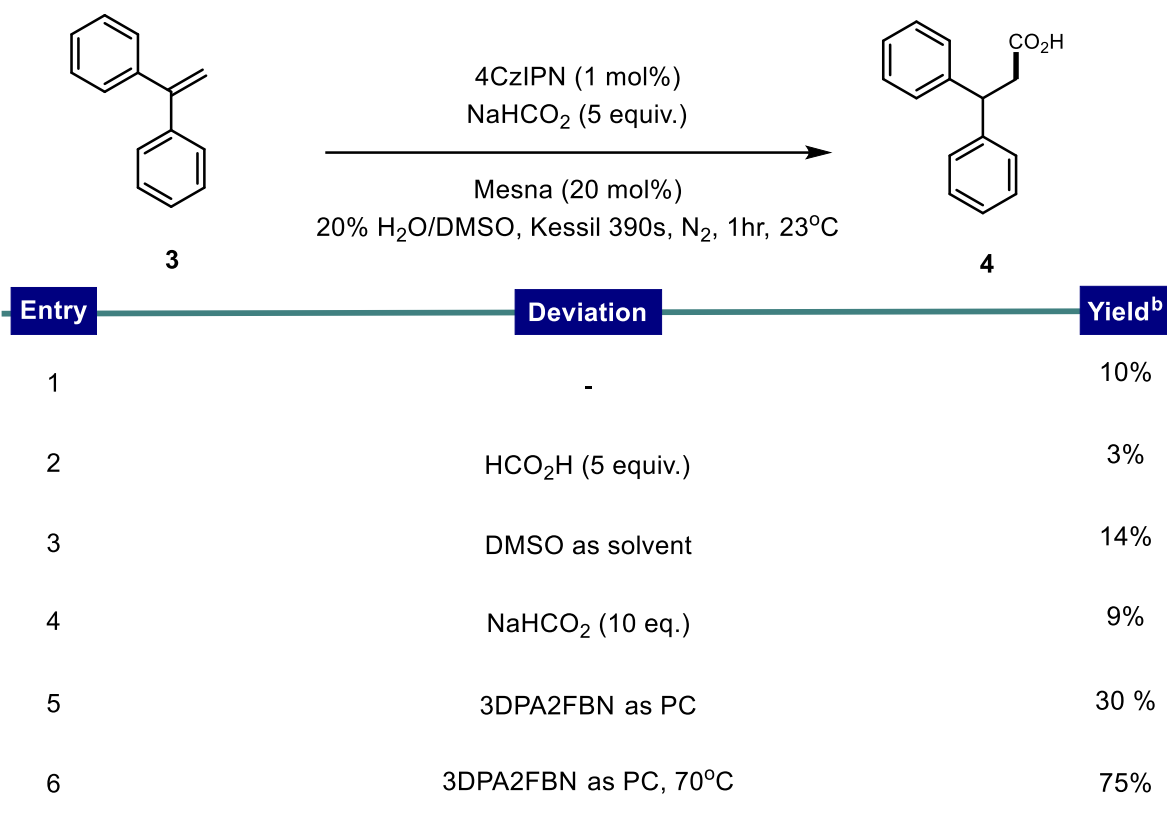
Entry	Solvent	Deviation	Yield ^b
1	DMSO	-	31%
2	10% H ₂ O/DMSO	-	47%
3	20% H ₂ O/DMSO	-	95%
4	50% H ₂ O/DMSO	-	73%
5	20% H ₂ O/DMSO	no mesna	15%
6	20% H ₂ O/DMSO	no HCO ₂ H	77%
7	20% H ₂ O/DMSO	no light	0%

^aConditions: **1** (1.0 equiv.), 4CzIPN (1 mol%), sodium formate (5.0 equiv.), formic acid (5.0 equiv.), mesna (20 mol%), Solvent [0.1M], 390 nm light, N₂, 1hr, 0.1 mmol scale. ^bYield determined via ¹H NMR with dibromomethane as an internal standard. ^cReaction ran for 16 hrs.

Furthermore, in the absence of Mesna the reaction proceeded in 15% yield, presumably a result of decomposed DMSO discussed in chapter 2. In the absence of formic acid, the reaction yield was slightly diminished (entry 6, 77%) and the absence of light so no product formation at all (entry 7, 0% yield).

Although this reaction system was proficient on Michael acceptors, we found that expanding the scope outside of electron-deficient alkenes was rather challenging. We first considered styrenes as an activated alkene using 1,1-diphenylethylene (**3**). Under our standard

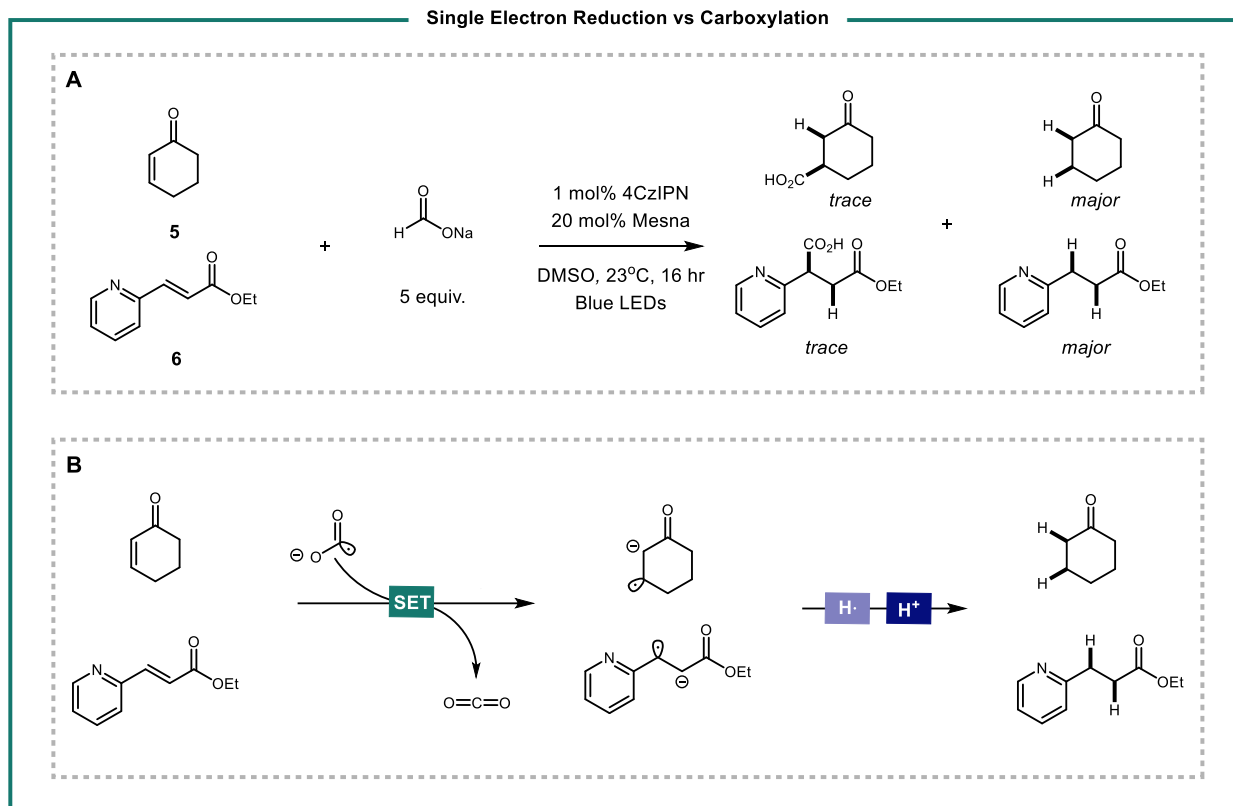
Figure 3.3: Optimization of Carboxylation for 1,1-Diphenylethylene



^aConditions: **1** (1.0 equiv.), 4CzIPN (1 mol%), sodium formate (5.0 equiv.), mesna (20 mol%), Solvent [0.1M], 390 nm light, N₂, 1hr, 0.1 mmol scale. ^bYield determined via ¹H NMR with dibromomethane as an internal standard. ^cReaction ran for 16 hrs.

conditions we observed small conversion to the carboxylated product (entry 1, 10% yield). Adding formic acid to formic a buffered system, changing the solvent to DMSO, and increasing formate equivalence were all ineffective at increasing product yield (entries 2-4, 3-15% yield). Given the relatively low reduction potential of **3** ($E_{1/2} = +1.54$ V vs SCE)³, we hypothesized that substrate oxidation by the photocatalyst may be inhibiting the reaction. Consistent with this hypothesis, switching out the photocatalyst for the substantially less oxidizing photocatalyst 3DPA2FBN ($E_{1/2} = +0.92$ V vs SCE)⁴ increased the yield substantially (entry 5, 30% yield). We further hypothesized that the resulting radical formed via conjugate addition would be tertiary, doubly benzylic, and sterically encumbered. In other words, it is stabilized and persistent, and therefore likely reversible.⁵ To drive this reaction forward, the addition of heat (70°C) increased the reaction yield substantially (entry 6, 75% yield). Despite extensive screening of different styrenes, we were unable to replicate this reactivity with polymerization or a return of starting material making up most of the reactivity. Although styrenes were not productive coupling partners in this transformation, we decided to examine the scope of electron-deficient alkenes.

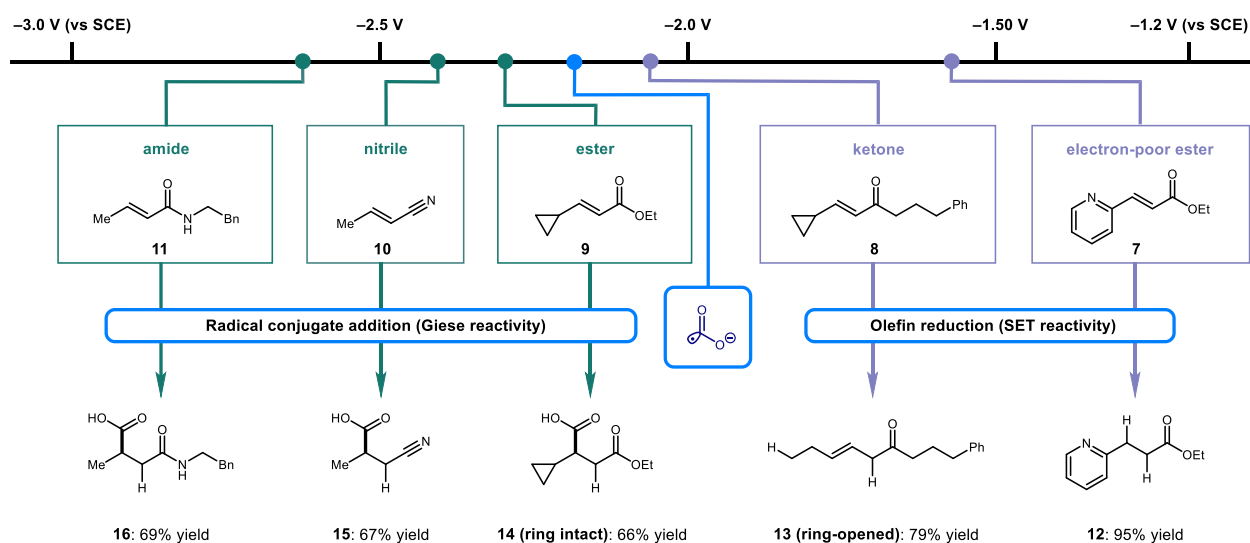
When coupling in electron-deficient alkenes (**5** and **6**) with similar electronics to ester **1**, we instead saw divergent reactivity where most of the mass balance consisted of reduced/hydrogenated forms of the alkenes with only trace amounts of carboxylation observed (**Figure 3.4A**). We hypothesized that this reactivity was likely occurring from single electron reduction of the olefin by the carbon dioxide radical anion instead of carboxylation.⁶ SET to these α,β -unsaturated systems should deliver the alkyl radical and alpha anion (enolate) after which subsequent HAT and protonation would deliver the “hydrogenated” product (**Figure 3.4B**).

Figure 3.4: Investigations into Michael Acceptor Single Electron Reduction

Intrigued by this divergent reactivity, we sought to quantify the reduction potentials of a series of α,β -unsaturated systems to identify any potential correlation between substrate reduction potential and reaction outcome. After calculating the reduction potentials of a series of Michael acceptors we saw an interesting split where electron-poor ester (**7**) and ketone (**8**) were within the reduction potential of the carbon dioxide radical anion while ester (**9**), nitrile (**10**), and amide (**11**), were outside the reduction potential. This split in reduction potential was directly correlated to the observed reactivity where olefins within the reduction potential underwent SET while those outside the reduction potential underwent Giese type addition. Efficient transformation of pyridyl cinnamate ester (**7**) to the hydrogenated product (**12**) in 95% yield was observed. To interrogate the radical nature of this system, we prepared β -cyclopropyl enone **8**

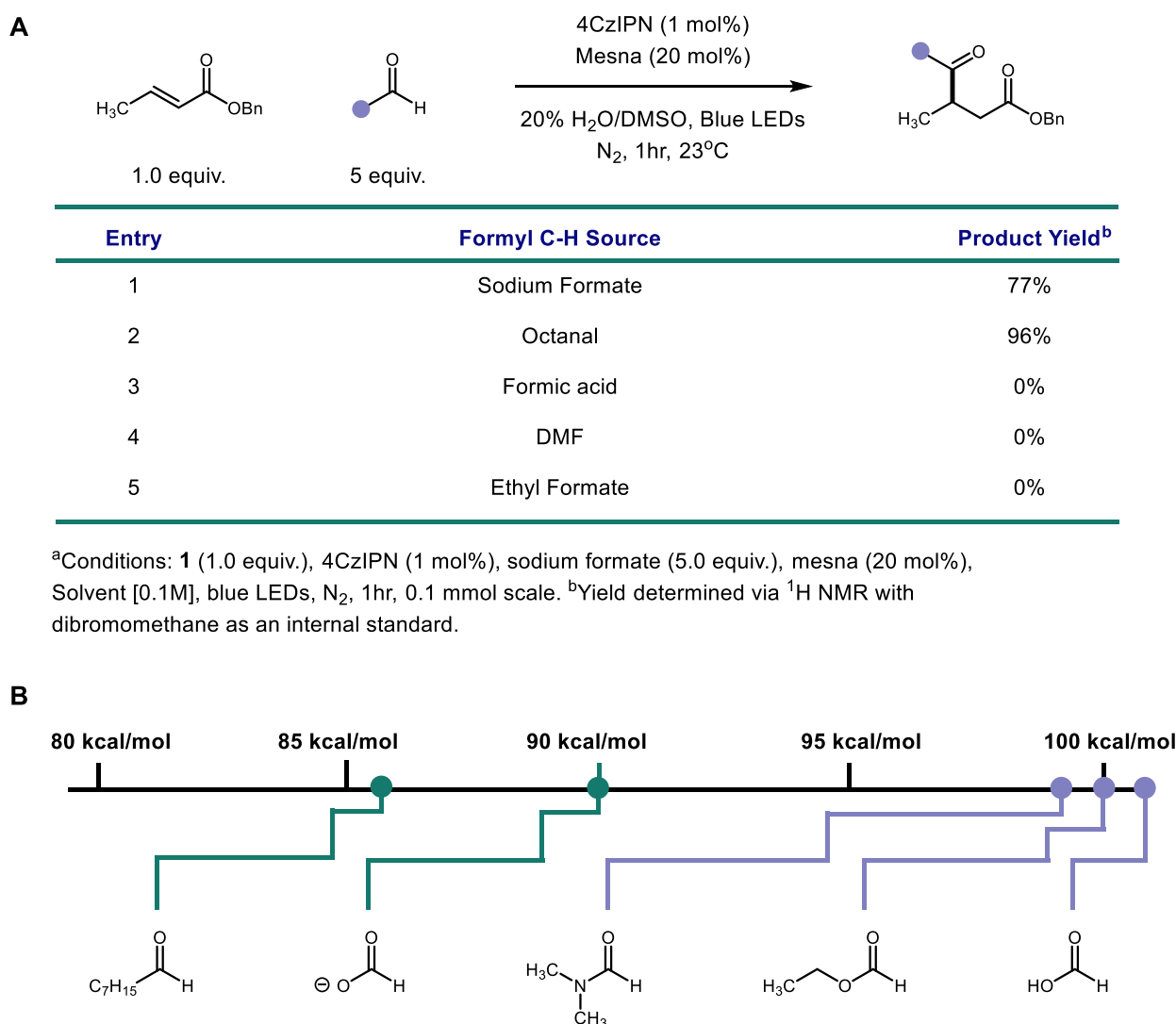
and subjected it to our standard conditions. The net transformation observed was cyclopropyl ring opening to the internal alkene **13** (79% yield)—an event consistent with SET as described in **Figure 3.4B**.⁷ With the analogous ester, we instead observed carboxylation to afford the corresponding 1,4-dicarboxyl **14** (66% yield) where cyclopropyl ring opening was not observed. These data indicate that olefin reduction potential and reaction outcome are correlated, where more electron-poor olefins ($E_{1/2}^{\circ} \geq -2.1$ V vs SCE) undergo SET and less electron-poor olefins ($E_{1/2}^{\circ} \leq -2.1$ V vs SCE) undergo radical hydrocarboxylation. Consistent with this observation, nitriles and amides (**10** & **11**) also underwent CO₂ incorporation to afford the corresponding hydrocarboxylation products **15** (67% yield) and **16** (69% yield). Although carbon dioxide is a common electrophilic coupling partner, we here demonstrate the nucleophilic behavior of its radical anion aiding in the construction of 1,4-dicarbonyls which have important implications in the synthesis of heterocycles⁸⁻¹⁰ and bioactive small molecules.¹¹

Figure 3.5: Reduction Potential Series Demonstrating the Split Reactivity for Michael Acceptors



Given the utility in generating nucleophilic acyl radicals for carbon-carbon bond formation, we sought to extend this reactivity to other systems which revealed yet another interesting trend. As expected, carboxylation with sodium formate proceeded in 77% yield (entry 1) while aliphatic aldehyde octanal also went addition in near quantitative yield (entry 2, 96% yield). However protonating formate to formic acid resulted in a complete return of starting material (entry 3, 0% yield). Similarly, DMF and ethyl formate were also unreactive (entry 4 & 5, 0% yield).

Figure 3.6: Evaluation of Olefin Conjugate Addition with Different Formyl C-H Sources^a

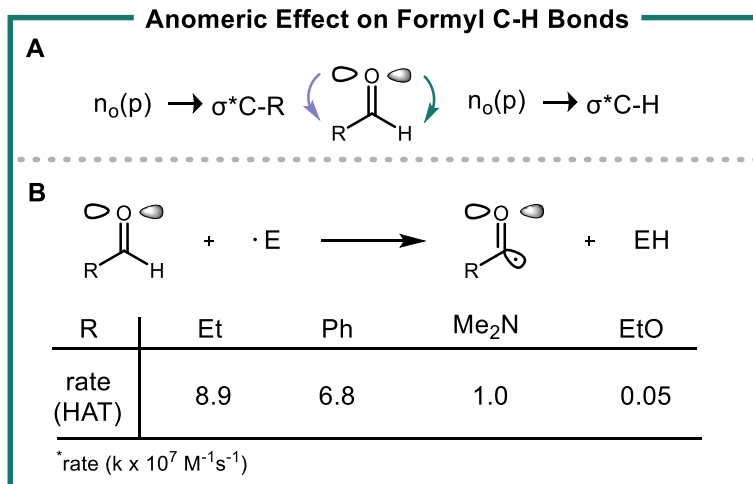


To further probe the change in reactivity in this system, we employed computational chemistry to calculate the BDE of the (formyl) C-H bonds for entries 1-5 and found a clean split in reactivity. While the formyl C-H bonds of sodium formate and octanal were found to be less than or equal to 90 kcal/mol, the BDE of formic acid, DMF, and ethyl formate were found to be between 98-101 kcal/mol. This substantial increase in BDE is likely to high in energy for a thiyl radical to abstract from and are therefore inert. The most likely explanation for this phenomenon is driven by an “anomeric effect”.

Although the anomeric effect has historically been used to describe the preference of certain functional groups to rest in the axial conformation at the anomeric position of sugars, it also has implications in other systems. In carbonyl species, the p-orbital lone pairs of the oxygen have hyperconjugative interactions on adjacent atoms, namely the σ^* C-R bonds directly adjacent to it. As shown in **Figure 3.7A**, there are two competing interactions—one guided by hyperconjugative donation from the oxygen lone pairs ($n_o(p)$) into the σ^* C-R orbital and the other into the σ^* C-H orbital.¹² When the “acceptor” capacity σ^* C-R orbital is high, a high degree of the p-orbital donation goes into this orbital and its effect on the σ^* C-H orbital is weakened therefore providing a stabilizing effect and the opposite is true when R acceptor capacity is low. This phenomenon is exemplified in **Figure 3.7B**, for aldehydes where the R acceptor capacity is low, the rate of HAT from the formyl C-H bond is fast and its BDE is low. However, when R is replaced with a heteroatom as is the case with DMF and ethyl formate, the rate of HAT decreases substantially, also consistent with our BDE calculations. When R is a heteroatom, the σ^* C-R orbital is more polarized and therefore capable of accepting electron density. This in turn pulls electron density away from the σ^* C-H orbital making it less inclined to participate in C-H activation. Although slightly more complicated, the same rationale for the

difference in BDE between formate and formic acid may also be used here. In the case of formate given its equivalent resonant structures, it is possible that it exhibits a “double” anomeric effect that is not present in formic acid thereby making its C-H bond labile.

Figure 3.7: Graphic Representation of the Anomeric Effect in Formyl C-H Systems

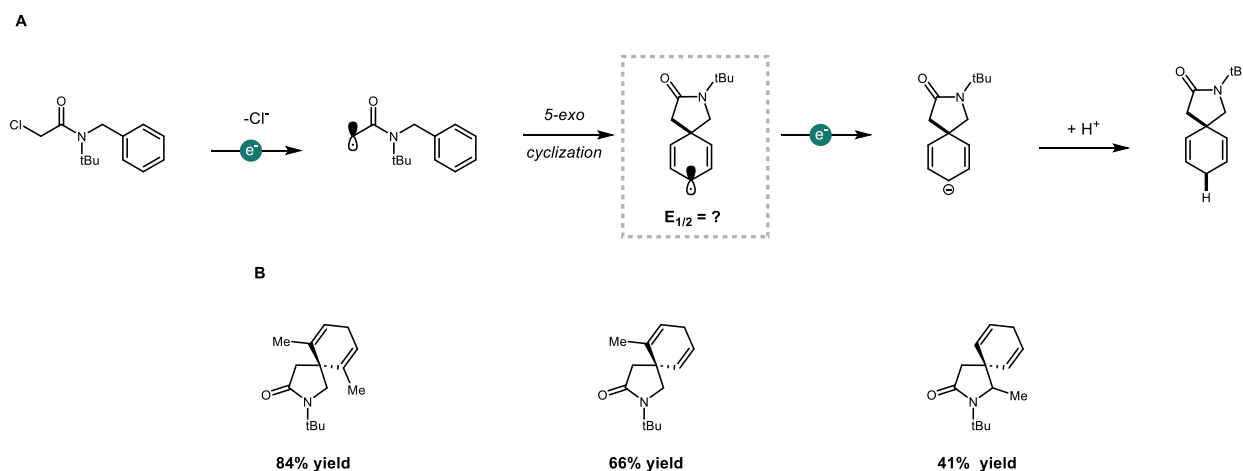


3.2: Mechanistic Questions Regarding Spirocyclic Dearomatization

In our efforts to elucidate the mechanistic details regarding our protocol for the synthesis of spirocyclic lactams via a dearomatization strategy we employed computational chemistry. Using DFT calculations we elucidate key features of this mechanism, first regarding the redox potential of a reactive intermediate that was shown to be consistent with the proposed redox states of the photocatalytic cycle. Furthermore, we optimized the geometry of multiple substrates to examine the structural minima. Upon close investigation, it was revealed the compounds bearing an ortho substituent were primed for intramolecular cyclization as the ortho substituted positioned the ring under the forming radical thereby minimizing the interatomic distance between the forming bonds.

After optimization and evaluation of the substrate scope, two key mechanistic features remained ambiguous in this transformation. Upon initial single electron reduction of the α -chloroacetamide, the forming radical may then undergo cyclization to form the corresponding dienyl radical.¹³ In order to match up the redox potentials of this catalytic system, the redox potential of this intermediate must be quantified (Scheme 5.1A). Furthermore, we noticed an interesting trend in our substrate scope where substrates bearing ortho substituents were particularly efficient at undergoing cyclization as opposed to hydrodehalogenation (Scheme 5.1B).

Scheme 3.1: Mechanistic Questions Regarding Spirocyclic Dearomatization

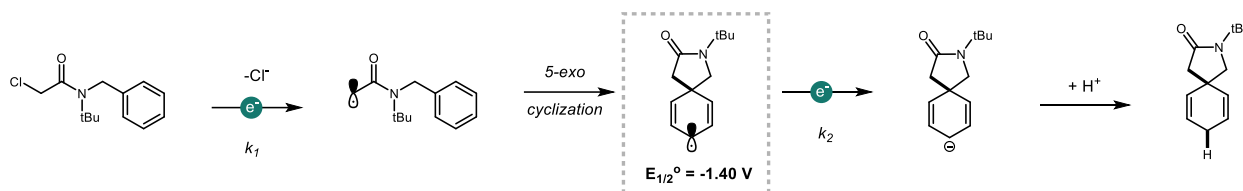


3.2.1: Computational Investigations

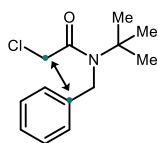
Using standard DFT techniques (see *Supporting Information*), we identified the reduction potential of the dienyl radical ($E_{1/2}^{\circ} = -1.40$ V vs SCE) which may then undergo radical polar crossover to the resultant dienyl anion (Scheme 5.2). Importantly, the rate of SET to the starting material (k_1) must be slower than the rate of radical polar crossover (k_2) as this would correspond

with good reaction efficiency. However, if k_2 is slower than k_1 then the build up of dienyl radical is observed and can lead to dimerization (via radical-radical coupling) instead of hydrogen incorporation.

Scheme 3.2: Reaction Mechanism for Intramolecular Dearomatization



When examining the substrate scope, there appeared to be a direct correlation when the pendant aromatic ring of the starting material was ortho-substituted. In order to examine this further, we carried out geometry optimizations of the starting materials and examined the resulting lowest energy confirmations. Upon first glance, it appeared that the compounds that were ortho substituted oriented themselves directly underneath the forming radical, presumably due to a steric effect¹⁴—this conformation would favor cyclization over hydrodehalogenation. As such, we quantified the interatomic distance between the bond forming sites and found a direct correlation between compounds that were ortho substituted and a smaller interatomic distance (Table 5.1). This fact is also reflected in the ratio of dearomatization and hydrodehalogenation where dearomatization is favored for compounds bearing ortho substituents.

Figure 3.8: Correlation Between Arene Substitution & Reaction Efficiency

Substrate	Interatomic Distance (Å)	DeAr/HDH (¹ H NMR)
	3.49	5.2
	3.42	9.3
	2.91	54
	3.41	7.9
	2.95	60
	3.42	8.4
	3.43	9.1
	3.43	7.8

3.3: References

- (1) Gant Kanegusuku, A. L., & Roizen, J. L. Recent Advances in Photoredox-Mediated Radical Conjugate Addition Reactions: An Expanding Toolkit for the Giese Reaction. *Angew. Chem. Int. Ed.*, **2021**, *60*, 211116-21149
- (2) Sharma, S., Singh, J., & Sharma, A. Visible Light Assisted Radical-Polar/Polar-Radical Crossover Reactions in Organic Synthesis. *Adv. Synth. Catal.*, **2021**, *363*, 3146-3169.
- (3) Roth, H. G., Romero, N. A., & Nicewicz, D. A. Experimental and Calculated Electrochemical Potentials of Common Organic Molecules for Applications to Single-Electron Redox Chemistry. *Synlett*, **2016**, *27*, 714–723.
- (4) Speckmeier, E., Fischer, T. G., & Zeitler, K. A Toolbox Approach to Construct Broadly Applicable Metal-Free Catalysts for Photoredox Chemistry: Deliberate Tuning of Redox Potentials and Importance of Halogens in Donor-Acceptor Cyanoarenes. *J. Am. Chem. Soc.*, **2018**, *140*, 15353–15365.
- (5) Sowndarya S. V., S., st. John, P. C., & Paton, R. S. A quantitative metric for organic radical stability and persistence using thermodynamic and kinetic features. *Chem. Sci.*, **2021**, *12*, 13158–13166.
- (6) (a) Ischay, M. A.; Anzovino, M. E.; Du, J.; Yoon, T. P. Efficient Visible Light Photocatalysis of [2 + 2] Enone Cycloadditions. *J. Am. Chem. Soc.* **2008**, *130*, 12886–12887.
- (b) Du, J.; Yoon, T. P. Crossed Intermolecular [2 + 2] Cycloadditions of Acyclic Enones via Visible Light Photocatalysis. *J. Am. Chem. Soc.* **2009**, *131*, 14604–14605.

- (7) Grilller, D.; Ingold, K. Free-Radical Clocks. *Acc. Chem. Res.*, **1980**, *13*, 317-323.
- (8) Minetto, G.; Raveglia, L. F.; Sega, A.; Taddei, M. Microwave-Assisted Paal-Knorr Reaction-Three-Step Regiocontrolled Synthesis of Polysubstituted Furans, Pyrroles and Thiophenes. *Eur. J. Org. Chem.* **2005**, *2005*, 5277–5288.
- (9) Knorr, L. Synthese Von Pyrrolderivaten. *Ber. Dtsch. Chem. Ges.* **1884**, *17*, 1635–1642.
- (10) O'Reilly, E.; Iglesias, C.; Ghislieri, D.; Hopwood, J.; Galman, J. L.; Lloyd, R. C.; Turner, N. J. A Regio- and Stereoselective ω -Transaminase/Monoamine Oxidase Cascade for the Synthesis of Chiral 2,5-Disubstituted Pyrrolidines. *Angew. Chem., Int. Ed.* **2014**, *53*, 2447–2450.
- (11) DeMartino, M. P.; Chen, K.; Baran, P. S. Intermolecular Enolate Heterocoupling: Scope, Mechanism, and Application. *J. Am. Chem. Soc.* **2008**, *130*, 11546–11560.
- (12) Alabugin, I. v., Kuhn, L., Medvedev, M. G., Krivoshchapov, N. v., Vil', V. A., Yaremenko, I. A., Mehaffy, P., Yarie, M., Terent'Ev, A. O., & Zolfigol, M. A. Stereoelectronic power of oxygen in control of chemical reactivity: The anomeric effect is not alone. *Chem. Soc. Rev.*, **2021**, *50*, 10253–10345.
- (13) a. Flynn, A. R., McDaniel, K. A., Hughes, M. E., Vogt, D. B., & Jui, N. T. Hydroarylation of Arenes via Reductive Radical-Polar Crossover. *J. Am. Chem. Soc.*, **2020**, *142*, 9163–9168.
- b. McDaniel, K. A., & Jui, N. T. Dearomatization through Photoredox Hydroarylation: Discovery of a Radical-Polar Crossover Strategy. *Org. Lett.*, **2021**, *23*, 5576–5580.
- (14) Boivin, J.; Yousfi, M.; Zard, S. Z. Spirolactams by a Novel ipso Radical Cyclisation and Loss of Aromaticity. *Tetrahedron Lett.* **1997**, *38* (34), 5985–5988.

Chapter 4: Nickel/Visible-Light Catalyzed Carboxylation of C(sp²) Bromides via Formate Activation

Adapted and reprinted in part with permission from Smith, G.; Zhang, D.; Zhang, W.; Soliven, A.; Wuest, W. *J. Org. Chem.*, **2023**, *88*, 9565-9568.

Copyright 2023 American Chemical Society

<https://pubs.acs.org/doi/10.1021/acs.joc.3c00895>

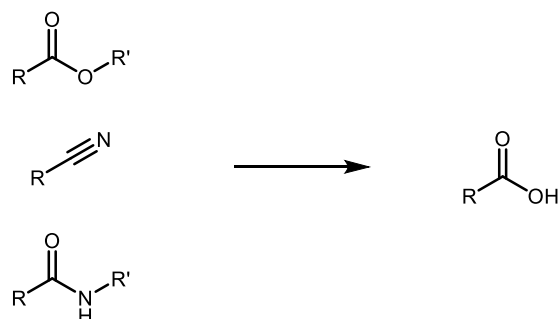
Abstract: A new visible-light-driven method for the carboxylation of (hetero)aryl/vinyl bromides has been developed using catalyzing 4CzIPN, nickel, phenyl triflimide, and sodium formate as a carboxylation agent. Interestingly, we found that catalytic phenyl triflimide plays an essential role in promoting the reaction. While many C(sp²) carboxylation reactions require harsh reagents or gaseous carbon dioxide, we demonstrate the mild and facile construction of carboxylic acid from readily available starting materials.

Chapter 4.1: Incentive and Overview of C(cp²) Carboxylations

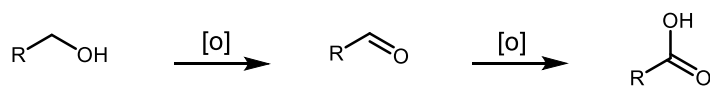
Carboxylic acids are one of the most ubiquitous functional groups found across a variety of pharmaceutically and biologically relevant compounds.¹ Outside of their relevance in bioactive compounds, carboxylic acids, are a valuable synthetic linchpin in organic chemistry providing a functional handle for a large range of useful transformations.² Classical methods of constructing carboxylic acids includes the hydrolysis of esters, amides, and nitriles; the oxidation of aldehydes/alcohols, and the addition of organometallic species to CO₂ (Figure 4.1). While these methods are valuable, they rely on the pre-existing frameworks for hydrolysis/oxidation or the use of harsh reagents and gaseous CO₂.

Figure 4.1: Classical Methods of Constructing Carboxylic Acids

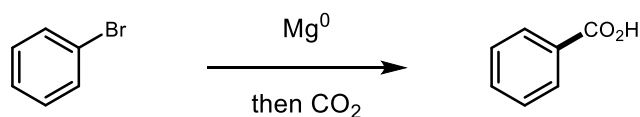
A. Hydrolysis of esters, nitriles, and amides



B. Oxidation of alcohols/aldehydes



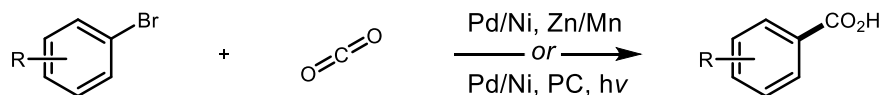
C. Organometallic Addition into CO₂



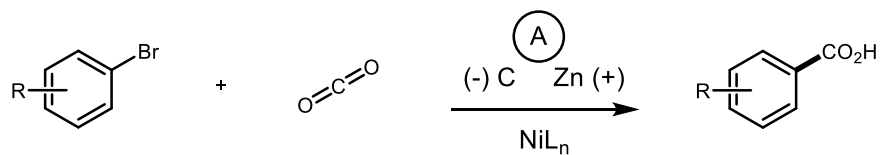
While these classical methods remain useful, the utility of catalytic carboxylation reactions with organic halides and CO₂ has emerged as a valuable alternative.³ Martin et al. have demonstrated several elegant methods for the carboxylation of aryl (pseudo)halides using either stoichiometric metal reducing agents or dual photocatalytic systems (Figure 4.2B).⁴ Nickel-catalyzed electrochemical processes have also been demonstrated as valuable alternatives to classical carboxylation reactions (Figure 4.2B).⁵ We recently disclosed a protocol for accessing the radical anion of carbon dioxide (CO₂^{•-}) through a polarity matched hydrogen atom transfer (HAT) between an electrophilic radical and a formate salt, demonstrating both its nucleophilic and reductive reactivity.⁶ Inspired by the emergence of dual photoredox/nickel catalysis pioneered by Molander, Doyle, and Macmillan,⁷ we sought to expand the reactivity of the carbon dioxide radical anion by binding it to a metal center thereby allowing formate salts to replace CO₂ in C(sp²) cross-couplings.

Figure 4.2: Catalytic Strategies for C(sp²) Carboxylation

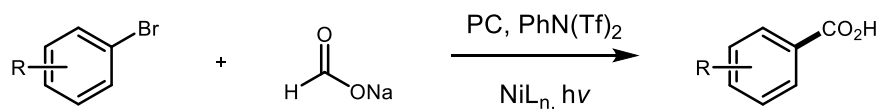
A. CO₂ driven carboxylations w/ metal reductants or photocatalysts



B. Ni-catalyzed Electrochemical driven carboxylation with CO₂



C. This work: CO₂ radical anion driven carboxylation

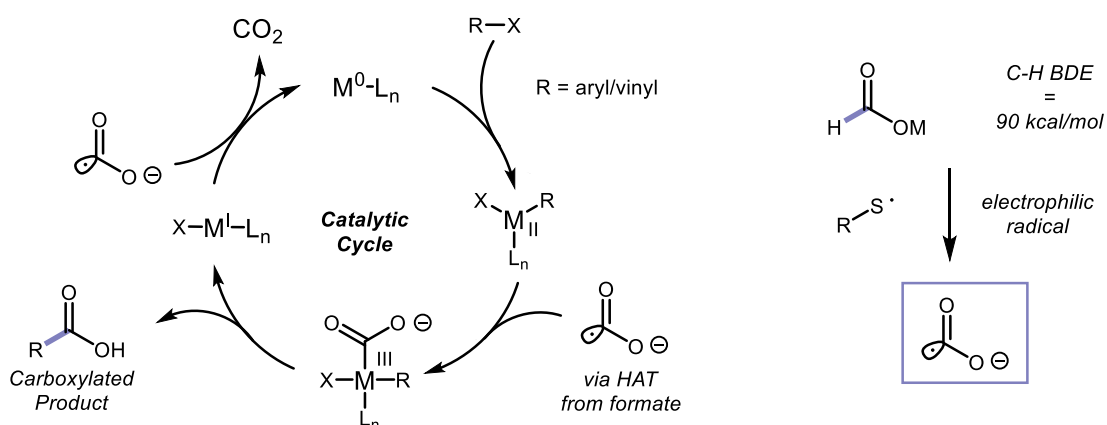


Fu et al. recently reported a similar system,⁸ where the use of more highly oxidizing photocatalysts and additives were necessary to access aryl bromide reactivity. In this report, we share our initial insights into this system where we hypothesize phenyl triflimide plays a key role in catalyzing this reaction (**Figure 4.2C**).

4.2: Initial Investigations Using Alternative Initiators

In a similar manner to classical metallophotoredox catalytic cycles, we envisioned the mechanistic scenario outlined in **Figure 4.3**. Upon oxidative addition to a metal species (M^0), the M^{II} complex may then intercept the carbon dioxide radical anion to form the corresponding M^{III} complex which would undergo reductive elimination to expel the carboxylated product alongside a M^{I} species. Finally, another equivalent of the carbon dioxide radical anion may turn over the catalytic cycle and release CO_2 gas in the process.

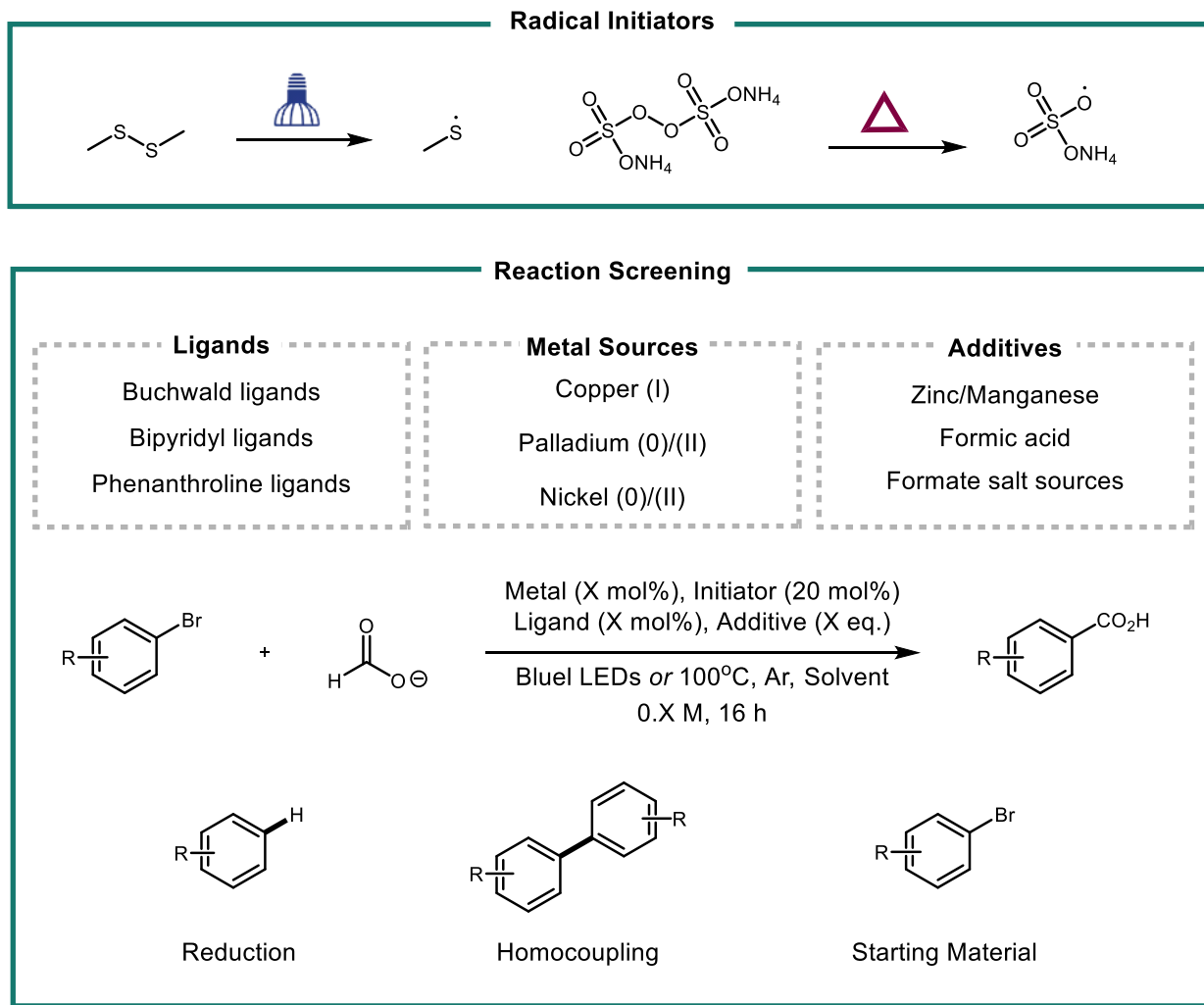
Figure 4.3: Initial Mechanistic Scenario for $C(sp^2)$ Carboxylation



While this mechanistic hypothesis is theoretically feasible, it places a significant amount of mechanistic responsibility on the carbon dioxide radical anion. The $CO_2^{\bullet-}$, in this scenario, would be responsible for generating M^0 *in situ*, binding the M^{II} complex, and also reducing

the $M^{(I)}$ complex back to $M^{(0)}$. In other words, it must operate as both the reductant and the CO_2 source reagent. We began investigation this process under our alternative initiator protocols—using either disulfide (in combination with blue LEDs) or persulfate (in combination with heat). Despite extensive screening with a variety of different metals, ligands, and additives that are known to catalyze similar transformation^x, product yield was never observed. The vast majority of these systems only produced unreacted starting material, homocoupling products, and reduction products—indicating CO_2 radical anion formation (Figure 4.4).

Figure 4.4: Overview of Reaction Screening for Alternative Initiators



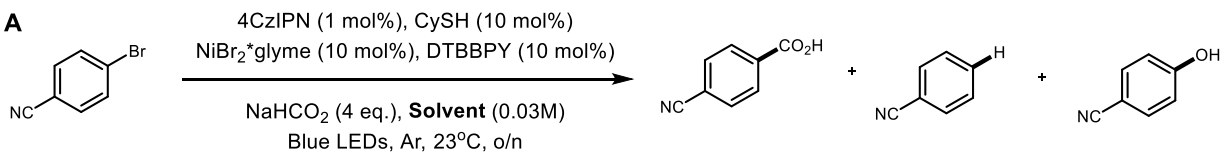
In order to target a system with more control, we decided to look at this transformation using more established chemistry. As such we began examining this transformation under photochemical conditions using nickel as our metal source—a reaction well established as facilitating radical processes.

4.3: Reaction Optimization Under Photochemical Conditions

Using 4CzIPN (1 mol%), cyclohexanethiol (10 mol%) as an HAT catalyst, nickel (II) bromide ethylene glycol dimethyl ether complex (10 mol%), di-tert-butylbipyridine (10 mol%), sodium formate (4 equiv.), solvent (0.03M), under irradiation with blue LEDs and argon. Although using dioxane as solvent did not yield any product (Table 4.1A, entry 1), we were excited to find that a 1:1 dioxane/DMSO cosolvent system or DMF as solvent furnished the product in 60% yield (entries 2-3). Interestingly, we found that another byproduct made up the

Table 4.1: Solvent Screen Under Photochemical Conditions

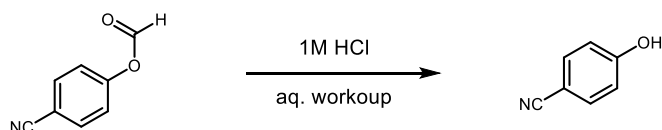
A



Entry	Conditions	Starting Material ^b	Product ^b	Reduction ^b	Phenol ^b
1	Dioxane	100%	0%	0%	0%
2	1:1 Dioxane/DMSO	0%	60%	0%	40%
3	DMF	0%	60%	0%	30%

^aConditions: Aryl chloride (1.0 eq.), sodium formate (5 eq.), initiator (20 mol%), DMSO [0.1M], N₂, Blue LEDs or 100oc, 16 hrs, 0.1 mmol scale. ^bYield determined via ¹H NMR using dibromomethane as an internal standard. Product yield determined via ¹H NMR using CH₂Br₂ as an internal standard.

B



rest of the mass balance which after close examination was revealed to be the phenol indicating carbon-heteroatom formation. After altering the reaction conditions, reducing sodium formate equivalence to 1.5 and increase solvent concentration to 0.1 molar, we next sought to examine the substrate scope of this reaction.

When these reaction conditions were applied to electron-neutral arene bromobenzene, no product yield was observed (Table 4.2, entry 1). The same result was observed with 3 and 4-bromoanisole, electron-neutral and electron-rich arenes (entries 2-3), and switching out the halide for 4-iodoanisole (entry 4) did not produce any product yield either. This divergence in

Table 4.2: Reaction Screening with Electron-Rich/Neutral Arenes^a

Entry	Substrate	Starting Material ^b	Product ^b	Reduction ^b	Phenol ^b
1	R = H	100%	0%	0%	0%
2	R = 3-OCH ₃	100%	0%	0%	0%
3	R = 4-OCH ₃	100%	0%	0%	0%
4	R = 4-OCH ₃ , X = I	100%	0%	0%	0%

^aConditions: Aryl bromide (1.5 eq.), sodium formate (1.55 eq.), initiator (20 mol%), 1:1 DMSO/dioxane [0.1M], N₂, Blue LED, 16 hrs, 0.1 mmol scale. ^bYield determined via ¹H NMR using dibromomethane as an internal standard.

reactivity was accompanied by a new reaction feature in which the system rapidly turned dark brown upon irradiation with blue LEDs. Although unfortunate, this setback was not surprising as many metallophotoredox catalyzed systems are unreactive or low-yielding in the absence of electron-withdrawing groups—this is most likely attributed to the slow rate of oxidative addition

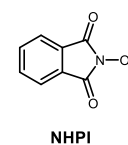
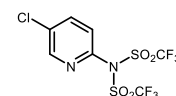
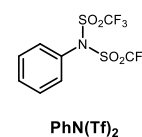
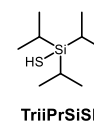
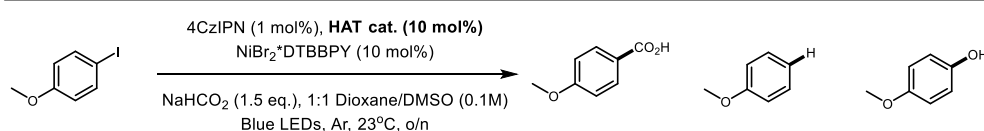
to electron rich/neutral aryl halides relative to their electron-deficient counterparts.¹⁰ Both 4CzIPN ($E_{1/2}^{\circ}(\text{PC}^*/\text{PC}^{*+}) = -1.2\text{V vs SCE}$)¹¹ and $\text{CO}_2^{\bullet-}$ ($E_{1/2}^{\circ} = -2.2\text{ V vs SCE}$) are capable of generating the active nickel species ($E_{1/2}^{\text{red}}[\text{Ni}^{\text{II}}/\text{Ni}^0] = -1.2\text{V vs SCE}$),¹² which may lead to rapid accumulation of Ni^0 consistent with nickel black formation.¹³

This potential bottleneck is outlined in **Figure 4.5**. As previously discussed, mismatched kinetics between oxidative addition of our aryl species alongside radical formation may prevent product formation from occurring. However, it is also possible that thiol is disrupting this process given its proclivity to coordinate metal catalysts and therefore inhibit product formation.¹⁴ As such, we sought to identify an HAT catalyst that was non-nucleophilic/bulky in order to prevent catalyst coordination with the right kinetics to interact with the metal system.

Table 4.3: HAT Catalyst Screen

Entry	Substrate	Starting Material ^b	Product ^b	Reduction ^b	Phenol ^b
1	CySH	100%	0%	0%	0%
2	PhSH	92%	trace	0%	0%
3	TriiPrSiSH	75%	15%	0%	0%
4	tBuSH	82%	7%	0%	0%
5	Ph_3SH	72%	0%	0%	0%
6	DABCO	40%	0%	60%	0%
7	NHPI	45%	trace	15%	0%
8	$\text{Mn}(\text{dpm})_3$	30%	56%	0%	0%
9	$\text{PhN}(\text{Tf})_2$	17%	75%	0%	0%
10	Comin's Reagent	60%	40%	0%	0%

^aConditions: Aryl bromide (1.5 eq.), sodium formate (1.55 eq.), initiator (20 mol%), 1:1 DMSO/dioxane [0.1M], N_2 , Blue LED, 16 hrs, 0.1 mmol scale. ^bYield determined via $^1\text{H NMR}$ using dibromomethane as an internal standard.

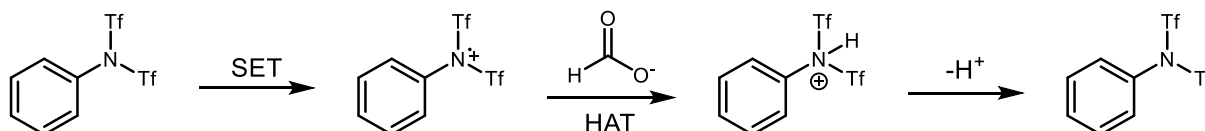


In order to find a suitable HAT catalyst, we screened a series of known and hypothesized HAT catalysts beginning with a series of thiols (Table 4.3, entries 1-5). While cyclohexanethiol and thiophenol lead to 0% product formation, small amounts of carboxylation were observed with triisopropylsilane thiol and tert-butyl thiol (entries 4-5, 15 and 7% yield). Both thiols are sterically encumbered potentially preventing thiol coordination, although the higher yield for triisopropyl silane thiol may also be attributed to its very low oxidation potential ($E_{1/2}^{ox} = +0.28$ V vs SCE).¹⁵ Despite a similar steric profile, triphenylmethane thiol (entry 5) did not correlate with product formation. Nitrogen and oxygen-centered heterocycles DABCO and NHPI¹⁶ were not productive in product formation either (entries 6-7). There are several established protocols using manganese as a hydrogen atom transfer agent¹⁷ for selective processes and interestingly Mn(dpm)₃ catalyzed product formation in 56% yield (entry 8). Although intriguing, we sought to keep expensive metals out of this reaction system and this hit was not pursued any further. Interestingly, the use of phenyl triflimide and Comin's reagent catalyzed product formation in 75% and 40% yield (entries 9-10).

4.4: Mechanistic Investigations into Phenyl Triflimide

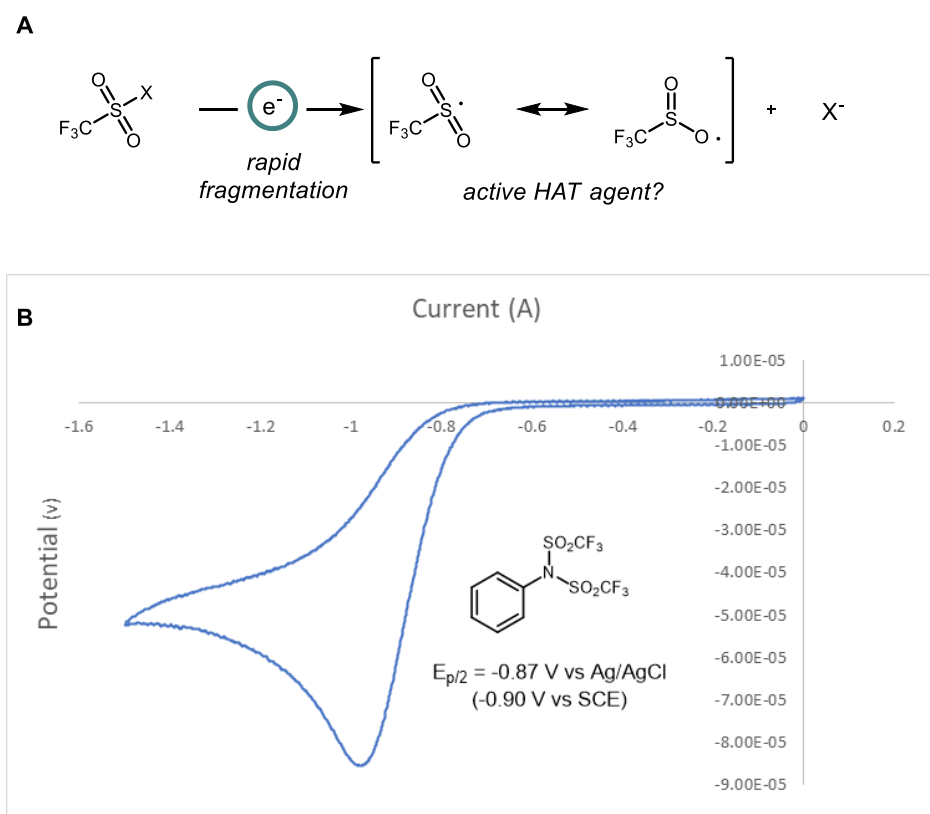
Our initial hypothesis regarding this system was that phenyl triflimide was playing a role as a unique and novel HAT catalyst (Scheme 4.1). Single electron transfer from phenyl triflimide

Scheme 4.1: Initial Hypothesis for the Role of Phenyl Triflimide



to the photocatalyst would generate the electrophilic radical cation of phenyl triflimide which could abstract from formate. Finally, deprotonation of corresponding sulfonamide salt by excess formate would regenerate phenyl triflimide. Given the bulky and electron-deficient nature of phenyl triflimide we initially hypothesized the unique additive was effective because it was unable to coordinate the catalyst and/or exhibited favorable kinetics. An alternative to single electron oxidation of phenyl triflimide could simply be single electron reduction. SET from 4CzIPN to phenyl triflimide would generate an electrophilic sulfinyl radical which may be capable of HAT¹⁸, alongside an anionic nitrogen byproduct (Figure 4.5A). The standard

Figure 4.5: Reduction Pathway and CV of Phenyl Triflimide

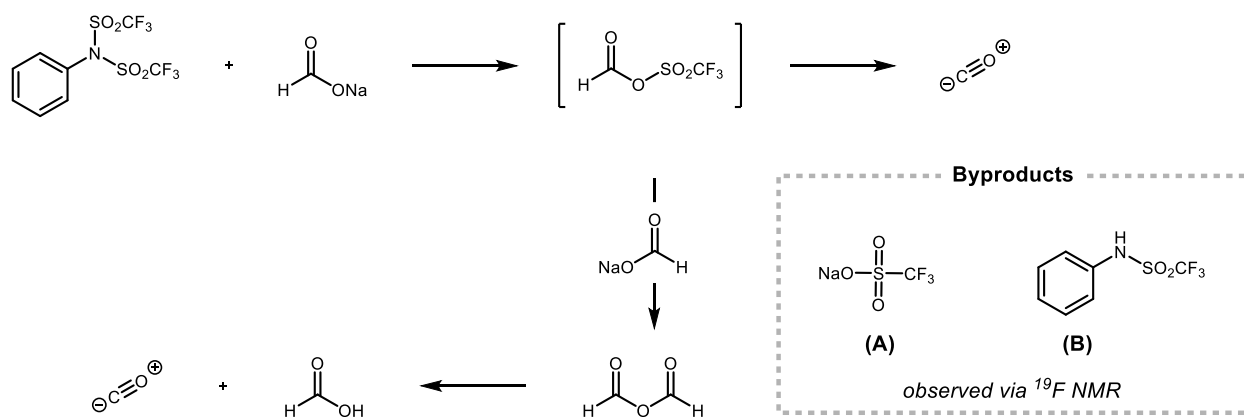


reduction potential of phenyl triflimide was measured using cyclic voltammetry (see *Supporting Information*), revealing an irreversible reduction potential ($E_{p/2} = -0.91 \text{ V vs SCE}$) indicating that

SET between 4CzIPN ($PC^*/PC^{++} = -1.2$ V vs SCE) and phenyl triflimide is favorable (Figure 4.5B). However, Stern-Volmer fluorescence quenching experiments indicate no quenching of the photocatalyst (4CzIPN) by phenyl triflimide (see *Supporting Information*).

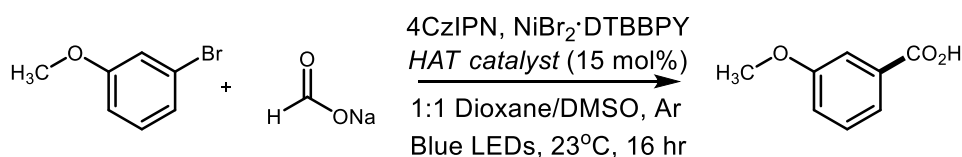
Although phenyl triflimide is an air-stable crystalline solid, we reconsidered its role in the reaction given its traditional role as an electrophile to make enol triflates from carbonyl compounds.¹⁹ Indeed, control experiments using ^{19}F NMR indicate a rapid reaction between phenyl triflimide and sodium formate that result in complete conversion to sodium trifluoromethanesulfonate (A) alongside the aniline byproduct (B) that would result from nucleophilic attack with formate (Scheme 4.2). Upon initial attack of phenyl triflimide, the intermediate anhydride may then undergo decarbonylation which computational studies predict should be a rapid process (17.3 kcal/mol for decarbonylation).²⁰ An alternative pathway would involve another equivalent of formate to intercept the anhydride thereby generating formic anhydride instead which also possesses a low barrier to decarbonylation. Regardless of the pathway, we began to examine how catalytic carbon monoxide may play a role in this reaction.

Scheme 4.2: Reaction Pathway for CO Generation

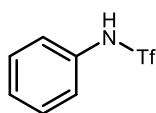


We first considered the potential that either sodium trifluoromethanesulfonate or the aniline byproduct were catalyzing the reaction. Neither trifluoro-*N*-phenylmethanesulfonamide (1) nor sodium trifluoromethanesulfonate (2) resulted in any product formation indicating that they play no part in catalyzing the reaction. Using sodium *p*-toluenesulfinate (3), known as an HAT catalyst, gave a complete return of starting material solidifying our belief that sulfinyl radicals are not at play in this system (Table 4.4, entries 1-3).

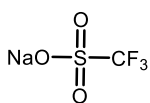
Table 4.4: Reaction Controls



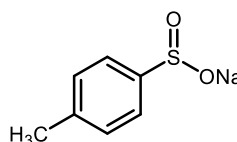
Entry	HAT Catalyst	Deviation	Yield ^b
1	Trifluoro- <i>N</i> -phenylmethanesulfonamide	-	0%
2	Sodium trifluoromethanesulfonate	-	0%
3	Sodium <i>p</i> -toluenesulfinate	-	0%



1



2



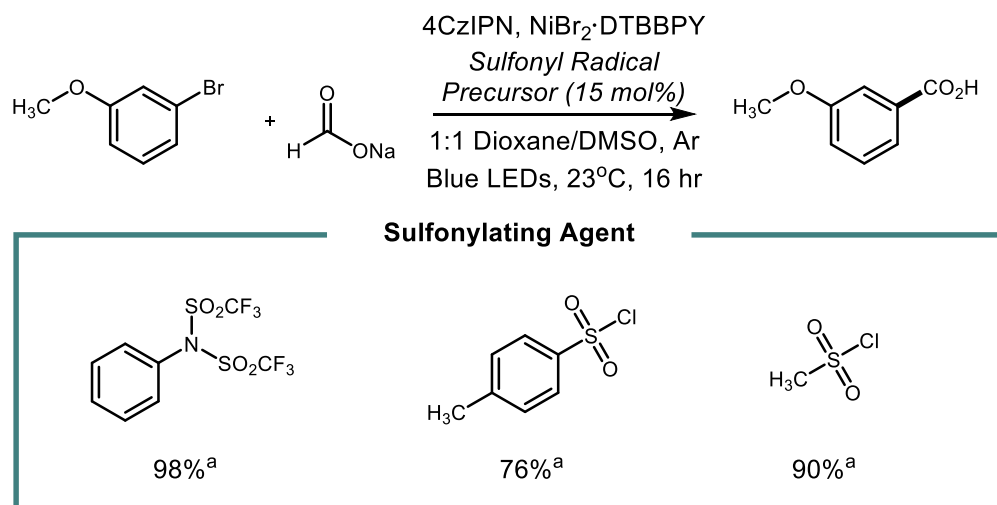
3

^aConditions: Aryl bromide (1.0 eq.), 4CzIPN (1 mol%), Ni cat. (10 mol%), sodium formate (1.5 eq.), additive (15 mol%), 1:1 DMSO/dioxane [0.1M], N₂, Blue LED, 16 hrs, 0.1 mmol scale. ^bYield determined via ¹H NMR using dibromomethane as an internal standard.

Given the reaction efficacy of a stoichiometric amount of a sulfonylating agent in this reaction system, we hypothesized other sulfonylating agents may be able to catalyze similar systems. Excitingly, we found that when phenyl triflimide was replaced with toluenesulfonyl

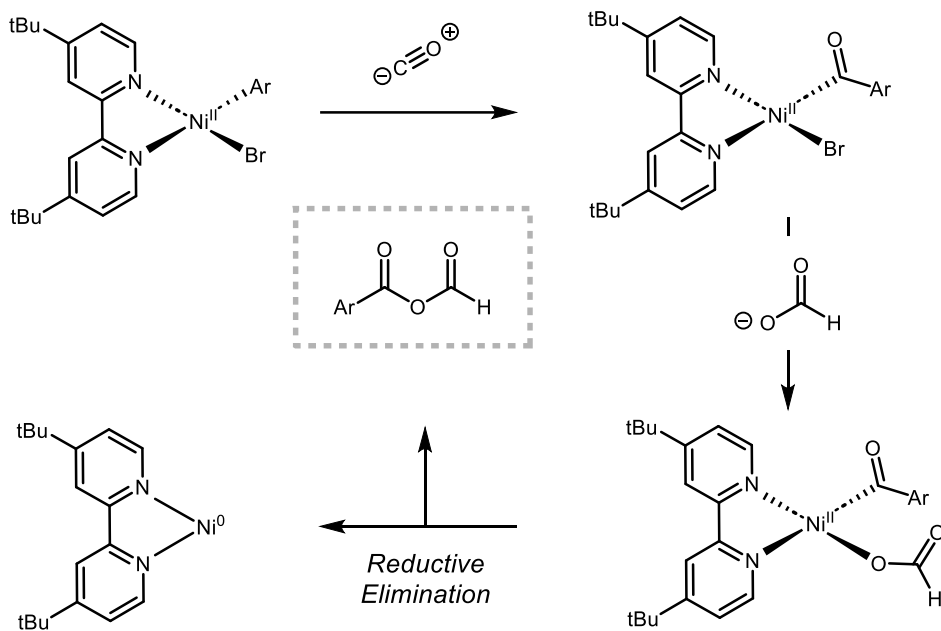
chloride the reaction proceeded in 76% yield. Furthermore, methanesulfonyl chloride also catalyzed the reaction in 90% yield in further support of our hypothesis that formate is engaging the sulfonylating agents in a decarbonylation process.

Figure 4.6: Evaluation of Alternative Sulfonylating Agents



^aConditions: Aryl bromide (1.0 eq.), 4CzIPN (1 mol%), Ni cat. (10 mol%), sodium formate (1.5 eq.), additive (15 mol%), 1:1 DMSO/dioxane [0.1M], N₂, Blue LED, 16 hrs, 0.1 mmol scale. Yield determined via ¹H NMR using dibromomethane as an internal standard.

Interestingly, Fu et al. recently reported a system regarding the nickel-catalyzed carboxylation of alkynes using formic acid and catalytic pivalic anhydride.²¹ Through a series of in depth computational analyses, they found that their system was proceeding through a thermally induced (100°C or greater) process in which carbon monoxide is recycled throughout the reaction and maintained at sub-stoichiometric amounts. This process is outlined in scheme 4.3. Upon oxidative addition, the Ni(II) complex may then undergo migratory insertion followed by transmetalation with formate. Upon reductive elimination, carbon-hetero atom bond formation furnishes the anhydride product. Under thermal conditions, this complex may then decarbonylate to deliver the carboxylated product alongside carbon monoxide.

Scheme 4.3: Carbon Monoxide Recycling System

To further probe this mechanism, we ran a series of screens to probe this reaction system. Consistent with other carbon monoxide recycling systems,²² we found a direct correlation between phenyl triflimide loading and product formation. At our standard 15 mol% phenyl triflimide, we see quantitative conversion to the product (Table 4.3, entry 1). However, doubling that loading leads to a significant drop in product yield (entry 2, 55% yield). This trend continues with a complete shut down of reactivity at 100 mol% phenyl triflimide. This is consistent with previous findings and is likely a result of catalyst poisoning by carbon monoxide.

We next considered the role of the photocatalyst and ligand given the use of a photocatalyst and bipyridine ligand often indicates radical reactivity. Although the use of bipyridine ligands is often related to stabilizing incoming radical species on the metal center, bipyridine ligands are also known to stabilize odd redox intermediates in nickel, namely Ni(I) and Ni(III)—reactive species known to facilitate carbon-heteroatom bond formation.²³

Table 4.5: Phenyl Triflimide Loading

4CzIPN (1 mol%), PhN(Tf)₂ (**X mol%**)
 NiBr₂·glyme (10 mol%), DTBBPY (10 mol%)
 NaHCO₂ (1.5 eq), 1:1 DMSO/Dioxane
 Ar, Blue LEDs, o/n

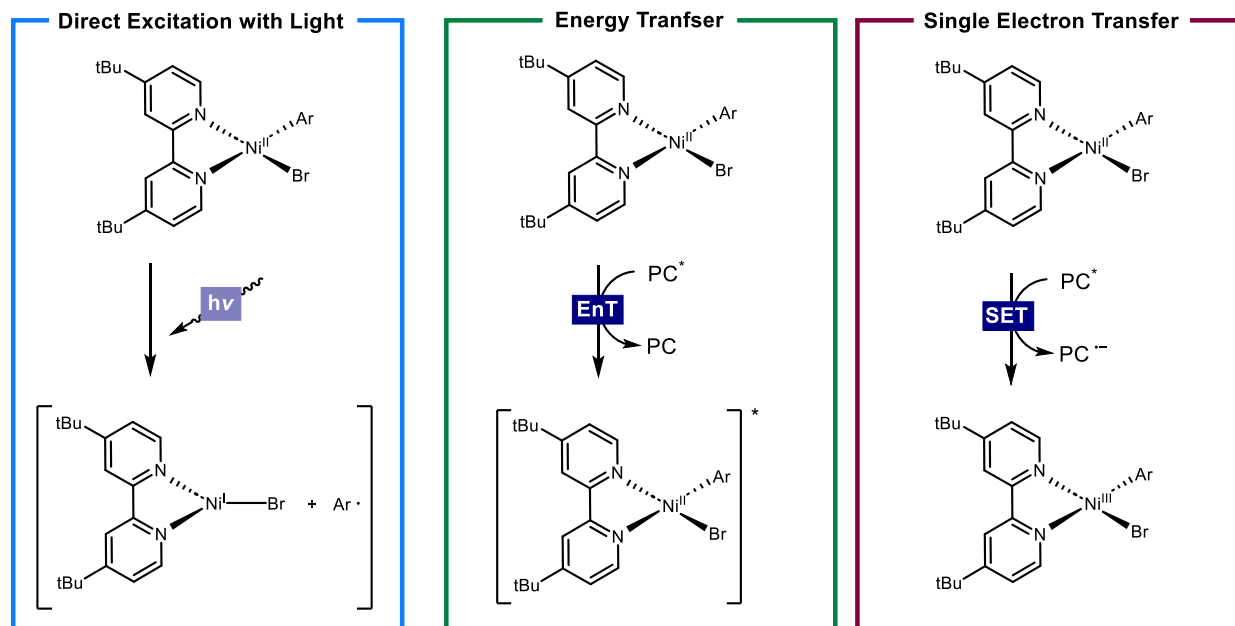
Entry	Conditions	Starting Material	Product
1	15 mol%	0%	100%
2	30 mol%	42%	55%
3	60 mol%	82%	20%
4	100 mol%	100%	0%

^aConditions: Aryl bromide (1.0 eq.), 4CzIPN (1 mol%), Ni cat. (10 mol%), sodium formate (1.5 eq.), additive (15 mol%), 1:1 DMSO/dioxane [0.1M], N₂, Blue LED, 16 hrs, 0.1 mmol scale. Yield determined via ¹H NMR using dibromomethane as an internal standard.

Some reports indicate that upon oxidative addition, Ni(II) complexes absorb visible light promoting the complex to its excited state. This complex may then undergo disproportionation to generate an active Ni(I) catalyst poised for oxidative addition²⁴. However, in the absence of a photocatalyst no product formation is observed indicating a photoexcited nickel complex is not at play here (Figure 4.7B, entry 1). Alternatively, energy transfer mechanisms may also be at play as energy transfer from a photocatalyst to a Ni(II) complex has been shown to facilitate carbon-heteroatom bond formation.²⁵ Although this possibility was unlikely given 4CzIPN is not well established in energy transfer mechanisms, we switched out the photocatalysts for benzophenone (a known energy transfer catalyst) but did not observe any product formation (Figure 4.7B, entry 2). A final possibility would be the direct regulation of the nickel redox state

by the photocatalyst.²⁶ The use of photocatalyst with highly oxidizing excited states is consistent with this mechanistic hypothesis delivering product in 69-100% yield (Figure 4.7B, entries 3-5).

Figure 4.7: Nickel Photocatalyst Dependence

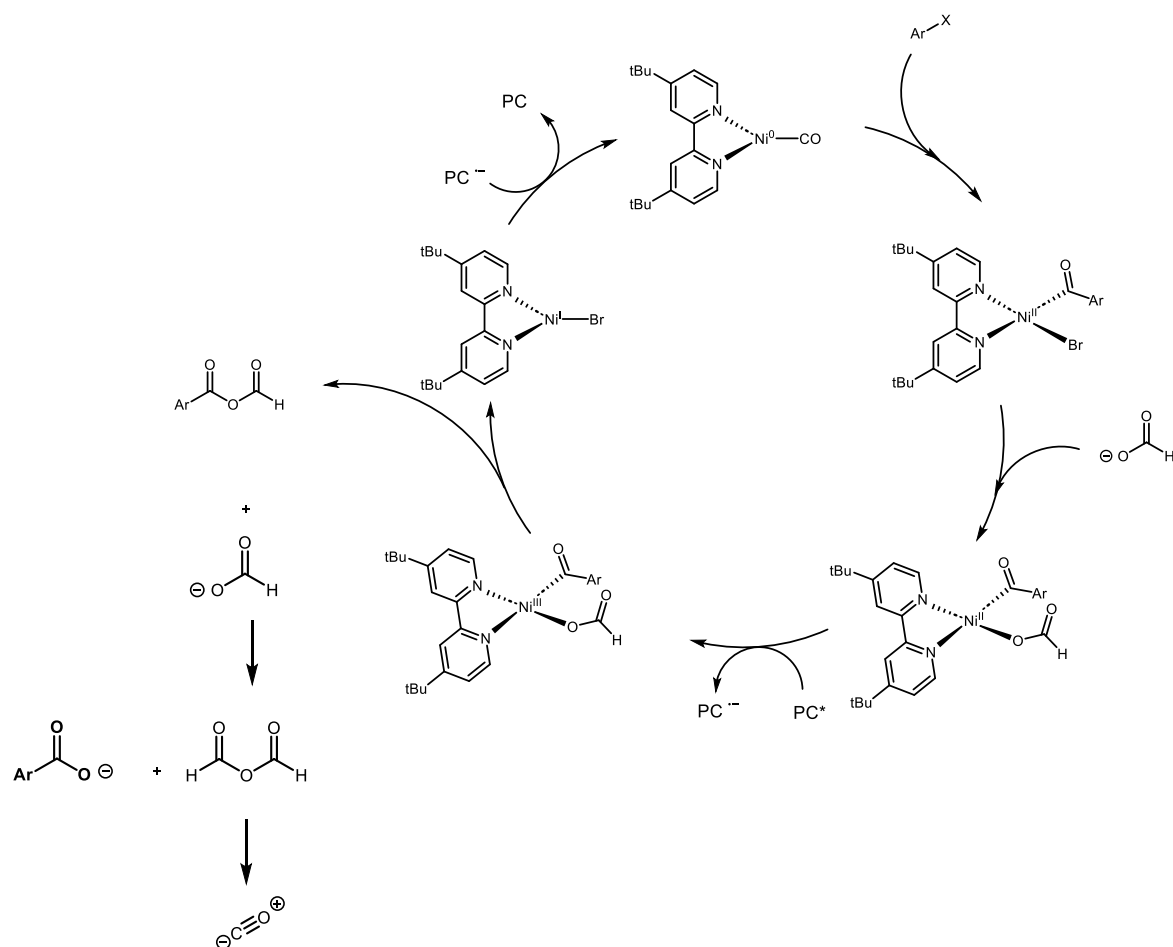


Entry	Conditions	Starting Material ^a	Product ^a
1	No PC	100%	0%
2	Benzophenone	100%	0%
3	Cl-4CzIPN	0%	95%
4	Ir[(dF(CF ₃)ppy) ₂ (dtbbpy) ₂ PF ₆	0%	100%
5	Ir[(ppy) ₂ dtbbpy]PF ₆	30%	69%

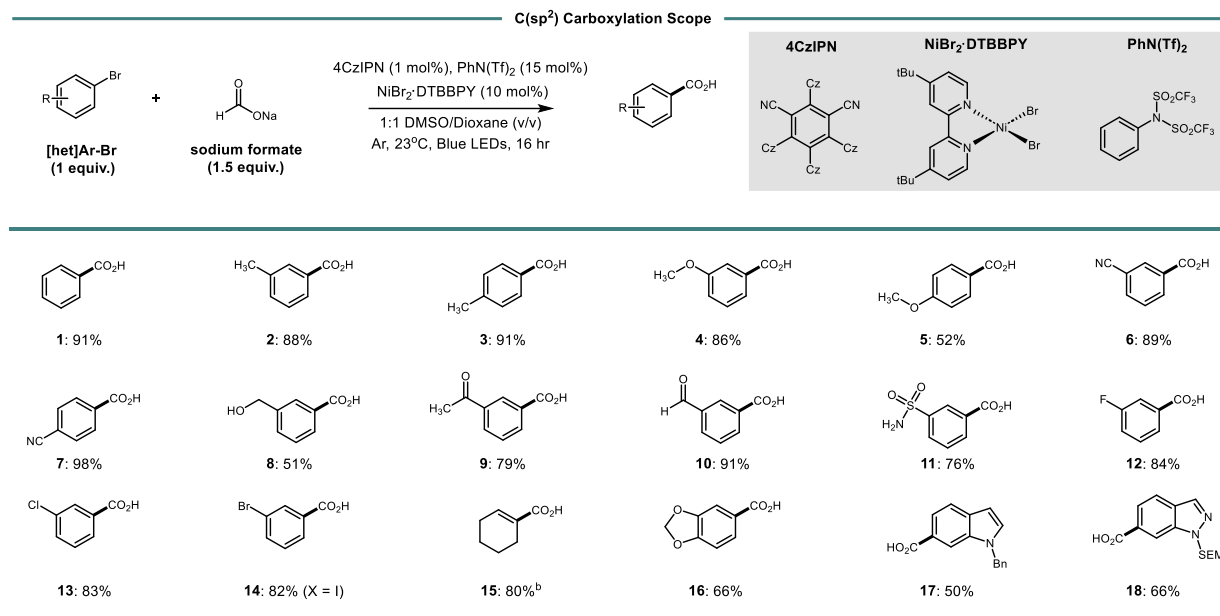
^aConditions: Aryl bromide (1.0 eq.), PC (1 mol%), Ni cat. (10 mol%), sodium formate (1.5 eq.), phenyl triflimide (15 mol%), 1:1 DMSO/dioxane [0.1M], N₂, Blue LED, 16 hrs, 0.1 mmol scale. Yield determined via ¹H NMR using dibromomethane as an internal standard.

With our mechanistic data in hand, we propose the following mechanistic scenario. Upon generation of Ni(0) *in situ* by the photocatalyst and coordination of carbon monoxide the active catalyst is formed. Oxidative addition of the aryl bromide followed by nucleophilic displacement with formate would yield the Ni(II) intermediate. This complex may then be oxidized by the photocatalyst (generation the radical anion of the photocatalyst) to Ni(III) which readily undergoes reductive elimination to deliver the mixed anhydride. Upon hydrolysis with another equivalent of formate, formic anhydride is generated (alongside the carboxylated product) which could then decarbonylate thereby regenerating carbon monoxide. The resultant Ni(I) species may then be reduced back to Ni(0) from the radical anion of the photocatalyst.

Scheme 4.6: Proposed Mechanistic Scenario



With our optimized conditions in hand, we sought to demonstrate the utility of this system with a variety of (hetero)aryl/vinyl bromides. We first considered a panel of neutral aryl bromides where bromobenzene, 2-bromotoluene, and 3-bromotoluene all underwent carboxylation in good yield (**Table 4.4**, 1-3, 88-91% yield). Interestingly, substrates with ortho substituents were not compatible coupling partners under this system, presumably due to steric effects. We next evaluated a series of electron-rich/electron-poor systems which all proceeded smoothly to the corresponding carboxylated product (**4-7**, 52-98% yield). This system was found to tolerate a variety of functional groups including primary alcohols, ketones, aldehydes, and sulfonamides (**8-11**, 51-91% yield). Interestingly, neither aryl ketone **9** nor benzaldehyde **10** showed signs of reduction to the corresponding benzylic alcohols—a further piece of evidence that the carbon dioxide radical anion is not involved in this transformation. Furthermore, despite the labile formyl C-H bond of **10**, we observed no traces of ketone formation from the aldehyde-derived acyl radical. Halogens were also well tolerated under this system (**12-14**, 82-84% yield) where coupling was selective for the C-I bond over the C-Br bond. Finally, we found this system also worked with vinyl bromide **15** (80% yield) alongside a variety of heterocyclic bromides including dioxalane, indole, and indazole further demonstrating the tolerance of this methodology (**16-18**, 50-66% yield).

Table 4.6: Substrate Scope for C(sp²) Carboxylation

^aCondition same as follows: Aryl bromide (1 equiv.), sodium formate (1.5 equiv.), 4CzIPN (1 mol%), NiBr₂·dtbbpy (10 mol%), PhN(Tf)₂ (15 mol%), 1:1 DMSO/Dioxane (v/v, 0.1M), blue LEDs, and Ar at 23°C for 16 h. Isolated yields are shown unless otherwise stated. Reactions were performed on a 0.5 mmol scale (see Supporting Information). ^bReaction performed on a 0.1 mmol scale, yields determined by ¹H NMR using CH₂Br₂ as an internal standard.

4.5 References

- (1) (a) Ertl, P.; Altmann, E.; McKenna, J. M. The Most Common Functional Groups in Bioactive Molecules and How Their Popularity Has Evolved over Time. *J. Med. Chem.* **2020**, *63*, 8408–8418.
- (b) Börjesson, M.; Moragas, T.; Gallego, D.; Martin, R. Metal-Catalyzed Carboxylation of Organic (Pseudo)halides with CO₂. *ACS Catal.* **2016**, *6*, 6739–6749.
- (c) Maag, H. *Prodrugs of Carboxylic Acids*; Springer: New York, 2007.
- (2) Gooßen, L. J.; Rodríguez, N.; Gooßen, K. Carboxylic acids as substrates in homogeneous photocatalysis. *Angew. Chem., Int. Ed.* **2008**, *47*, 3100–3120.

- (3) Tortajada, A.; Juliá-Hernández, F.; Börjesson, M.; Moragas, T.; Martín, R. Transition-Metal-Catalyzed Carboxylation Reactions with Carbon Dioxide. *Angew. Chem., Int. Ed.* **2018**, *130*, 16178–16214.
- (4) (a) Correa, A.; Martín, R. Palladium-catalyzed direct carboxylation of aryl bromides with carbon dioxide. *J. Am. Chem. Soc.* **2009**, *131*, 15974–15975.
- (b) Börjesson, M.; Moragas, T.; Martín, R. Ni-Catalyzed Carboxylation of Unactivated Alkyl Chlorides with CO₂. *J. Am. Chem. Soc.* **2016**, *138*, 7504–7507.
- (c) Shimomaki, K.; Murata, K.; Martín, R.; Iwasawa, N. Visible-Light-Driven Carboxylation of Aryl Halides by the Combined Use of Palladium and Photoredox Catalysts. *J. Am. Chem. Soc.* **2017**, *139*, 9467–9470.
- (5) Sun, G. Q.; Zhang, W.; Liao, L. L.; Li, L.; Nie, Z. H.; Wu, J. G.; Zhang, Z.; Yu, D. G. Nickel-catalyzed electrochemical carboxylation of unactivated aryl and alkyl halides with CO₂. *Nat. Commun.* **2021**, *12*, 1–10.
- (6) Hendy, C. M.; Smith, G. C.; Xu, Z.; Lian, T.; Jui, N. T. Radical Chain Reduction via Carbon Dioxide Radical Anion (CO₂^{•-}). *J. Am. Chem. Soc.* **2021**, *143*, 8987–8992.
- (7) (a) Tellis, J.; Primer, D.; Molander, G. Single-electron transmetalation in organoboron cross-coupling by photoredox/nickel dual catalysis. *Science* **2014**, *345*, 433–436.
- (b) Zuo, Z.; Ahneman, D. T.; Chu, L.; Terrett, J. A.; Doyle, A. G.; Macmillan, D. W. C. Merging photoredox with nickel catalysis: Coupling of α-carboxyl sp³-carbons with aryl halides. *Science* **2014**, *345*, 437–440.

- (c) Chan, A. Y.; Perry, I. B.; Bissonnette, N. B.; Buksh, B. F.; Edwards, G. A.; Frye, L. I.; Garry, O. L.; Lavagnino, M. N.; Li, B. X.; Liang, Y.; Mao, E.; Millet, A.; Oakley, J. v.; Reed, N. L.; Sakai, H. A.; Seath, C. P.; MacMillan, D. W. C. Metallaphotoredox: The Merger of Photoredox and Transition Metal Catalysis. *Chem. Rev.* **2022**, *122*, 1485–1542.
- (8) Fu, M. C.; Wang, J. X.; Ge, W.; Du, F. M.; Fu, Y. Dual nickel/ photoredox catalyzed carboxylation of C(sp²)-halides with formate. *Org. Chem. Front.* **2022**, *10*, 35–41.
- (9) Speckmeier, E.; Fischer, T. G.; Zeitler, K. A Toolbox Approach to Construct Broadly Applicable Metal-Free Catalysts for Photoredox Chemistry: Deliberate Tuning of Redox Potentials and Importance of Halogens in Donor-Acceptor Cyanoarenes. *J. Am. Chem. Soc.*, **2018**, *140*, 15353–15365.
- (10) Zhang, X.; MacMillan, D. W. C. Direct Aldehyde C-H Arylation and Alkylation via the Combination of Nickel, Hydrogen Atom Transfer, and Photoredox Catalysis. *J. Am. Chem. Soc.*, **2017**, *139*, 11353–11356.
- 11)(a) Gisbertz, S.; Reischauer, S.; Pieber, B. Overcoming limitations in dual photoredox/nickel-catalysed C–N cross-couplings due to catalyst deactivation. *Nat. Catal.*, **2020**, *3*, 611–620.
- (b) Dorsheimer, J. R.; Ashley, M. A.; Rovis, T. Dual Nickel/Photoredox-Catalyzed Deaminative Cross-Coupling of Sterically Hindered Primary Amines. *J. Am. Chem. Soc.*, **2021**, *143*, 19294–19299.
- (c) Kawamata, Y.; Vantourout, J. C.; Hickey, D. P.; Bai, P.; Chen, L.; Hou, Q.; Qiao, W.; Barman, K.; Edwards, M. A.; Garrido-Castro, A. F.; deGruyter, J. N.; Nakamura, H.; Knouse, K.; Qin, C.; Clay, K. J.; Bao, D.; Li, C.; Starr, J. T.; Garcia-Irizarry, C.; Sach, N.; White, H. S.; Neurock, M.; Minter, S.

D.; Baran, P. S. Electro-chemically Driven, Ni-Catalyzed Aryl Amination: Scope, Mechanism, and Applications. *J. Am. Chem. Soc.*, **2019**, *141*, 6392–6402.

(11) Speckmeier, E.; Fischer, T. G.; Zeitler, K. A Toolbox Approach to Construct Broadly Applicable Metal-Free Catalysts for Photoredox Chemistry: Deliberate Tuning of Redox Potentials and Importance of Halogens in Donor-Acceptor Cyanoarenes. *J. Am. Chem. Soc.*, **2018**, *140*, 15353–15365.

(12) Zhang, X.; MacMillan, D. W. C. Direct Aldehyde C-H Arylation and Alkylation via the Combination of Nickel, Hydrogen Atom Transfer, and Photoredox Catalysis. *J. Am. Chem. Soc.*, **2017**, *139*, 11353–11356.

(13) Gisbertz, S., Reischauer, S., & Pieber, B. Overcoming limitations in dual photoredox/nickel-catalysed C–N cross-couplings due to catalyst deactivation. *Nat. Cat.*, **2020**, *3*, 611–620.

(14) (a) Oderinde, M. S.; Frenette, M.; Robbins, D. W.; Aquila, B.; Johannes, J. W. Photoredox Mediated Nickel Catalyzed Cross Coupling of Thiols with Aryl and Heteroaryl Iodides via Thiyl Radicals. *J. Am. Chem. Soc.* **2016**, *138*, 1760–1763.

(b) Xu, T.; Zhou, X.; Xiao, X.; Yuan, Y.; Liu, L.; Huang, T.; Li, C.; Tang, Z.; Chen, T. Nickel-Catalyzed Decarbonylative Thioetherification of Carboxylic Acids with Thiols. *J. Org. Chem.* **2022**, *87*, 8672–8684.

(c) Liu, S.; Jin, S.; Wang, H.; Qi, Z.; Hu, X.; Qian, B.; Huang, H. Nickel-catalyzed oxidative dehydrogenative coupling of alkane with thiol for C(sp³)-S bond formation. *Tetrahedron Lett.* **2021**, *68*, 152950.

(15) Zhou, R.; Goh, Y. Y.; Liu, H.; Tao, H.; Li, L.; Wu, J. Visible Light-Mediated Metal-Free

Hydrosilylation of Alkenes through Selective Hydrogen Atom Transfer for Si-H Activation.

Angew. Chem., Int. Ed., **2017**, *56*, 16621.

(16) Seath, C. P., Vogt, D. B., Xu, Z., Boyington, A. J., & Jui, N. T. Radical Hydroarylation of Functionalized Olefins and Mechanistic Investigation of Photocatalytic Pyridyl Radical Reactions. *J. Am. Chem. Soc.*, **2020**, *140*, 15525–15534.

(17) Crossley, S. W. M., Obradors, C., Martinez, R. M., & Shenvi, R. A. Mn-, Fe-, and Co-Catalyzed Radical Hydrofunctionalizations of Olefins. *Chem. Rev.*, **2016**, *116*, 8912-9000.

(18) Kamijo, S., Takao, G., Kamijo, K., Hirota, M., Tao, K., & Murafuji, T. Photo-induced Substitutive Introduction of the Aldoxime Functional Group to Carbon Chains: A Formal Formylation of Non-Acidic C(sp³)–H Bonds. *Angew. Chem. Int. Ed.*, **2016**, *128*, 9847–9851.

(19) Combs, D. L., & Dehghani, A. (n.d.). Pyridine-Derived Triflating Reagents: An Improved Preparation of Vinyl Triflates from Metallo Enolates. *Tett. Let.*, **1992**, *33*, 6299-6302.

(20) Jiang, J., Fu, M., Li, C., Shang, R., & Fu, Y. Theoretical Investigation on Nickel-Catalyzed Hydrocarboxylation of Alkynes Employing Formic Acid. *Organometallics*, **2017**, *36*, 2818–2825.

(21) Fu, M. C., Shang, R., Cheng, W. M., & Fu, Y. Nickel-Catalyzed Regio- and Stereoselective Hydrocarboxylation of Alkynes with Formic Acid through Catalytic CO Recycling. *ACS Catal.*, **2016**, *6*, 2501–2505.

(22) Zhu, C., Yue, H., Jia, J., & Rueping, M. (2021). Nickel-Catalyzed C-Heteroatom Cross-Coupling Reactions under Mild Conditions via Facilitated Reductive Elimination. *Angew. Chem. Int. Ed.*, **2021**, *60*, 17810-17831.

(23) B. J. Shields, B. Kudisch, G. D. Scholes, A. G. Doyle, *J. Am. Chem. Soc.* 2018, 140, 3035 – 3039.

(24) E. B. Corcoran, M. T. Pirnot, S. Lin, S. D. Dreher, D. A. DiRocco, I. W. Davies, S. L. Buchwald, D. W. MacMillan. Aryl amination using ligand-free Ni(II) salts and photoredox catalysis. *Science*, **2016**, 353, 279 – 283.

(25) Terrett, J. A., Cuthbertson, J. D., Shurtleff, V. W., & MacMillan, D. W. C. Switching on elusive organometallic mechanisms with photoredox catalysis. *Nature*, **2015**, 524, 330–334.

Chapter 5 Supporting Information

S2.4 Supporting Information

S2.4.1 General Information

A. General Reagent Information

Reagents were purchased from Sigma-Aldrich, Alfa Aesar, Acros Organics, Combi-Blocks, Oakwood Chemicals, Astatech, and TCI America and used as received, unless stated otherwise. All reactions were set up on the bench top and conducted under nitrogen atmosphere while subject to irradiation from blue LEDs (LEDwholesalers PAR38 Indoor Outdoor 16-Watt LED Flood Light Bulb, Blue; or Hydrofarm® PPB1002 PowerPAR LED Bulb-Blue 15W/E27 (available from Amazon). Flash chromatography was carried out using Siliaflash® P60 silica gel obtained from Silicycle. Thin-layer chromatography (TLC) was performed on 250 µm SiliCycle silica gel F-254 plates. Visualization of the developed chromatogram was performed by fluorescence quenching or staining using KMnO₄, p-anisaldehyde, or ninhydrin stains. DMSO was purchased from Fisher Scientific and was distilled over CaH₂ and degassed by sonication

under vacuum and stored under nitrogen. Photoredox catalyst 4CzIPN was prepared according to literature procedures.¹

B. General Analytical Information

Unless otherwise noted, all yields refer to chromatographically and spectroscopically (¹H NMR) homogenous materials. New compounds were characterized by NMR and HRMS. ¹H and ¹³C NMR spectra were obtained from the Emory University NMR facility and recorded on a Bruker Avance III HD 600 equipped with cryo-probe (600 MHz), Bruker 400 (400 MHz), INOVA 600 (600 MHz), INOVA 500 (500 MHz), INOVA 400 (400 MHz), or VNMR 400 (400 MHz), and are internally referenced to residual protio solvent signals. Data for ¹H NMR are reported as follows: δ chemical shift (ppm), multiplicity (s = singlet, d = doublet, t = triplet, q = quartet, m = multiplet, dd = doublet of doublets, dt = doublet of triplets, ddd = doublet of doublet of doublets, dtd = doublet of triplet of doublets, b = broad, etc.), coupling constant (Hz), integration, and assignment, when applicable. Data for decoupled ¹³C NMR are reported in terms of chemical shift and multiplicity when applicable. High Resolution mass spectra were obtained from the Emory University Mass Spectral facility.

C. General Photoredox Reaction Setup

To run multiple reactions, an appropriately sized 3D printed carousel was used, which exposed the reactions to the blue light evenly (photo 1). A 15 W LED array lamp was used as a blue light source (photo 2,3). These lamps were routinely used for up to 12 reactions at a time (photo 2,3). The blue LEDs were positioned approximately 6 inches above the reaction vials to get good light coverage without overheating the reactions (photo 2,3). Reactions run at elevated temperatures were irradiated in a shallow oil bath (photo 4,5).

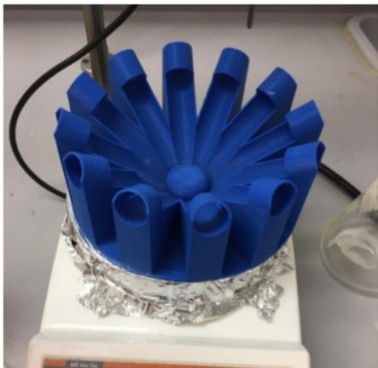


Photo 1



Photo 2



Photo 3

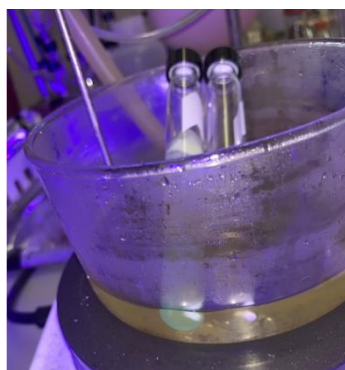


Photo 4



Photo 5

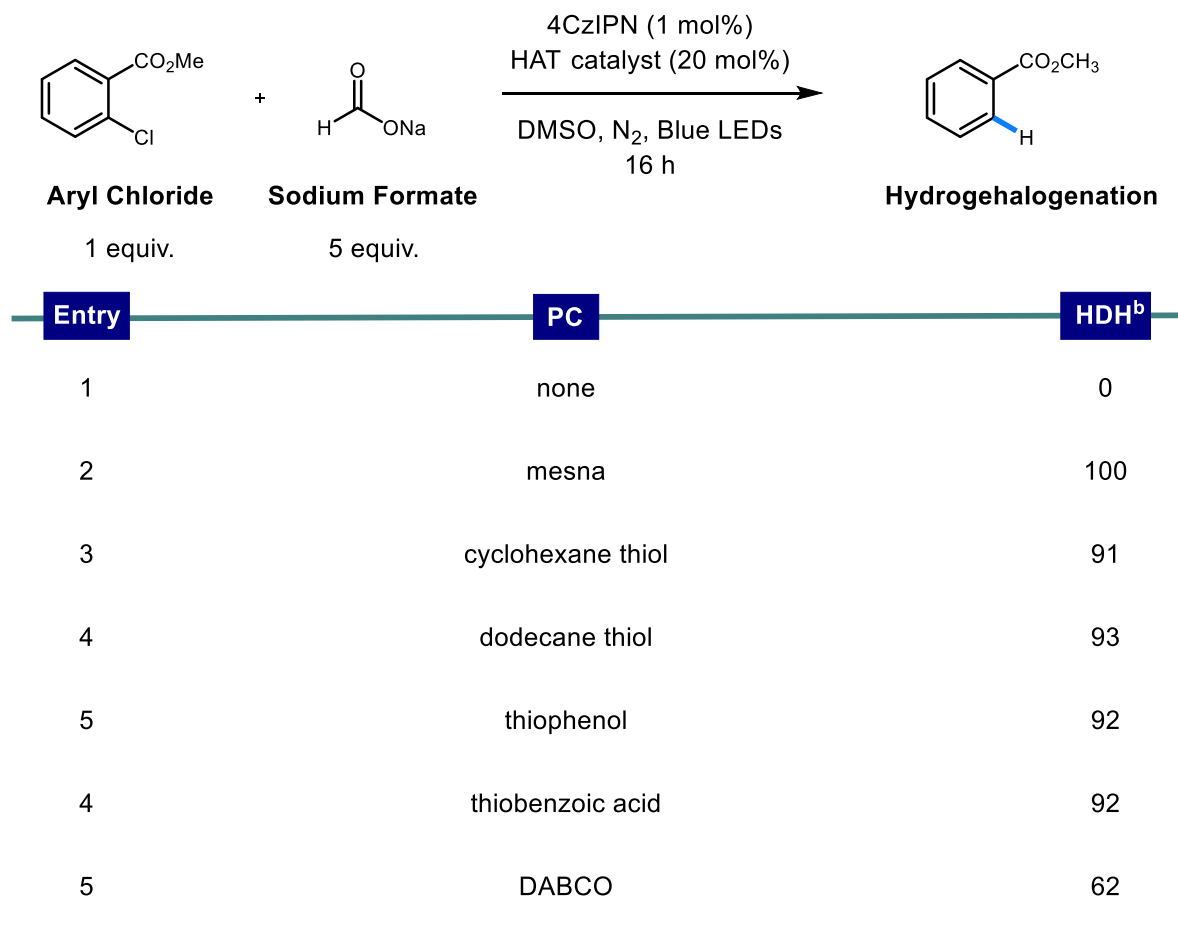
S2.4.2 Optimization of Hydrodehalogenation with CO_2^-

Procedure:

An 8 mL screw-top test tube was charged with 4CzIPN (1 mol%, 0.001 mol), sodium formate (5.0 equiv, 0.5 mmol) and mesna (20 mol%, 0.02 mol). The tube was equipped with a stir bar and sealed with a PTFE/silicon septum. Under nitrogen atmosphere, separately degassed DMSO (1 Photo 4 Photo 5 45 mL) was added via syringe, followed by 2-chloromethylbenzoate (1 equiv, 0.1 mmol). The resulting mixture was stirred at 1400 RPM for 16 h under irradiation by blue LEDs. The reaction was then extracted with ethyl acetate (3 x). The organic layer was passed through a small silica plug with 100% EtOAc and concentrated. Deutero-chloroform with an

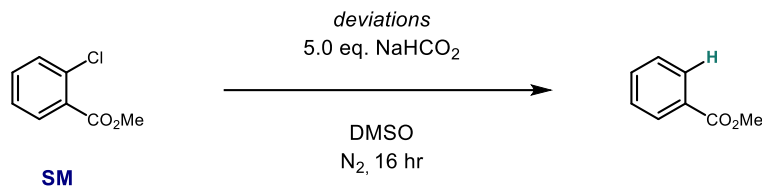
internal standard of dibromomethane (7 μ L, 0.1 mmol) was added. The sample was analyzed by ^1H NMR ($d = 5$ s), and the integral values were used to calculate the data given in Table S1- S3.

HAT Catalysts Screen:



^a Conditions: aryl chloride (1 equiv.), sodium formate (5 equiv.), photocatalyst (PC, 1 mol%), HAT catalyst (20 mol%), DMSO [0.1 M], N_2 , Blue LEDs, 16 h. Reactions performed on a 0.1 mmol scale. ^bYield determined via ^1H NMR using CH_2Br_2 as an internal standard.

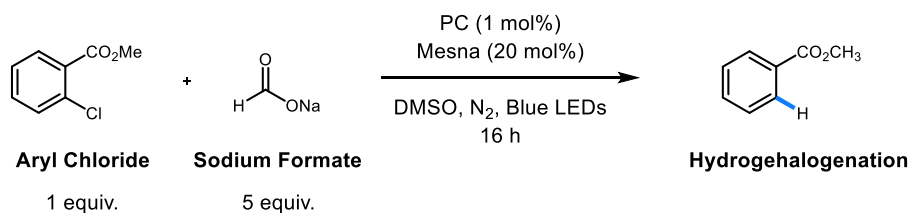
Controls



Entry	deviations	SM	HDH
1	no 4CzIPN	100	0
2	no formate	99	0
3	no light	102	0
4	in presence of air	3	94

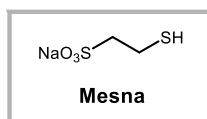
^a Conditions: aryl chloride (1 equiv.), sodium formate (5 equiv.), photocatalyst (PC, 1 mol%), Mesna (20 mol%), DMSO [0.1 M], N₂, Blue LEDs, 16 h. Reactions performed on a 0.1 mmol scale. ^bYield determined via ¹H NMR using CH₂Br₂ as an internal standard.

Photocatalyst Screen:



Entry	PC	HDH ^b
1	4CzIPN	98
2	4CzTPN	98
3	Ir(df-CF ₃ -ppy) ₂ (dtbbpy)PF ₆	99
4	Ir(ppy) ₂ (dtbbpy)PF ₆	98
5	DCA	90

^a Conditions: aryl chloride (1 equiv.), sodium formate (5 equiv.), photocatalyst (PC, 1 mol%), Mesna (20 mol%), DMSO [0.1 M], N₂, Blue LEDs, 16 h. Reactions performed on a 0.1 mmol scale. ^bYield determined via ¹H NMR using CH₂Br₂ as an internal standard.



S2.4.3: General Procedures

General Procedure A

A 20 mL screw-top test tube was charged with 4CzIPN (1 mol%), sodium formate (5.0 equiv), mesna (20 mol%), (hetero)aryl halide (if solid, 1.0 equiv) and alkene (if solid, 5.0 equiv). The tube was equipped with a stir bar and was sealed with a PTFE/silicon septum. The atmosphere was exchanged by applying vacuum and backfilling with nitrogen (this process was conducted a total of three times). Under nitrogen atmosphere, separately degassed solvents were added via syringe in a 1:1 ratio (50% MeCN/ 50% DMSO, 0.1 M) followed by the (hetero)aryl halide (if liquid, 1.0 equiv) and the alkene (if liquid, 1.0 equiv). The resulting mixture was stirred at 1400 RPM for 16 h under irradiation by blue LEDs. Water was added and then the reaction mixture was extracted with ethyl acetate (3 x). The organic layer was passed through a small silica plug with 100% EtOAc and concentrated. The residue was purified on silica using the indicated solvent mixture as eluent to afford the title compound.

General Procedure B

A 20 mL screw-top test tube was charged with 4CzIPN (1 mol%), sodium formate (5.0 equiv), mesna (20 mol%), and the phenyl ammonium salt (1.0 equiv). The tube was equipped with a stir bar and was sealed with a PTFE/silicon septum. The atmosphere was exchanged by applying vacuum and backfilling with nitrogen (this process was conducted a total of three times). Under nitrogen atmosphere, degassed DMSO (0.1 M) was added via syringe. The resulting mixture was stirred at 1400 RPM for 16 h under irradiation by blue LEDs. Water was added and then the 60 reaction mixture was extracted with ethyl acetate (3 x). The organic layer was passed through a small silica plug with 100% EtOAc and concentrated to afford the title compound.

General Procedure C

A 20 mL screw-top test tube was charged with 4CzIPN (1 mol%), sodium formate (10.0 equiv), mesna (20 mol%), and the N-tosyl (hetero)arene (1.0 equiv). The tube was equipped with a stir bar and was sealed with a PTFE/silicon septum. The atmosphere was exchanged by applying vacuum and backfilling with nitrogen (this process was conducted a total of three times). Under nitrogen atmosphere, a degassed solution of 20% H₂O/DMSO (0.1 M) was added via syringe. The resulting mixture was stirred at 1400 RPM for 16 h under irradiation by blue LEDs, unless noted otherwise. Water was added and then the reaction mixture was extracted with ethyl acetate (3 x). The organic layer was passed through a small silica plug with 100% EtOAc and concentrated. The residue was purified on silica using the indicated solvent mixture as eluent to afford the title compound.

General Procedure D

A 20 mL screw-top test tube was charged with 4CzIPN (1 mol%), sodium formate (10.0 equiv), mesna (20 mol%), and the trifluoromethyl- arene (if solid, 1.0 equiv). The tube was equipped with a stir bar and was sealed with a PTFE/silicon septum. The atmosphere was exchanged by applying vacuum and backfilling with nitrogen (this process was conducted a total of three times). Under nitrogen atmosphere, degassed DMSO (0.1 M) was added via syringe followed by trifluoromethyl arene (if liquid, 1.0 equiv) and buten-1-ol (3.0 equiv). The resulting mixture was stirred at 1400 RPM for 16 h under irradiation by blue LEDs, unless noted otherwise. Water was added and then the reaction mixture was extracted with ethyl acetate (3 x). The organic layer was passed through a small silica plug with 100% EtOAc and concentrated. The residue was purified on silica using the indicated solvent mixture as eluent to afford the title compound.

General Procedure E

A 20 mL screw-top test tube was charged with 4CzIPN (1 mol%), sodium formate (10.0 equiv), and mesna (20 mol). The tube was equipped with a stir bar and was sealed with a PTFE/silicon septum. The atmosphere was exchanged by applying vacuum and backfilling with nitrogen (this process was conducted a total of three times). Under nitrogen atmosphere, a degassed solution of 20% H₂O/DMSO (0.1 M) was added via syringe followed by the aldehyde (1.0 equiv). The resulting mixture was stirred at 1400 RPM for 16 h under irradiation by blue LEDs. Water was added and then the reaction mixture was extracted with ethyl acetate (3 x). The organic layer was passed through a small silica plug with 100% EtOAc and concentrated. The residue was purified on silica using the indicated solvent mixture as eluent to afford the title compound.

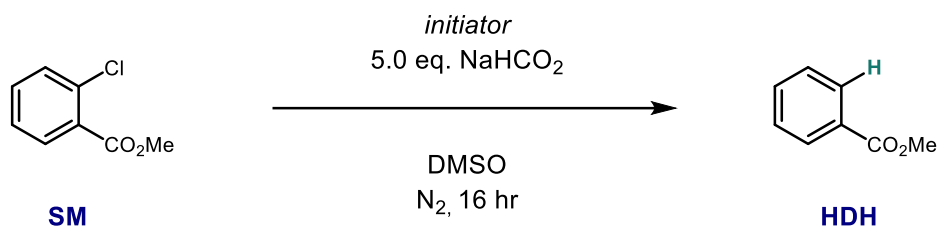
S2.4.4: Alternative Initiators

Procedure

An 8 mL screw-top test tube was charged with appropriate initiator (20 mol%, 0.02 mol), sodium formate (5.0 equiv, 0.5 mmol) and mesna (20 mol%, 0.02 mol, *if needed- refer to table below*). The tube was equipped with a stir bar and sealed with a PTFE/silicon septum. The atmosphere was exchanged by applying vacuum and backfilling with nitrogen (this process was conducted a total of three times). Under nitrogen atmosphere, separately degassed DMSO (0.1 M, 1 mL) was added via syringe, followed by 2-chloromethylbenzoate (1 equiv, 0.1 mmol) . The resulting mixture was stirred at 1400 RPM for 16 h under irradiation by blue LEDs or heated to 100 °C (*refer to table below*). The reaction was then extracted with ethyl acetate (3 x). The organic layer was passed through a small silica plug with 100% EtOAc to remove any excess DMSO and concentrated. Deutro-chloroform with an internal standard of dibromomethane (7 µL, 0.1 mmol)

was added. The sample was analyzed by ^1H NMR ($d = 5$ s), and the integral values were used to calculate the data given in Table S4.

Initiators:

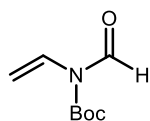


Entry	initiator	SM	HDH
1	20 mol% methyl disulfide, blue LEDs	0	99
2	20 mol% ammonium persulfate, 20 mol% mesna, 100 °C	0	96
3	20 mol% AIBN, 20 mol% mesna, 100 °C	50	48

yields determined by ^1H NMR with dibromomethane as internal standard

Table S4

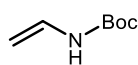
S2.4.5: Preparation of Starting Materials



Tert-butyl formyl(vinyl)carbamate (S1): To a round bottom flask under nitrogen was added di-tert-butyl decarbonate (15.7 g, 72 mmol, 1.2 equiv.), 4-dimethylaminopyridine (0.073 g, 0.6 mmol, 0.01 equiv.), freshly distilled N-vinylformamide (4.21 g, 60 mmol, 1 equiv.), and THF (200 mL). The reaction was stirred at 23 °C for 16 h and concentrated *in vacuo*. The crude product was purified by silica chromatography (5% EtOAc/hexanes as the eluent) to give the title compound as a clear oil (10.15 g, 99% yield). The physical properties and spectral data were consistent with the reported values.²

¹H NMR (600 MHz, Chloroform-d) δ 9.26 (s, 1H), 6.59 (dd, J = 16.3, 9.7 Hz, 1H), 5.67 (d, J = 16.2 Hz, 1H), 5.06 (d, J = 9.6 Hz, 1H), (s, 12 H).

Tert-butyl vinylcarbamate (S2): To a round bottom flask was added *tert*-butyl



formyl(vinyl)carbamate (7.19 g, 42 mmol, 1 equiv) followed by THF. The reaction mixture was cooled to 0 °C then a solution of 2M NaOH (25 mL) was added over a

period of 20 minutes. The reaction mixture was warmed to room temperature and monitored via

GCMS until complete consumption of starting material (1 hour). The reaction mixture was

diluted with H₂O (20 mL) and extracted with MTBE (4x). The combined organic extracts were

washed with H₂O (20 mL) and brine (20 mL), dried over MgSO₄, and concentrated *in vacuo*.

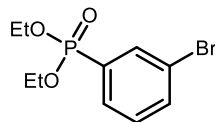
The crude product was recrystallized in pentanes at -20°C overnight to afford the title compound

as a crystalline white solid (4.94 g, 82% yield). The physical properties and spectral data were

consistent with the reported values.²

¹H NMR (600 MHz, DMSO-d₆) δ (9.20, s, 1H), 6.51 (ddd, J = 15.9, 10.4, 8.9 Hz, 1H), 4.45 (d, J = 15.9 Hz, 1H), 4.09 (d, J = 8.9 Hz, 1H), 1.41 (s, 9H).

Diethyl (3-bromophenyl)phosphonate (S3): Pd(OAc)₂ (0.224 g, 1 mmol, 0.1 equiv) was added



to a flame dried round bottom flask and the atmosphere was exchanged three times with N₂. 3-bromoiodobenzene (10 mmol, 1.27 mL, 1 equiv) was then

added followed by triethyl phosphite (10.5 mmol, 1.8 mL, 1.05 equiv) and the reaction was

heated to 90 °C overnight under N₂. After cooling to room temperature, the reaction mixture was

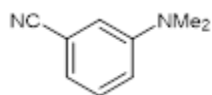
diluted with Et₂O and pushed through a celite plug using Et₂O (50 mL). The crude reaction

mixture was then concentrated *in vacuo* and purified by silica chromatography (50- 100%

EtOAc/Hexanes as the eluent) to afford the title compound as a red-orange oil (1.7 g, 58% yield).

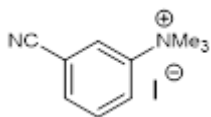
The spectral data were consistent with the reported values.³

¹H NMR (500 MHz, Chloroform-*d*) δ 7.94 (ddd, $J = 13.6, 1.9, 1.4$ Hz, 1H), 7.73 (ddd, $J = 12.9, 7.6, 1.2$ Hz, 1H), 7.67 (ddd, $J = 8.1, 2.1, 1.0$ Hz, 1H), 7.34 (td, $J = 7.8, 4.7$ Hz, 1H), 4.11 (m, 4H), 1.32 (t, $J = 7.1$ Hz, 6H).



3-(dimethylamino)benzonitrile (S4): A round bottom flask equipped with a stirbar was added 3-aminobenzonitrile (10 mmol, 1.2 g, 1.0 equiv), Na₂CO₃ (20 mmol, 2.1 g, 2.0 equiv) and DMF (10 mL). Methyl Iodide (25 mmol, 1.6 mL, 2.5 equiv) was added dropwise to the solution a few minutes later. The reaction was heated to 80 °C and stirred overnight. The reaction was allowed to cool to room temp. and it was diluted in EtOAc. The solution was washed with a solution of 1 M LiCl, extracted with EtOAc (3 x), dried over Na₂SO₄ and concentrated *in vacuo*. The crude reaction mixture was pushed through a silica plug (10% EtOAc/hexanes) to afford the title compound as an orange oil (1.0 g, 69% yield). The spectral properties were consistent with the reported values.⁴

¹H NMR (500 MHz, Chloroform-*d*) δ 7.32 – 7.26 (m, 1H), 6.95 (dt, $J = 7.5, 1.1$ Hz, 2H), 6.91 – 6.82 (m, 1H), 2.98 (s, 6H).



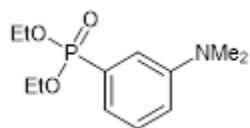
3-cyano-N,N,N-trimethylbenzenaminium iodide (S5): A round bottom flask equipped with a stir bar was added methyl 3-(dimethylamino)benzonitrile S4 (6.0 mmol, 0.88 g, 1.0 equiv) and DMF (4 mL). Methyl Iodide (12 mmol, 0.74 mL, 2.0 equiv) was added dropwise. The reaction was heated to 50 °C and stirred overnight. The reaction was allowed to cool to room temp. and it was diluted with Et₂O. The

solid precipitate was collected by vacuum filtration to afford the title compound as a white solid (1.26 g, 73% yield).

¹H NMR (500 MHz, DMSO-*d*₆) δ 8.58 (dd, *J* = 2.4, 1.3 Hz, 1H), 8.34 (ddd, *J* = 8.7, 2.8, 0.9 Hz, 1H), 8.15 – 8.06 (m, 1H), 7.90 – 7.85 (m, 1H), 3.64 (s, 9H).

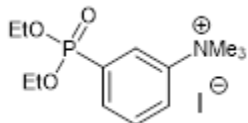
¹³C NMR (151 MHz, DMSO-*d*₆) δ 147.43, 133.94, 131.33, 125.86, 125.13, 117.47, 112.81, 56.47.

HRMS (APCI) *m/z*: [M⁺] calcd. for C₁₀H₁₃N₂, 161.0709; found, 161.0711. [M⁻] calcd. for I, 126.9050; found, 126.9057.



diethyl (3-(dimethylamino)phenyl)phosphonate (S6): A pressure tube equipped with a stirbar was added 3-(dimethylamino)benzoic acid (5.0 mmol, 0.83 g, 1.0 equiv), Pd(OAc)₂ (0.25 mmol, 0.056 g, 5 mol%) and 1,4-Bis(diphenylphosphino)butane (0.5 mmol, 0.213 g, 10 mol%). The atmosphere was exchanged by applying vacuum and backfilling with nitrogen (this process was conducted a total of three times). Diethyl phosphonate (7.5 mmol, 0.97 mL, 1.5 equiv), trimethylacetic anhydride (7.5 mmol, 0.83 mL, 1.5 equiv), and triethyl amine (7.5 mmol, 1.0 mL, 1.5 equiv) was added to the tube under nitrogen followed by degassed 1,4-dioxane (25 mL). The reaction was heated to 160 °C and allowed to stir overnight. The reaction was cooled to room temperature and concentrated *in vacuo*. The crude reaction mixture was purified by silica chromatography (30- 100% EtOAc eluent) to give the title compound as an opaque yellow oil (0.83 g, 65% yield). The spectral properties were consistent with the reported values.⁵

^1H NMR (400 MHz, Chloroform-*d*) δ 7.36 – 7.26 (m, 1H), 7.20 – 7.05 (m, 2H), 6.87 (d, $J = 8.4$ Hz, 1H), 4.20 – 3.99 (m, 4H), 2.98 (s, 6H), 1.32 (t, $J = 7.1$ Hz, 6H).



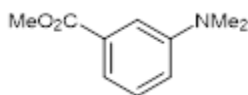
3-(diethoxyphosphoryl)-N,N,N-trimethylbenzenaminium iodide (S7): A round bottom flask equipped with a stir bar was added diethyl (3-(dimethylamino)phenyl)phosphonate **S6** (2.0 mmol, 0.51 g, 1.0 equiv) and DMF (1.5 mL). Methyl Iodide (4 mmol, 0.25 mL, 2.0 equiv) was added dropwise. The reaction was heated to 50 °C and stirred overnight. The reaction was allowed to cool to room temp. and it was diluted with Et₂O. The solid precipitate was collected by vacuum filtration to give the title compound as a white solid (0.65 g, 81% yield).

^1H NMR (400 MHz, Methanol-*d*₄) δ 8.26 (dd, $J = 14.8, 3.3$ Hz, 2H), 8.02 (ddt, $J = 12.7, 7.5, 1.0$ Hz, 1H), 7.94 – 7.83 (m, 1H), 4.31 – 4.12 (m, 4H), 3.77 (s, 9H), 1.38 (t, $J = 7.1$ Hz, 6H).

^{13}C NMR (151 MHz, Methanol-*d*₄) δ 148.80 (d, $J = 18.9$ Hz), 134.72 (d, $J = 8.9$ Hz), 132.56 (d, $J = 15.7$ Hz), 132.52 (d, $J = 192.1$ Hz), 124.15 (d, $J = 12.7$ Hz), 64.56 (d, $J = 6.0$ Hz), 57.84, 16.64 (d, $J = 6.1$ Hz).

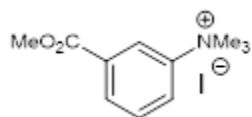
^{31}P NMR (162 MHz, Methanol-*d*₄) δ 15.49.

HRMS (APCI) m/z : [M^+] calcd. for C₁₃H₂₃NO₃P, 272.1410; found, 272.1410. [M^-] calcd. for I, 126.9050; found, 126.9056.



methyl 3-(dimethylamino)benzoate (S8): To a round bottom flask equipped with a stirbar was added 3-(dimethylamino)benzoic acid (20 mmol, 3.3 g, 1.0 equiv) and MeOH (20 mL). A few drops of concentrated HCl was added and the reaction was refluxed overnight and then concentrated *in vacuo*. The crude product was diluted in EtOAc and washed with sat. NaHCO₃ (3 x), dried over Na₂SO₄ and concentrated *in vacuo*. The crude reaction mixture was pushed through a silica plug (5% EtOAc) to give the title compound as a clear oil (1.7 g, 47% yield). .) The physical and spectral properties were consistent with the reported values.⁶

¹H NMR (500 MHz, Chloroform-*d*) δ 7.42 – 7.36 (m, 2H), 7.29 (t, *J* = 7.8 Hz, 1H), 6.91 (d, *J* = 7.8 Hz, 1H), 3.90 (s, 3H), 3.00 (s, 6H).

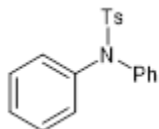


3-(methoxycarbonyl)-N,N,N-trimethylbenzenaminium iodide (S9): A round bottom flask equipped with a stir bar was added methyl 3-(dimethylamino)benzoate **S8** (9.0 mmol, 1.6 g, 1.0 equiv) and DMF (7 mL). Methyl Iodide (15 mmol, 0.93 mL, 1.5 equiv) was added dropwise. The reaction was heated to 50 °C and stirred overnight. The reaction was allowed to cool to room temp. and it was diluted with Et₂O. The solid precipitate was collected by vacuum filtration to give the title compound as a white solid (2.4 g, 84% yield).

¹H NMR (400 MHz, DMSO-*d*₆) δ 8.43 (dd, *J* = 2.8, 1.4 Hz, 1H), 8.30 (ddd, *J* = 8.6, 2.9, 0.9 Hz, 1H), 8.14 (ddd, *J* = 7.8, 1.4, 0.9 Hz, 1H), 7.82 (t, 1H), 3.92 (s, 3H), 3.66 (s, 9H).

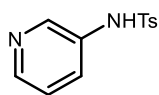
¹³C NMR (101 MHz, DMSO-*d*₆) δ 165.03, 147.48, 131.29, 130.83, 130.60, 125.55, 121.14, 56.40, 52.81.

HRMS (APCI) m/z : $[M^+]$ calcd. for $C_{11}H_{16}NO_2$, 194.0812; found, 194.0813. $[M^-]$ calcd. for I, 126.9050; found, 126.9056.



4-methyl-N,N-diphenylbenzenesulfonamide (S10): A round bottom flask was charged with diphenylamine (0.68 g, 4 mmol, 1 equiv.) and pyridine (10 mL). The reaction mixture was then cooled to 0 °C followed by the addition of toluenesulfonyl chloride (1.14 g, 6 mmol, 1.5 equiv). The reaction mixture was warmed to room temperature, stirred overnight, and then concentrated *in vacuo*. The reaction mixture was then diluted with water (10 mL) extracted with CH_2Cl_2 (3x), dried over Na_2SO_4 and concentrated *in vacuo*. The crude product was purified by silica chromatography (0- 10% EtOAc/Hexanes as the eluent) to give the title compound as a white solid (0.43 g, 36% yield). The physical and spectral properties were consistent with the reported values.⁷

1H NMR (600 MHz, Chloroform-*d*) δ 7.58 (d, J = 6.7 Hz, 2H), 7.35 – 7.22 (m, 12H), 2.43 (s, 3H).¹

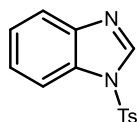


4-methyl-N-(pyridine-3-yl)benzenesulfonamide (S11): A round bottom flask was charged with 3-aminopyridine (10 mmol, 0.94 g, 1 equiv.), pyridine (25 mL) and cooled to 0 °C. The reaction mixture was then treated with toluenesulfonyl chloride (11 mmol, 2.09 g, 1.1 equiv), equipped with a reflux condenser and refluxed at 115 °C for 3 hours. After cooling to room temperature, the reaction mixture was concentrated *in vacuo*, diluted with water (20 mL), and extracted with CH_2Cl_2 (3 x). The crude product was purified by silica chromatography (10- 100%

EtOAc/hexanes as the eluent) to give the title compound as a white solid (0.33 g, 13% yield).

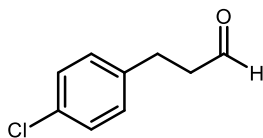
The physical and spectral properties were consistent with the reported values.⁸

¹H NMR (400 MHz, DMSO-d₆): δ 10.49 (bs, 1H), 8.26 (d, J = 2.6 Hz, 1H), 8.23 (dd, J = 4.7, J = 1.5 Hz, 1H), 7.65 (d, J = 8.3 Hz, 2H), 7.48 (ddd, J = 8.3, 2.7, 1.5 Hz, 1H), 7.35 (d, J = 8.1 Hz, 1H), 7.27 (dd, J = 8.3, 4.7 Hz, 1H), 2.33 (s, 3H).



1-tosyl-1H-benzo[d]imidazole (S12): A round bottom flask was charged with benzimidazole (0.47 g, 4 mmol, 1 equiv.) and pyridine (10 mL). The reaction mixture was then cooled to 0°C followed by the addition of toluenesulfonyl chloride (1.14 g, 6 mmol, 1.5 equiv.). The reaction mixture was warmed to room temperature, stirred overnight, and then concentrated *in vacuo*. The reaction mixture was then diluted with water (10 mL) extracted with CH₂Cl₂ (3 x), dried over Na₂SO₄ and concentrated *in vacuo*. The crude product was purified by silica chromatography (10- 100% EtOAc/Hexanes as the eluent) to give the title compound as a white solid (0.78 g, 72% yield). The physical and spectral properties were consistent with the reported values.⁹

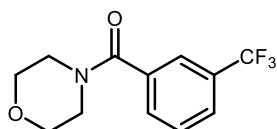
¹H NMR (600 MHz, Chloroform-d) δ 8.39 (s, 1H), 7.86 (m, 3H), 7.76 (m, 1H), 7.37 (m, 2H), 7.30 (m, 2H), 2.38 (s, 3H).



3-(4-chlorophenyl)propanal (S13): To a round bottom flask was added 3-(4-chlorophenyl)propan-1-ol (10 mmol, 1.5 mL, 1 equiv), [Cu(CH₃CN)₄]PF₆ (0.5 mmol, 0.19 g, 0.05 equiv.), TEMPO (0.5 mmol, 0.078 g, 0.05 equiv.), 2,2-bipyridine (0.5 mmol, 0.078 g, 0.05

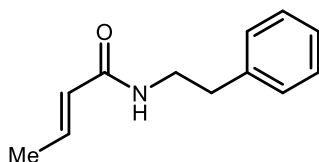
equiv), NMI (1 mmol, 80 μ L, 0.1 equiv) and CH₃CN (50 mL). The reaction was then sparged with air overnight then pushed through a silica plug using EtOAc and concentrated *in vacuo*. The crude product was then purified by silica chromatography (0-30% EtOAc/Hexanes as the eluent) to give the title compound as a light yellow oil (0.519 g, 31% yield.) The physical and spectral properties were consistent with the reported values.¹⁰

¹H NMR (400 MHz, Chloroform-d) δ 9.80 (t, J = 1.3 Hz, 1H), 7.27-7.21 (m, 2H), 7.15-7.08 (m, 2H), 2.96-2.87 (m, 2H), 2.80-2.73 (m, 2H).



morpholino(3-(trifluoromethyl)phenyl)methanone (S14): A round bottom flask equipped with a stir bar was added morpholine (11 mmol, 0.95 mL, 1.1 equiv), triethylamine (12.5 mmol, 1.7 g, 1.25 equiv) and CH₂Cl₂ (20 mL) and stirred for 10 minutes. 3-(trifluoromethyl)benzoyl chloride (10 mmol, 1.5 mL, 1.0 equiv) was added dropwise and the solution was allowed to stir for 1 hour. The reaction mixture was quenched with 1 M HCl, extracted with CH₂Cl₂ (3 x), and concentrated *in vacuo*. The crude reaction mixture was pushed through a silica plug (50% EtOAc/hexanes as the eluent) and concentrated *in vacuo* to afford the title compound as a white solid (2.3 g, 90% yield). The spectral properties were consistent with the reported values.¹¹

¹H NMR (600 MHz, Chloroform-d) δ 7.70 (d, J = 11.7 Hz, 2H), 7.62 – 7.53 (m, 2H), 3.99 – 3.30 (m, 8H).



(E)-N-phenethylbut-2-enamide (S15): To a flame dried round bottom flask was added crotonic acid (5 mmol, 0.43 g, 1 equiv) after which the atmosphere was exchanged three times with nitrogen. CH₂Cl₂ (20 mL) was then added followed by oxalyl chloride (5.5 mmol, 0.46 mL, 1.5 equiv) and DMF (2 drops)—the reaction mixture was then allowed to stir for 1 hour.

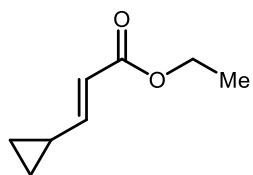
Phenethylamine (6 mmol, 0.76 mL, 1.2 equiv) was then added in one portion followed by triethylamine (5.5 mmol, 0.77 mL, 1.1 equiv). The reaction mixture was allowed to stir overnight, diluted with CH₂Cl₂ (20 mL) and 1M HCl (10 mL). The organic phase was separated from the aqueous phase and washed with 1M HCl (10 ml), brine (2x), dried over Na₂SO₄, and concentrated *in vacuo*. The crude product was pushed through a silica plug with (50% EtOAc/Hexanes as the eluent) to afford the title compound as white solid (0.96 g, 99% yield).

¹H NMR (600 MHz, Chloroform-d) δ 7.31 (t, J = 7.6 Hz, 1H), 7.24 (t, J = 7.9 Hz, 2H), 7.20 (d, J = 7.3 Hz, 2H), 6.83 (dq, J = 15.2, 6.9 Hz, 1H), 5.72 (dd, J = 15.2 Hz, 1.6 Hz, 1H), 5.39 (bs, 1H), 3.59 (td, J = 6.9 Hz, 5.9 Hz, 2H), 2.84 (t, J = 6.9 Hz, 2H), 1.83 (dd, J = 6.9, 1.6 Hz, 3H).

¹³C NMR (600 MHz, Chloroform-d) δ 165.9, 140.5, 138.5, 128.8, 128.7, 125.9, 124.9, 40.53, 35.7, 17.2.

HRMS (APCI) *m/z*: [M+H] calcd. for C₁₂H₁₆NO, 190.1226; found, 190.1229.

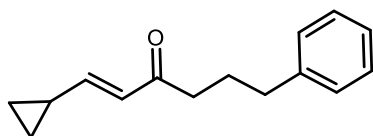
Rf: 0.34 (50% EtOAc/Hexanes)



Ethyl (E)-3-cyclopropylacrylate (S16): To a flame dried round bottom flask was added sodium hydride (3.6 mmol, 0.14 g, 1.2 equiv) after which the atmosphere was exchanged three times

with N₂. THF was added (5 mL) and the flask was then cooled to 0 °C followed by the dropwise addition of triethyl phosphonoacetate (3.3 mmol, 0.65 mL, 1.2 equiv). The reaction mixture was then stirred at 0 °C for thirty minutes after which cyclopropane carboxaldehyde (3 mmol, 0.22 mL, 1 equiv) was added dropwise as a solution in THF (5 mL). The reaction mixture was then allowed to warm to room temperature, stirred overnight, and then quenched with saturated aqueous ammonium chloride (10 mL) at 0 °C. The aqueous phase was extracted with EtOAc (3x) dried over Na₂SO₄, and concentrated *in vacuo*. The crude product was then pushed through a silica plug using (10% EtOAc/Hexanes as the eluent) to afford the title compound as yellow oil (0.42 g, 99% yield). The physical and spectral properties were consistent with the reported values.¹²

¹H NMR (600 MHz, Chloroform-d) δ 6.41 (dd, J = 15.4 Hz, 10.1 Hz, 1H), 5.89 (d, J = 15.4 Hz, 1H), 4.17 (q, J = 10.7 Hz, 2H), 1.58-1.53 (m, 1H), 1.26 (t, J = 7.1 Hz, 3H), 0.95-0.91 (m, 2H), 0.65-0.61 (m, 2H).



(E)-1-cyclopropyl-6-phenylhex-1-en-3-one (S17): To a flame dried round bottom flask was added 1-(triphenylphosphoraneylidene)-2-propanone (4 mmol, 1.27 g, 1 equiv) after which the atmosphere was exchanged three times with nitrogen followed. THF was added (30 mL), the reaction mixture was cooled to -78°C and n-butyllithium (5.2 mmol, 2.5 mL, 1.3 equiv.) was added dropwise. The reaction mixture was stirred at -78°C for 1 hour followed by the dropwise addition of (2-bromoethyl)benzene (5.2 mmol, 0.71 mL, 1.3 equiv). The reaction mixture was warmed to room temperature, stirred for 7 hours, and concentrated *in vacuo*. The crude mixture was then dissolved in CH₂Cl₂ (40 mL), washed with water (3x), dried over Na₂SO₄ and

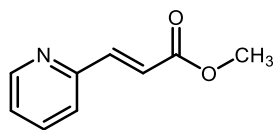
concentrated *in vacuo*. The crude reaction mixture was then dissolved in CHCl_3 followed by the addition of cyclopropane carboxaldehyde (6 mmol, 0.45 mL, 1.5 equiv.). The reaction mixture was refluxed overnight at 60 °C, concentrated *in vacuo*, and purified by silica chromatography (0-5% EtOAc/ Hexanes as the eluent) to give the title compound as a colorless oil (0.35 g, 41% yield).

^1H NMR (600 MHz, Chloroform-*d*) δ 7.28-7.22 (m, 2H), 7.19-7.13 (m, 3H), 6.27-6.14 (m, 2H), 2.61 (t, $J = 7.6$ Hz, 2H), 2.47 (t, $J = 6.8$ Hz, 2H), 1.96-1.88 (m, 2H), 1.55-1.48 (m, 1H), 0.98-0.91 (m, 2H), 0.64-0.59 (m, 2H).

^{13}C NMR (151 MHz, Chloroform-*d*) δ 199.65, 152.58, 141.92, 128.65, 128.49, 127.34, 126.03, 77.37, 77.16, 76.95, 39.59, 35.33, 25.95, 14.78, 9.08.

HRMS (APCI) m/z : $[\text{M}+\text{H}]$ calcd. for $\text{C}_{15}\text{H}_{19}\text{O}$, 215.1430; found, 215.1233.

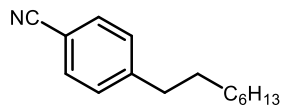
Rf: 0.48 (10% EtOAc/Hexanes)



Methyl (*E*)-3-(pyridine-2-yl)acrylate (S18): A round bottom flask was equipped with 2-pyridinecarboxaldehyde (5 mmol, 0.48 mL, 1 equiv), methyl (triphenylphosphoranylidene)acetate (7.5 mmol, 2.50 g, 1.5 equiv) and benzene (10 mL) under nitrogen. The reaction was then heated to 80 °C for three hours, cooled to room temperature, and concentrated *in vacuo*. The crude product was purified by silica chromatography (30- 40% EtOAc/Hexanes as the eluent) to give the title compound as a light brown solid (0.59 g, 73% yield). The physical properties and spectral data were consistent with the reported values.¹³

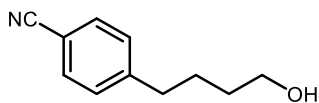
^1H NMR (600 MHz, CDCl_3) δ 8.64 (d, $J = 4.8$ Hz, 1H), 7.73-7.64 (m, 2H), 7.42 (d, $J = 7.8$ Hz, 1H), 7.29-7.24 (m, 1H), 6.93 (d, $J = 15.7$ Hz, 1H), 3.81 (s, 3H).

2.4.6: Preparation of Substrates from the Substrate Table



4-octylbenzonitrile (1): Prepared according to general procedure A using 4-chlorobenzonitrile (0.5 mmol, 0.069 g, 1 equiv.), 1-octene (2.5 mmol, 390 μ L, 5.0 equiv), sodium formate (2.5 mmol, 0.17 g, 5.0 equiv), mesna (0.1 mmol, 0.016 g, 20 mol%) and 4CzIPN (0.005 mmol, 0.0039 g, 1 mol%) in 0.1 M 50% MeCN/ DMSO (5 mL). After 16 hours the reaction was purified by silica chromatography (5% EtOAc/Hexanes as the eluent) to afford the title compound as a clear oil (0.071 g, 66% yield). The physical and spectral properties were consistent with the reported values.¹⁴

¹H NMR (500 MHz, Chloroform-d) δ 7.55 (d, J = 8.0 Hz, 2H), 7.25 (d, J = 8.0 Hz, 2H), 2.65 (t, J = 7.6 Hz, 2H), 1.60 (m, 2H), 1.35-1.16 (m, 10H), 0.87 (t, J = 6.8 Hz, 3H).



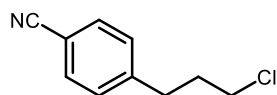
4-(4-hydroxybutyl)benzonitrile (2): Prepared according to general procedure A using 4-chlorobenzonitrile (0.5 mmol, 0.069 g, 1 equiv.), 3-buten-1-ol (2.5 mmol, 215 μ l, 5 equiv.), sodium formate (2.5 mmol, 0.17 g, 5.0 equiv.), mesna (0.1 mmol, 0.016 g, 20 mol%) and 4CzIPN (0.005 mmol, 0.0039 g, 1 mol%) in 0.1 M 50% MeCN/ DMSO (5 mL). After 16 hours, the crude product was purified by silica gel chromatography (30% EtOAc/Hexanes to 50% EtOAc:/Hexanes as the eluent) to afford the title compound as a colorless solid (0.040 g, 46% yield).

¹H NMR (500 MHz, Benzene-*d*6) δ 7.01 (d, J = 8.0 Hz, 2H), 6.56 (d, J = 8. Hz, 2H), 3.22 (t, J = 6.3 Hz, 2H), 2.13 (t, J = 7.6 Hz, 2H), 1.32-1.24 (m, 2H), 1.20-1.13 (m, 2H).

^{13}C NMR (100 MHz, Chloroform-d) δ 148.17, 132.27, 129.31, 119.23, 109.71, 62.57, 35.88, 32.18, 27.23.

HRMS (APCI) m/z : $[\text{M}+\text{H}]$ calcd. for $\text{C}_{11}\text{H}_{14}\text{NO}$, 176.1069; found, 176.1071.

Rf: 0.23 (30% EtOAc/Hexanes)



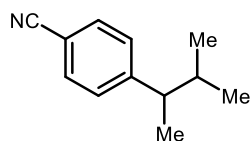
4-(6-chlorohexyl)benzonitrile (3): Prepared according to general procedure A using 4-chlorobenzonitrile (0.5 mmol, 0.069 g, 1.0 equiv), 6-chlorohex-1-ene (2.5 mmol, 0.33 mL, 5.0 equiv), sodium formate (2.5 mmol, 0.17 g, 5.0 equiv), mesna (0.1 mmol, 0.016 g, 20 mol%) and 4CzIPN (0.005 mmol, 0.0039 g, 1 mol%) in 0.1 M 50% MeCN/ DMSO (5 mL). After 16 hours the reaction was purified by silica chromatography (0%- 20% EtOAc/hexanes as eluent) to afford the title compound as a clear oil (0.094 g, 85% yield)

^1H NMR (400 MHz, Chloroform-d) δ 7.57 (d, J = 8.3 Hz, 2H), 7.27 (d, J = 6.9 Hz, 2H), 3.53 (t, J = 6.6 Hz, 2H), 2.71 – 2.58 (m, 2H), 1.82 – 1.70 (m, 2H), 1.64 (p, J = 7.6 Hz, 2H), 1.54 – 1.41 (m, 2H), 1.40 – 1.31 (m, 2H).

^{13}C NMR (101 MHz, Chloroform-d) δ 148.35, 132.44, 132.29, 129.31, 119.29, 109.73, 45.14, 36.07, 32.55, 30.89, 28.51, 26.74.

HRMS (APCI) m/z : $[\text{M}+\text{H}]$ calcd. for $\text{C}_{13}\text{H}_{17}\text{NCl}$, 222.1044; found, 222.1043.

Rf: 0.40 (10% EtOAc/ Hexanes)



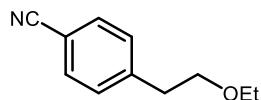
4-(3-methylbutan-2-yl)benzonitrile (4): Prepared according to general procedure A using 4-chlorobenzonitrile (0.5 mmol, 0.069 g, 1 equiv.), 2-methyl-2-butene (2.5 mmol, 265 μ l, 5 equiv.), sodium formate (2.5 mmol, 0.17 g, 5.0 equiv), mesna (0.1 mmol, 0.016 g, 20 mol%) and 4CzIPN (0.005 mmol, 0.0039 g, 1 mol%) in 0.1 M 50% MeCN/ DMSO (5 mL). After 16 hours, the crude product was purified by silica gel chromatography (5% EtOAc/Hexanes as the eluent) to afford the title compound as a light yellow oil (0.057 g, 66% yield).

^1H NMR (500 MHz, Benzene-*d*6) δ 7.01 (d, J = 8.0 Hz, 2H), 6.56 (d, J = 8.0 Hz, 2H), 1.99 (q, J = 7.2 Hz, 1H), 1.43-1.31 (m, 1H), 0.88 (d, J = 7.1 Hz, 3H), 0.71 (d, J = 6.7 Hz, 3H), 0.53 (d, J = 6.7 Hz, 3H).

^{13}C NMR (100 MHz, Chloroform-*d*) δ 152.95, 132.11, 128.56, 119.35, 109.69, 47.24, 34.41, 36.62, 21.17, 20.16, 18.60.

HRMS (APCI) m/z : [M+H] calcd. for $\text{C}_{12}\text{H}_{16}\text{N}$, 174.1277; found, 174.1277.

Rf: 0.66 (5% EtOAc/Hexanes)



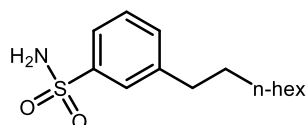
4-(2-ethoxyethyl)benzonitrile (5): Prepared according to general procedure A using 4-chlorobenzonitrile (0.5 mmol, 0.07 g, 1.0 equiv), ethyl vinyl ether (2.5 mmol, 0.24 mL, 5.0 equiv), sodium formate (2.5 mmol, 0.17 g, 5.0 equiv), mesna (0.1 mmol, 0.016 g, 20 mol%) and 4CzIPN (0.005 mmol, 0.0039 g, 1 mol%) in 0.1 M 50% MeCN/ DMSO (5 mL). After 16 hours the reaction was purified by silica chromatography (0%- 50% EtOAc/hexanes as eluent) to provide the title compound as a clear oil (0.070 g, 81% yield)

^1H NMR (500 MHz, Chloroform-*d*) δ 7.58 (d, J = 8.2 Hz, 2H), 7.34 (d, J = 8.1 Hz, 2H), 3.64 (t, J = 6.7 Hz, 2H), 3.48 (q, J = 7.0 Hz, 2H), 2.93 (t, J = 6.7 Hz, 2H), 1.18 (t, J = 7.0 Hz, 3H).

^{13}C NMR (151 MHz, Chloroform-d) δ 145.24, 132.25, 129.85, 119.22, 110.23, 70.57, 66.53, 36.62, 15.24.

HRMS (APCI) m/z : [M+H] calcd. for $\text{C}_{11}\text{H}_{14}\text{NO}$, 176.1069; found, 176.1070.

Rf: 0.25 (10% EtOAc/ Hexanes)



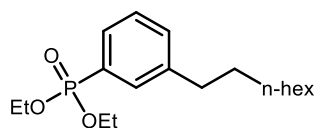
3-octylbenzenesulfonamide (6): Prepared according to general procedure A using 3-bromobenzenesulfonamide (0.5 mmol, 0.118 g, 1 equiv.), 1-octene (2.5 mmol, 390 μl , 5 equiv.), sodium formate (2.5 mmol, 0.17 g, 5.0 equiv.), mesna (0.1 mmol, 0.016 g, 20 mol%) and 4CzIPN (0.005 mmol, 0.0039 g, 1 mol%) in 0.1 M 50% MeCN/ DMSO (5 mL). After 16 hours, the crude product was purified by silica gel chromatography (30% EtOAc/Hexanes to 50% EtOAc/Hexanes as the eluent) to afford the title compound as a clear amorphous solid (0.068 g, 51% yield).

^1H NMR (500 MHz, Chloroform-d) δ 7.76-7.72 (m, 2H), 7.44-7.37 (m, 2H), 4.75 (s, 2H), 2.67 (t, $J = 7.8$ Hz, 2H), 1.66-1.58 (m, 2H), 1.36-1.21 (m, 10H), 0.88f (t, $J = 6.7$ Hz, 3H).

^{13}C NMR (101 MHz, Chloroform-d) δ 144.60, 141.91, 133.03, 129.15, 126.24, 123.80, 35.89, 31.97, 31.34, 29.51, 29.37, 29.33, 22.78, 14.23.

HRMS (APCI) m/z : [M+H] calcd. for $\text{C}_{14}\text{H}_{24}\text{NO}_3\text{S}$, 270.1522; found, 270.1515.

Rf: 0.75 (40% EtOAc/Hexanes)



Diethyl (4-octylphenyl)phosphonate (7): Prepared according to general procedure A using diethyl (3-bromophenyl)phosphonate **S3** (0.5 mmol, 0.147 g, 1 equiv.), 1-octene (2.5 mmol, 390 μ L, 5 equiv.), sodium formate (2.5 mmol, 0.17 g, 5.0 equiv.), mesna (0.1 mmol, 0.016 g, 20 mol%) and 4CzIPN (0.005 mmol, 0.0039 g, 1 mol%) in 0.1 M 50% MeCN/ DMSO (5 mL). After 16 hours, the crude product was purified by silica gel chromatography (15% EtOAc/Hexanes to 50% EtOAc/Hexanes as the eluent) to afford the title compound as a colorless oil (0.060 g, 37% yield).

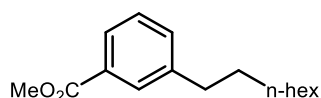
^1H NMR (500 MHz, Chloroform-*d*) δ 7.65-7.57 (m, 2H), 7.38-7.34 (m, 2H), 4.19-4.02 (m, 2H), 2.64 (t, $J = 7.7$ Hz, 2H), 1.65-1.58 (m, 2H), 1.35-1.22 (m, 10H), 0.87 (t, $J = 12.9$ Hz, 3H).

^{13}C NMR (151 MHz, Chloroform-*d*) δ 143.46 (d, $J = 14.5$ Hz), 132.67 (d, $J = 3.2$ Hz), 131.89 (d, $J = 10.2$ Hz), 129.13 (d, $J = 9.8$ Hz), 128.51 (d, $J = 15.6$ Hz), 128.21 (d, $J = 186.5$ Hz), 62.16 (d, $J = 5.4$ Hz), 35.92, 31.98, 31.46, 29.53, 29.39, 29.36, 22.78, 16.46 (d, $J = 6.5$ Hz), 14.21.

^{31}P NMR (243 MHz, Chloroform-*d*) δ 19.42

HRMS (APCI) m/z : [M+H] calcd. for $\text{C}_{18}\text{H}_{32}\text{O}_3\text{P}$, 327.2084; found, 327.2078.

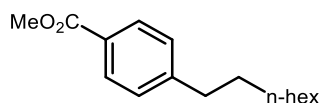
Rf: 0.62 (50% EtOAc/Hexanes)



Methyl 3-octylbenzoate (8): Prepared according to general procedure A using methyl 3-chlorobenzoate (0.5 mmol, 70 μ L, 1.0 equiv), 1-octene (2.5 mmol, 390 μ L, 5.0 equiv), sodium formate (2.5 mmol, 0.17 g, 5.0 equiv), mesna (0.1 mmol, 0.016 g, 20 mol%) and 4CzIPN (0.005 mmol, 0.0039 g, 1 mol%) in 0.1 M 50% MeCN/ DMSO (5 mL). After 16 hours, the crude product was pushed through a silica plug using EtOAc, concentrated *in vacuo*, and left under vacuum overnight to afford the title compound as a colorless oil (0.086 g, 69% yield). The

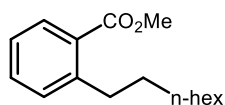
physical and spectral properties were consistent with the reported values.¹⁵

¹H NMR (500 MHz, Chloroform-d) δ 7.88-7.82 (m, 2H), 7.39-7.31 (m, 2H), 3.91 (s, 3H), 2.65 (t, J = 7.9 Hz 2H), 1.61 (m, 2H), 1.36-1.21 (m, 10H), 0.88 (t, J = 6.9 Hz , 3H).



Methyl-4-octylbenzoate (9): Prepared according to general procedure A using methyl 4-chlorobenzoate (0.5 mmol, 0.085 g, 1.0 equiv), 1-octene (2.5 mmol, 390 μ L, 5.0 equiv), sodium formate (2.5 mmol, 0.17 g, 5.0 equiv), mesna (0.1 mmol, 0.016 g, 20 mol%) and 4CzIPN (0.005 mmol, 0.0039 g, 1 mol%) in 0.1 M 50% MeCN/ DMSO (5 mL). After 16 hours, the crude product was pushed through a silica plug using EtOAc, concentrated *in vacuo*, and left under vacuum overnight to afford the title compound as a light yellow oil (0.093 g, 75% yield). The physical and spectral properties were consistent with the reported values.¹⁶

¹H NMR (500 MHz, Chloroform-d) δ 7.95 (d, J = 8.0 Hz, 2H), 7.24 (d, J = 8.0 Hz, 2H), 3.90 (s, 3H), 2.65 (t, J = 7.8 Hz 2H), 1.64-1.59 (m, 2H), 1.32-1.22 (m, 10H), 0.89 (t, J = 7.0 Hz , 3H).



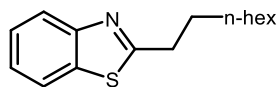
Methyl-2-octylbenzoate (10): Prepared according to general procedure A using methyl 2-chlorobenzoate (0.5 mmol, 72 μ l , 1 equiv.), 1-octene (2.5 mmol, 390 μ l, 5 equiv.), sodium formate (2.5 mmol, 0.17 g, 5.0 equiv.), mesna (0.1 mmol, 0.016 g, 20 mol%) and 4CzIPN (0.005 mmol, 0.0039 g, 1 mol%) in 0.1 M 50% MeCN/ DMSO (5 mL). After 16 hours, the crude product was purified by silica gel chromatography (5% EtOAc/Hexanes as the eluent) to afford the title compound as a colorless oil (0.040 g, 32% yield).

^1H NMR (500 MHz, Chloroform-*d*) δ 7.84 (dd, $J = 7.8, 1.5$ Hz, 2H), 7.41 (td, $J = 7.5, 1.3$ Hz, 2H), 3.89 (s, 3H), 2.93 (t, $J = 7.8$ Hz, 2H), 1.62-1.54 (m, 2H), 1.36-1.21 (m, 10H), 0.87 (t, $J = 7.04$ Hz, 3H).

^{13}C NMR (151 MHz, Chloroform-*d*) δ 168.41, 144.87, 131.91, 131.03, 130.66, 129.66, 125.77, 52.00, 34.61, 32.04, 31.98, 29.91, 29.63, 29.43, 22.82, 14.25.

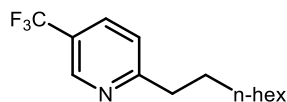
HRMS (APCI) m/z : [M+H] calcd. for $\text{C}_{16}\text{H}_{25}\text{O}_2$, 249.1849; found, 249.1851.

Rf: 0.59 (5% EtOAc/Hexanes).



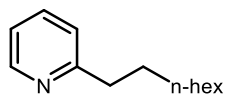
2-octylbenzo[*d*]thiazole (11): Prepared according to general procedure A at 100 °C using 2-bromobenzothiazole (0.5 mmol, 0.107 g, 1.0 equiv), 1-octene (2.5 mmol, 390 μL , 5.0 equiv), sodium formate (2.5 mmol, 0.17 g, 5.0 equiv), mesna (0.1 mmol, 0.016 g, 20 mol%) and 4CzIPN (0.005 mmol, 0.0039 g, 1 mol%) in 0.1 M 50% MeCN/ DMSO (5 mL). After 16 hours the reaction was purified by silica chromatography (5% EtOAc/Hexanes as the eluent) to afford the title compound as a yellow oil (0.099 g, 80% yield). The physical and spectral properties were consistent with the reported values.¹⁷

^1H NMR (500 MHz, Chloroform-*d*) δ 7.97 (dd, $J = 8.2, 1.2$ Hz, 1H), 7.83 (d, $J = 8.0, 1.3$ Hz, 1H), 7.44 (dt, $J = 8.3, 1.3$ Hz, 1H), 7.33 (dt, $J = 7.4, 1.2$ Hz, 1H), 3.11 (t, $J = 7.4$ Hz, 2H), 1.46-1.24 (m, 12H), 0.88 (t, $J = 6.9$ Hz, 3H).



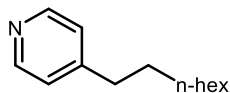
2-octyl-5-(trifluoromethyl)pyridine (12): Prepared according to general procedure A using 2-chloro-5-(trifluoromethyl)pyridine (0.5 mmol, 0.091 g, 1.0 equiv), 1-octene (2.5 mmol, 0.39 mL, 5.0 equiv), sodium formate (2.5 mmol, 0.17 g, 5.0 equiv), mesna (0.1 mmol, 0.016 g, 20 mol%) and 4CzIPN (0.005 mmol, 0.0039 g, 1 mol%) in 0.1 M 50% MeCN/ DMSO (5 mL). After 16 hours the reaction was purified by silica chromatography (0%- 50% EtOAc/hexanes as eluent) to provide the title compound as a clear oil (0.09 g, 70% yield). The spectral properties were consistent with the reported values.¹⁸

¹H NMR (400 MHz, Chloroform-*d*) δ 8.81 (d, $J = 2.4$ Hz, 1H), 7.84 (dd, $J = 8.2, 2.5$ Hz, 1H), 7.29 (d, $J = 8.2$ Hz, 1H), 2.92 – 2.78 (m, 2H), 1.76 (p, $J = 7.8$ Hz, 2H), 1.41 – 1.18 (m, 10H), 0.96 – 0.84 (m, 3H).



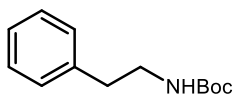
2-octylpyridine (13): Prepared according to general procedure A using 2-chloro-pyridine (0.25 mmol, 24 μ L, 1.0 equiv), 1-octene (1.25 mmol, 0.20 mL, 5.0 equiv), sodium formate (1.25 mmol, 0.085 g, 5.0 equiv), formic acid (1.25 mmol, 47 μ L, 5.0 equiv), mesna (0.05 mmol, 0.0082 g, 20 mol%) and 4CzIPN (0.0025 mmol, 0.0020 g, 1 mol%) in 0.1 M 50% MeCN/ DMSO (2.5 mL). After 16 hours the reaction was purified quenched with NaHCO₃ and extracted with EtOAc (3x). It was purified by silica chromatography (0%- 50% EtOAc/hexanes as eluent) to provide the title compound as a pale yellow oil (0.020 g, 43% yield). The spectral properties were consistent with the reported values.¹⁹

¹H NMR (600 MHz, Chloroform-*d*) δ 8.70 – 8.26 (m, 1H), 7.58 (td, $J = 7.6, 1.9$ Hz, 1H), 7.14 (d, $J = 7.8$ Hz, 1H), 7.09 (ddd, $J = 7.6, 4.9, 1.2$ Hz, 1H), 2.81 – 2.75 (m, 2H), 1.76 – 1.68 (m, 2H), 1.41 – 1.19 (m, 10H), 0.87 (t, $J = 7.0$ Hz, 3H).



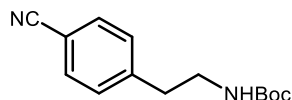
4-octylpyridine (14): Prepared according to general procedure A using 4-chloropyridin-1-ium chloride (0.5 mmol, 0.075 g, 1.0 equiv), 1-octene (2.5 mmol, 0.39 mL, 5.0 equiv), sodium formate (2.5 mmol, 0.17 g, 5.0 equiv), mesna (0.1 mmol, 0.016 g, 20 mol%) and 4CzIPN (0.005 mmol, 0.0039 g, 1 mol%) in 0.1 M 50% MeCN/ DMSO (5 mL). After 16 hours the reaction was purified quenched with NaHCO₃ and extracted with EtOAc (3x). It was purified by silica chromatography (10%- 50% EtOAc/hexanes as eluent) to provide the title compound as a yellow oil (0.056 g, 70% yield). The spectral properties were consistent with the reported values.²⁰

¹H NMR (500 MHz, Chloroform-*d*) δ 8.48 (d, J = 5.2 Hz, 2H), 7.10 (d, J = 4.4 Hz, 2H), 2.63 – 2.56 (m, 2H), 1.62 (p, J = 7.3 Hz, 2H), 1.48 – 1.12 (m, 10H), 0.88 (t, J = 6.9 Hz, 3H).



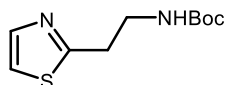
Tert-butyl phenethylcarbamate (15): Prepared according to general procedure A using bromobenzene (0.5 mmol, 53 μ L, 1.0 equiv), *tert*-butyl vinylcarbamate **S2** (1.5 mmol, 0.214 g, 3.0 equiv), sodium formate (2.5 mmol, 0.17 g, 5.0 equiv), mesna (0.1 mmol, 0.016 g, 20 mol%) and 4CzIPN (0.005 mmol, 0.0039 g, 1 mol%) in 0.1 M 50% MeCN/ DMSO (5 mL). After 16 hours the reaction was purified by silica chromatography (10- 15% EtOAc/Hexanes as the eluent) to afford the title compound as a white solid (0.082 g, 74% yield). The spectral properties were consistent with the reported values.²¹

¹H NMR (500 MHz, Chloroform-*d*) δ 7.32-7.28 (m, 2H), 7.24-7.17 (m, 3H), 3.42-2.32 (m, 2H), 2.80 (t, J = 7.0 Hz, 2H), 1.43 (s, 9H).



***Tert*-butyl (4-cyanophenethyl)carbamate (16):** Prepared according to general procedure A using 4-chlorobenzonitrile (0.5 mmol, 0.069 g, 1 equiv.) and *tert*-butyl vinylcarbamate **S2** (1.5 mmol, 0.214 g, 3 equiv.). The crude product was purified on silica gel (20:80 EtOAc:Hexanes to 30:70 EtOAc:Hexanes) to afford the title compound as a white solid (0.100 g, 81% yield). The physical and spectral properties were consistent with the reported values.²²

¹H NMR (500 MHz, Chloroform-*d*): δ 7.59 (d, J = 7.8 Hz 2H), 7.65-7.57 (m, 2H), 4.53 (br s, 1H) 3.43-3.34 (m, 2H), 2.89- 2.83 (m, 2H), 1.42 (m, 9H).



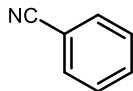
***Tert*-butyl (2-(thiazol-2-yl)ethyl) carbamate (17):** Prepared according to general procedure A using 2-bromothiazole (0.5 mmol, 45 μ l, 1 equiv.), *tert*-butyl vinylcarbamate **S2** (1.5 mmol, 0.214 g, 1 equiv.), sodium formate (2.5 mmol, 0.17 g, 5.0 equiv.), mesna (0.1 mmol, 0.016 g, 20 mol%) and 4CzIPN (0.005 mmol, 0.0039 g, 1 mol%) in 0.1 M 50% MeCN/ DMSO (5 mL). After 16 hours, the crude product was purified by silica gel chromatography (20% EtOAc/Hexanes to 50% EtOAc/Hexanes as the eluent) to afford the title compound as a yellow solid (0.112 g, 98% yield).

¹H NMR (500 MHz, Chloroform-*d*) δ 7.70 (d, J = 3.4 Hz, 1H), 7.23 (d, J = 3.3 Hz, 1H), 5.12 (s, 1H), 3.62-3.53 (m, 2H), 3.22 (t, J = 6.4 Hz, 2H), 1.44 (s, 9H).

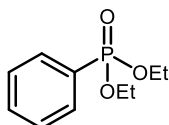
¹³C NMR (100 MHz, Chloroform-*d*) δ 168.11, 155.93, 142.56, 118.71, 79.43, 39.92, 33.41, 28.49.

HRMS (APCI) m/z : $[M+H]$ calcd. for $C_{10}H_{17}N_2O_2$, 229.1005; found, 229.1007.

Rf: 0.50 (40% EtOAc/Hexanes)

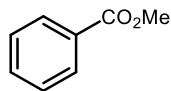


Benzonitrile (18): Prepared according to general procedure A 3-cyano-N,N,N-trimethylbenzenaminium iodide **S5** (0.25 mmol, 0.072 g, 1.0 equiv), sodium formate (1.25 mmol, 0.085 g, 5.0 equiv), mesna (0.05 mmol, 0.0082 g, 20 mol%) and 4CzIPN (0.0025 mmol, 0.0020 g, 1 mol%) in d_6 -DMSO (2.5 mL). After 16 hours the reaction was stopped and dibromomethane was added (0.25 mmol, 17.5 μ L, 1.0 equiv) as internal standard. The sample was analyzed by 1H NMR ($d = 5$ s), and the integral values were used to calculate the product yield (86% yield by NMR).



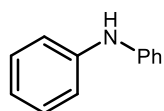
diethyl phenylphosphonate (19): Prepared according to general procedure A 3-(diethoxyphosphoryl)-N,N,N-trimethylbenzenaminium iodide **S7** (0.25 mmol, 0.099 g, 1.0 equiv), sodium formate (1.25 mmol, 0.085 g, 5.0 equiv), mesna (0.05 mmol, 0.0082 g, 20 mol%) and 4CzIPN (0.0025 mmol, 0.0020 g, 1 mol%) in 0.1 M 20% H_2O / DMSO (2.5 mL). After 16 hours the reaction was washed with water and extracted with EtOAc (3x) to provide the title compound with no extra purification needed as a tan oil (0.050 g, 94% yield). The spectral properties were consistent with the reported values.²³

¹H NMR (600 MHz, Chloroform-*d*) δ 7.81 (ddd, $J = 13.3, 8.3, 1.4$ Hz, 2H), 7.61 – 7.51 (m, 1H), 7.46 (td, $J = 7.5, 4.3$ Hz, 2H), 4.19 – 4.02 (m, 4H), 1.32 (t, $J = 6.8$ Hz, 6H).



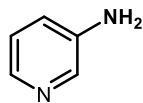
Methylbenzoate (20): Prepared according to general procedure A using 3-(methoxycarbonyl)-N,N,N-trimethylbenzenaminium iodide **S9** (0.5 mmol, 0.16 g, 1.0 equiv), sodium formate (2.5 mmol, 0.17 g, 5.0 equiv), mesna (0.1 mmol, 0.016 g, 20 mol%) and 4CzIPN (0.005 mmol, 0.0039 g, 1 mol%) in in 0.1 M DMSO (5 mL). After 16 hours the reaction was washed with water and extracted with EtOAc (3x) to provide the title compound with no extra purification needed as a yellow oil (0.047 g, 70% yield). The spectral properties were consistent with the reported values.²⁴

¹H NMR (600 MHz, Chloroform-*d*) δ 8.04 (d, $J = 7.1$ Hz, 2H), 7.56 (t, $J = 7.4$ Hz, 1H), 7.47 – 7.42 (m, 2H), 3.92 (s, 3H).

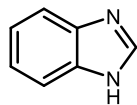


diphenyl amine (21): Prepared according to general procedure A at 100 °C 4-methyl-N,N-diphenylbenzenesulfonamide **S10** (0.5 mmol, 0.162 g, 1.0 equiv), sodium formate (5.0 mmol, 0.34 g, 5.0 equiv), mesna (0.1 mmol, 0.0164 g, 20 mol%) and 4CzIPN (0.0039 mmol, 0.0039 g, 1 mol%) in 0.1 M 20% H₂O/ DMSO (5 mL). After 16 hours the reaction was purified by silica chromatography (30%- 100% EtOAc/hexanes as eluent) to provide the title compound as an off white solid (0.044 g, 52% yield). The spectral properties were consistent with the reported values.²⁵

¹H NMR (600 MHz, Chloroform-*d*) δ 7.28 (d, $J = 7.3$ Hz, 4H), 7.08 (d, $J = 7.4$ Hz, 4H), 6.93 (t, $J = 7.4$ Hz, 2H), 5.71 (br s, 1H)

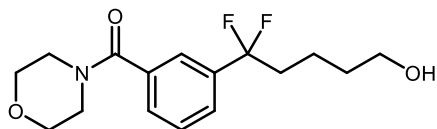


3-aminopyridine (22): Prepared according to general procedure A at 100 °C 4-methyl-*N*-(pyridine-3-yl)benzenesulfonamide **S11** (0.25 mmol, 0.062 g, 1.0 equiv), sodium formate (2.5 mmol, 0.17 g, 10.0 equiv), mesna (0.05 mmol, 0.0082 g, 20 mol%) and 4CzIPN (0.0025 mmol, 0.0020 g, 1 mol%) in 0.1 *d*₆-DMSO (2.5 mL). After 16 hours the reaction was stopped and dibromomethane was added (0.25 mmol, 17.5 μ L, 1.0 equiv) as internal standard. The sample was analyzed by ¹H NMR ($d = 5$ s), and the integral values were used to calculate the product yield (84% yield by NMR).



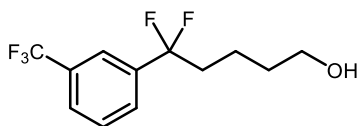
1H-benzo[d]imidazole (23): Prepared according to general procedure A 1-tosyl-1*H*-benzo[*d*]imidazole **S12** (0.25 mmol, 0.068 g, 1.0 equiv), sodium formate (1.25 mmol, 0.085 g, 5.0 equiv), mesna (0.05 mmol, 0.0082 g, 20 mol%) and 4CzIPN (0.0025 mmol, 0.0020 g, 1 mol%) in 0.1 M 20% H₂O/ DMSO (2.5 mL). After 16 hours the reaction was purified by silica chromatography (30%- 100% EtOAc/hexanes as eluent) to provide the title compound as an off white solid (0.024 g, 81% yield). The spectral properties were consistent with the reported values.²⁶

¹H NMR (600 MHz, Chloroform-*d*) δ 8.14 (s, 1H), 7.69 (br s, 2H), 7.31 (dd, $J = 6.1, 3.0$ Hz, 2H).



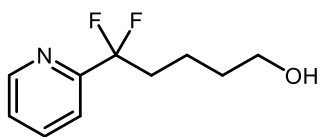
(3-(1,1-difluoro-5-hydroxypentyl)phenyl)(morpholino)methanone (24): Prepared according to general procedure A using morpholino(3-(trifluoromethyl)phenyl)methanone **S14** (0.5 mmol, 0.129 g, 1 equiv.) and 3-buten-1-ol (1.5 mmol, 130 μ l, 3 equiv.). The crude product was purified on silica gel (20:80 EtOAc:Hexanes to 30:70 EtOAc:Hexanes) to afford the title compound as a clear oil (0.078 g, 56% yield). The physical and spectral properties were consistent with the reported values.¹¹

¹H NMR (600 MHz, Chloroform-d): δ 7.55-7.43 (m, 4H), 3.78 (bs, 4H), 3.66-3.54 (m, 4H), 3.42 (bs, 2H), 2.23-2.04 (m, 2H), 1.73 (bs, 1H), 1.61-1.47 (m, 4H).



5,5-difluoro-5-(3-(trifluoromethyl)phenyl)pentan-1-ol (25): Prepared according to general procedure A using 1,3-bis(trifluoromethyl)benzene (0.5 mmol, 78 μ l, 1 equiv.) and 3-buten-1-ol (1.5 mmol, 130 μ l, 3 equiv.). The crude product was purified on silica gel (20:80 EtOAc:Hexanes to 40:60 EtOAc:Hexanes) to afford the title compound as a light yellow oil (0.073 g, 56% yield). The physical and spectral properties were consistent with the reported values.¹¹

¹H NMR (600 MHz, Chloroform-d): δ 7.78 (d, J = 7.9 Hz 2H), 7.30 (d, J = 7.9 Hz, 2H), 4.54 (br s, 1H), 3.42-3.33 (m, 2H), 2.89-2.82 (m, 2H), 1.42 (s, 9H).



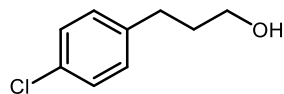
4,4-difluoro-4-(pyridine-2-yl)butan-1-ol (26): Prepared according to general procedure A at 100°C using 2-(trifluoromethyl)pyridine (0.5 mmol, 58 μ l, 1 equiv.) and 3-buten-1-ol (1.5 mmol, 130 μ l, 3 equiv.). The crude product was purified on silica gel (20:80 EtOAc:Hexanes to 30:70 EtOAc:Hexanes) to afford the title compound as a clear oil (0.031 g, 30% yield). The physical and spectral properties were consistent with the reported values.¹¹

¹H NMR (600 MHz, Chloroform-d): δ 8.66 (d, *J* = 4.8 Hz, 1H), 7.81 (t, *J* = 7.8 Hz, 1H), 7.64 (d, *J* = 7.9 Hz, 1H), 7.36 (t, *J* = 7.6 Hz, 1H), 3.66 (t, *J* = 6.3 Hz, 2H), 2.37 (dp, *J* = 16.5 Hz, *J* = 8.0 Hz, 2H), 1.66-1.50 (m, 4H).



Octanol (27): Prepared according to general procedure A using octanal (0.5 mmol, 78 μ L, 1.0 equiv), sodium formate (2.5 mmol, 0.17 g, 5.0 equiv), mesna (0.1 mmol, 0.016 g, 20 mol%) and 4CzIPN (0.005 mmol, 0.0039 g, 1 mol%) in 0.1 M 20% H₂O/ DMSO (5 mL). After 16 hours the reaction was purified by silica chromatography (5%- 30% EtOAc/hexanes as eluent) to provide the title compound as a yellow oil (0.057 g, 87% yield). The spectral properties were consistent with the reported values.²⁷

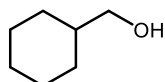
¹H NMR (500 MHz, Chloroform-d) δ 3.64 (t, *J* = 6.5 Hz, 2H), 1.56 (p, *J* = 6.7 Hz, 2H), 1.39 – 1.22 (m, 10H), 0.88 (t, *J* = 6.6 Hz, 3H).



3-(4-chlorophenyl)propanol (28): Prepared according to general procedure A using 3-(4-chlorophenyl)propanal **S13** (0.25 mmol, 0.042 g, 1.0 equiv), sodium formate (1.25 mmol, 0.085 g, 5.0 equiv), mesna (0.05 mmol, 0.0082 g, 20 mol%) and 4CzIPN (0.0025 mmol, 0.0020 g, 1 mol%) in 0.1 M 20% H₂O/ DMSO (2.5 mL). After 16 hours the reaction was purified by silica

chromatography (0%- 30% EtOAc/hexanes as eluent) to provide the title compound as a pale yellow oil (0.033 g, 80% yield). The spectral properties were consistent with the reported values.²⁸

¹H NMR (600 MHz, Chloroform-*d*) δ 7.25 (d, J = 8.3 Hz, 2H), 7.13 (d, J = 8.4 Hz, 2H), 3.66 (t, J = 6.4 Hz, 2H), 2.74 – 2.65 (m, 2H), 1.92 – 1.82 (m, 2H).



Cyclohexylmethanol (29): Prepared according to general procedure A using cyclohexanecarbaldehyde (0.5 mmol, 60 μ L, 1.0 equiv), sodium formate (2.5 mmol, 0.17 g, 5.0 equiv), mesna (0.1 mmol, 0.016 g, 20 mol%) and 4CzIPN (0.005 mmol, 0.0039 g, 1 mol%) in 0.1 M 20% H₂O/ DMSO (5 mL). After 16 hours the reaction was purified by silica chromatography (0%- 20% EtOAc/hexanes as eluent) to provide the title compound as a pale yellow oil (0.033 g, 80% yield). The spectral properties were consistent with the reported values.²⁹

¹H NMR (600 MHz, Chloroform-*d*) δ 3.44 (d, J = 6.4 Hz, 2H), 1.86 – 1.60 (m, 5H), 1.52 – 1.42 (m, 1H), 1.31 – 1.12 (m, 4H), 0.99 – 0.88 (m, 2H).

S2.4.7: Fluorescence Quenching Experiments

Fluorescence spectra is measured on a Horiba Fluoromax_Plus C. The sample is placed in a 1 cm pathlength cell. Quenching studies were conducted in DMSO with a photocatalyst (4CzIPN) concentration of 70 μ M with varying concentrations of quenchers (*refer to Table S5*). All samples were prepared and stored under a nitrogen atmosphere. The sample is placed in a 1 cm pathlength cell. The sample is excited at 435 nm and the PL spectra is detected with 1 nm

resolution at a 90 degree angle. Data is analyzed by Igor Pro and the points were fitted with a linear trend.

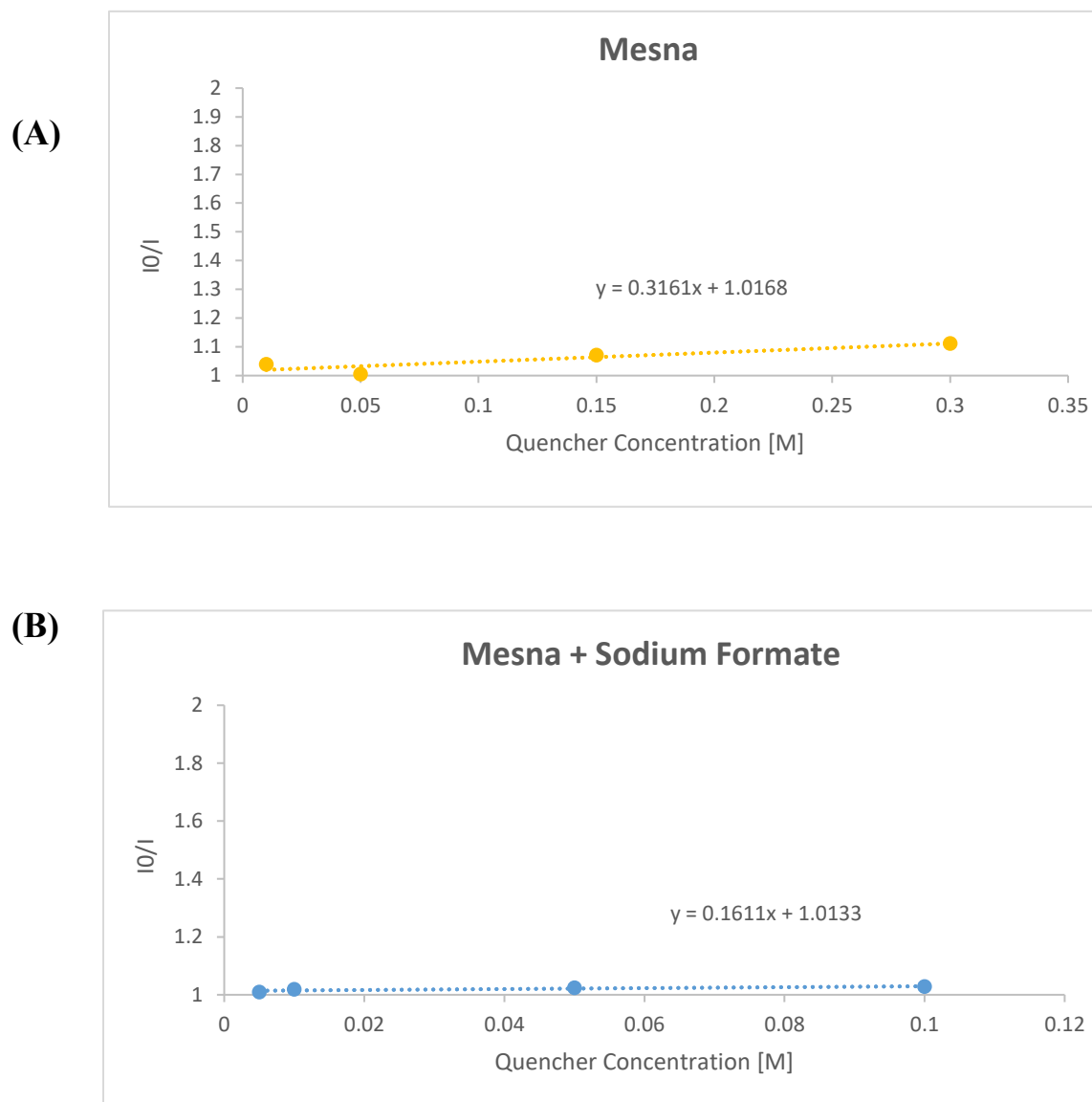


Figure S1. (a) Stern- Volmer plot with Mesna (b) Stern-Volmer plot with Mesna and sodium formate

2.4.8: Transient Absorption Spectroscopy

Methods

Transient spectroscopy is performed on Ultrafast Systems Helios and EOS system. The laser system is based on a Coherent Legend regenerative amplifier system, with 150 fs pulse width, 1 kHz repetition rate, and 2 mJ pulse energy. For the measurement within 1 ns, the fundamental 800 nm light is split to generate the 400 nm excitation light via a BBO crystal (pump) and a broadband white light extended into UV region by focusing on a rotating CaF₂ window (probe). The pump and probe are focused on the sample cell (1 mm) and the probe light is collected via a fiber. For longer delay time the white light is generated by a supercontinuum laser. The detection scheme is similar. The data is analyzed by Surface Explorer and Igor Pro.

Analysis

Transient spectroscopy is employed to investigate the single electron transfer (SET) from the photosensitizer to the thiol at the initialization of the reaction. First, we studied the photosensitizer by exciting at 400 nm, at the ground state absorption. The transient absorption spectrum shows an intersystem crossing process of PS from singlet to triplet excited state at delay time ranging from 10 ns to 10 ms as shown in Figure 1a, 1b, and 1c. The singlet and triplet excited state shows similar ground state bleach (GSB, ~390-400 nm) and broad excited state absorption (ESA, ~450-900 nm) position, but different amplitude. The SET is observed by comparing the kinetics at one of the ESA signal at 473 nm, where the triplet state of PS decays faster with more thiol added as shown in Figure 1c. The SET occurs on a relatively slow time scale where the singlet state decay away as both systems show no difference within 1 ns as shown in Figure S1. Since the excited PS concentration is significant lower (more than 1000 times) than the thiol concentration, the bimolecular reaction rate can be simplified to a pseudo-first order reaction.

Fitting functions and quantum yield calculation

The singlet and triplet lifetime of photosensitizer can be fitted with a bi-exponential function to the kinetics shown in Figure 1c:

$$\Delta A = \Delta A_0(a_1 e^{k_1 t} + a_2 e^{k_2 t})$$

where k_1 and k_2 are the decay rate of the singlet and triplet state. From the fitting shown in Figure 1c, $k_1=13.8\pm 0.1 \text{ ns}^{-1}$, $k_2=1.80\pm 0.06 \text{ ms}^{-1}$.

With the thiol in the system, since the SET occurs in the triplet state, the additional decay rate k leads to faster reaction, which is:

$$\Delta A = \Delta A_0(a_1 e^{k_1 t} + a_2 e^{(k_2+k)t})$$

Fitting result at different concentrations in Figure 1c gives the k value at different concentration and the pseudo-first order reaction rate k_0 can be obtained by:

$$k_0 = k[\text{thiol}] = 0.402 \mu\text{s}^{-1}\text{M}^{-1}$$

Although the absolute quantum yield of triplet state of the photosensitizer cannot be determined by the transient study, we can estimate the upper limit of the quantum yield of the SET from triplet state by assuming a unity intersystem crossing efficiency.

The upper limit of SET quantum yield in real experimental condition (0.01M thiol) can be calculated by:

$$QY_{SET} = \frac{k_{ET}[\text{thiol}]}{k_{ET}[\text{thiol}] + k_{triplet}} = \frac{0.402 * 0.01}{0.402 * 0.01 + 1/1.80} = 0.72\%$$

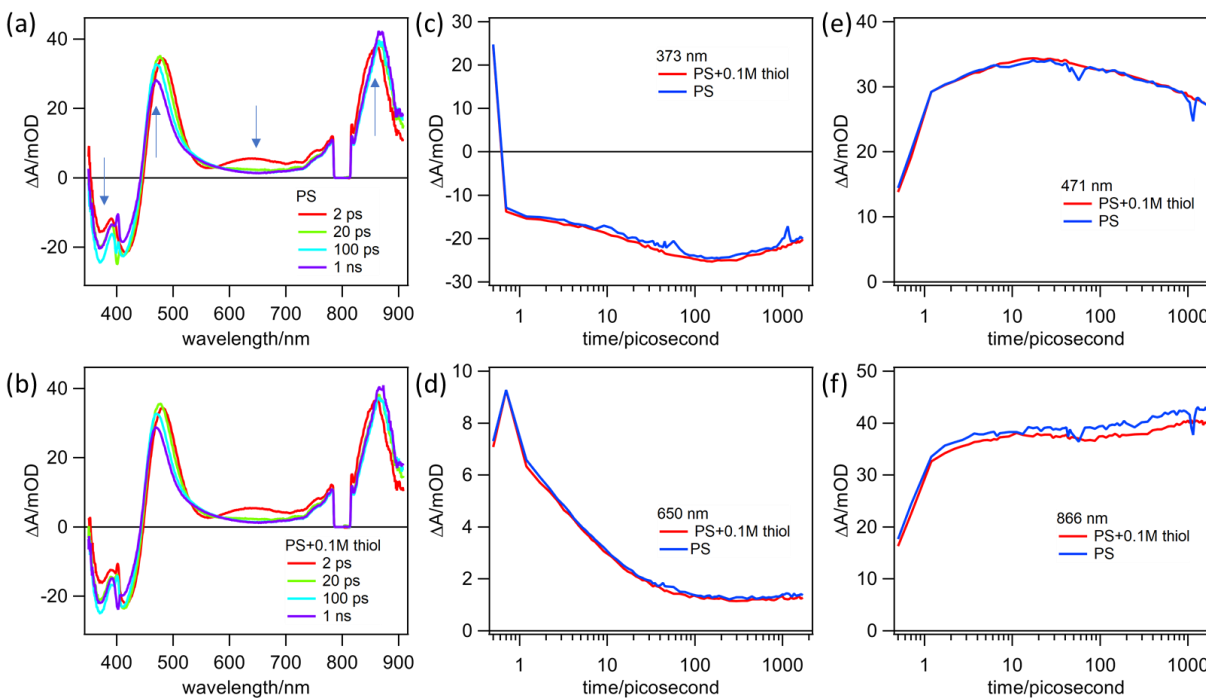


Figure S2. TAS of photosensitizer and with 0.1M thiol within 1 ns time window. (a)-(b) TA spectra of PS and PS+0.1M thiol. (c)-(f) Kinetics comparison at various indicated wavelength. The spectra and kinetics show no difference at this time range.

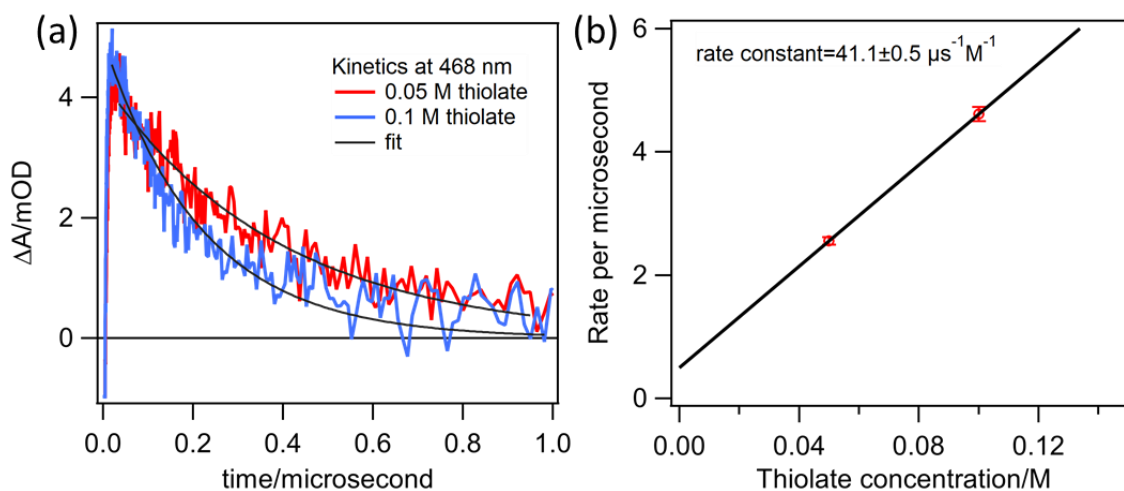


Figure S3. (a) Quenching kinetics of thiolate with photosensitizer at 0.05M and 0.1M concentration. (b) Pseudo-first order rate constant of thiolate.

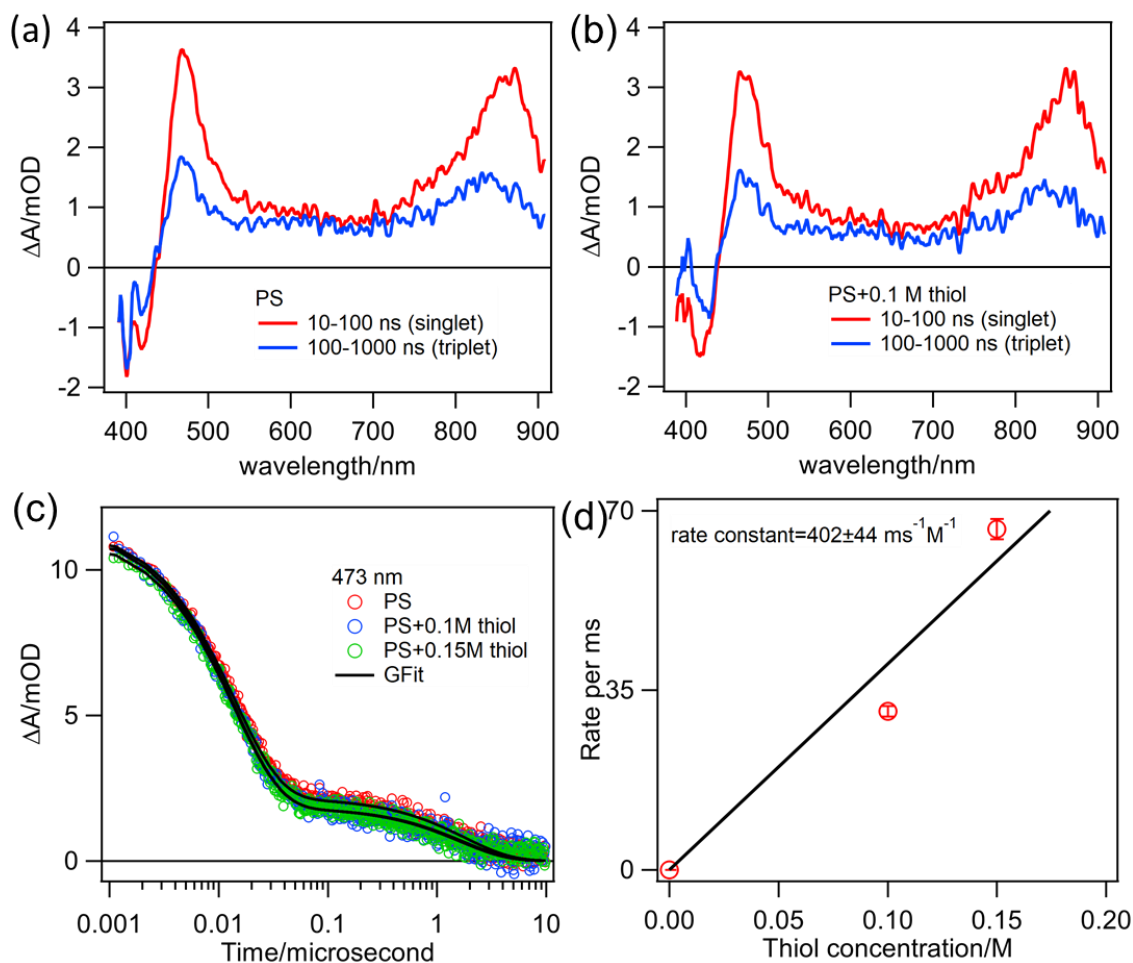


Figure S4. Transient absorption spectroscopy (TAS) of the photosensitizer with thiol. (a) TA spectra of photosensitizer and (b) photosensitizer with 0.1M thiol after 400 nm excitation with delay time at 10-100 ns and 100-1000 ns, which corresponds to the singlet and triplet excited state, respectively. (c) Kinetics probed at 473 nm of photosensitizer, photosensitizer with 0.1M and 0.15M thiol. The higher concentration of thiol leads to faster decay of triplet state. (d) The thiol induced quenching rate of the triplet state is plotted against the thiol concentration, the fitting gives the pseudo-first order rate constant of thiol quenching to be $402 \text{ ms}^{-1}\text{M}^{-1}$.

2.4.9: Quantum Yield Experiments

Determination of the light intensity at 436 nm:

The photon flux of the spectrophotometer was determined by standard ferrioxalate actinometry.¹⁸ A 0.15 M solution of ferrioxalate was prepared by dissolving 2.21 g of potassium ferrioxalate hydrate in 30 mL of 0.05 M H₂SO₄. A buffered solution of phenanthroline was prepared by dissolving 50 mg of phenanthroline and 11.25 g of sodium acetate in 50 mL of 0.5 M H₂SO₄. Both solutions were covered in foil and stored in the dark. To determine the photon flux of our lamp source, 2.0 mL of the ferrioxalate solution was placed in an 8 mL screw-top test tube and irradiated for 10.0s with a blue LED lamp ($\lambda = 435$ nm, LED wholesalers PAR38 Indoor Outdoor 16-Watt LED Flood Light Bulb, Blue) at a distance of exactly 7.0 cm. After irradiation, 0.35 mL of the phenanthroline solution was added to the test tube. The solution was then allowed to rest for 1 h in the dark to allow the ferrous ions to completely coordinate to the phenanthroline. The absorbance of the solution was measured at 510 nm. Conversion was calculated using eq. 1.

$$(1) \text{ mol Fe}^{2+} = \frac{V \cdot \Delta A}{l \cdot \epsilon}$$

Where V is the total volume (0.00235 L) of the solution after addition of phenanthroline, ΔA is the difference in absorbance at 510 nm between the irradiated and non-irradiated solutions, l is the path length (1.000 cm), and ϵ is the molar absorptivity at 510 nm (11,100 L mol⁻¹ cm⁻¹).¹⁸ The photon flux can be calculated using eq 2.

$$(2) \text{ Photon flux} = \frac{\text{mol Fe}^{2+}}{\Phi \cdot t \cdot f}$$

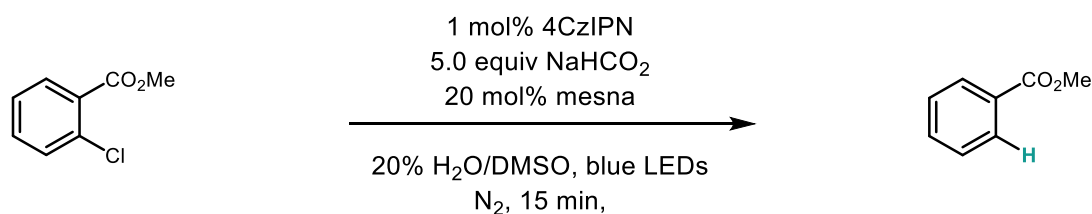
Where Φ is the quantum yield for the ferrioxalate actinometer (1.01 for a 0.15 M solution at $\lambda = 436 \text{ nm}$),¹⁸ t is the time (10.0 s), and f is the fraction of light absorbed at $\lambda = 436 \text{ nm}$ (0.99833, vide infra)¹⁸. The photon flux was calculated (average of three experiments) to be $4.02 \times 10^{-8} \text{ einstein s}^{-1}$.

Sample Calculation:

$$\text{Mol Fe}^{2+} = \frac{0.0235 \text{ L} \cdot 1.91328}{1.00 \text{ cm} \cdot 11,100 \text{ L mol}^{-1} \text{ cm}^{-1}} = 4.05 \times 10^{-7} \text{ mol}$$

$$\text{Photon flux} = \frac{4.05 \times 10^{-7} \text{ mol}}{1.01 \cdot 10 \text{ s} \cdot 0.99833} = 4.02 \times 10^{-8} \text{ einsteins s}^{-1}$$

Determination of quantum yield



An 8 mL screw-top test tube was charged with 4CzIPN (0.002, 29 μL , 1 mol%), sodium formate (1.0 mmol, 0.068 g, 5.0 equiv) and mesna (0.04, 20 mol%, 0.02 mol). The tube was equipped with a stir bar and sealed with a PTFE/silicon septum. Under nitrogen atmosphere, separately degassed DMSO (2 mL) was added via syringe, followed by 2-chloromethylbenzoate (0.2 mmol, 29 μL , 1.0 equiv). The resulting mixture was stirred at 1400 RPM for 15 min. under irradiation by blue LEDs at a distance of exactly 7.0 cm, unless noted otherwise. The reaction was then extracted with ethyl acetate (3 x). The organic layer was passed through a small silica plug with 100% EtOAc and concentrated. Deutro-chloroform with an internal standard of dibromomethane

(14 μL , 0.2 mmol) was added. The sample was analyzed by ^1H NMR ($d = 5$ s), and the integral values were used to calculate the data. Essentially all incident light ($f > 0.999$, *vide infra*) is absorbed by the 4CzIPN at the reaction conditions described above. The quantum yield was calculated using eq. 3 the average yield of three experiments to be 2.63.

$$(3) \Phi = \frac{\text{mol product}}{\text{flux} \cdot t \cdot f}$$

Average yield of 3 experiments: 47% yield (avg. mmol= 0.095)

Sample quantum yield calculation:

$$\Phi = \frac{9.5 \times 10^{-5} \text{ mol}}{4.02 \times 10^{-8} \cdot 900 \text{ s} \cdot 1.00} = 2.63$$

2.4.10: Chain Length Approximation

Chain length

Chain length values calculated in this paper are a lower limit approximation of the actual chain lengths and were calculated using eq. 4, where QY (initial SET) was calculated through transient absorption spectroscopy experimentation (refer to pg. 30 for calculation).

$$(1) \text{Chain length} = \frac{\Phi(\text{overall reation})}{\Phi(\text{inital SET})}$$

Sample Calculation:

$$\text{Chain length} = \frac{2.63}{0.0072} = 365$$

The lower limit of the chain length was determined to be 365.

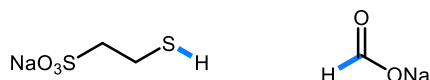
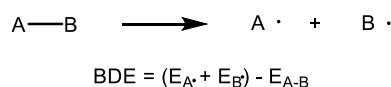
2.4.11: Computational Details

General.

All DFT calculations were carried out using the Gaussian 9 software package³² at the (U)B3LYP³³ or R(B3LYP)³³ level of theory with the 6-311+G(d,p)³⁴ basis set. The CPCM formalism for the Self Consistent Reaction Field (SCRF) model of solvation was employed in calculations to account for solvation in DMSO, and the default parameters as implemented in Gaussian were used.

Calculated Bond Dissociation Energies

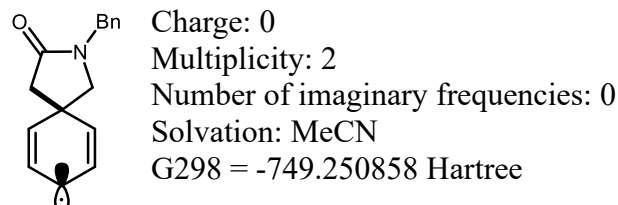
Calculations were carried out at the (U)B3LYP³² level of theory with the 6-311+G(d,p)³⁴ basis set. Bond dissociation energies (BDEs) were calculated according to the following equation:



BDE =	87.8	89.6
(kcal/mol)		

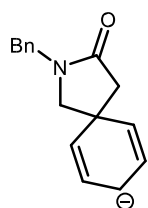
Steric effects of the arene substituents on cyclization were observed from the minimized geometries of the relevant compounds. The structural minima were visualized using GaussView⁵⁶ allowing the interatomic distances between the two carbons which form the spirocyclic center to be obtained.

Molecular Coordinates of Optimized Structures:



C -0.67021525 1.67383904 -3.52647222
 C 1.62256455 1.29631778 -3.73626915
 C 0.07672390 2.37458623 -2.38022356
 H -1.57793076 2.15145972 -3.83115408
 H -0.90383945 0.67001427 -3.23897339
 H 1.48810123 0.31261662 -3.33733101
 H 2.55355683 1.31829279 -4.26321362
 O -0.45691413 2.90442774 -1.37122951
 N 1.53966646 2.32415369 -2.66562245
 C 1.99332151 3.62922748 -3.16749843
 H 1.41849308 3.89967664 -4.02850339
 H 3.02787126 3.56890337 -3.43389629
 C 1.80692420 4.69402465 -2.07065614
 C 2.83996131 4.94875764 -1.15858849
 C 0.60426554 5.40825710 -1.98459730
 C 2.67034073 5.91772490 -0.16046362
 H 3.75821850 4.40342648 -1.22429734
 C 0.43464415 6.37722284 -0.98647109
 H -0.18448079 5.21376361 -2.68098190
 C 1.46768203 6.63195728 -0.07440472
 H 3.45908884 6.11222174 0.53591803
 H -0.48361187 6.92255620 -0.92076418
 H 1.33817319 7.37178573 0.68768538
 C 0.41715892 1.68130187 -4.58869847
 C 0.60945176 3.15768691 -5.12274815

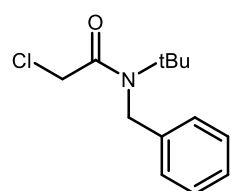
C 0.13949927 0.65242991 -5.75754249
 C 0.94414182 3.32317391 -6.39869152
 H 0.51126987 3.99542129 -4.46437028
 C -0.31675236 1.12588223 -6.91301264
 H 0.27797525 -0.39785205 -5.60710243
 C 0.27516439 2.42711245 -7.42686688
 H 1.69198010 4.03440692 -6.68115480
 H -1.10493686 0.62654268 -7.43677329
 H 0.22350066 2.69870937 -8.46053316



Charge: -1
 Multiplicity: 1
 Number of imaginary frequencies: 0
 Solvation: MeCN
 $G_{298} = -749.361362$ Hartree

C -0.67021525 1.67383904 -3.52647222
 C 1.62256455 1.29631778 -3.73626915
 C 0.07672390 2.37458623 -2.38022356
 H -1.57793076 2.15145972 -3.83115408
 H -0.90383945 0.67001427 -3.23897339
 H 1.48810123 0.31261662 -3.33733101
 H 2.55355683 1.31829279 -4.26321362
 O -0.45691413 2.90442774 -1.37122951
 N 1.53966646 2.32415369 -2.66562245
 C 1.99332151 3.62922748 -3.16749843
 H 1.41849308 3.89967664 -4.02850339
 H 3.02787126 3.56890337 -3.43389629
 C 1.80692420 4.69402465 -2.07065614
 C 2.83996131 4.94875764 -1.15858849
 C 0.60426554 5.40825710 -1.98459730

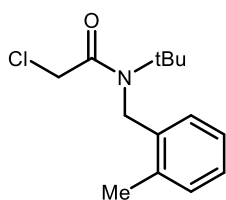
C 2.67034073 5.91772490 -0.16046362
 H 3.75821850 4.40342648 -1.22429734
 C 0.43464415 6.37722284 -0.98647109
 H -0.18448079 5.21376361 -2.68098190
 C 1.46768203 6.63195728 -0.07440472
 H 3.45908884 6.11222174 0.53591803
 H -0.48361187 6.92255620 -0.92076418
 H 1.33817319 7.37178573 0.68768538
 C 0.41715892 1.68130187 -4.58869847
 C 0.60945176 3.15768691 -5.12274815
 C 0.13949927 0.65242991 -5.75754249
 C 0.94414182 3.32317391 -6.39869152
 H 0.51126987 3.99542129 -4.46437028
 C -0.31675236 1.12588223 -6.91301264
 H 0.27797525 -0.39785205 -5.60710243
 C 0.27516439 2.42711245 -7.42686688
 H 1.69198010 4.03440692 -6.68115480
 H -1.10493686 0.62654268 -7.43677329
 H 0.22350066 2.69870937 -8.46053316



Charge: 0
 Multiplicity: 1
 Solvation: MeCN
 Number of imaginary frequencies: 0
 Interatomic Distance: 3.49 Å

C -1.42928837 1.11221039 0.41076646
 O -1.33747937 1.09112177 1.66563575
 N -0.21375667 1.09002359 -0.41560538
 C -2.81505622 1.16126145 -0.25918986
 H -3.16450854 0.16432840 -0.42921214
 H -2.74146226 1.67760837 -1.19346486

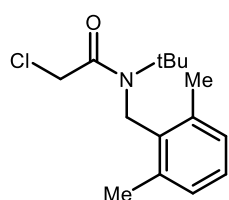
Cl -3.94504256 2.00781660 0.79155999
C 0.84595957 0.35633052 0.29121565
C 0.38046073 -1.08711028 0.55840376
H 1.15181881 -1.62115898 1.07289253
H 0.17044641 -1.57212133 -0.37195008
H -0.50431405 -1.07096071 1.15991251
C 1.14822317 1.05438379 1.63022959
H 1.91958125 0.52033510 2.14471837
H 0.26344839 1.07053337 2.23173835
H 1.47165419 2.05729396 1.44458591
C 2.11937374 0.33308720 -0.57450723
H 2.89073182 -0.20096150 -0.06001846
H 2.44280476 1.33599736 -0.76015092
H 1.90935943 -0.15192384 -1.50486107
C -0.50228101 0.42370000 -1.69375505
H 0.38249377 0.40755043 -2.29526381
H -0.82571202 -0.57921016 -1.50811136
C -1.61245993 1.19233084 -2.43423422
C -2.48811378 0.50857202 -3.28841580
C -1.74706889 2.57554372 -2.25388869
C -3.49837493 1.20802651 -3.96225391
H -2.38533832 -0.54754210 -3.42611180
C -2.75733089 3.27499799 -2.92772574
H -1.07848790 3.09760871 -1.60170192
C -3.63298329 2.59123954 -3.78190911
H -4.16695566 0.68596158 -4.61444100
H -2.86010661 4.33111204 -2.79002943
H -4.40433884 3.12528890 -4.29640101



Charge: 0
 Multiplicity: 1
 Number of imaginary frequencies: 0
 Solvation: MeCN
 Interatomic Distance: 3.42 Å

C -0.43282831 -0.79332914 0.01121010
 O -1.15350877 -1.79569780 -0.23260806
 N 1.03169377 -0.91818165 -0.01085634
 C -1.08513793 0.56414367 0.33270619
 H -1.23097314 1.11340606 -0.57390449
 H -0.44744177 1.12003940 0.98785774
 Cl -2.63967693 0.29771101 1.11374532
 C 1.42013417 -1.96127084 -0.97105371
 C 2.95439540 -2.09206871 -0.99417094
 H 3.23713774 -2.85132411 -1.69309011
 H 3.30449213 -2.35723106 -0.01845520
 H 3.38756900 -1.15853001 -1.28702948
 C 0.91625664 -1.57963532 -2.37535488
 H 1.19899898 -2.33889072 -3.07427405
 H 1.34943024 -0.64609662 -2.66821341
 H -0.14975603 -1.48875628 -2.35929291
 C 0.79668805 -3.30486860 -0.54955638
 H 1.07943039 -4.06412400 -1.24847556
 H -0.26932462 -3.21398956 -0.53349441
 H 1.14678478 -3.57003094 0.42615936
 C 1.62680143 0.36434348 -0.41319471
 H 1.27670470 0.62950582 -1.38891045
 H 2.69281410 0.27346444 -0.42925668
 C 1.21986386 1.45710358 0.59272635
 C 1.09241111 2.78690766 0.16928938

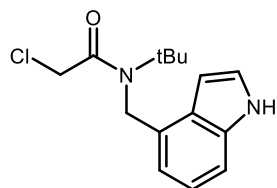
C 0.97700342 1.12171120 1.93155147
 C 0.72209430 3.78131876 1.08467673
 C 0.60668597 2.11612218 2.84693868
 H 1.07431902 0.10637671 2.25485557
 C 0.47923215 3.44592608 2.42350147
 H 0.62478130 4.79665368 0.76137321
 H 0.42125398 1.86004221 3.86916078
 H 0.19648575 4.20518080 3.12241974
 C 1.35929469 3.15547139 -1.30194613
 H 1.72782650 4.15848454 -1.35716320
 H 0.44934096 3.07862445 -1.85960082
 H 2.08614872 2.48538517 -1.71129646



Charge: 0
 Multiplicity: 1
 Number of imaginary frequencies: 0
 Solvation: MeCN
 Interatomic Distance: 2.91 Å

C -0.46509528 0.55862783 0.17643923
 O -1.11792889 -0.50351715 0.00548049
 N 0.99291720 0.56343212 -0.01084802
 C -1.19361469 1.85342254 0.58186015
 H -1.48812414 2.38725389 -0.29745111
 H -0.53748551 2.46370861 1.16662114
 Cl -2.62102207 1.45127518 1.52969224
 C 1.36083931 -0.44177984 -1.01836092
 C 0.67065848 -0.10673774 -2.35365012
 H 0.93846576 -0.83842258 -3.08700986
 H 0.98458438 0.86123309 -2.68438097
 H -0.39061595 -0.11023476 -2.21732540

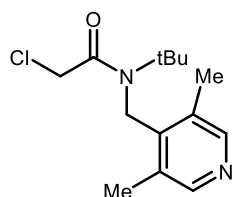
C 0.90902068 -1.83493418 -0.54235572
H 1.17682788 -2.56661908 -1.27571541
H -0.15225374 -1.83843116 -0.40603096
H 1.38856193 -2.06772318 0.38541010
C 2.88828097 -0.43674675 -1.21456659
H 3.15608824 -1.16843160 -1.94792629
H 3.36782219 -0.66953570 -0.28680076
H 3.20220688 0.53122407 -1.54529744
C 1.42419860 1.89326126 -0.46521659
H 0.94465737 2.12605024 -1.39298246
H 2.48547299 1.89675826 -0.60154133
C 1.03875641 2.94634046 0.59027312
C 0.74834651 4.25951975 0.19638959
C 0.97841390 2.59146326 1.94465228
C 0.39759530 5.21782213 1.15688535
C 0.62766535 3.54976632 2.90514834
C 0.33725629 4.86294581 2.51126490
H 0.17586062 6.22046358 0.85614650
H 0.58159357 3.27880998 3.93924700
H 0.06944982 5.59463092 3.24462471
C 0.81465566 4.64949437 -1.29193930
H 1.08524402 5.68107847 -1.37863557
H -0.14199254 4.49242142 -1.74476641
H 1.54678741 4.04593963 -1.78651457
C 1.29754143 1.14840803 2.37749085
H 1.70949193 1.15507812 3.36498888
H 2.00541810 0.72069865 1.69861295
H 0.39944568 0.56680505 2.3696092



Charge: 0
 Multiplicity: 1
 Number of imaginary frequencies: 0
 Solvation: MeCN
 Interatomic Distance: 3.41 Å

C -0.50779625 1.50532687 0.33496392
 O -1.15791776 0.45474692 0.09581049
 N 0.95129954 1.44454317 0.50302599
 C -1.24076953 2.85467982 0.45156918
 H -1.29019019 3.31812571 -0.51158995
 H -0.70944740 3.49197138 1.12718464
 Cl -2.87111364 2.58623869 1.05780137
 C 1.49214433 0.34225853 -0.30527808
 C 1.15581445 0.58071586 -1.78906391
 H 1.54949055 -0.22162741 -2.37742131
 H 1.59051752 1.50449655 -2.10931771
 H 0.09375155 0.62495983 -1.91139483
 C 0.86649699 -0.98729501 0.15564797
 H 1.26017309 -1.78963827 -0.43270941
 H -0.19556591 -0.94305104 0.03331709
 H 1.10018077 -1.15297640 1.18659006
 C 3.02072084 0.27858039 -0.12921309
 H 3.41439695 -0.52376286 -0.71757049
 H 3.25440467 0.11289902 0.90172898
 H 3.45542381 1.20236111 -0.44946690
 C 1.54850833 2.71366245 0.06305114
 H 1.31482454 2.87934380 -0.96789094
 H 2.61057125 2.66941854 0.18538202
 C 0.98190907 3.86843687 0.90984587
 C 0.85691106 5.15148359 0.38937984

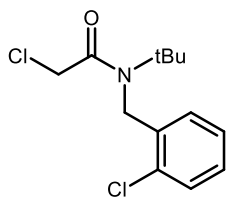
C 0.57797504 3.66702136 2.24537631
 C 0.28995697 6.17897067 1.08982434
 C 0.07149149 4.75199263 3.00918067
 H 0.65659470 2.69506976 2.68586357
 C -0.07451198 6.02921740 2.42534016
 H -0.20387837 4.59989838 4.03189215
 H -0.45919004 6.85348853 2.98881146
 C 1.30281089 5.70566587 -0.95218599
 H 1.77466013 5.16100102 -1.74313384
 C 1.00986056 7.03255115 -0.94292059
 H 1.35306981 7.73623853 -1.67225692
 N 0.14972544 7.37497755 0.22779087
 H -0.80086996 7.48509673 -0.06245413



Charge: 0
 Multiplicity: 1
 Number of imaginary frequencies: 0
 Solvation: MeCN
 Interatomic Distance: 2.95 Å

C 2.18821795 1.15575564 -1.92603099
 O 2.78368334 0.66024971 -2.91772923
 N 2.95555049 1.83421108 -0.87161220
 C 0.65562940 1.05138115 -1.81704346
 H 0.20600082 1.90176989 -2.28562977
 H 0.37263454 1.02133901 -0.78558266
 Cl 0.10916246 -0.41725914 -2.61833592
 C 2.12875659 2.88700819 -0.26421602
 H 2.68729115 3.38084986 0.50328614
 H 1.84790004 3.59695636 -1.01387807
 C 4.16382720 2.43521874 -1.45449914

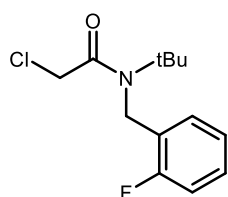
C 5.02999225 1.33228845 -2.09081892
H 5.90948618 1.76975660 -2.51509717
H 4.47145770 0.83844672 -2.85832104
H 5.31084886 0.62234032 -1.34115685
C 3.75960369 3.45701324 -2.53345204
H 4.63909764 3.89448139 -2.95773029
H 3.15778772 4.22333495 -2.09133377
H 3.20106914 2.96317151 -3.30095416
C 4.96769935 3.14598163 -0.34986994
H 5.84719328 3.58344980 -0.77414818
H 5.24855595 2.43603351 0.39979215
H 4.36588336 3.91230333 0.09224833
C 0.86294285 2.25738114 0.34642737
C -0.32966103 2.99049776 0.41391645
C 0.89268568 0.95148609 0.83775696
C -0.27219432 0.41145146 1.38462852
C -1.43705684 1.18968051 1.42674257
H -0.27597075 -0.58743090 1.76819045
H -2.33361790 0.78175801 1.84468694
N -1.43592273 2.44433269 0.94602106
C -0.37241114 4.43225234 -0.12563537
H -1.09216047 4.99884195 0.42739004
H -0.64768225 4.41814592 -1.15952455
H 0.59290631 4.88150770 -0.01965502
C 2.18814983 0.12097726 0.77752642
H 2.20814867 -0.56851182 1.59551472
H 3.03358497 0.77379063 0.84056721
H 2.22281108 -0.41938888 -0.14535116



Charge: 0
 Multiplicity: 1
 Number of imaginary frequencies: 0
 Solvation: MeCN
 Interatomic Distance: 3.42 Å

C -0.99633452 0.18519537 -0.16020934
 O -1.62020267 -0.87186988 -0.43764791
 N 0.46878452 0.16454722 -0.04231174
 C -1.76774614 1.50043808 0.05580161
 H -1.86432111 2.01469876 -0.87753071
 H -1.23465676 2.11684354 0.74917022
 Cl -3.36736441 1.14378531 0.69737794
 C 1.01711452 -0.87224924 -0.92847612
 C 0.62362710 -0.56330213 -2.38495109
 H 1.02275166 -1.31797710 -3.02998230
 H 1.01755263 0.39100131 -2.66606963
 H -0.44282009 -0.54827252 -2.47076771
 C 0.45015628 -2.24573269 -0.52387561
 H 0.84928084 -3.00040766 -1.16890682
 H -0.61629092 -2.23070308 -0.60969223
 H 0.72355338 -2.46039075 0.48809077
 C 2.55200114 -0.89388064 -0.80496435
 H 2.95112570 -1.64855561 -1.44999557
 H 2.82539824 -1.10853870 0.20700202
 H 2.94592667 0.06042280 -1.08608289
 C 1.00997194 1.47559960 -0.42852132
 H 0.73657483 1.69025766 -1.44048770
 H 2.07641913 1.46056999 -0.34270470
 C 0.43553098 2.56176732 0.49984136
 C 0.25787743 3.86791526 0.02409065
 C 0.09044326 2.24403201 1.82040211

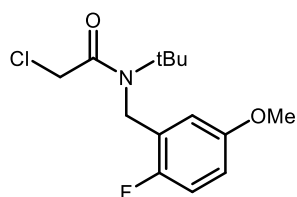
C -0.26486135 4.85632852 0.86890149
 C -0.43229680 3.23244494 2.66521254
 H 0.22608547 1.24675902 2.18364826
 C -0.60994818 4.53859343 2.18946253
 H -0.40050316 5.85360161 0.50565546
 H -0.69577712 2.98984744 3.67349056
 H -1.00906898 5.29326936 2.83449495
 Cl 0.69126501 4.26695399 -1.63438555



Charge: 0
 Multiplicity: 1
 Number of imaginary frequencies: 0
 Solvation: MeCN
 Interatomic Distance: 3.43 Å

C -0.61568894 0.26849260 0.52217769
 O -1.18280256 -0.82303094 0.78775079
 N 0.85162121 0.35651459 0.53454962
 C 1.42378791 -0.94638530 0.16579882
 C 0.94481915 -1.33665208 -1.24483252
 H 1.36129423 -2.28502138 -1.51324297
 H 1.26359618 -0.59537172 -1.94753064
 H -0.12322293 -1.40072250 -1.25383794
 C 0.96498733 -2.01327478 1.17715873
 H 1.38146241 -2.96164409 0.90874829
 H -0.10305474 -2.07734521 1.16815331
 H 1.29777731 -1.74211540 2.15727271
 C 2.96096997 -0.85417179 0.17875989
 H 3.37744504 -1.80254109 -0.08965056
 H 3.29375994 -0.58301240 1.15887387
 H 3.27974699 -0.11289143 -0.52393824
 C 1.28956721 1.37490909 -0.43083939

H 0.95677723 1.10374971 -1.41095337
 H 2.35760929 1.43897952 -0.42183398
 C -1.45885082 1.51205963 0.18421457
 H -1.63090453 1.55026933 -0.87117045
 H -0.93494532 2.39269024 0.49229369
 Cl -3.00121129 1.42191558 1.02718446
 C 0.69015448 2.73985183 -0.04452903
 C 0.40768852 3.68743915 -1.03761171
 C 0.42715486 3.03436241 1.30009608
 C -0.13777457 4.92953807 -0.68606902
 C -0.11830950 4.27646080 1.65163863
 H 0.64282365 2.31085836 2.05833672
 C -0.40077329 5.22404901 0.65855618
 H -0.35344298 5.65304227 -1.44430962
 H -0.31911375 4.50132690 2.67828993
 H -0.81724459 6.17241986 0.92696703
 F 0.66103916 3.40372938 -2.33291948



Charge: 0
 Multiplicity: 1
 Number of imaginary frequencies: 0
 Solvation: MeCN
 Interatomic Distance: 3.43 Å

C -0.53706787 0.37443739 0.68435628
 O -1.11307434 -0.69793748 1.00341623
 N 0.92925254 0.42180201 0.59183032
 C 1.43849310 -0.90045013 0.20039280
 C 0.85021447 -1.29270053 -1.16769633
 H 1.22088617 -2.25515616 -1.45262024
 H 1.13812537 -0.56830622 -1.90067668

H -0.21710719 -1.32717681 -1.10034750
C 1.02411667 -1.94303633 1.25533649
H 1.39478838 -2.90549196 0.97041258
H -0.04320499 -1.97751261 1.32268532
H 1.43285572 -1.67049871 2.20589192
C 2.97463829 -0.85083005 0.10346084
H 3.34531000 -1.81328569 -0.18146307
H 3.38337735 -0.57829243 1.05401628
H 3.26254919 -0.12643574 -0.62951951
C 1.32479368 1.41699793 -0.41516138
H 0.91605462 1.14446031 -1.36571682
H 2.39211534 1.45147421 -0.48251022
C -1.36831004 1.63716418 0.39083027
H -1.61379233 1.66856837 -0.65015591
H -0.80032440 2.50622755 0.64971473
Cl -2.84877388 1.59913760 1.34181965
C 0.79130357 2.80221445 -0.00508398
C 0.46464029 3.74634028 -0.98785532
C 0.63249084 3.11863567 1.35085779
C -0.02083759 5.00688661 -0.61468493
C 0.14701590 4.37918311 1.72402826
C -0.17964861 5.32330846 0.74125689
H -0.27025496 5.72774660 -1.36505274
H -0.55031993 6.28576425 1.02618081
F 0.61762651 3.44152402 -2.29406443
H 0.88190600 2.39777484 2.10122553
O -0.01503554 4.70206279 3.10764239
C 0.17093435 6.10760855 3.29407287
H 0.04967908 6.34920383 4.32936456
H -0.55284110 6.64295259 2.71575130

H 1.15511737 6.38237129 2.97659970

2.4.12: Electrochemical Measurements

Electrochemical potentials were obtained with a standard set of conditions according to literature procedure.³⁵ Cyclic voltammograms (CVs) were collected with a VersaSTAT 4Potentiostat. Samples were prepared with 0.1 mmol of substrate in 10 mL of 0.1 M tetra-n-butylammonium hexafluorophosphate in dry, degassed DMSO. Measurements employed a glassy carbon working electrode, platinum wire counter electrode, 3M NaCl silver-silver chloride reference electrode, and a scan rate of 100 mV/s. Reductions were measured by scanning potentials in the negative direction and oxidations in the positive direction; the glassy carbon electrode was polished between each scan. Data was analyzed using Microsoft Excel by subtracting a background current prior to identifying the maximum current (C_p) and determining the potential ($E_p/2$) at half this value ($C_p/2$). The obtained value was referenced to Ag|AgCl and converted to SCE by subtracting 0.035 V.

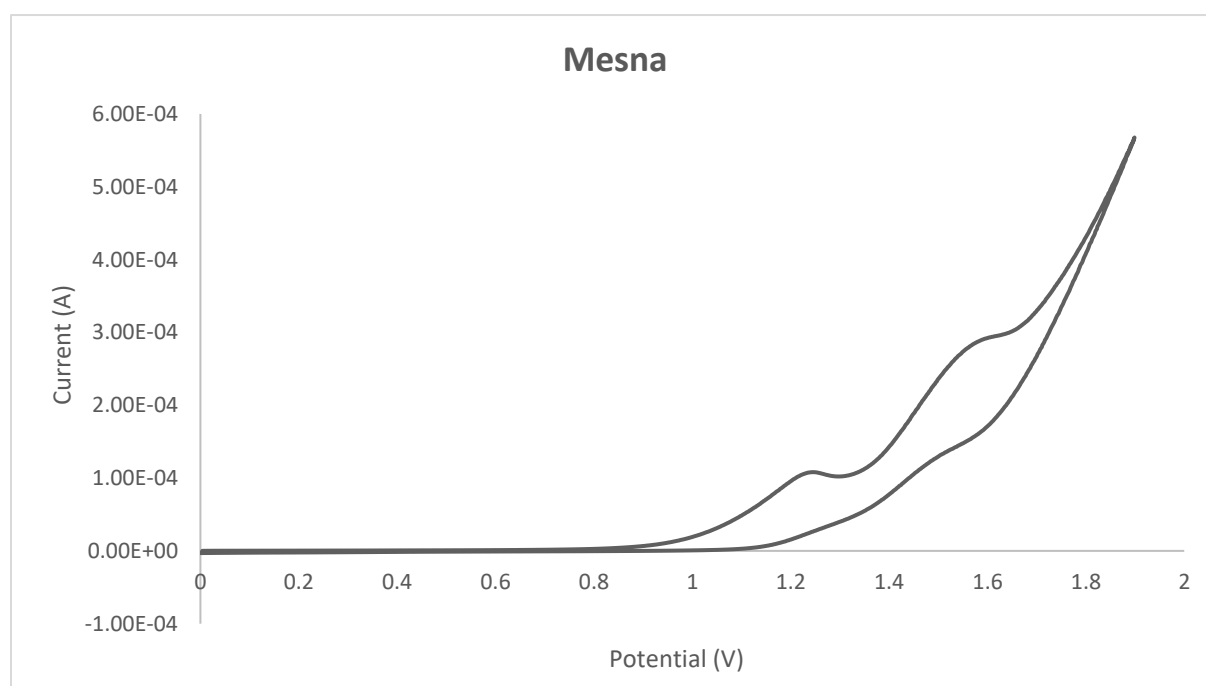


Figure S4. CV of Mesna

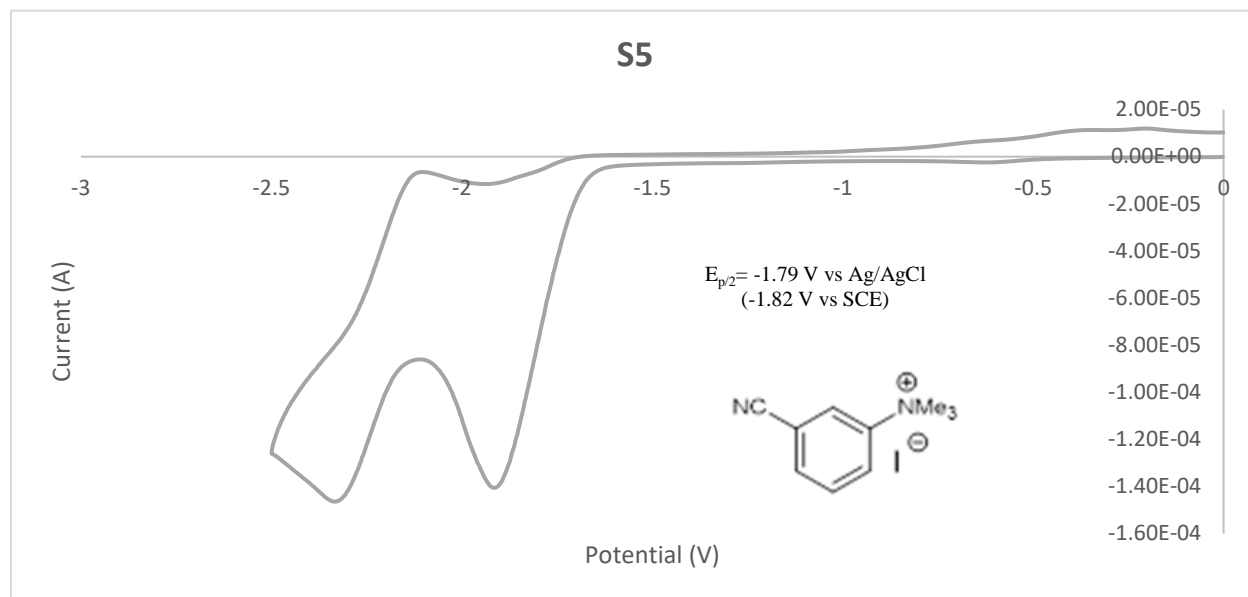


Figure S5. CV of 3-cyano-N,N,N-trimethylbenzenaminium iodide (S5)

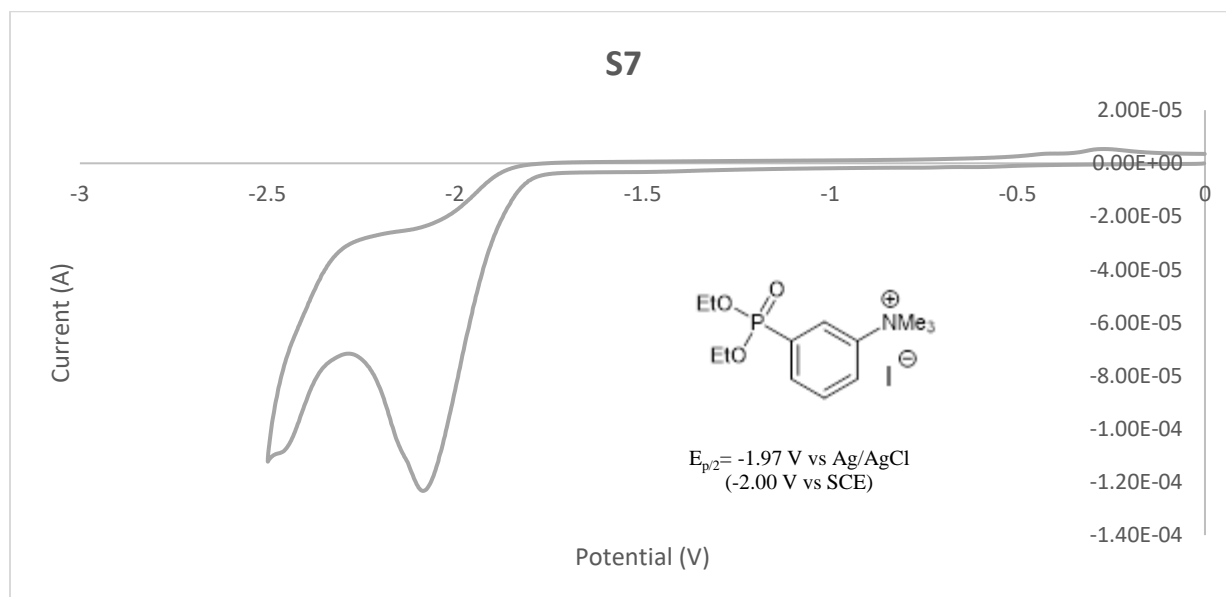


Figure S6. CV of 3-(diethoxyphosphoryl)-N,N,N-trimethylbenzenaminium iodide (S7)

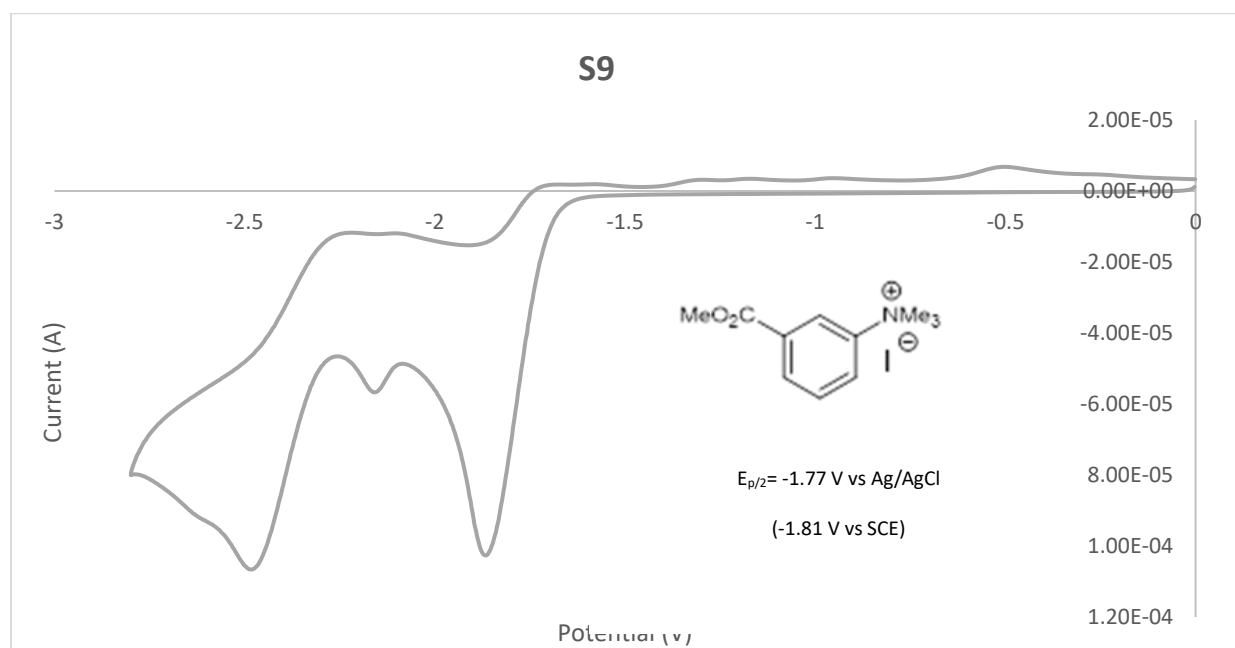


Figure S7. CV of 3-(methoxycarbonyl)-N,N,N-trimethylbenzenaminium iodide (S9)

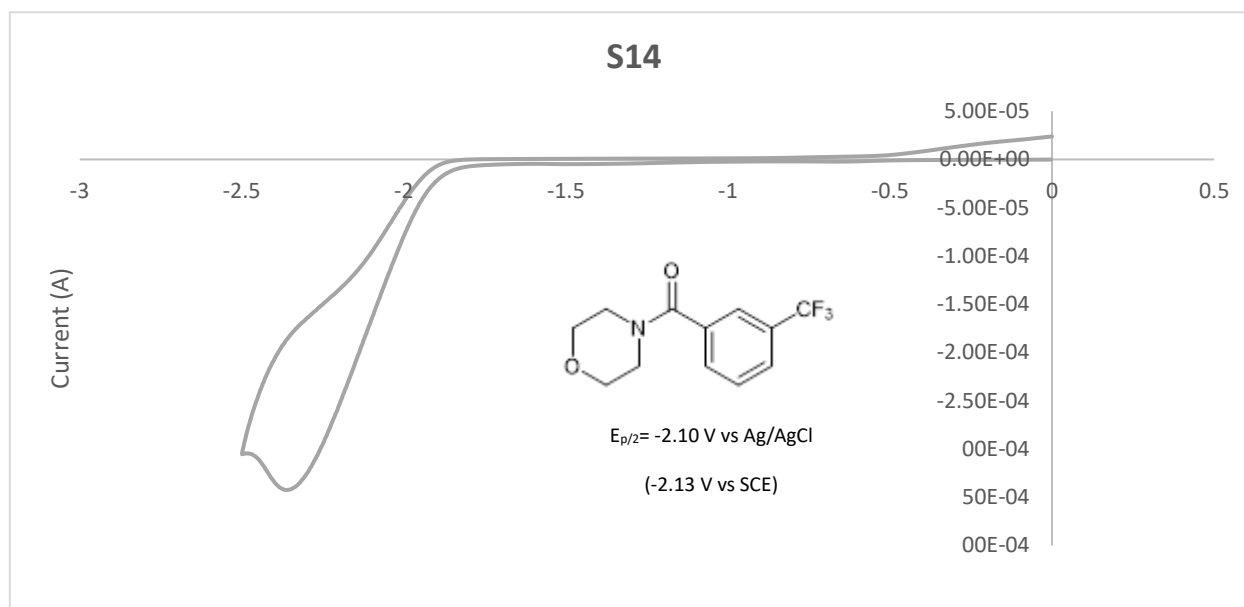


Figure S7. CV of morpholino(3-(trifluoromethyl)phenyl)methanone (S14)

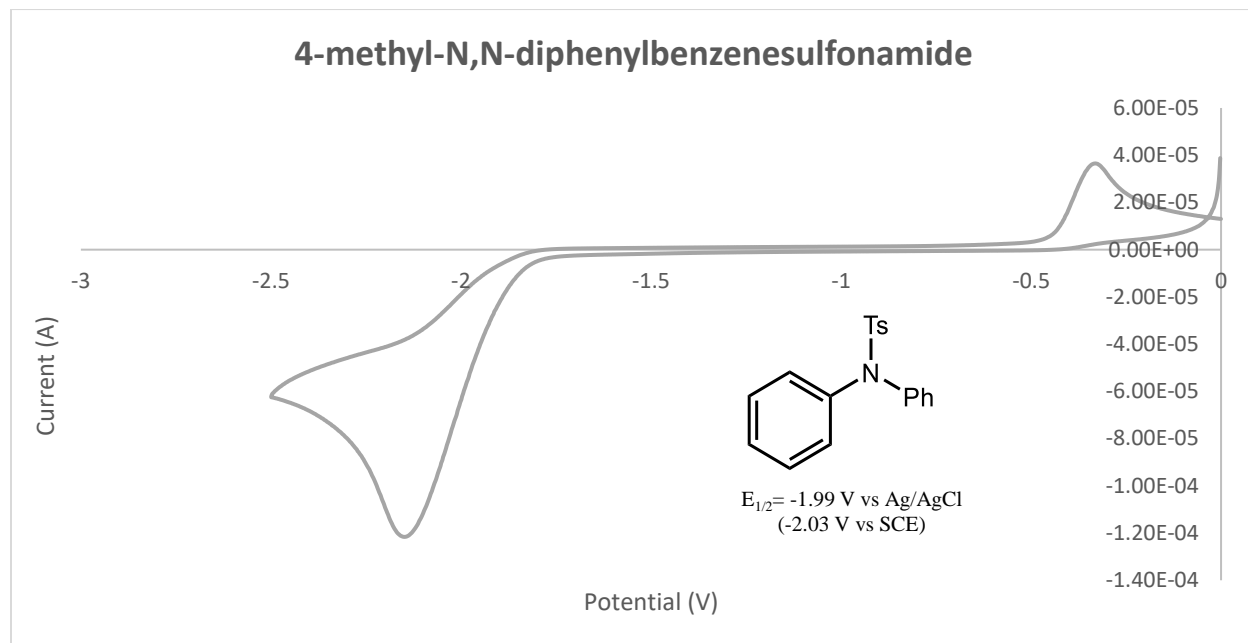


Figure S8. CV of 4-methyl-N,N-diphenylbenzenesulfonamide

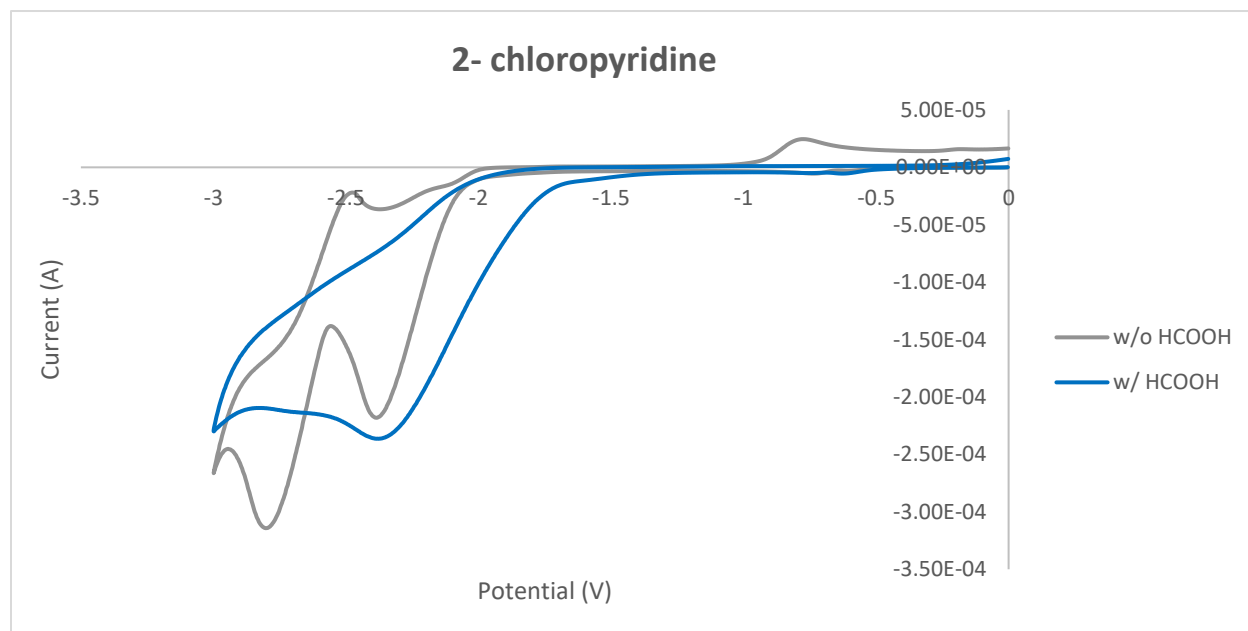


Figure S9. CV of 2-chloropyridine in the absence of formic acid (gray line) and in the presence of 5.0 eq. of formic acid (blue)

2.4.13: References

1. Luo, J.; Zhang, J. "Donor-Acceptor Fluorophores for Visible-Light-Promoted Organic Synthesis: Photoredox/ Ni Dual Catalytic C(sp³)-C(sp²) Cross- Coupling." *ACS Catal.* **2016**, *6*, 873–877.
2. Kassir, A.; Ragab, S.; Nguyen, T.; Pouget, F.; Guillot, R.; Scherrmann, M.; Boddaert, T.; Aitken, D. "Synthetic Access to All Four Stereoisomers of Oxetin." *J. Org. Chem.*, **2016**, *81*, 9983-9991.
3. Andaloussi, M.; Lindh, J.; Savmarker, J.; Sjoberg, P.; Larhed, M. Microwave-Promoted Palladium (II)-Catalyzed C-P Bond Formation by Using Arylboronic Acids or Aryltrifluoroborates. *Chem. Eur. J.*, **2009**, *15*, 13069-13074.
4. Takise, R.; Itami, K.; Yamaguchi, J. "Cyanation of Phenol Derivatives with Aminoacetonitriles by Nickel Catalysis." *Org. Lett.* **2016**, *18*, 17, 4428–4431.
5. Liu, C.; Ji, C.; Zhou, T.; Hong, X.; Szostak, M. "Decarbonylative Phosphorylation of Carboxylic Acids via Redox- Neutral Palladium Catalysis." *Org. Lett.* **2019**, *21*, 22, 9256–9261.
6. Naksomboon, K.; Poater, J.; Bickelhaupt M.; Fernandez-Ibanez, M. A. "para-Selective C-H olefination of Aniline Derivatives via Pd/S,O-Ligand Catalysis." *J. Am. Chem. Soc.* **2019**, *141*, 16, 6719–6725.
7. Takise, R.; Itami, K.; Yamaguchi, J. "Cyanation of Phenol Derivatives with Aminoacetonitriles by Nickel Catalysis." *Org. Lett.* **2016**, *18*, 17, 4428–4431.
8. Bordi, S.; Starr, J. "Hydropyridylation of Olefins by Intramolecular Minisci Reaction." *Org. Lett.*, **2017**, *19*, 2290-2293
9. Peng, Z.; Wong, J.; Hansen, E.; Dermenci, A.; Clarke, H. "Development of a Concise, Asymmetric Synthesis of a Smoothed Receptor (SMO) Inhibitor: Enzymatic Transamination of a 4-Piperidinone with Dynamic Kinetic Resolution." *Org. Lett.*, **2014**, *16*, 860-863.

- 10 Huang, H.; Bellotti, P.; Pfluger, P.; Schwarz, L.; Heidrich, B.; Glorius, F. Three-Component, Interrupted Radical Heck/Allylic Substitution Cascade Involving Unactivated Alkyl Bromides. *J. Am. Chem. Soc.*, **2020**, *142*, 10173-10183.
11. Wang, H.; Jui, N. "Catalytic Defluoroalkylation of Trifluoromethylaromatics with Unactivated Alkenes." *J. Am. Chem. Soc.* **2018**, *140*, 1, 163–166
12. Cheng, R.; Shi, Z.; Ding, W.; Liu, Z.; Jin, H.; Yu, X.; Wang, S. Facile Synthesis of alpha-beta unsaturated esters through a one-pot copper catalyzed aerobic oxidation-Wittig reaction. *Tett. Lett.*, **2018**, *59*, 14-17.
13. Li, W.; Tang, J.; Li, S.; Zheng, X.; Yuan, M.; Xu, B.; Jiang, W.; Fu, H.; Li, R.; Chen, H. Stereodivergent Synthesis of Alkenylpyridines via Pd/Cu Catalyzed C–H Alkenylation of Pyridinium Salts with Alkynes. *Org. Lett.*, **2020**, *22*, 7814-7819.
14. Liu, Z.; Dong, N.; Xu, M.; Sum, Z.; Tu, T. "Mild Negishi Cross-Coupling Reactions Catalyzed by Acenaphthoimidazolide Palladium Complexes at Low Catalyst Loadings." *J. Org. Chem.*, **2013**, *78*, 7436-7444.
15. Mader, P.; Bartholomäus, R.; Nicolussi, S.; Baumann, A.; Weis, M.; Chicca, A.; Rau, M.; Simao, A.; Gertsch, J.; Altmann, K. "Synthesis and Biological Evaluation of Endocannabinoid Uptake Inhibitors Derived from WOBE437." *ChemMedChem.*, **2021**, *16*, 145-154.
16. Kim, S.; Goldfogel, M.; Gilbert, M.; Weix, D. "Nickel-Catalyzed Cross-Electrophile Coupling of Aryl Chlorides with Primary Alkyl Chlorides." *J. Am. Chem. Soc.*, **2020**, *142*, 9902-9907.

17. Ackermann, L.; Punji, B.; Song, W. "User-Friendly [(Diglyme)NiBr₂]-Catalyzed Direct Alkylations of Heteroarenes with Unactivated Alkyl Halides through C-H Bond Cleavages." *Adv. Synth. Catal.*, **2011**, 353, 3325-3329.
18. Boyington, A.; Riu, M.; Jui, N. "Anti-Markovnikov Hydroarylation of Unactivated Olefins via Pyridyl Radical Intermediates." *J. Am. Chem. Soc.* **2017**, 139, 19, 6582–6585.
19. Hara, N.; Saito, T.; Semba, K.; Kuriakose, N.; Zheng, H.; Sakaki, S.; Nako, Y. "Rhodium Complexes Bearing PAIP Pincer Ligands." *J. Am. Chem. Soc.* **2018**, 140, 23, 7070–7073
20. Kondolff, I.; Doucet, H.; Santelli, M. "Tetrphosphine/palladium catalysed Suzuki cross-coupling reactions of aryl halides with alkylboronic acids." *Tetrahedron Lett.* **2004**, 60, 3813-3818.
21. Cassani, C.; Bergonzini, G.; Wallentin, C. "Photocatalytic Decarboxylative Reduction of Carboxylic Acids and Its Application in Asymmetric Synthesis." *Org. Lett.*, **2014**, 16, 4228-4231.
22. Cassani, C.; Bergonzini, G.; Wallentin, C. Photocatalytic Decarboxylative Reduction of Carboxylic Acids and Its Application in Asymmetric Synthesis. *Org. Lett.*, **2014**, 16, 4228-4231.
23. Wang, T.; Sang, S.; Liu, L.; Qiao, H.; Gao, Y.; Zhao, Y. "Experimental and Theoretical Study on Palladium- Catalyzed C-P Bond Formation via Direct Coupling of Triarylbismuths with P(O)-H Compounds." *J. Org. Chem.* **2014**, 79, 2, 608–617.
24. Xia, Q.; Liu, X.; Zhang, Y.; Chen, C.; Chen, W. "Copper- Catalyzed N-Methylation of Amides and O-Methylation of Carboxylic Acids by Using Peroxides as the Methylating Reagents." *Org. Lett.* **2013**, 15, 13, 3326–3329

25. Suarez-Pantiga, S.; Hernandez-Ruiz, R.; Virumbrales, C.; Pedrosa, M.; Sanz, R. “Reductive Molybdenum-Catalyzed Direct Amination of Boronic Acids with Nitro Compounds.” *Angew. Chem. Int. Ed.* **2019**, 58, 2129–2133.
26. Z.; Sun, Q.; Xia, C.; Sun, W. “CO₂ as a C1 Source: B(C₆F₅)₃-Catalyzed Cyclization of *o*-Phenylene-diamines To Construct Benzimidazoles in the Presence of Hydrosilane.” *Org. Lett.* **2016**, 18, 24, 6316–6319.
27. Bonfio, C.; Caumes, C.; Duffy, C.; Patel, B.; Percivalle, C.; Tsnakopoulou, M.; Sutherland, J. “Length-Selective Synthesis of Acylglycerol-Phosphates through Energy-Dissipative Cycling.” *J. Am. Chem. Soc.* **2019**, 141, 9, 3934–3939
28. Houjeiry, T.; Poe, S.; McQuade, T. “Synthesis of Optically Active 4-Substituted 2-Cyclohexenones.” *Org. Lett.* **2012**, 14, 17, 4394–4397
29. Tamang, S.; Bedi, D.; Shafiei-Haghighi, S.; Smith, C Crawford, C.; Findlater, M. “Cobalt-Catalyzed Hydroboration of Alkenes, Aldehydes, and Ketones.” *Org. Lett.* **2018**, 20, 6695–6700.
30. Li, W.; Tang, J.; Li, S.; Zheng, X.; Yuan, M.; Xu, B.; Jiang, W.; Fu, H.; Li, R.; Chen, H. Stereodivergent Synthesis of Akenylpyridines via Pd/Cu Catalyzed C-H Alkenylation of Pyridinium Salts with Alkynes. *Org. Lett.*, **2020**, 22, 7814-7819.
31. Cismesia, M.; Yoon, T. “Characterizing chain processes in visible light photoredox catalysis.” *Chem. Sci.*, **2015**, 6, 5426–5434.
32. Zhang, Z.; Sun, Q.; Xia, C.; Sun, W. CO₂ as a C1 Source: B(C₆F₅)₃-Catalyzed Cyclization of *o*-Phenylene-diamines to Construct Benzimidazoles in the Presence of Hydrosilane. *Org. Lett.*, **2016**, 18, 6316-6319.

33. M. J. Frisch, G. W. Trucks, H. B. Schlegel, G. E. Scuseria, M. A. Robb, J. R. Cheeseman, G. Scalmani, V. Barone, G. A. Petersson, H. Nakatsuji, X. Li, M. Caricato, A. Marenich, J. Bloino, B. G. Janesko, R. Gomperts, B. Mennucci, H. P. Hratchian, J. V. Ortiz, A. F. Izmaylov, J. L. Sonnenberg, D. Williams-Young, F. Ding, F. Lipparini, F. Egidi, J. Goings, B. Peng, A. Petrone, T. Henderson, D. Ranasinghe, V. G. Zakrzewski, J. Gao, N. Rega, G. Zheng, W. Liang, M. Hada, M. Ehara, K. Toyota, R. Fukuda, J. Hasegawa, M. Ishida, T. Nakajima, Y. Honda, O. Kitao, H. Nakai, T. Vreven, K. Throssell, J. A. Montgomery, Jr., J. E. Peralta, F. Ogliaro, M. Bearpark, J. J. Heyd, E. Brothers, K. N. Kudin, V. N. Staroverov, T. Keith, R. Kobayashi, J. Normand, K. Raghavachari, A. Rendell, J. C. Burant, S. S. Iyengar, J. Tomasi, M. Cossi, J. M. Millam, M. Klene, C. Adamo, R. Cammi, J. W. Ochterski, R. L. Martin, K. Morokuma, O. Farkas, J. B. Foresman, and D. J. Fox, Gaussian, Inc., Wallingford CT, **2016**.
34. (a) Lee, C.; Yang, W.; Parr, R. G. *Phys. Rev. B*, **1988**, 37 (2), 785–789. (b) Becke, A. D. *J. Chem. Phys.* **1993**, 98 (7), 5648–5652.
35. Roth, H. G.; Romero, N. A.; Nicewicz, D. A. Experimental and Calculated Electrochemical Potentials of Common Organic Molecules for Applications to Single Electron Redox Chemistry. *Synlett*. **2016**, 27 (05), 714–723

S3.3: Supporting Information

S3.3.1 General Information

A. General Reagent Information

Reagents were purchased from Sigma-Aldrich, Alfa Aesar, Acros Organics, Combi-Blocks, Oakwood Chemicals, Astatech, and TCI America and used as received, unless stated otherwise. All reactions were set up on the bench top and conducted under nitrogen atmosphere while subject to irradiation from blue LEDs (LEDwholesalers PAR38 Indoor Outdoor 16-Watt LED

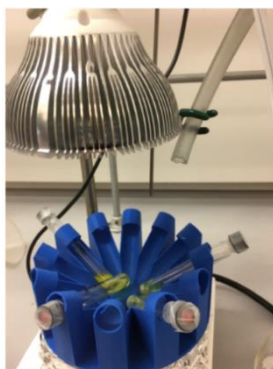
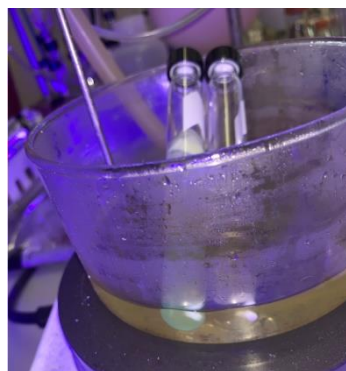
Flood Light Bulb, Blue; or Hydrofarm® PPB1002 PowerPAR LED Bulb-Blue 15W/E27 (available from Amazon). Flash chromatography was carried out using Siliaflash® P60 silica gel obtained from Silicycle. Thin-layer chromatography (TLC) was performed on 250 μm SiliCycle silica gel F-254 plates. Visualization of the developed chromatogram was performed by fluorescence quenching or staining using KMnO_4 , p-anisaldehyde, or ninhydrin stains. DMSO was purchased from Fisher Scientific and was distilled over CaH_2 and degassed by sonication under vacuum and stored under nitrogen. Photoredox catalyst 4CzIPN was prepared according to literature procedures.¹

B. General Analytical Information

Unless otherwise noted, all yields refer to chromatographically and spectroscopically (^1H NMR) homogenous materials. New compounds were characterized by NMR and HRMS. ^1H and ^{13}C NMR spectra were obtained from the Emory University NMR facility and recorded on a Bruker Avance III HD 600 equipped with cryo-probe (600 MHz), Bruker 400 (400 MHz), INOVA 600 (600 MHz), INOVA 500 (500 MHz), INOVA 400 (400 MHz), or VNMR 400 (400 MHz), and are internally referenced to residual protio solvent signals. Data for ^1H NMR are reported as follows: δ chemical shift (ppm), multiplicity (s = singlet, d = doublet, t = triplet, q = quartet, m = multiplet, dd = doublet of doublets, dt = doublet of triplets, ddd = doublet of doublet of doublets, dtd = doublet of triplet of doublets, b = broad, etc.), coupling constant (Hz), integration, and assignment, when applicable. Data for decoupled ^{13}C NMR are reported in terms of chemical shift and multiplicity when applicable. High Resolution mass spectra were obtained from the Emory University Mass Spectral facility.

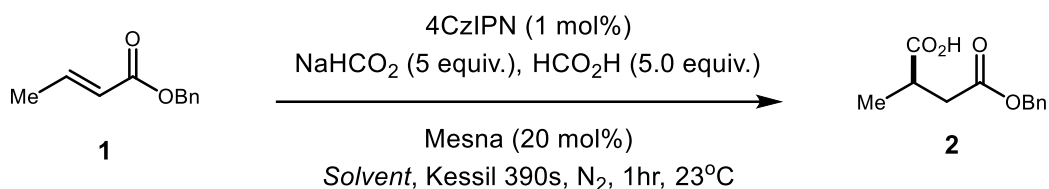
C. General Photoredox Reaction Setup

To run multiple reactions, an appropriately sized 3D printed carousel was used, which exposed the reactions to the blue light evenly (photo 1). A 15 W LED array lamp was used as a blue light source (photo 2,3). These lamps were routinely used for up to 12 reactions at a time (photo 2,3). The blue LEDs were positioned approximately 6 inches above the reaction vials to get good light coverage without overheating the reactions (photo 2,3). Reactions run at elevated temperatures were irradiated in a shallow oil bath (photo 4,5).

**Photo 1****Photo 2****Photo 3****Photo 4****Photo 5**

3.3.2: Optimization of Carboxylation of Michael Acceptors

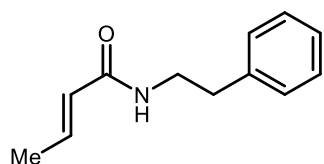
Procedure: An 8 mL screw-top test tube was charged with benzyl (E)-but-2-enoate S1 (1.0 equiv, 0.1 mmol), 4CzIPN (1 mol%, 0.001 mol), sodium formate (5.0 equiv, 0.5 mmol), formic acid (5.0 equiv, 0.5 mmol) and mesna (20 mol%, 0.02 mol). The tube was equipped with a stir bar and sealed with a PTFE/silicon septum. Under nitrogen atmosphere, separately degassed solvent (1 mL) was added via syringe. The resulting mixture was stirred at 1400 RPM for 16 h under irradiation by a kessil 390s lamp. Saturated aqueous potassium carbonate was added and reaction was then extracted with ethyl acetate (3 x). The organic layer was passed through a small silica plug with 100% EtOAc and concentrated. Deutro-chloroform with an internal standard of dibromomethane (7 μ L, 0.1 mmol) was added. The sample was analyzed by ^1H NMR ($d = 5$ s), and the integral values were used to calculate the data given in Table 2.1.

Table S-1. Optimization and Controls of Michael Acceptor Carboxylation**3.3.3: Preparation of Substrates**

Entry	Solvent	Deviation	Yield ^b
1	DMSO	-	31%
2	10% H ₂ O/DMSO	-	47%
3	20% H ₂ O/DMSO	-	95%
4	50% H ₂ O/DMSO	-	73%
5	20% H ₂ O/DMSO	no mesna	15%
6	20% H ₂ O/DMSO	no HCO ₂ H	77%
7	20% H ₂ O/DMSO	no light	0%

^aConditions: **1** (1.0 equiv.), 4CzIPN (1 mol%), sodium formate (5.0 equiv.), formic acid (5.0 equiv.), mesna (20 mol%), Solvent [0.1M], 390 nm light, N₂, 1hr, 0.1 mmol scale. ^bYield determined via ¹H NMR with dibromomethane as an internal standard. ^cReaction ran for 16 hrs.

(E)-N-phenethylbut-2-enamide (S15): To a flame dried round bottom flask was added crotonic acid (5 mmol, 0.43 g, 1 equiv) after which the atmosphere was exchanged three times with nitrogen. CH₂Cl₂ (20 mL) was then added followed by oxalyl chloride (5.5 mmol, 0.46 mL, 1.5



equiv) and DMF (2 drops)—the reaction mixture was then allowed to stir for 1 hour. Phenethylamine (6 mmol, 0.76 mL, 1.2 equiv) was

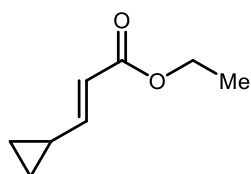
then added in one portion followed by triethylamine (5.5 mmol, 0.77 mL, 1.1 equiv). The reaction mixture was allowed to stir overnight, diluted with CH₂Cl₂ (20 mL) and 1M HCl (10 mL). The organic phase was separated from the aqueous phase and washed with 1M HCl (10 mL), brine (2x), dried over Na₂SO₄, and concentrated *in vacuo*. The crude product was pushed through a silica plug with (50% EtOAc/Hexanes as the eluent) to afford the title compound as white solid (0.96 g, 99% yield).

¹H NMR (600 MHz, Chloroform-d) δ 7.31 (t, J = 7.6 Hz, 1H), 7.24 (t, J = 7.9 Hz, 2H), 7.20 (d, J = 7.3 Hz, 2H), 6.83 (dq, J = 15.2, 6.9 Hz, 1H), 5.72 (dd, J = 15.2 Hz, 1.6 Hz, 1H), 5.39 (bs, 1H), 3.59 (td, J = 6.9 Hz, 5.9 Hz, 2H), 2.84 (t, J = 6.9 Hz, 2H), 1.83 (dd, J = 6.9, 1.6 Hz, 3H).

¹³C NMR (600 MHz, Chloroform-d) δ 165.9, 140.5, 138.5, 128.8, 128.7, 125.9, 124.9, 40.53, 35.7, 17.2.

HRMS (APCI) *m/z*: [M+H] calcd. for C₁₂H₁₆NO, 190.1226; found, 190.1229.

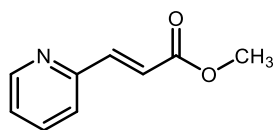
Rf: 0.34 (50% EtOAc/Hexanes)



Ethyl (*E*)-3-cyclopropylacrylate (S16): To a flame dried round bottom flask was added sodium hydride (3.6 mmol, 0.14 g, 1.2 equiv) after which the atmosphere was exchanged three times with N₂. THF was added (5 mL) and the flask was then cooled to 0 °C followed by the dropwise addition of triethyl phosphonoacetate (3.3 mmol, 0.65 mL, 1.2 equiv). The reaction mixture was then stirred at 0 °C for thirty minutes after which cyclopropane carboxaldehyde (3 mmol, 0.22 mL, 1 equiv) was added dropwise as a solution in THF (5 mL). The reaction mixture was then allowed to warm to room temperature, stirred overnight, and then quenched with saturated

aqueous ammonium chloride (10 mL) at 0 °C. The aqueous phase was extracted with EtOAc (3x) dried over Na₂SO₄, and concentrated *in vacuo*. The crude product was then pushed through a silica plug using (10% EtOAc/Hexanes as the eluent) to afford the title compound as yellow oil (0.42 g, 99% yield). The physical and spectral properties were consistent with the reported values.¹²

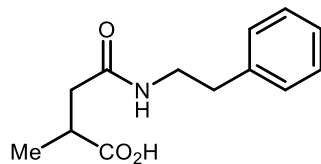
¹H NMR (600 MHz, Chloroform-d) δ 6.41 (dd, J = 15.4 Hz, 10.1 Hz, 1H), 5.89 (d, J = 15.4 Hz, 1H), 4.17 (q, J = 10.7 Hz, 2H), 1.58-1.53 (m, 1H), 1.26 (t, J = 7.1 Hz, 3H), 0.95-0.91 (m, 2H), 0.65-0.61 (m, 2H).



Methyl (*E*)-3-(pyridine-2-yl)acrylate (S18): A round bottom flask was equipped with 2-pyridinecarboxaldehyde (5 mmol, 0.48 mL, 1 equiv), methyl (triphenylphosphoranylidene)acetate (7.5 mmol, 2.50 g, 1.5 equiv) and benzene (10 mL) under nitrogen. The reaction was then heated to 80 °C for three hours, cooled to room temperature, and concentrated *in vacuo*. The crude product was purified by silica chromatography (30- 40% EtOAc/Hexanes as the eluent) to give the title compound as a light brown solid (0.59 g, 73% yield). The physical properties and spectral data were consistent with the reported values.¹³

¹H NMR (600 MHz, CDCl₃) δ 8.64 (d, J = 4.8 Hz, 1H), 7.73-7.64 (m, 2H), 7.42 (d, J = 7.8 Hz, 1H), 7.29-7.24 (m, 1H), 6.93 (d, J = 15.7 Hz, 1H), 3.81 (s, 3H).

3.3.4: Preparation of Products from Figure 3.5



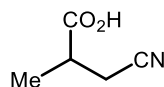
2-methyl-4-oxo-4-(phenethylamino)butanoic acid (30): Prepared according to general procedure A using (*E*)-*N*-phenethylbut-2-enamide **S15** (1 mmol, 0.189 g, 1 equiv), sodium formate (5 mmol, 0.34 g, 5.0 equiv), formic acid (5 mmol, 0.19 mL, 5 equiv), mesna (0.2 mmol, 0.032 g, 20 mol%) and 4CzIPN (0.01 mmol, 0.0078 g, 1 mol%) in 0.1 M 20% H₂O/ DMSO (10 mL). After 16 hours under irradiation by Kessil 390 nm light, the crude product was purified by silica chromatography (10- 100% EtOAc/Hexanes + 1% AcOH as eluent) to afford the title compound as a white solid (0.162 g, 69% yield).

¹H NMR (400 MHz, Chloroform-*d*) δ 7.31 (m, 2H), 7.23 (m, 3H), 5.72 (br s, 1H), 3.64 – 3.47 (m, 2H), 3.01 – 2.87 (m, 1H), 2.83 (t, *J* = 6.9 Hz, 2H), 2.54 (dd, *J* = 15.6, 8.8 Hz, 1H), 2.30 (dd, *J* = 15.5, 4.3 Hz, 1H), 1.23 (d, *J* = 7.2 Hz, 3H).

¹³C NMR (151 MHz, DMSO-*d*₆) δ 176.72, 170.30, 139.48, 128.61, 128.27, 126.02, 40.15, 38.66, 35.45, 35.17, 16.65.

HRMS (APCI) *m/z*: [M+H] calcd. for C₁₃H₁₈NO₃, 236.1281; found, 236.1285.

R_f: 0.14 (85% EtOAc/Hexanes)



3-cyano-2-methylpropanoic acid (31): Prepared according to general procedure A using crotonitrile (1 mmol, 0.076 g, 1 equiv), sodium formate (5 mmol, 0.34 g, 5.0 equiv), formic acid (5 mmol, 0.19 mL, 5 equiv), mesna (0.2 mmol, 1.032 g, 20 mol%) and 4CzIPN (0.01 mmol, 0.0078 g, 1 mol%) in 0.1 M 20% H₂O/ DMSO (10 mL). After 16 hours under irradiation by

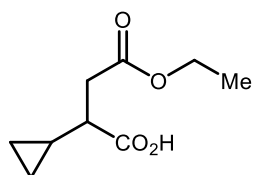
Kessil 390 nm light, the crude reaction mixture was diluted with EtOAc (10 mL) and washed with saturated aqueous potassium carbonate. The organic phase was collected in a flask and the aqueous phase was acidified with concentrated HCl to pH 1-2. The aqueous phase was then extracted with EtOAc (3 x) and the combined organic extracts were pushed through a silica plug (100% EtOAc as eluent) and concentrated *in vacuo* to afford the title compound as a yellow oil (0.071 g, 63% yield).

¹H NMR (600 MHz, Chloroform-*d*): δ 2.94-2.84 (m, 1H), 2.70 (dd, $J = 16.7, 5.91$ Hz, 1H), 2.57 (dd, $J = 16.8, 7.4$ Hz, 1H), 1.43 (d, $J = 7.2$ Hz, 3H).

¹³C NMR (151 MHz, Chloroform-*d*) δ 178.31, 117.59, 77.37, 77.16, 76.95, 36.09, 20.93, 16.60.

HRMS (APCI) m/z : [M+H] calcd. for C₅H₈NO₂, 114.0550; found, 114.0553.

Rf: 0.35 (50% EtOAc/Hexanes)



2-cyclopropyl-4-ethoxy-4-oxobutanoic acid (32): Prepared according to general procedure A using ethyl (*E*)-3-cyclopropylacrylate **S16** (1 mmol, 0.140 g, 1 equiv), sodium formate (5 mmol, 0.34 g, 5.0 equiv), formic acid (5 mmol, 0.19 mL, 5 equiv), mesna (0.2 mmol, 0.032 g, 20 mol%) and 4CzIPN (0.01 mmol, 0.0078 g, 1 mol%) in 0.1 M 20% H₂O/ DMSO (10 mL). After 16 hours under irradiation by Kessil 390 nm light, the crude product was purified by silica chromatography (10-70% EtOAc/Hexanes + 1% AcOH as eluent) to afford the title compound as a yellow oil (0.122 g, 66% yield).

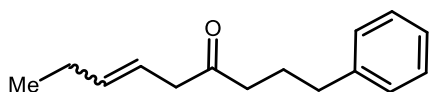
¹H NMR (600 MHz, Chloroform-*d*) δ 4.24 – 3.95 (m, 2H), 2.82 (dd, $J = 16.1, 10.2$ Hz, 1H),

2.59 (dd, $J = 16.1, 5.5$ Hz, 1H), 2.06 (td, $J = 9.7, 4.9$ Hz, 1H), 1.24 (t, $J = 7.1$ Hz, 3H), 0.97 – 0.80 (m, 1H), 0.63 – 0.52 (m, 2H), 0.52 – 0.43 (m, 1H), 0.25 – 0.16 (m, 1H).

^{13}C NMR (151 MHz, Chloroform-*d*) δ 180.30, 171.96, 60.88, 46.27, 36.53, 14.23, 13.59, 4.44.

HRMS (APCI) m/z : [M+H] calcd. for $\text{C}_9\text{H}_{15}\text{O}_4$, 187.0965; found, 187.0968.

Rf: 0.52 (50% EtOAc/Hexanes)



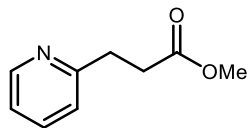
(E)-1-phenylnon-6-en-4-one (33): Prepared according to general procedure A using (*E*)-1-cyclopropyl-6-phenylhex-1-en-3-one **S17** (1 mmol, 0.214 g, 1 equiv), sodium formate (5 mmol, 0.34 g, 5.0 equiv), formic acid (5 mmol, 0.19 mL, 5 equiv), mesna (0.2 mmol, 0.032 g, 20 mol%) and 4CzIPN (0.01 mmol, 0.0078 g, 1 mol%) in 0.1 M 20% H_2O / DMSO (10 mL). After 16 hours under irradiation by Kessil 390 nm light, the crude product was purified by silica chromatography (5- 20% EtOAc/Hexanes) to afford the title compound as a mixture of E/Z isomers as a clear oil (0.168 g, 77% yield).

^1H NMR (600 MHz, Chloroform-*d*): δ 7.28 (t, $J = 7.4$ Hz, 2H), 7.21-7.15 (m, 3H), 5.61—5.53 (m, 1H), 5.51-5.46 (m, 1H), 3.14-3.12 (d, $J = 7.1$ Hz, 0.37 H, Z isomer), 3.07 (d, $J = 6.7$ Hz, 1.70 H, E isomer), 2.61 (t, $J = 7.6$ Hz, 2H), 2.44 (t, $J = 7.1$ Hz, 2H), 2.08-1.99 (m, 2H), 1.94-1.87 (m, 2H), 0.98 (t, $J = 7.3$ Hz, 3H).

^{13}C NMR (151 MHz, Chloroform-*d*) δ 209.50, 208.89, 141.78, 136.84, 135.46, 128.61, 128.51, 126.07, 121.01, 120.38, 46.97, 41.78, 41.53, 41.38, 35.20, 25.75, 25.33, 25.26, 20.95, 14.06, 13.66.

HRMS (APCI) m/z : [M+H] calcd. for $\text{C}_{15}\text{H}_{21}\text{O}$, 217.1587; found, 217.1590.

Rf: 0.60 (10% EtOAc/Hexanes)



Methyl 3-(pyridin-2-yl)propanoate (34): Prepared according to general procedure A using methyl (*E*)-3-(pyridine-2-yl)acrylate **S18** (1 mmol, 0.163 g, 1 equiv), sodium formate (5 mmol, 0.34 g, 5.0 equiv), formic acid (5 mmol, 0.19 mL, 5 equiv), mesna (0.2 mmol, 0.032 g, 20 mol%) and 4CzIPN (0.01 mmol, 0.0078 g, 1 mol%) in 0.1 M 20% H₂O/ DMSO (10 mL). After 16 hours under irradiation by Kessil 390 nm light, the crude product was by silica chromatography (30-50% EtOAc/as the eluent) to afford the title compound as a colorless oil (0.157 g, 95% yield). The physical and spectral properties are consistent with the reported values.³⁰

¹H NMR (600 MHz, CDCl₃): δ 8.51 (d, *J* = 3.2 Hz, 1H), 7.59 (td, *J* = 7.7, 2.0 Hz, 1H), 7.18 (d, *J* = 7.8 Hz, 1H), 7.14-7.07 (m, 1H), 3.66 (s, 3H), 3.11 (t, *J* = 7.5 Hz, 2H), 2.81 (t, *J* = 7.5 Hz, 2H).

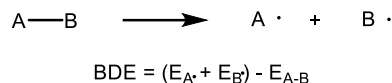
3.3.5: Computational Details

General.

All DFT calculations were carried out using the Gaussian 9 software package at the (U)B3LYP or R(B3LYP)³³ level of theory with the 6-311+G(d,p)³⁴ basis set. The CPCM formalism for the Self Consistent Reaction Field (SCRF) model of solvation was employed in calculations to account for solvation in DMSO, and the default parameters as implemented in Gaussian were used.

Calculated Bond Dissociation Energies

Calculations were carried out at the (U)B3LYP³² level of theory with the 6-311+G(d,p)³⁴ basis set. Bond dissociation energies (BDEs) were calculated according to the following equation:



Calculated BDEs (kcal/mol):

Sodium Formate: 90 kcal/mol

Formic acid: 101 kcal/mol

Ethyl Formate: 100 kcal/mol

DMF: 99 kcal/mol

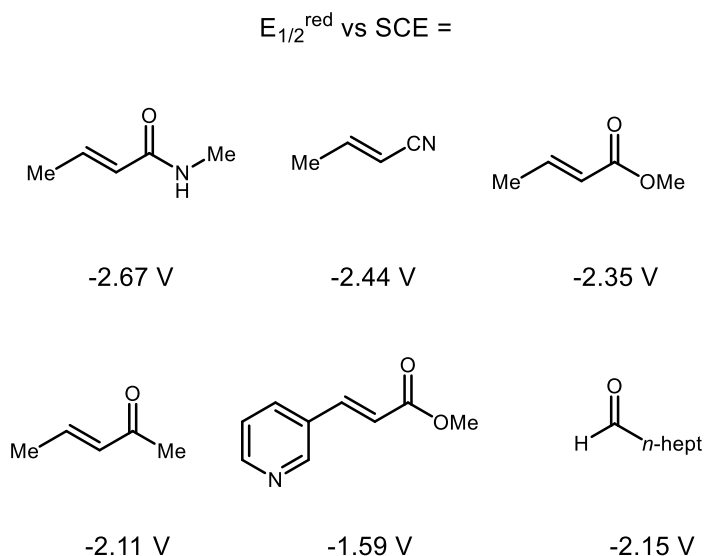
Octanal: 86 kcal/mol

Calculated Reduction Potentials

Reduction potentials were calculated using a modified procedure as described by Nicewicz and coworkers.³⁵ Geometry optimizations were carried out for the reduced and neutral forms of each molecule, and frequency calculations were performed on the minimized structures to ensure no imaginary frequencies existed. Geometry optimizations that did not converge to an energy minimum upon the initial calculation were sequentially optimized using a tight convergence criteria. Gibbs free energies (G_{298}) were obtained from the calculation and employed in the following equation:

$$E_{1/2}^{0,calc} = -\frac{(G_{298}[reduced] - G_{298}[oxidized])}{n_e \mathcal{F}} - E_{1/2}^{0,SHE} + E_{1/2}^{0,SCE}$$

Where n_e is the number of electrons transferred ($n_e = 1$ for all calculations here), \mathcal{F} is the Faraday constant (value $23.061 \text{ kcal mol}^{-1} \text{ V}^{-1}$), $E_{1/2}^{0,SHE}$ is the absolute value for the standard hydrogen electrode (SHE, value = 4.281 V) and $E_{1/2}^{0,SCE}$ is the potential of the saturated calomel electrode (SCE) relative to the SHE in DMSO (value = -0.279)²⁸, and $G_{298}[\text{oxidized}]$ and $G_{298}[\text{reduced}]$ are the Gibbs free energies in DMSO obtained from DFT calculations.



3.3.6: References

1. Luo, J.; Zhang, J. "Donor-Acceptor Fluorophores for Visible-Light-Promoted Organic Synthesis: Photoredox/ Ni Dual Catalytic C(sp³)-C(sp²) Cross- Coupling." *ACS Catal.* **2016**, 6, 873–877.
2. Cheng, R.; Shi, Z.; Ding, W.; Liu, Z.; Jin, H.; Yu, X.; Wang, S. Facile Synthesis of alpha-beta unsaturated esters through a one-pot copper catalyzed aerobic oxidation-Wittig reaction. *Tett. Lett.*, **2018**, 59, 14-17.

3. Li, W.; Tang, J.; Li, S.; Zheng, X.; Yuan, M.; Xu, B.; Jiang, W.; Fu, H.; Li, R.; Chen, H. Stereodivergent Synthesis of Alkenylpyridines via Pd/Cu Catalyzed C–H Alkenylation of Pyridinium Salts with Alkynes. *Org. Lett.*, **2020**, *22*, 7814–7819.

4. Li, W.; Tang, J.; Li, S.; Zheng, X.; Yuan, M.; Xu, B.; Jiang, W.; Fu, H.; Li, R.; Chen, H. Stereodivergent Synthesis of Alkenylpyridines via Pd/Cu Catalyzed C–H Alkenylation of Pyridinium Salts with Alkynes. *Org. Lett.*, **2020**, *22*, 7814–7819

5. (a) Lee, C.; Yang, W.; Parr, R. G. *Phys. Rev. B*, **1988**, *37* (2), 785–789. (b) Becke, A. D. *J. Chem. Phys.* **1993**, *98* (7), 5648–5652.

6. Roth, H. G.; Romero, N. A.; Nicewicz, D. A. Experimental and Calculated Electrochemical Potentials of Common Organic Molecules for Applications to Single Electron Redox Chemistry. *Synlett* **2016**, *27* (05), 714–723.

S4.6 Supporting Information

I. General Information

I-A. General Reagent Information

Reagents were purchased from Sigma-Aldrich, Alfa Aesar, Acros Organics, Combi-Blocks, Oakwood Chemicals, Astatech, and TCI America and used as received, unless stated otherwise.

All reactions were set up on the bench top and conducted under nitrogen atmosphere while

subject to irradiation from blue LEDs (LEDwholesalers PAR38 Indoor Outdoor 16-Watt LED Flood Light Bulb, Blue; or Hydrofarm® PPB1002 PowerPAR LED Bulb-Blue 15W/E27 (available from Amazon). Flash chromatography was carried out using Siliaflash® P60 silica gel obtained from Silicycle. Thin-layer chromatography (TLC) was performed on 250 μm SiliCycle silica gel F-254 plates. Visualization of the developed chromatogram was performed by fluorescence quenching or staining using KMnO_4 , p-anisaldehyde, or ninhydrin stains. DMSO was purchased from Fisher Scientific and was distilled over CaH_2 and degassed by sonication under vacuum and stored under nitrogen. Photoredox catalyst 4CzIPN was prepared according to literature procedures.¹

I-B. General Analytical Information.

Unless otherwise noted, all yields refer to chromatographically and spectroscopically (^1H NMR) homogenous materials. New compounds were characterized by NMR and HRMS. ^1H and ^{13}C NMR spectra were obtained from the Emory University NMR facility and recorded on a Bruker Avance III HD 600 equipped with cryo-probe (600 MHz), Bruker 400 (400 MHz), INOVA 600 (600 MHz), INOVA 500 (500 MHz), INOVA 400 (400 MHz), or VNMR 400 (400 MHz), and are internally referenced to residual protio solvent signals. Data for ^1H NMR are reported as follows: chemical shift (ppm), multiplicity (s = singlet, d = doublet, t = triplet, q = quartet, m = multiplet, dd = doublet of doublets, dt = doublet of triplets, ddd = doublet of doublet of doublets, dtd = doublet of triplet of doublets, b = broad, etc.), coupling constant (Hz), integration, and assignment, when applicable. Data for decoupled ^{13}C NMR are reported in terms of chemical shift and multiplicity when applicable. High Resolution mass spectra were obtained from the

Emory University Mass Spectral facility using a Thermo Scientific Extractive Plus with an orbitrap mass analyzer.

I-C. General Photoredox Reaction Setup

To run multiple reactions, an appropriately sized 3D printed carousel was used, which exposed the reactions to the blue light evenly (photo 1). While our 3D printed carousel was helpful for screening reactions, it is not necessary in this system—any rack will suffice and our scaled reactions are simply held by a clamp. A 15 W LED array lamp was used as a blue light source (photo 2,3). These lamps were routinely used for up to 12 reactions at a time (photo 2,3). The blue LEDs were positioned approximately 6 inches above the reaction vials to get good light coverage without overheating the reactions (photo 2,3).

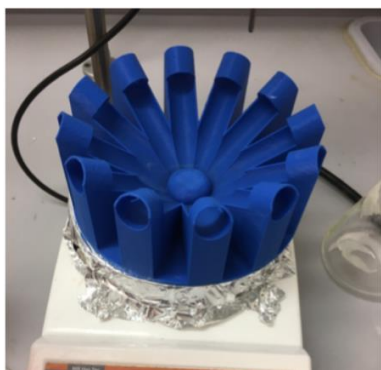


Photo 1

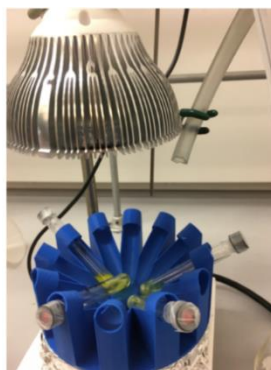


Photo 2



Photo 3

S4.6.1 General Procedures

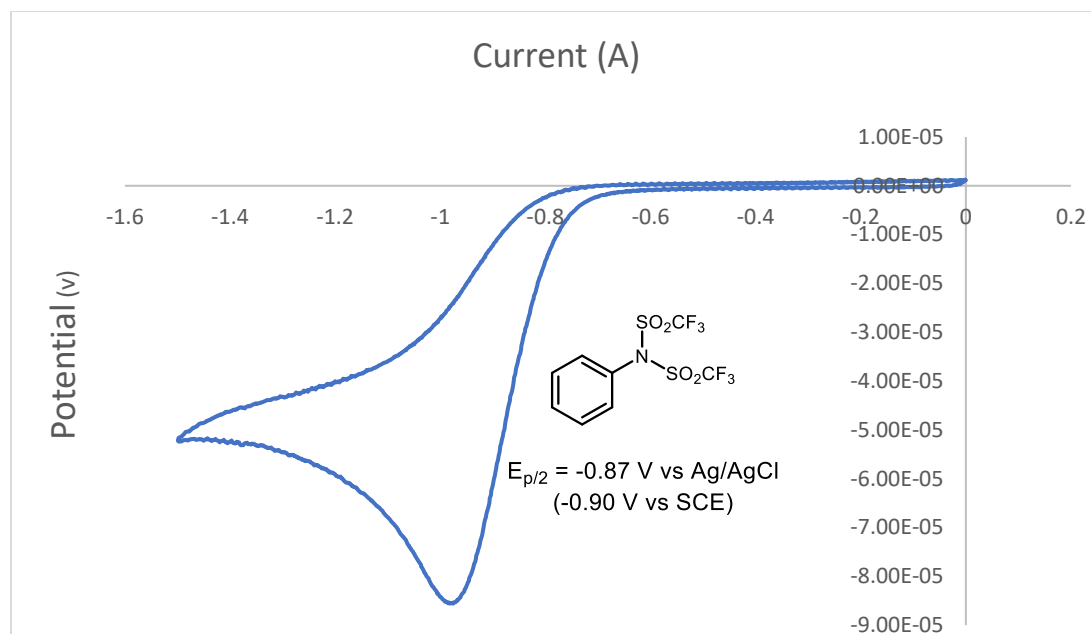
General Procedure A

A 20 mL screw-top test tube was charged with 4CzIPN (1 mol%), sodium formate (1.5 equiv), mesna (20 mol%), N-phenyl-bis(trifluoromethanesulfonimide) (15 mol%) and [4,4'-Bis(1,1-

dimethyl)-2,2'-bipyridine] nickel (II) bromide (10 mol%)) and substrate (1 equiv., *if solid*). The tube was equipped with a stir bar and was sealed with a PTFE/silicon septum. The atmosphere was exchanged by applying vacuum and backfilling with argon (this process was conducted a total of three times). Under argon atmosphere, separately the indicated degassed solvent (0.1 M) was added via syringe followed by the substrate (*if liquid*, 1.0 equiv). The resulting mixture was stirred at 1400 RPM for 16 h under irradiation by blue LEDs. 1M HCl was added and then the reaction mixture was extracted with ethyl acetate (3 x). The organic layer was dried over MgSO₄ and concentrated. The residue was purified on silica using the indicated solvent mixture as eluent to afford the title compound.

S4.6.2 Electrochemical Measurements

Electrochemical potentials were obtained with a standard set of conditions according to literature procedure.¹ Cyclic voltammograms (CVs) were collected with a VersaSTAT 4Potentiostat. Samples were prepared with 0.1 mmol of substrate in 10 mL of 0.1 M tetra-n-butylammonium hexafluorophosphate in dry, degassed acetonitrile. Measurements employed a glassy carbon working electrode, platinum wire counter electrode, 3M NaCl silver-silver chloride reference electrode, and a scan rate of 100 mV/s. Reductions were measured by scanning potentials in the negative direction and oxidations in the positive direction; the glassy carbon electrode was polished between each scan. Data was analyzed using Microsoft Excel by subtracting a background current prior to identifying the maximum current (C_p) and determining the potential (E_{p/2}) at half this value (C_p/2). The obtained value was referenced to Ag|AgCl and converted to SCE by subtracting 0.035 V.

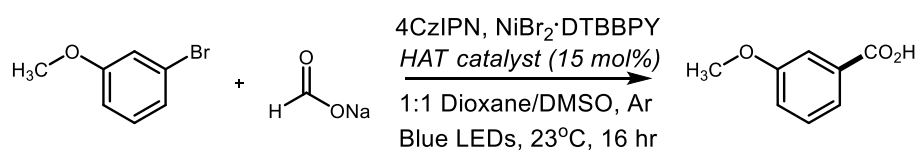


S4.6.3. Optimization Details

Optimization Procedure

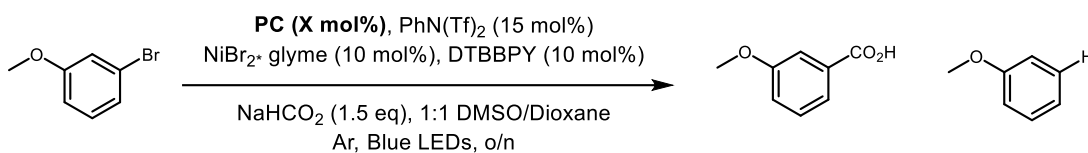
A 20 mL screw-top test tube was charged with 4CzIPN (1 mol%), sodium formate (1.5 equiv), mesna (20 mol%), N-phenyl-bis(trifluoromethanesulfonyl)benzamide (15 mol%) and [4,4'-Bis(1,1-dimethyl)-2,2'-bipyridine] nickel (II) bromide (10 mol%) and substrate (1 equiv., *if solid*). The tube was equipped with a stir bar and was sealed with a PTFE/silicon septum. The atmosphere was exchanged by applying vacuum and backfilling with argon (this process was conducted a total of three times). Under argon atmosphere, separately the indicated degassed solvent (0.1 M) was added via syringe followed by the substrate (*if liquid*, 1.0 equiv). The resulting mixture was stirred at 1400 RPM for 16 h under irradiation by blue LEDs. 1M HCl was added and then the reaction mixture was extracted with ethyl acetate (3 x). The organic layer was dried over MgSO₄ and concentrated. Deutero-chloroform with an internal standard of dibromomethane (7 μL, 0.1 mmol) was added. The sample was analyzed by ¹H NMR (d = 5 s), and the integral values were used to calculate the data given in Table S1- S3.

HAT Catalysts:



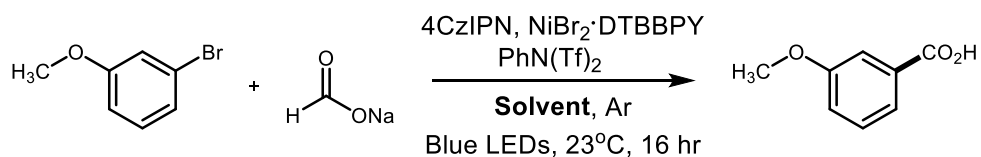
Entry	HAT Catalyst	Deviation	Yield ^a
1	Cyclohexanethiol	-	0%
2	Triphenylmethanethiol	-	0%
3	Triisopropylsilanethiol	-	0%
4	DABCO	-	0%
5	HOBt	-	0%
6	PhN(SO ₂ CF ₃) ₂	-	98%
7	Methanesulfonyl Chloride	-	90%
8	p-toluenesulfonyl chloride	-	76%
9	Sodium p-toluenesulfinate	-	0%

Photocatalyst Screen:



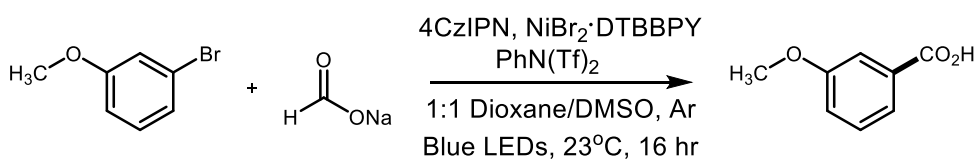
Entry	Conditions	Starting Material	Product	HDH	Phenyl Formate
1	Cl-4CzIPN	0%	95%	--	--
2	3DPAFIPN	70%	32%	--	--
3	3DPA2FBN	91%	8%	--	--
4	Ir(ppy) ₃	70%	30%	--	--
5	Ir[(dF(CF ₃)ppy) ₂ (dtbbpy) ₂ PF ₆	0%	100%	--	--
6	Ir[(ppy) ₂ dtbbpy]PF ₆	30%	69%	--	--
7	Benzophenone	100%	0%	--	--

Solvent Screen



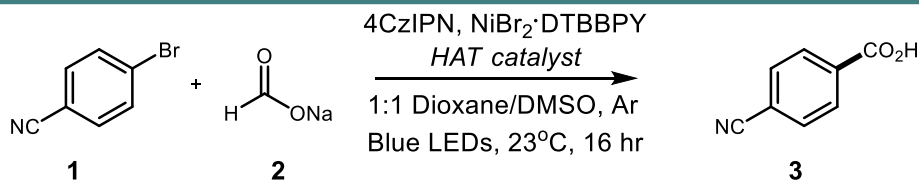
Entry	Solvent	Yield
1	1:1 Dioxane/DMSO	98%
2	Dioxane	0%
3	DMSO	85%
4	DMF	34%

Control Experiments:



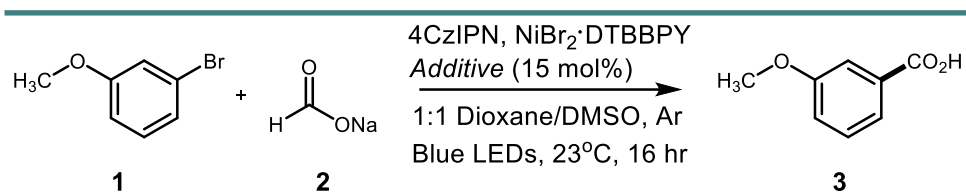
Entry	Deviation	Yield
1	No 4CzIPN	0%
2	No PhN(Tf) ₂	0%
3	No NaHCO ₂	0%
4	No light	0%
5	No air-free precautions	60%

HAT Catalyst Screen with Electron-Deficient Arene:



Entry	HAT Catalyst	Deviation	Yield ^a
1	Cyclohexanethiol	-	75%
2	Mesna	-	30%
3	Thiophenol	-	73%
4	Tert-butylthiol	-	51%
5	Thioacetic Acid	-	57%

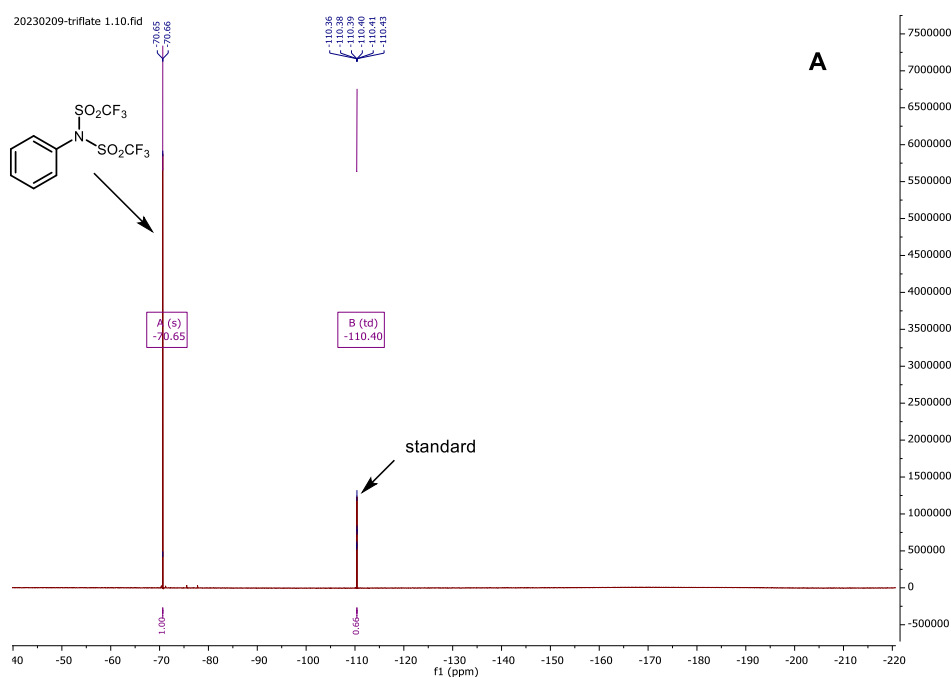
Reaction Controls for Sulfinyl Radical HAT processes:

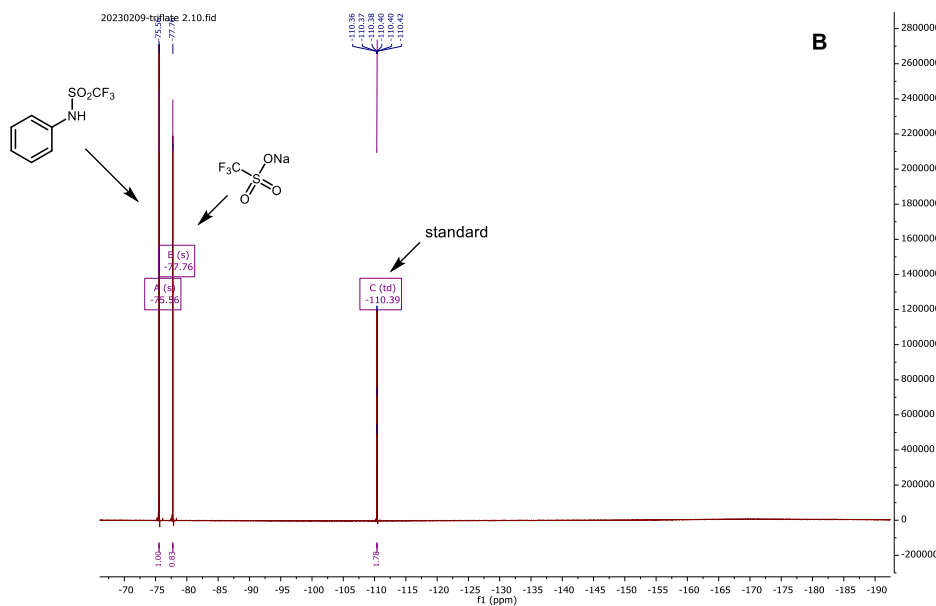


Entry	HAT Catalyst	Deviation	Yield ^a
1	Trifluoro- <i>N</i> -phenylmethanesulfonamide	-	0%
2	Sodium trifluoromethanesulfonate	-	0%
3	Sodium <i>p</i> -toluenesulfinate	-	0%

S4.6.4: Investigations into the Role of Phenyl Triflimide

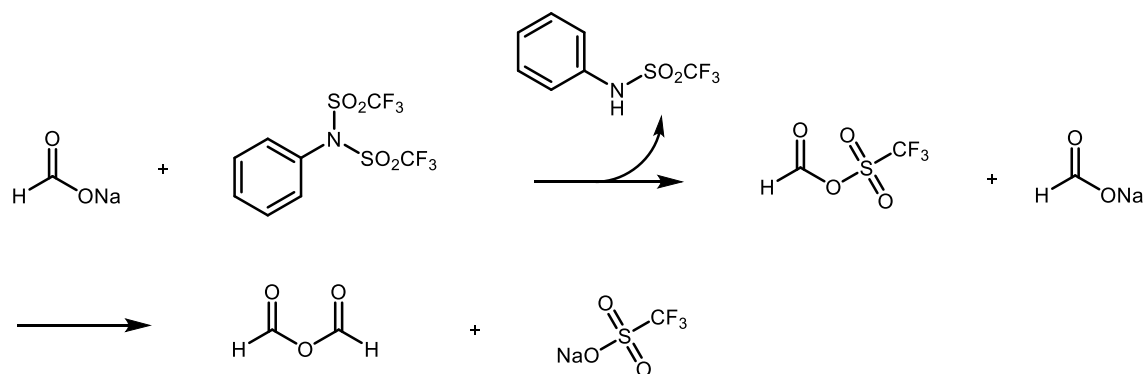
Samples were prepared using 0.015 mmol of phenyl triflimide (**A**) alongside a combination of 0.015 mmol phenyl triflimide and 0.15 mmol sodium formate (**B**) using 1-bromo-3-fluorobenzene as an internal standard in DMSO- d_6 .



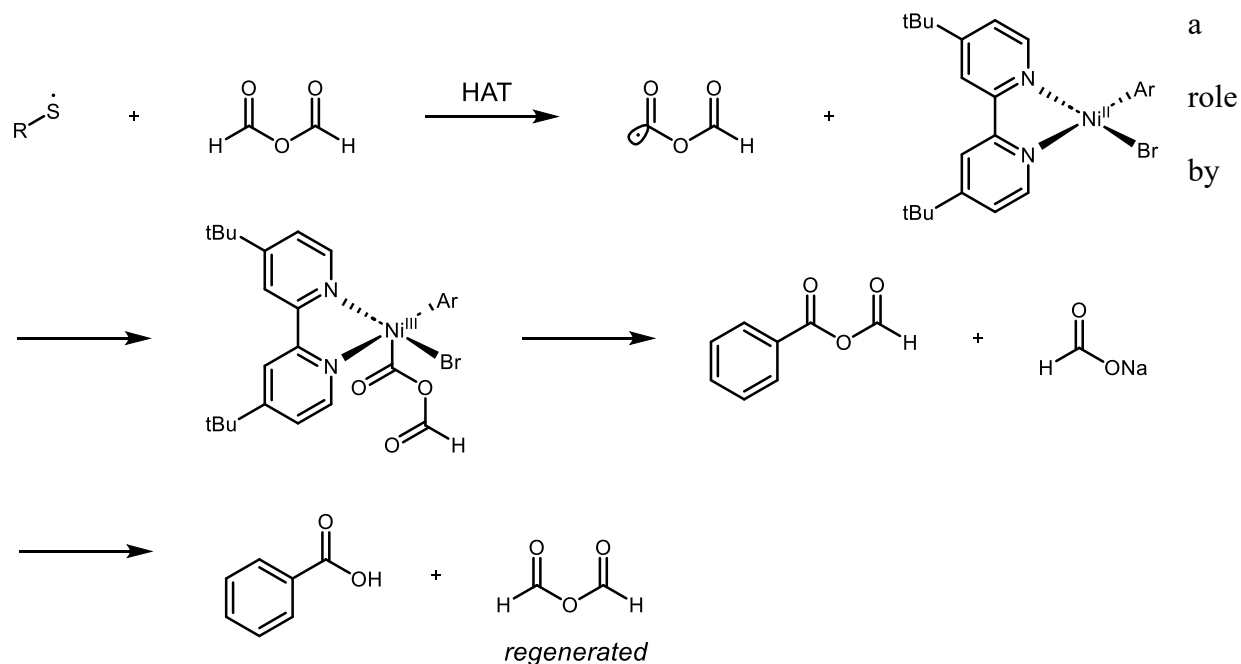


Spectra B shows

trifluoro-N-phenylmethanesulfonamide at -75.56 ppm alongside sodium trifluoromethanesulfonate at -77.76 ppm, these chemical shifts are consistent with the literature spectra.²¹ The presence of trifluoro-N-phenylmethanesulfonamide and sodium trifluoromethanesulfonate when sodium formate and phenyl triflimide are in solution together suggests the following reaction pathway.



In this reaction pathway, trifluoro-N-phenylmethanesulfonamide and sodium trifluoromethanesulfonate are generated—when tested independently as additives (**Table S-4**) no product formation is observed indicating that *in situ* generated formic anhydride may be playing

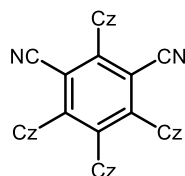


masking formate as the anhydride. A potential role for formic anhydride is shown below.

In this mechanistic scenario, DMSO may serve as a source of electrophilic HAT catalysts in the form of thiol. Our previous work has demonstrated that DMSO decomposes to various thiol/sulfur based impurities that catalyze radical formation²². HAT from formic anhydride would generate the acyl radical that may bind the metal center. Upon reductive elimination the mixed anhydride is formed which may be hydrolyzed by formate to release the carboxylate while reforming formic anhydride. Given phenyl triflimide is catalytic in this reaction (15 mol%), formic anhydride must be regenerated. Masking formate as the anhydride may prevent undesired reduction chemistry from the carbon dioxide radical anion to substrates or metal centers making this reaction more efficacious. Given the complexities of this system and how phenyl triflimide

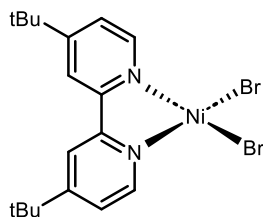
and its degradation products fit into the catalytic cycles, further mechanistic studies are required to elucidate the details of this mechanism.

S4.6.5: Preparation of Starting Materials



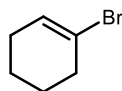
2,4,5,6-Tetrakis(carbazole-9-yl)-4,6-dicyanobenzene (4CzIPN) (S1): To a flame dried round bottom flask was added carbazole (1.67 g, 10.0 mmol) in anhydrous THF (40 mL). Sodium hydride (60% in oil, 0.60 g, 15.0 mmol) was carefully added portion wise to the solution. After 30 minutes, tetrafluoroisophthalonitrile (0.40 g, 2.00 mmol) was added and allow to stir at room temperature for 16 h. Water (2 mL) was then added carefully and the reaction mixture was then concentrated *in vacuo*. The resulting solid was then washed with water and ethanol then recrystallized from hexanes/ CH_2Cl_2 to yield the product was a vibrant yellow solid (1.4 g, 89% yield). The physical and spectral properties were consistent with reported values.³

^1H NMR (400 MHz, CDCl_3) δ 8.21 (d, $J = 7.8$ Hz, 2H), 7.75-7.65 (m, 8H), 7.52-7.45 (m, 2H), 7.33 (d, $J = 7.5$ Hz, 2H), 7.24-7.19 (m, 4H), 7.12-7.03 (m, 8H), 6.86-6.79 (m, 4H) 6.69-6.61 (m, 2H).



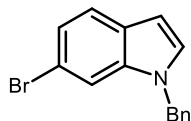
[4,4'-Bis(1,1-dimethyl)-2,2'-bipyridine] nickel (II) bromide (S2): Following a previously reported synthesis, a flame-dried round bottom flask was charged with NiBr₂(glyme) (0.616 g, 2.0 mmol, 1 equiv.) and 4,4'-di-*tert*-butyl-2,2'-bipyridyl (0.536 g, 2.0 mmol, 1 equiv.) before being placed under argon. Anhydrous THF (60 mL) was added and the reaction mixture was stirred for 20 h. The resulting green solid was filtered off and washed with diethyl ether and dried under vacuum to afford the title compound as a green powder that was used without further purification (0.89g, 91% yield).²⁰

¹H NMR (400 MHz, DMSO-*d*₆) δ 6.04 (1.53, 9H). The paramagnetic product shows only a broad peak at 1.53 ppm.²⁰



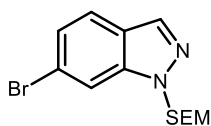
1-bromocyclohex-1-ene (S3): To a flame-dried round bottom flask was added triphenyl phosphite (6.8 g, 22.0 mmol, 1.1 equiv.). The atmosphere was exchanged three times with argon and equipped with an argon balloon. Anhydrous CH₂Cl₂ was added (60 mL) and the reaction was cooled to -78°C. Bromine (1.2 mL, 24.0 mmol, 1.2 equiv.) was added slowly and allowed to stir for five minutes before the slow addition of triethylamine (3.6 mL, 26.0 mmol, 1.3 equiv.). The reaction mixture was stirred for another five minutes before the addition of cyclohexanone (2.1 mL, 20.0 mmol, 1 equiv.). The reaction mixture was warmed to room temperature overnight then refluxed in an oil bath for two hours. The crude reaction mixture was then concentrated and purified by silica chromatography (100% Hexanes as the eluent) to afford the title compound as a pale yellow oil (1.83 g, 56% yield). The physical and spectral properties match the reported values.⁴

¹H NMR (400 MHz, CDCl₃) δ 6.04 (m, 1H), 2.42 (m, 2H), 2.08-2.07 (m, 2H), 1.77-1.71 (m, 2H), 1.64-1.58 (m, 2H).



1-benzyl-6-bromo-1H-indole (S4): To a flame-dried round bottom flask was added 6-bromoindole (0.98 g, 5.0 mmol, 1 equiv.) followed by anhydrous DMF (5 mL). The reaction mixture was cooled to 0°C and sodium hydride (0.24 g, 6.0 mmol, 1.2 equiv.) portion wise. Stir for thirty minutes at 0°C then add benzyl bromide (0.9 mL, 7.5 mmol, 1.5 equiv., dissolved in 2.5 mL DMF) slowly. The reaction mixture was warmed to room temperature and stirred overnight. After cooling back down to 0°C, the reaction was quenched with water (5 mL), extracted three times with ethyl acetate, dried over MgSO₄ and concentrated *in vacuo*. The crude reaction mixture was then purified by silica chromatography (2.5 % EtOAc/Hexanes as the eluent) to afford the title compound as an off white solid (1.08 g, 76% yield). The physical and spectral properties match the reported values.⁵

¹H NMR (400 MHz, CDCl₃) δ 7.50 (d, J = 8.4 Hz, 1H), 7.45-7.41 (m, 1H), 7.36-7.27 (m, 3H), 7.21 (dd, J = 8.4 Hz, 1.7 Hz, 1H), 7.12-7.03 (m, 3H), 6.52 (dd, J = 3.1, 1.0 Hz, 1H), 5.28 (s, 2H).



6-bromo-1-((2-(trimethylsilyl)ethoxy)methyl)-1H-indazole (S5): To a round bottom flask was added 6-bromoindazole (0.493 g, 2.5 mmol, 1 equiv.) and CH₂Cl₂ (10 mL). The reaction mixture was cooled to 0°C and potassium hydroxide (0.168 g, 3.0 mmol, 3 equiv., dissolved in 0.6 mL H₂O) was added followed by tetrabutylammonium bromide (0.080 g, 0.25 mmol, 0.1 equiv.). SEM-chloride (0.49 mL, 2.75 mmol, 1.1 equiv.) was then added dropwise and stirred at 0°C for 1 hour. The reaction mixture was allowed to warm to room temperature, stirred overnight, quenched with H₂O (10 mL) and extracted three times with CH₂Cl₂. The crude reaction mixture was dried over MgSO₄, concentrated *in vacuo*, and purified via silica chromatography (5-10% EtOAc/Hexanes as the eluent) to afford the title compound as a light brown oil (0.412 g, 50% yield).

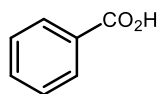
¹H NMR (400 MHz, CDCl₃) δ 7.97 (d, J = 1.0 Hz, 1H), 7.79-7.77 (m, 1H), 7.60 (dd, J = 8.6 Hz, 0.7 Hz, 1H), 7.30 (dd, J = 8.5 Hz, 1.6 Hz, 1H), 5.70 (s, 2H), 3.56-3.50 (m, 2H), 0.91-0.85 (m, 2H), -0.06 (s, 9H).

¹³C{¹H} NMR (100 MHz, CDCl₃) δ 140.6, 134.2, 125.1, 123.7, 122.3, 121.3, 112.9, 77.9, 66.6, 17.8, -1.1, -1.3, -1.6.

HRMS (APCI) *m/z*: [M⁺] calcd. for C₁₂H₂₀ON₂Si, 327.0523, found 327.0520.

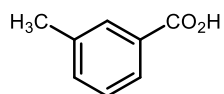
R_f: 0.47 (5% EtOAc/Hexanes)

4.6.6: Preparation of Products from Substrate Table



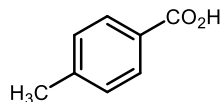
Benzoic acid (4): Prepared according to the general procedure using bromobenzene (0.5 mmol, 53 μ l, 1 equiv.), sodium formate (0.75 mmol, 0.051 g, 1.5 equiv.), 4CzIPN (.005 mmol, 0.0039 g, 1 mol%), N-phenyl-bis(trifluoromethanesulfonimide) (0.075 mmol, 0.027 g, 15 mol%), and [4,4'-Bis(1,1-dimethyl)-2,2'-bipyridine] nickel (II) bromide (0.05 mmol, 0.024 g, 10 mol%), in 1:1 DMSO/dioxane (5 mL). After 16 hours the reaction was quenched with 1M HCl (10 mL), extracted three times with ethyl acetate, dried over MgSO₄ and concentrated *in vacuo*. The crude reaction mixture was purified by silica chromatography (10% EtOAc/hexanes + 1% AcOH as the eluent) to afford the title compound as a pale yellow solid (0.065 g, 86% yield). The physical and spectral properties were consistent with the reported values.⁶

¹H NMR (400 MHz, DMSO-d₆) δ 12.94 (s, 1H), 7.95 (d, J = 7.3 Hz, 2H), 7.62 (t, J = 7.3 Hz, 2H), 7.50 (t, J = 7.7 Hz, 1H).



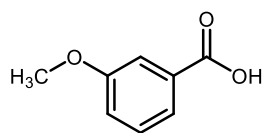
3-methylbenzoic acid (5): Prepared according to the general procedure using 3-bromotoluene (0.5 mmol, 61 μ l, 1 equiv.), sodium formate (0.75 mmol, 0.051 g, 1.5 equiv.), 4CzIPN (.005 mmol, 0.0039 g, 1 mol%), N-phenyl-bis(trifluoromethanesulfonimide) (0.075 mmol, 0.027 g, 15 mol%), and [4,4'-Bis(1,1-dimethyl)-2,2'-bipyridine] nickel (II) bromide (0.05 mmol, 0.024 g, 10 mol%), in 1:1 DMSO/dioxane (5 mL). After 16 hours the reaction was quenched with 1M HCl (10 mL), extracted three times with ethyl acetate, dried over MgSO₄ and concentrated *in vacuo*. The crude reaction mixture was purified by silica chromatography purified by silica chromatography (20% EtOAc/hexanes + 1% AcOH as the eluent) to afford the title compound as a white solid (0.060 g, 88% yield). The physical and spectral properties were consistent with the reported values.⁷

¹H NMR (600 MHz, CDCl₃) δ 7.95-7.90 (m, 2H), 7.43 (d, J = 7.6 Hz, 2H), 7.38 (t, J = 7.4 Hz, 1H), 2.43 (s, 3H).



4-methylbenzoic acid (6): Prepared according to the general procedure using 4-bromotoluene (0.5 mmol, 61 μl, 1 equiv.), sodium formate (0.75 mmol, 0.051 g, 1.5 equiv.), 4CzIPN (.005 mmol, 0.0039 g, 1 mol%), N-phenyl-bis(trifluoromethanesulfonimide) (0.075 mmol, 0.027 g, 15 mol%), and [4,4'-Bis(1,1-dimethyl)-2,2'-bipyridine] nickel (II) bromide (0.05 mmol, 0.024 g, 10 mol%), in 1:1 DMSO/dioxane (5 mL). After 16 hours the reaction was quenched with 1M HCl (10 mL), extracted three times with ethyl acetate, dried over MgSO₄ and concentrated *in vacuo*. The crude reaction mixture was purified by silica chromatography purified by silica chromatography (20% EtOAc/hexanes + 1% AcOH as the eluent) to afford the title compound as a white solid (0.062 g, 91% yield). The physical and spectral properties were consistent with the reported values.⁸

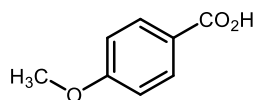
¹H NMR (600 MHz, CDCl₃) δ 7.95-7.90 (m, 2H), 7.43 (d, J = 7.6 Hz, 2H), 7.38 (t, J = 7.4 Hz, 1H), 2.43 (s, 3H).



3-methoxybenzoic acid (7): Prepared according to the general procedure using 3-bromoanisole (0.5 mmol, 63 μl, 1 equiv.), sodium formate (0.75 mmol, 0.051 g, 1.5 equiv.), 4CzIPN (.005 mmol, 0.0039 g, 1 mol%), N-phenyl-bis(trifluoromethanesulfonimide) (0.075 mmol, 0.027 g, 15 mol%), and [4,4'-Bis(1,1-dimethyl)-2,2'-bipyridine] nickel (II) bromide (0.05 mmol, 0.024 g, 10

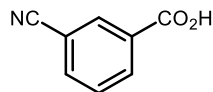
mol%), in 1:1 DMSO/dioxane (5 mL). After 16 hours the reaction was quenched with 1M HCl (10 mL), extracted three times with ethyl acetate, dried over MgSO₄ and concentrated *in vacuo*. The crude reaction mixture was purified by silica chromatography purified by silica chromatography (20-30% EtOAc/hexanes + 1% AcOH as the eluent) to afford the title compound as a pale yellow solid (0.065 g, 86% yield). The physical and spectral properties were consistent with the reported values.⁹

¹H NMR (400 MHz, DMSO-d₆) δ 13.00 (s, 1H), 7.53 (dt, J = 7.6, 1.3 Hz, 1H), 7.44-7.38 (m, 2H), 7.18 (ddd, J = 8.20, 2.7, 1.0 Hz, 1H), 3.80 (s, 3H).



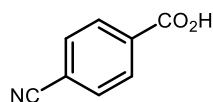
4-methoxybenzoic acid (8): Prepared according to the general procedure using 4-bromoanisole (0.5 mmol, 63 μl, 1 equiv.), sodium formate (0.75 mmol, 0.051 g, 1.5 equiv.), 4CzIPN (.005 mmol, 0.0039 g, 1 mol%), N-phenyl-bis(trifluoromethanesulfonimide) (0.075 mmol, 0.027 g, 15 mol%), and [4,4'-Bis(1,1-dimethyl)-2,2'-bipyridine] nickel (II) bromide (0.05 mmol, 0.024 g, 10 mol%), in 1:1 DMSO/dioxane (5 mL). After 16 hours the reaction was quenched with 1M HCl (10 mL), extracted three times with ethyl acetate, dried over MgSO₄ and concentrated *in vacuo*. The crude reaction mixture was purified by silica chromatography purified by silica chromatography (20-30% EtOAc/hexanes + 1% AcOH as the eluent) to afford the title compound as a pale yellow solid (0.039 g, 52% yield). The physical and spectral properties were consistent with the reported values.⁹

^1H NMR (400 MHz, DMSO- d_6) δ 13.00 (s, 1H), 7.89 (d, $J = 8.9$, 2H), 7.02 (d, $J = 8.8$ Hz, 2H), 3.82 (s, 3H).



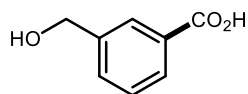
3-cyanobenzoic acid (9): Prepared according to the general procedure using 3-bromobenzonitrile (0.5 mmol, 0.091g, 1 equiv.), sodium formate (0.75 mmol, 0.051 g, 1.5 equiv.), 4CzIPN (.005 mmol, 0.0039 g, 1 mol%), N-phenyl-bis(trifluoromethanesulfonimide) (0.075 mmol, 0.027 g, 15 mol%), and [4,4'-Bis(1,1-dimethyl)-2,2'-bipyridine] nickel (II) bromide (0.05 mmol, 0.024 g, 10 mol%), in 1:1 DMSO/dioxane (5 mL). After 16 hours the reaction was quenched with 1M HCl (10 mL), extracted three times with ethyl acetate, dried over MgSO_4 and concentrated *in vacuo*. The crude reaction mixture was purified by silica chromatography purified by silica chromatography (20-30% EtOAc/hexanes + 1% AcOH as the eluent) to afford the title compound as a white solid (0.062 g, 89% yield). The physical and spectral properties were consistent with the reported values.¹⁰

^1H NMR (400 MHz, DMSO- d_6) δ 13.00 (s, 1H), 8.30-8.26 (m 1H), 8.25-8.20 (dt, $J = 7.9$, 1.4 Hz, 1H), 8.13-8.07 (dt, $J = 7.7$, 1.3, 1H), 7.73 (t, $J = 7.8$ Hz, 1H).



4-cyanobenzoic acid (10): Prepared according to the general procedure using 4-bromobenzonitrile (0.5 mmol, 0.091 g, 1 equiv.), sodium formate (0.75 mmol, 0.051 g, 1.5 equiv.), 4CzIPN (.005 mmol, 0.0039 g, 1 mol%), N-phenyl-bis(trifluoromethanesulfonimide) (0.075 mmol, 0.027 g, 15 mol%), and [4,4'-Bis(1,1-dimethyl)-2,2'-bipyridine] nickel (II) bromide (0.05 mmol, 0.024 g, 10 mol%), in 1:1 DMSO/dioxane (5 mL). After 16 hours the reaction was quenched with 1M HCl (10 mL), extracted three times with ethyl acetate, dried over MgSO₄ and concentrated *in vacuo*. The crude reaction mixture was purified by silica chromatography purified by silica chromatography (20-30% EtOAc/hexanes + 1% AcOH as the eluent) to afford the title compound as a pale yellow solid (0.073 g, 98% yield). The physical and spectral properties were consistent with the reported values.¹¹

¹H NMR (400 MHz, CDCl₃) δ 8.22 (d, J = 8.2 Hz, 2H), 7.80 (d, J = 8.2 Hz, 2H.)



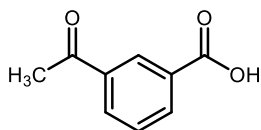
3-(hydroxymethyl)benzoic acid (11): Prepared according to the general procedure using 3-bromobenzyl alcohol (0.5 mmol, 60 μl, 1 equiv.), sodium formate (0.75 mmol, 0.051 g, 1.5 equiv.), 4CzIPN (.005 mmol, 0.0039 g, 1 mol%), N-phenyl-bis(trifluoromethanesulfonimide) (0.075 mmol, 0.027 g, 15 mol%), and [4,4'-Bis(1,1-dimethyl)-2,2'-bipyridine] nickel (II) bromide (0.05 mmol, 0.024 g, 10 mol%), in 1:1 DMSO/dioxane (5 mL). After 16 hours the reaction was quenched with 1M HCl (10 mL), extracted three times with ethyl acetate, dried over MgSO₄ and concentrated *in vacuo*. The crude reaction mixture was purified by silica chromatography purified by silica chromatography (20-50% EtOAc/hexanes + 1% AcOH as the eluent) to afford the title compound as a white solid (0.039 g, 51% yield).

¹H NMR (400 MHz, DMSO-d₆) δ 7.92 (s, 1H), 7.81 (d, J = 7.7 Hz, 1H), 7.54 (d, J = 7.7 Hz, 1H) 7.44 (t, J = 7.6 Hz, 1H) 5.32 (bs, 1H), 4.55 (s, 2H).

¹³C {¹H} NMR (100 MHz, CDCl₃) δ 167.4, 143.1 130.8, 130.7, 128.3, 127.6, 127.2, 62.4.

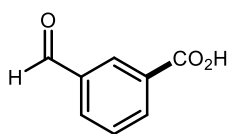
HRMS (APCI) *m/z*: [M+H] calcd. for C₈H₉O₃, 153.0546, found 153.0546.

R_f: 0.36 (40% EtOAc/Hexanes + 1% AcOH).



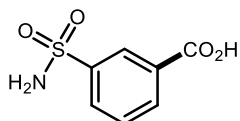
3-acetylbenzoic acid (12): Prepared according to the general procedure using 3-bromoacetophenone (0.5 mmol, 66 μl, 1 equiv.), sodium formate (0.75 mmol, 0.051 g, 1.5 equiv.), 4CzIPN (.005 mmol, 0.0039 g, 1 mol%), N-phenyl-bis(trifluoromethanesulfonimide) (0.075 mmol, 0.027 g, 15 mol%), and [4,4'-Bis(1,1-dimethyl)-2,2'-bipyridine] nickel (II) bromide (0.05 mmol, 0.024 g, 10 mol%), in 1:1 DMSO/dioxane (5 mL). After 16 hours the reaction was quenched with 1M HCl (10 mL), extracted three times with ethyl acetate, dried over MgSO₄ and concentrated *in vacuo*. The crude reaction mixture was purified by silica chromatography purified by silica chromatography (20-30% EtOAc/hexanes + 1% AcOH as the eluent) to afford the title compound as a white solid (0.065 g, 79% yield). The physical and spectral properties were consistent with the reported values.¹²

¹H NMR (400 MHz, CDCl₃) δ 8.68 (s, 1H), 8.32 (d, J = 7.7 Hz, 1H), 8.23 (d, J = 7.9 Hz, 1H), 7.62 (t, J = 7.8 Hz, 1H), 2.68 (s, 3H)



3-formylbenzoic acid (13): Prepared according to the general procedure using 3-bromobenzaldehyde (0.5 mmol, 0.093 g, 1 equiv.), sodium formate (0.75 mmol, 0.051 g, 1.5 equiv.), 4CzIPN (.005 mmol, 0.0039 g, 1 mol%), N-phenyl-bis(trifluoromethanesulfonimide) (0.075 mmol, 0.027 g, 15 mol%), and [4,4'-Bis(1,1-dimethyl)-2,2'-bipyridine] nickel (II) bromide (0.05 mmol, 0.024 g, 10 mol%), in 1:1 DMSO/dioxane (5 mL). After 16 hours the reaction was quenched with 1M HCl (10 mL), extracted three times with ethyl acetate, dried over MgSO₄ and concentrated *in vacuo*. The crude reaction mixture was purified by silica chromatography purified by silica chromatography (20% EtOAc/hexanes + 1% AcOH as the eluent) to afford the title compound as a pale yellow solid (0.068 g, 91% yield). The physical and spectral properties were consistent with the reported values.¹³

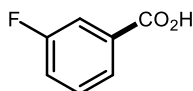
¹H NMR (400 MHz, DMSO-d₆) δ 13.37 (s, 1H), 10.09 (s, 1H), 8.44 (s, 1H), 8.24 (d, J = 7.6 Hz, 1H), 8.14 (d, J = 7.7 Hz, 1H), 7.74 (t, J = 7.6 Hz, 1H).



3-sulfamoylbenzoic acid (14): Prepared according to the general procedure using 3-bromobenzenesulfonamide (0.5 mmol, 0.118 g, 1 equiv.), sodium formate (0.75 mmol, 0.051 g, 1.5 equiv.), 4CzIPN (.005 mmol, 0.0039 g, 1 mol%), N-phenyl-bis(trifluoromethanesulfonimide) (0.075 mmol, 0.027 g, 15 mol%), and [4,4'-Bis(1,1-dimethyl)-2,2'-bipyridine] nickel (II) bromide (0.05 mmol, 0.024 g, 10 mol%), in 1:1 DMSO/dioxane (5 mL). After 16 hours the reaction was quenched with 1M HCl (10 mL), extracted three times with ethyl acetate, dried over MgSO₄ and concentrated *in vacuo*. The crude reaction mixture was purified by silica chromatography purified by silica chromatography (0-50% EtOAc/hexanes + 1% AcOH followed by 0-10% MeOH/CH₂Cl₂ as the eluent) to afford the title compound as a pale yellow

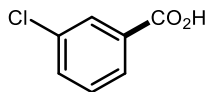
solid (0.077 g, 76% yield). The physical and spectral properties were consistent with the reported values.¹⁴

¹H NMR (400 MHz, DMSO-d₆) δ 13.42 (bs, 1H), 8.39 (s, 1H), 8.14 (d, J = 7.8 Hz, 1H), 8.05 (d, J = 8.1 Hz, 1H), 7.71 (t, J = 7.7 Hz, 1H), 7.50 (s, 2H).



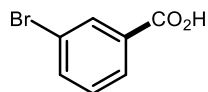
3-fluorobenzoic acid (15): Prepared according to the general procedure using 1-bromo-3-fluorobenzene (0.5 mmol, 56 μ l, 1 equiv.), sodium formate (0.75 mmol, 0.051 g, 1.5 equiv.), 4CzIPN (.005 mmol, 0.0039 g, 1 mol%), N-phenyl-bis(trifluoromethanesulfonimide) (0.075 mmol, 0.027 g, 15 mol%), and [4,4'-Bis(1,1-dimethyl)-2,2'-bipyridine] nickel (II) bromide (0.05 mmol, 0.024 g, 10 mol%), in 1:1 DMSO/dioxane (5 mL). After 16 hours the reaction was quenched with 1M HCl (10 mL), extracted three times with ethyl acetate, dried over MgSO₄ and concentrated *in vacuo*. The crude reaction mixture was purified by silica chromatography purified by silica chromatography (0-50% EtOAc/hexanes + 1% AcOH followed by 0-10% MeOH/CH₂Cl₂ as the eluent) to afford the title compound as a white solid (0.058 g, 84% yield). The physical and spectral properties were consistent with the reported values.¹⁵

¹H NMR (400 MHz, DMSO-d₆) δ 13.30 (bs, 1H), 7.80 (dt, J = 7.6, 1.3 Hz, 1H), 7.69-7.63 (m, 1H), 7.61-7.54 (m, 1H), 7.53-7.46 (m, 1H).



3-chlorobenzoic acid (16): Prepared according to the general procedure using 1-bromo-3-chlorobenzene (0.5 mmol, 59 μ l, 1 equiv.), sodium formate (0.75 mmol, 0.051 g, 1.5 equiv.), 4CzIPN (.005 mmol, 0.0039 g, 1 mol%), N-phenyl-bis(trifluoromethanesulfonimide) (0.075 mmol, 0.027 g, 15 mol%), and [4,4'-Bis(1,1-dimethyl)-2,2'-bipyridine] nickel (II) bromide (0.05 mmol, 0.024 g, 10 mol%), in 1:1 DMSO/dioxane (5 mL). After 16 hours the reaction was quenched with 1M HCl (10 mL), extracted three times with ethyl acetate, dried over MgSO₄ and concentrated *in vacuo*. The crude reaction mixture was purified by silica chromatography purified by silica chromatography (0-50% EtOAc/hexanes + 1% AcOH followed by 0-10% MeOH/CH₂Cl₂ as the eluent) to afford the title compound as a white solid (0.065 g, 83% yield). The physical and spectral properties were consistent with the reported values.¹⁶

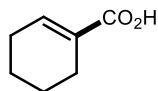
¹H NMR (400 MHz, DMSO-d₆) δ 13.34 (bs, 1H), 7.93-7.89 (m, 2H), 7.74-7.69 (m, 1H), 7.55 (t, J = 8.1 Hz, 1H).



3-bromobenzoic acid (17): Prepared according to the general procedure using 1-bromo-3-iodobenzene (0.5 mmol, 64 μ l, 1 equiv.), sodium formate (0.75 mmol, 0.051 g, 1.5 equiv.), 4CzIPN (.005 mmol, 0.0039 g, 1 mol%), N-phenyl-bis(trifluoromethanesulfonimide) (0.075 mmol, 0.027 g, 15 mol%), and [4,4'-Bis(1,1-dimethyl)-2,2'-bipyridine] nickel (II) bromide (0.05 mmol, 0.024 g, 10 mol%), in 1:1 DMSO/dioxane (5 mL). After 16 hours the reaction was quenched with 1M HCl (10 mL), extracted three times with ethyl acetate, dried over MgSO₄ and concentrated *in vacuo*. The crude reaction mixture was purified by silica chromatography purified by silica chromatography (10-20% EtOAc/hexanes + 1% AcOH as the eluent) to afford the title compound as a light yellow solid (0.082 g, 82% yield). The physical and spectral

properties were consistent with the reported values.¹⁷

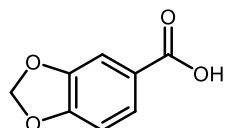
¹H NMR (400 MHz, DMSO-d₆) δ 13.32 (bs, 1H), 8.04 (t, J = 1.8 Hz, 1H), 7.93 (dt, J = 7.8, 1.3 Hz, 1H), 7.86-7.82 (m, 1H), 7.47 (t, J = 7.9 Hz).



Cyclohex-1-ene-1-carboxylic acid (18): Prepared according to the general procedure **S3** (0.1 mmol, 12 μl, 1 equiv.), sodium formate (0.15 mmol, 0.010 g, 1.5 equiv.), 4CzIPN (.0001 mmol, 0.0008 g, 1 mol%), N-phenyl-bis(trifluoromethanesulfonimide) (0.015 mmol, 0.0053 g, 15 mol%), and [4,4'-Bis(1,1-dimethyl)-2,2'-bipyridine] nickel (II) bromide (0.01 mmol, 0.0048 g, 10 mol%), in 1:1 DMSO/dioxane (5 mL). After 16 hours the reaction was quenched with 1M HCl (10 mL), extracted three times with ethyl acetate, dried over MgSO₄ and concentrated *in vacuo*. Dibromomethane (0.1 mmol, 7.0 μl, 1.0 equiv.) was added to the crude reaction mixture as an internal standard and the sample was analyzed via ¹H NMR (d = 5 s), and the integral values were used to calculate product yield (80% yield by NMR).¹⁸

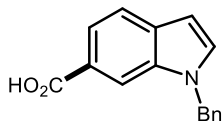
Note: Vinyl bromides suffered from issues with scalability/purification in this transformation, as such this reaction was performed on a 0.1 mmol scale and yield was determined via ¹H NMR using CH₂Br₂ as an internal standard..

¹H NMR (400 MHz, DMSO-d₆) δ 12.06 (s, 1H), 6.86 (m, 1H), 2.17-2.09 (m, 4H), 1.61-1.47 (m, 4H).



Benzo[*d*][1,3]dioxole-5-carboxylic acid (19): Prepared according to the general procedure using 5-bromo-1,3-benzodioxole (0.5 mmol, 60 μ l, 1 equiv.), sodium formate (0.75 mmol, 0.051 g, 1.5 equiv.), 4CzIPN (.005 mmol, 0.0039 g, 1 mol%), N-phenyl-bis(trifluoromethanesulfonimide) (0.075 mmol, 0.027 g, 15 mol%), and [4,4'-Bis(1,1-dimethyl)-2,2'-bipyridine] nickel (II) bromide (0.05 mmol, 0.024 g, 10 mol%), in 1:1 DMSO/dioxane (5 mL). After 16 hours the reaction was quenched with 1M HCl (10 mL), extracted three times with ethyl acetate, dried over MgSO₄ and concentrated *in vacuo*. The crude reaction mixture was purified by silica chromatography purified by silica chromatography (20-30% EtOAc/hexanes + 1% AcOH as the eluent) to afford the title compound as a white solid (0.055 g, 66% yield). The physical and spectral properties were consistent with the reported values.¹⁹

¹H NMR (400 MHz, DMSO-*d*₆) δ 12.76 (s, 1H), 7.54 (dd, *J* = 8.3, 1.7 Hz, 1H), 7.36 (d, *J* = 1.7 Hz, 1H), 7.00 (d, *J* = 8.1 Hz, 1H), 6.12 (s, 2H).



1-benzyl-1H-indole-6-carboxylic acid (20): Prepared according to the general procedure using 1-benzyl-6-bromo-1H-indole (0.5 mmol, 0.143 g, 1 equiv.), sodium formate (0.75 mmol, 0.051 g, 1.5 equiv.), 4CzIPN (.005 mmol, 0.0039 g, 1 mol%), N-phenyl-bis(trifluoromethanesulfonimide) (0.075 mmol, 0.027 g, 15 mol%), and [4,4'-Bis(1,1-dimethyl)-2,2'-bipyridine] nickel (II) bromide (0.05 mmol, 0.024 g, 10 mol%), in 1:1 DMSO/dioxane (5 mL). After 16 hours the reaction was quenched with 1M HCl (10 mL), extracted three times with ethyl acetate, dried over MgSO₄ and concentrated *in vacuo*. The crude reaction mixture was purified by silica chromatography purified by silica chromatography (10-30% EtOAc/hexanes + 1% AcOH as the eluent) to afford the title compound as a light yellow solid (0.063 g, 50% yield).

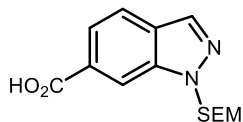
The physical and spectral properties were consistent with the reported values.¹

¹H NMR (400 MHz, DMSO-d₆) δ 12.57 (bs, 1H), 8.05-8.04 (m, 1H), 7.77 (d, J = 3.0 Hz, 1H), 7.63-7.61 (m, 2H), 7.31 (t, J = 7.1 Hz, 2H), 7.25 (t, J = 7.4 Hz, 1H), 7.16 (d, J = 7.4 Hz, 2H), 6.59 (dd, J = 3.1, 0.9 Hz, 1H), 5.53 (s, 2H).

¹³C {¹H} NMR (100 MHz, DMSO-d₆) δ 168.2, 138.1, 135.1, 132.8, 131.8, 128.6, 127.4, 126.7, 123.5, 120.2, 120.1, 112.2, 101.4, 49.2.

HRMS (APCI) *m/z*: [M+H] calcd. for C₁₆H₁₄O₂N, 252.1019, found 252.1015.

R_f: 0.49 (30% EtOAc/Hexanes + 1% AcOH)



1-((2-(trimethylsilyl)ethoxy)methyl)-1H-indazole-6-carboxylic acid (21): Prepared according to the general procedure using **S5** (0.5 mmol, 0.143 g, 1 equiv.), sodium formate (0.75 mmol, 0.051 g, 1.5 equiv.), 4CzIPN (.005 mmol, 0.0039 g, 1 mol%), N-phenyl-bis(trifluoromethanesulfonimide) (0.075 mmol, 0.027 g, 15 mol%), and [4,4'-Bis(1,1-dimethyl)-2,2'-bipyridine] nickel (II) bromide (0.05 mmol, 0.024 g, 10 mol%), in 1:1 DMSO/dioxane (5 mL). After 16 hours the reaction was quenched with 1M HCl (10 mL), extracted three times with ethyl acetate, dried over MgSO₄ and concentrated *in vacuo*. The crude reaction mixture was purified by silica chromatography (10-30% EtOAc/hexanes + 1% AcOH as the eluent) to afford the title compound as a light yellow solid (0.066 g, 66% yield). The physical and spectral properties were consistent with the reported values.¹

¹H NMR (400 MHz, DMSO-d₆) δ 13.13 (bs, 1H), 8.35 (d, J = 1.1 Hz, 1H), 8.25 (d, J = 1.0 Hz,

1H), 7.89 (dd, J = 8.5, 0.8 Hz, 1H), 7.75 (dd, J = 8.4, 1.3 Hz, 1H), 5.85 (s, 2H), 3.51 (t, J = 8.1 Hz, 2H), 0.79 (t, J = 7.9 Hz, 2H), -0.13 (s, 9H).

¹³C {¹H} NMR (100 MHz, DMSO-d₆) δ 167.5, 139.2, 134.1, 128.9, 126.7, 121.5, 121.0, 112.0, 76.9, 65.6, 17.1, -1.2, -1.4, -1.7.

HRMS (APCI) *m/z*: [M+H] calcd. for C₁₄H₂₁O₃N₂Si, 293.1316, found 293.1313.

Rf: 0.52 (30% EtOAc/Hexanes + 1% AcOH)

S4.6.7: References

1. Roth, G.; Romero, N.; Nicewicz, D. Experimental and Calculated Electrochemical Potentials of Common Organic Molecules for Applications to Single-Electron Redox Chemistry. *Synlett.*, **2017**, *5*, 714-723.
2. Shi, S.; Lalancette, R.; Szostak, R.; Szostak, M. Triflamides: Highly Reactive, Electronically Activated N-Sulfonyl Amides in Catalytic N-C(O) Amide Cross-Coupling. *Org. Lett.*, **2019**, *21*, 1253-1257.
3. Grotjahn, S.; Konig, B. Photosubstitution in Dicyanobenzene-based Photocatalysts. *Org. Lett.*, **2021**, *23*, 3146-3150.
4. Ojha, D. P., & Prabhu, K. R. . Regioselective Synthesis of Vinyl Halides, Vinyl Sulfones, and Alkynes: A Tandem Intermolecular Nucleophilic and Electrophilic Vinylation of Tosylhydrazones. *Org. Lett.*, **2015**, *17*, 18–21.
5. Zhang, X. L., Guo, R. L., Wang, M. Y., Zhao, B. Y., Jia, Q., Yang, J. H., & Wang, Y. Q. .Palladium-Catalyzed Three-Component Regioselective Dehydrogenative Coupling of Indoles, 2-Methylbut-2-ene, and Carboxylic Acids. *Org. Lett.*, **2021**, *23*, 9574–9579.

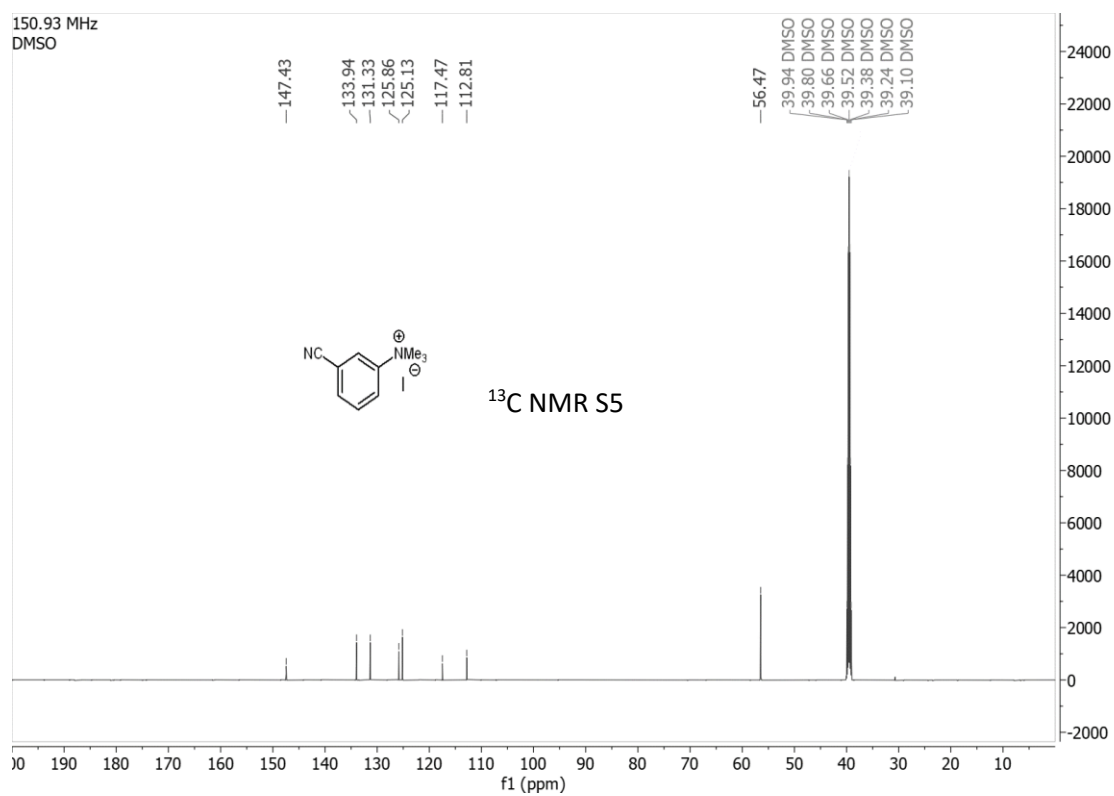
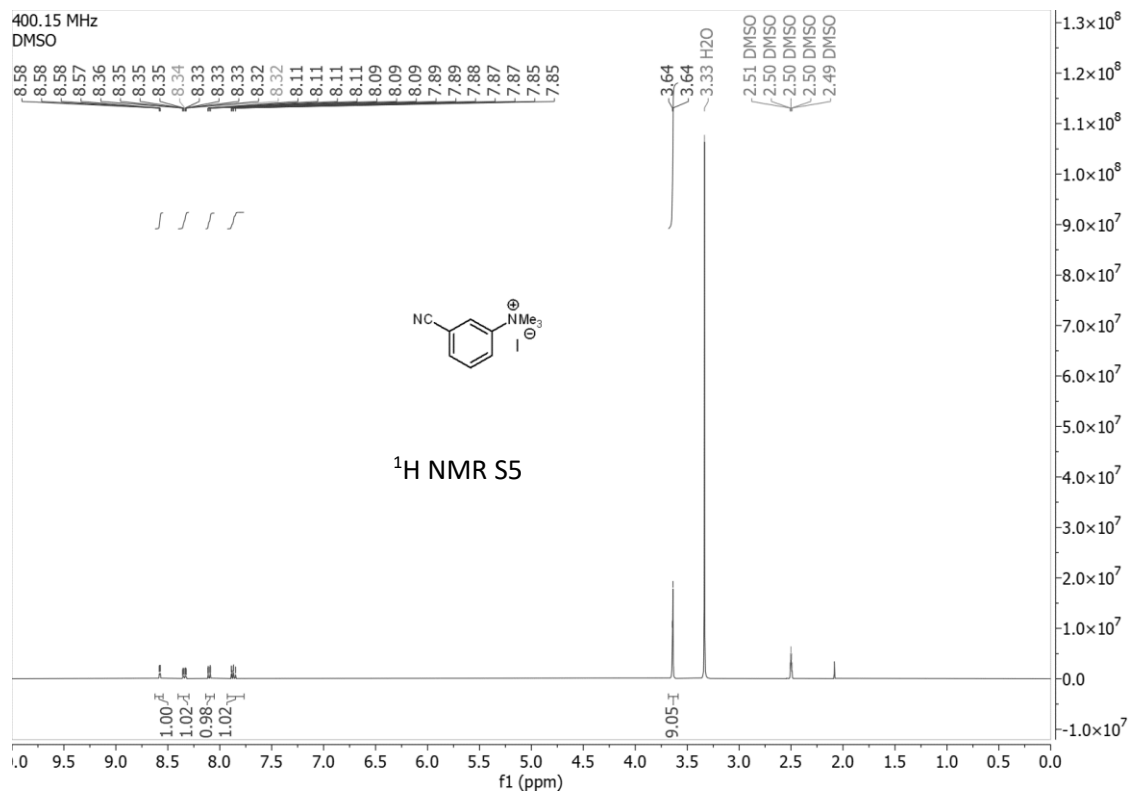
6. Tang, S., Rauch, M., Montag, M., Diskin-Posner, Y., Ben-David, Y., & Milstein, D. Catalytic Oxidative Deamination by Water with H₂ Liberation. *J. Am. Chem. Soc.*, **2020**, *142*, 20875–20882.
7. Farizyan, M., Mondal, A., Mal, S., Deufel, F., & van Gemmeren, M. Palladium-Catalyzed Nondirected Late-Stage C-H Deuteration of Arenes. *J. Am. Chem. Soc.*, **2021**, *143*, 16370–16376.
8. Kim, S. M., Kim, D. W., & Yang, J. W. Transition-metal-free and Chemoselective NaOtBu-O₂-mediated oxidative cleavage reactions of vic-1,2-diols to carboxylic acids and mechanistic insight into the reaction pathways. *Org. Lett.*, **2014**, *16*, 2876–2879.
9. Wang, Y., Zhao, Z., Pan, D., Wang, S., Jia, K., Ma, D., Yang, G., Xue, X. S., & Qiu, Y. Metal-Free Electrochemical Carboxylation of Organic Halides in the Presence of Catalytic Amounts of an Organomediator. *Angew. Chem. Int. Ed.*, **2022**, *61*, e202210201.
10. Ma, C., Zhao, C. Q., Xu, X. T., Li, Z. M., Wang, X. Y., Zhang, K., & Mei, T. S. Nickel-catalyzed carboxylation of aryl and heteroaryl fluorosulfates using carbon dioxide. *Org. Lett.*, **2019**, *21*, 2464–2467.
11. (a) Peixoto, D.; Figueiredo, M.; Gawande, M.; Corvo, M.; Vanhoenacker, G.; Afonso, C.; Ferreira, L.; Branco, P. Developments in the Reactivity of 2-Methylimidazolium Salts. *J. Org. Chem.*, **2017**, *82*, 6232–6241.
(b) Bhunia, S.; Das, P.; Nandi, S.; Jana, R. Carboxylation of Aryl Triflates with CO₂ Merging Palladium and Visible-Light-Photoredox Catalysts. *Org. Lett.*, **2019**, *21*, 4632–4737.

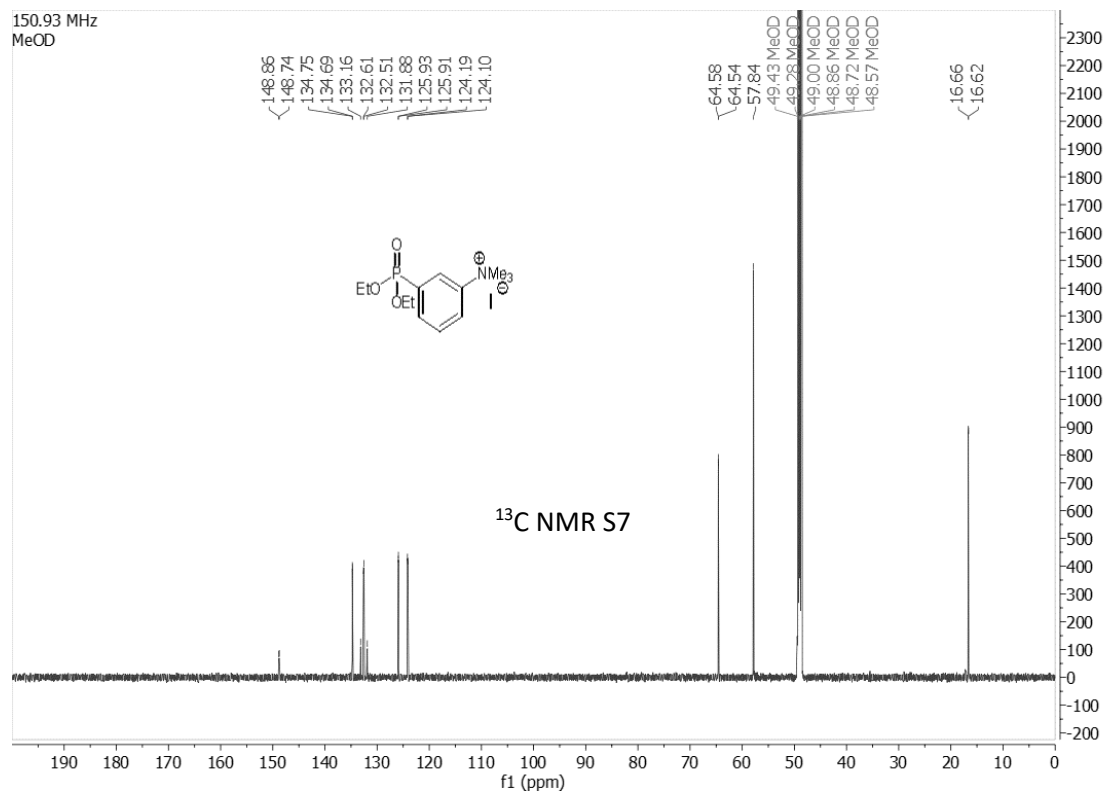
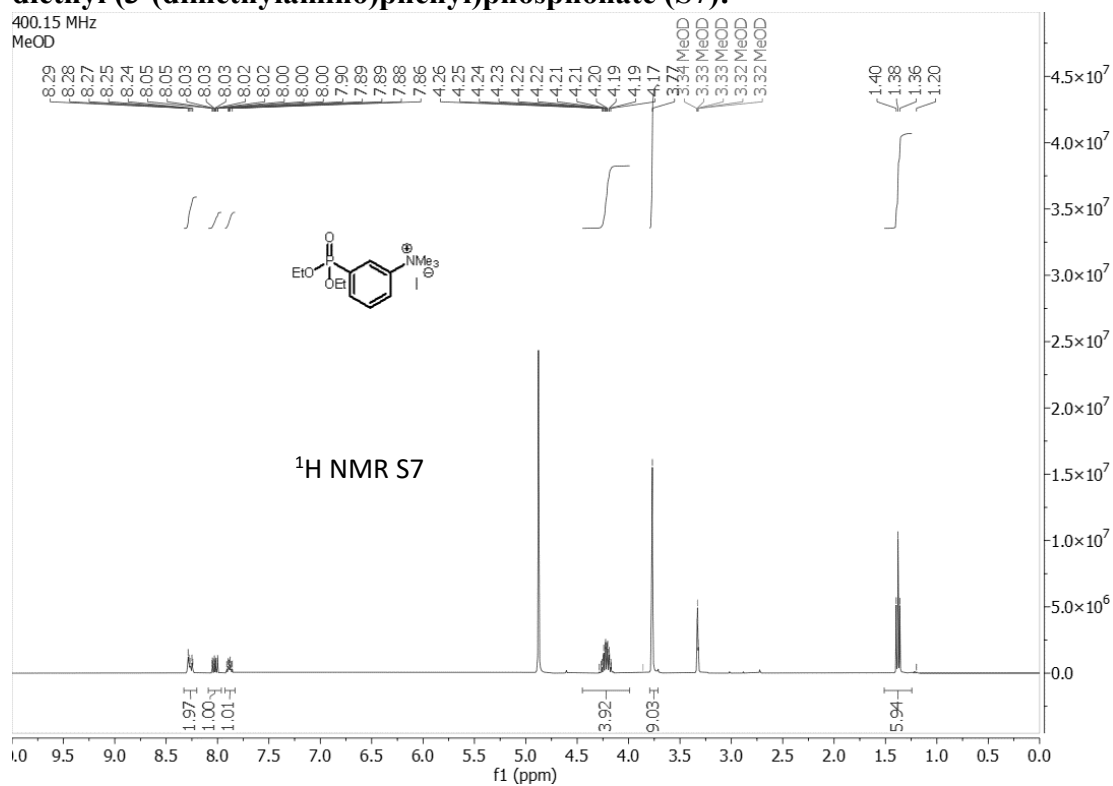
12. Liu, W., Wang, H., & Li, C. J. Metal-Free Markovnikov-Type Alkyne Hydration under Mild Conditions. *Org. Lett.*, **2016**, *18*, 2184–2187.
13. Wise, D. E., Gogarnoiu, E. S., Duke, A. D., Paolillo, J. M., Vacala, T. L., Hussain, W. A., & Parasram, M. Photoinduced Oxygen Transfer Using Nitroarenes for the Anaerobic Cleavage of Alkenes. *J. Am. Chem. Soc.*, **2022**, *144*, 15437–15442.
14. Weidel, E., de Jong, J. C., Brengel, C., Storz, M. P., Braunshausen, A., Negri, M., Plaza, A., Steinbach, A., Müller, R., & Hartmann, R. W. Structure optimization of 2-benzamidobenzoic acids as PqsD inhibitors for *Pseudomonas aeruginosa* infections and elucidation of binding mode by SPR, STD NMR, and molecular docking. *J. Med. Chem.*, **2013**, *56*, 6146–6155.
15. Xia, A., Qi, X., Mao, X., Wu, X., Yang, X., Zhang, R., Xiang, Z., Lian, Z., Chen, Y., & Yang, S. Metal-Free Aerobic Oxidative Selective C-C Bond Cleavage in Heteroaryl-Containing Primary and Secondary Alcohols. *Org. Lett.*, **2019**, *2*, 3028–3033.
16. Zhang, Z., Zhang, G., Xiong, N., Xue, T., Zhang, J., Bai, L., Guo, Q., & Zeng, R. Oxidative α -C-C Bond Cleavage of 2° and 3° Alcohols to Aromatic Acids with O₂ at Room Temperature via Iron Photocatalysis. *Org. Lett.*, **2021**, *23*, 2915–2920.
17. Wang, W., Yang, X., Dai, R., Yan, Z., Wei, J., Dou, X., Qiu, X., Zhang, H., Wang, C., Liu, Y., Song, S., & Jiao, N. Catalytic Electrophilic Halogenation of Arenes with Electron-Withdrawing Substituents. *J. Am. Chem. Soc.*, **2022**, *144*, 13415–13425.
18. Monda, F., & Madsen, R. Zinc Oxide-Catalyzed Dehydrogenation of Primary Alcohols into Carboxylic Acids. *Chem. Eur. J.*, **2018**, *24*, 17832–17837.

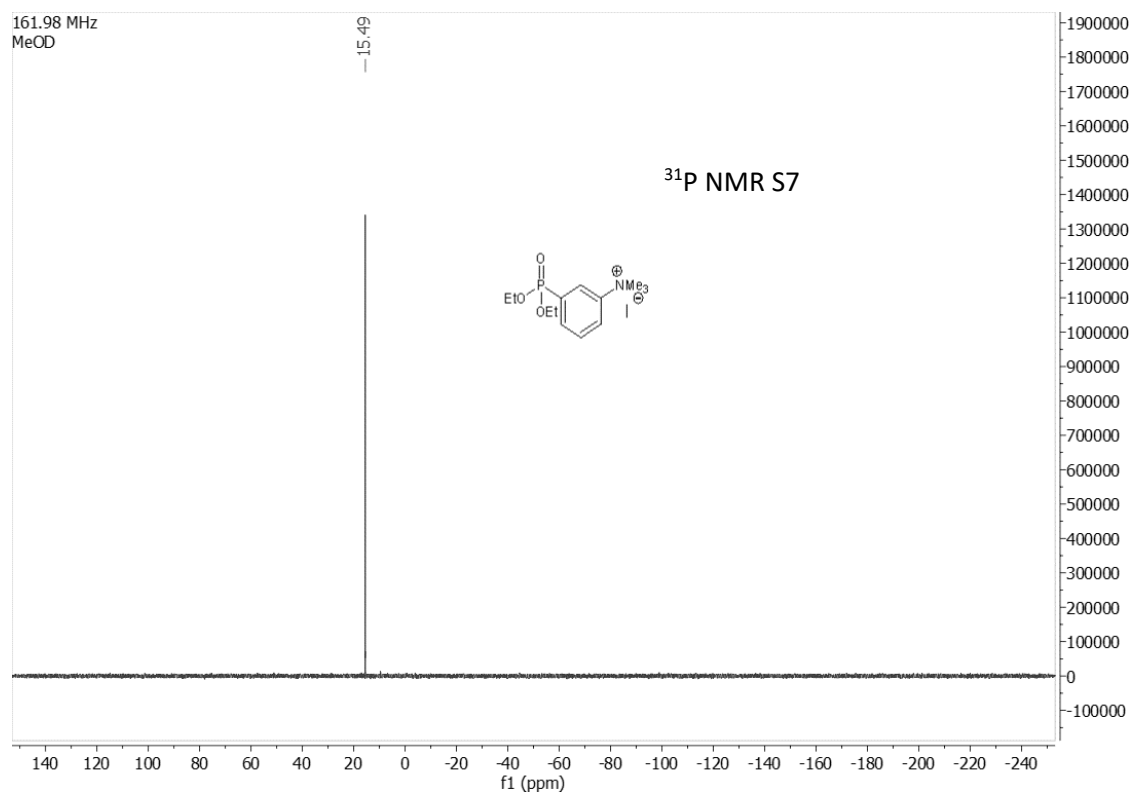
19. Ou, J., Tan, H., He, S., Wang, W., Hu, B., Yu, G., & Liu, K. 1,2-Dibutoxyethane-Promoted Oxidative Cleavage of Olefins into Carboxylic Acids Using O₂ under Clean Conditions. *J. Org. Chem.*, **2021**, *86*, 14974–14982.
20. (a) Ai, Y.; Ye, N.; Wang, Q.; Yahata, K.; Kishi, Y. Zirconium/Nickel-Mediated One-Pot Ketone Synthesis. *Angew. Chem. Int. Ed.*, **2017**, *56*, 10791-10795.
- (b) Ren, H.; Li, G.; Zhu, B.; Lv, X.; Yao, L.; Wang, X.; Su, Z.; Guan, W. How Does Iridium (III) Photocatalyst Regulate Nickel (II) Catalyst in Metallaphotoredox-Catalyzed C-S Cross-Coupling? Theoretical and Experimental Insights. *ACS. Catal.*, **2019**, *9*, 5, 3858-3865.
21. (a) Shi, S.; Lalancette, R.; Szostak, R.; Szostak, M. Triflamides: Highly Reactive, Electronically Activated N-Sulfonyl Amides in Catalytic N-C(O) Amide Cross-Coupling. *Org. Lett.*, **2019**, *21*, 1253-1257.
- (b) Ball-Jones, N.; Badillo, J.; Tran, N.; Franz, A. Catalytic Enantioselective Carboannulation with Allylsilanes. *Angew. Chem. Int. Ed.*, **2014**, *53*, 9462-9465.
22. Hendy, C.; Smith, G.; Xu, Z.; Lian, T.; Jui, N. Radical Chain Reduction via Carbon Dioxide Radical Anion (CO₂^{•-}). *J. Am. Chem. Soc.*, **2021**, *143*, 8987-8992.

5.1: Appendix—Spectra

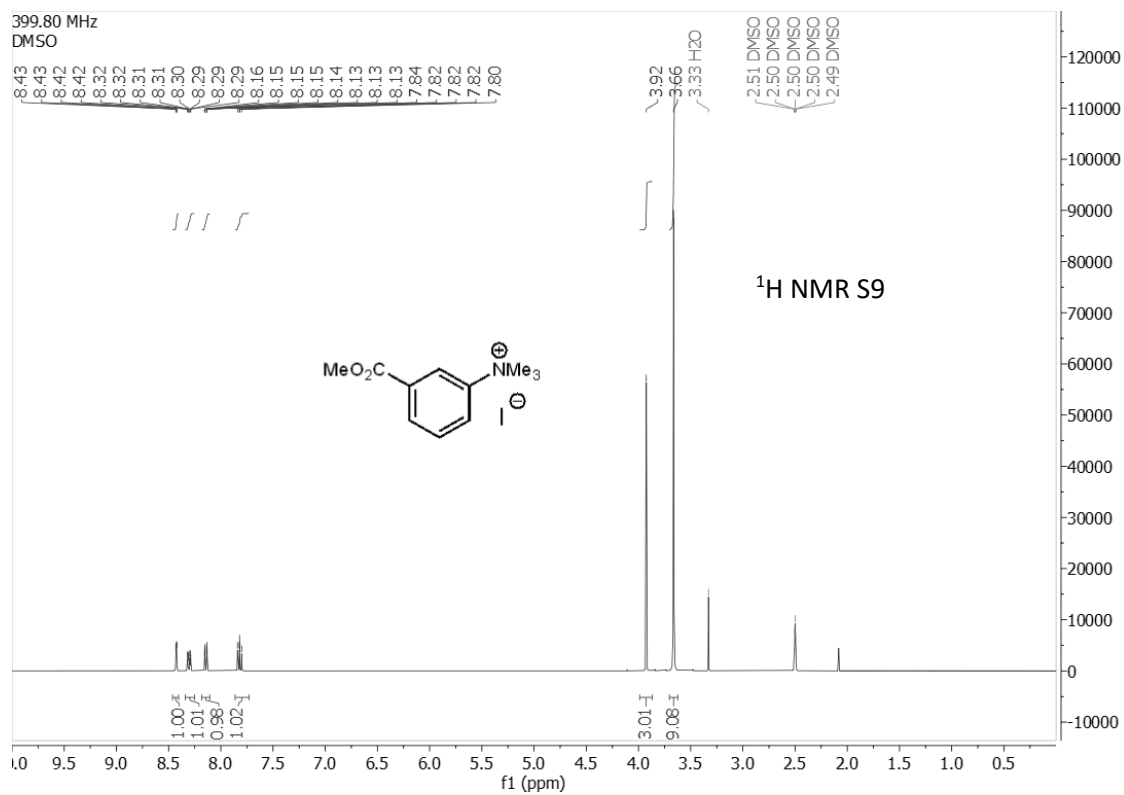
3-cyano-N,N,N-trimethylbenzenaminium iodide (S5):

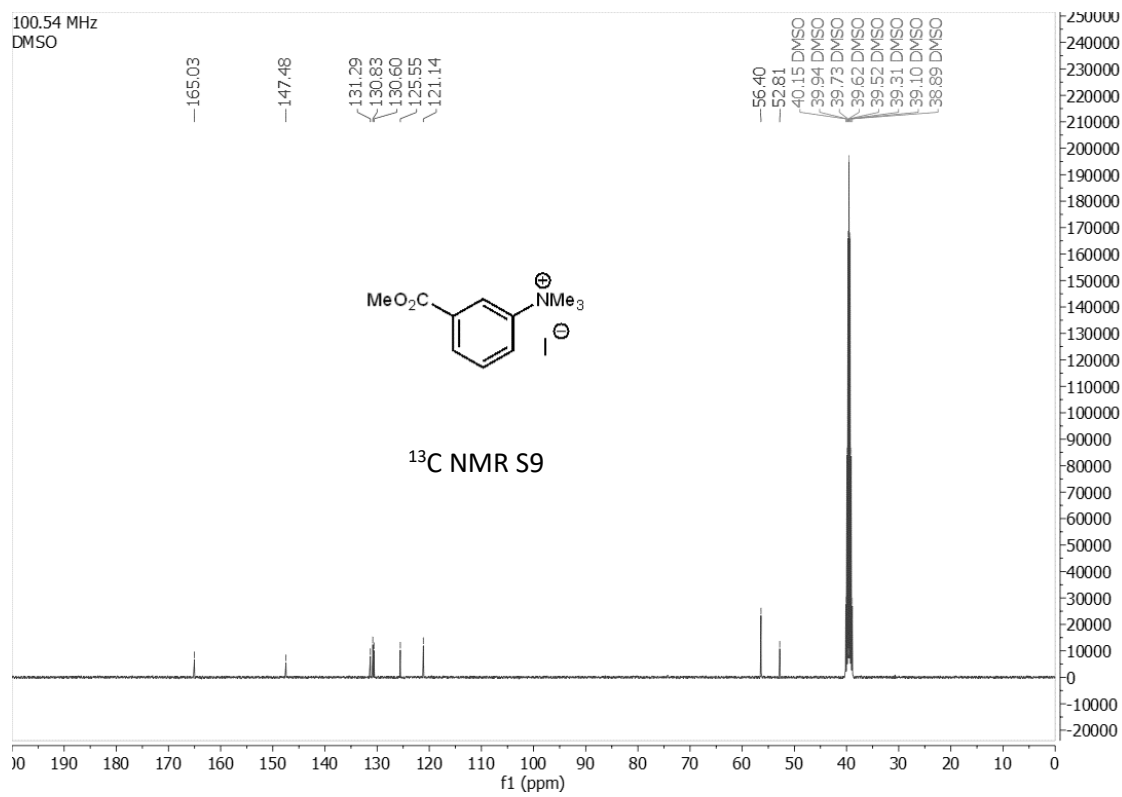


diethyl (3-(dimethylamino)phenyl)phosphonate (S7):


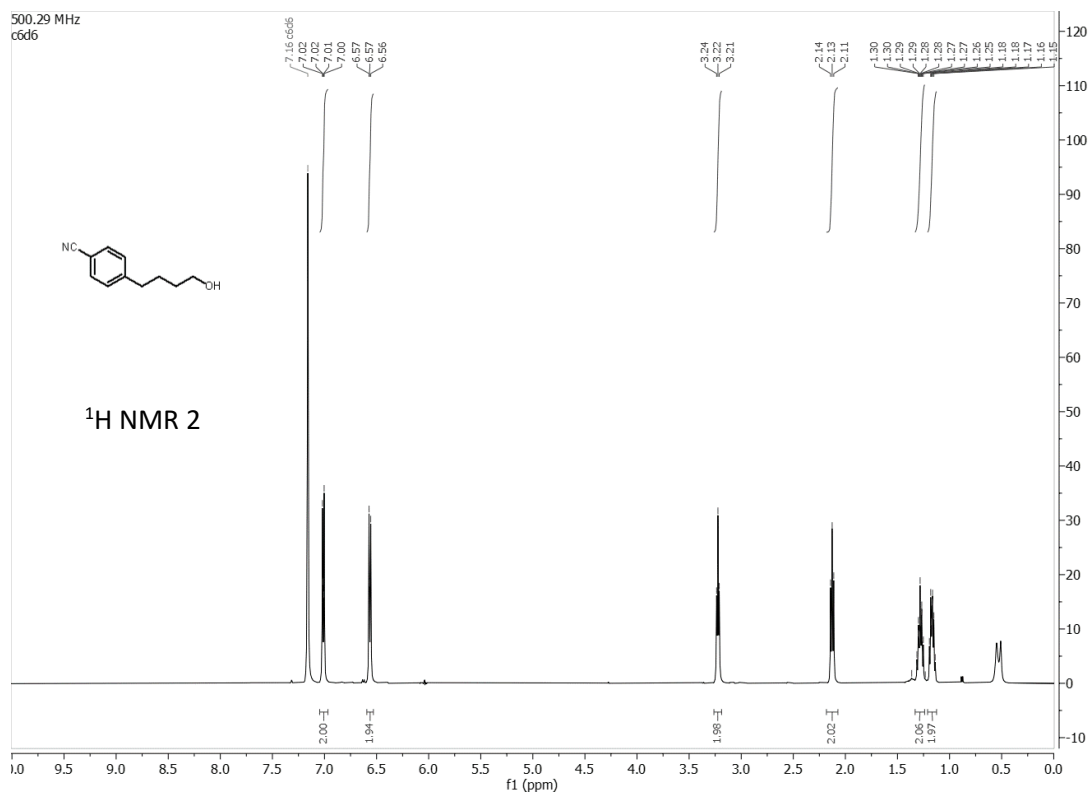


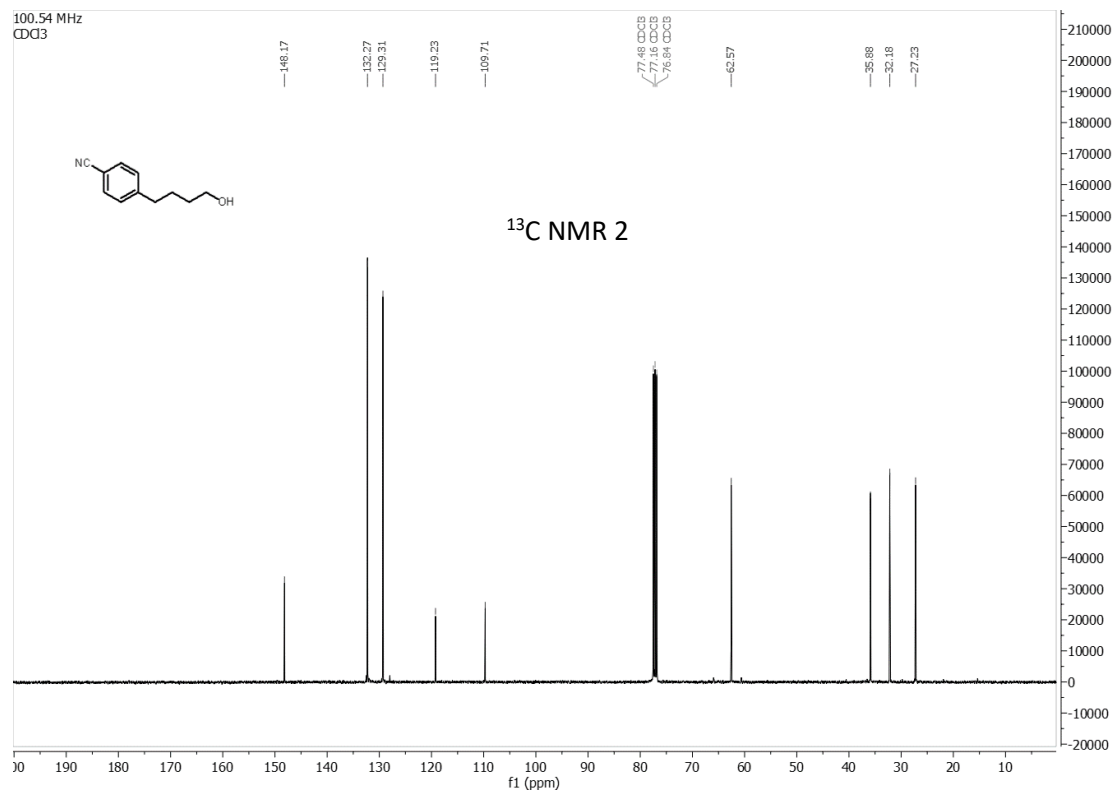
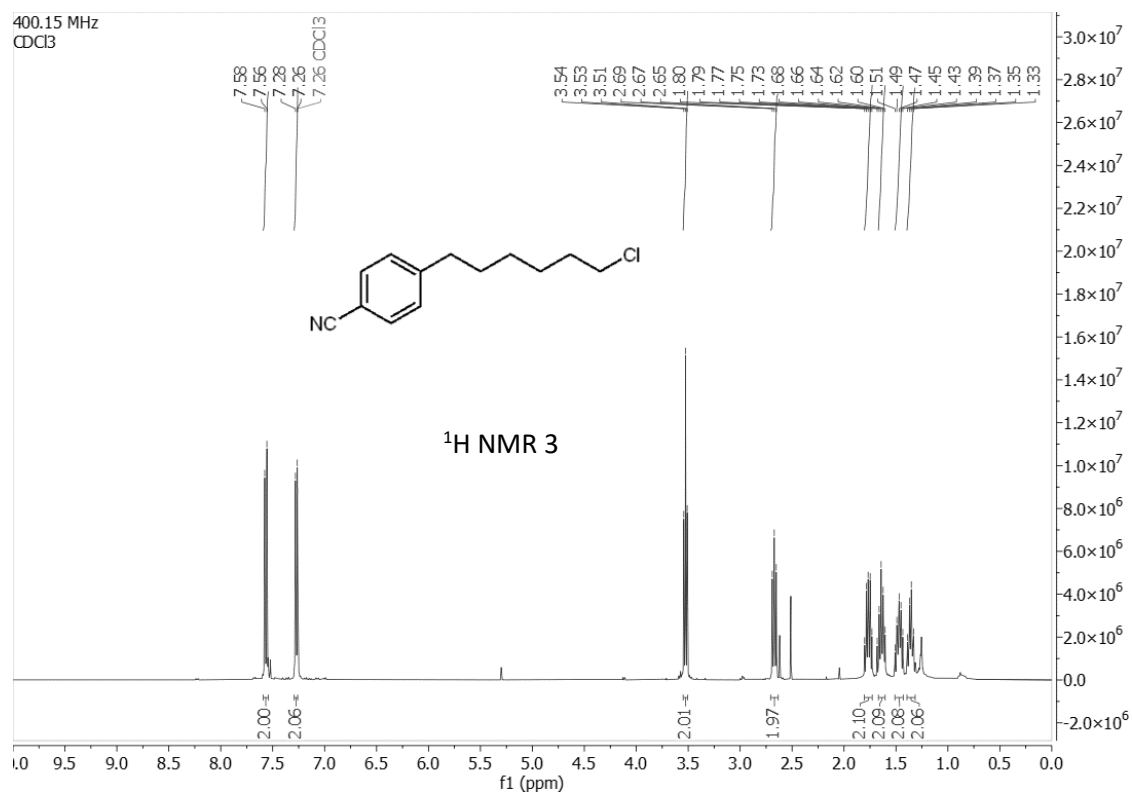
3-(methoxycarbonyl)-N,N,N-trimethylbenzenaminium iodide (S9)

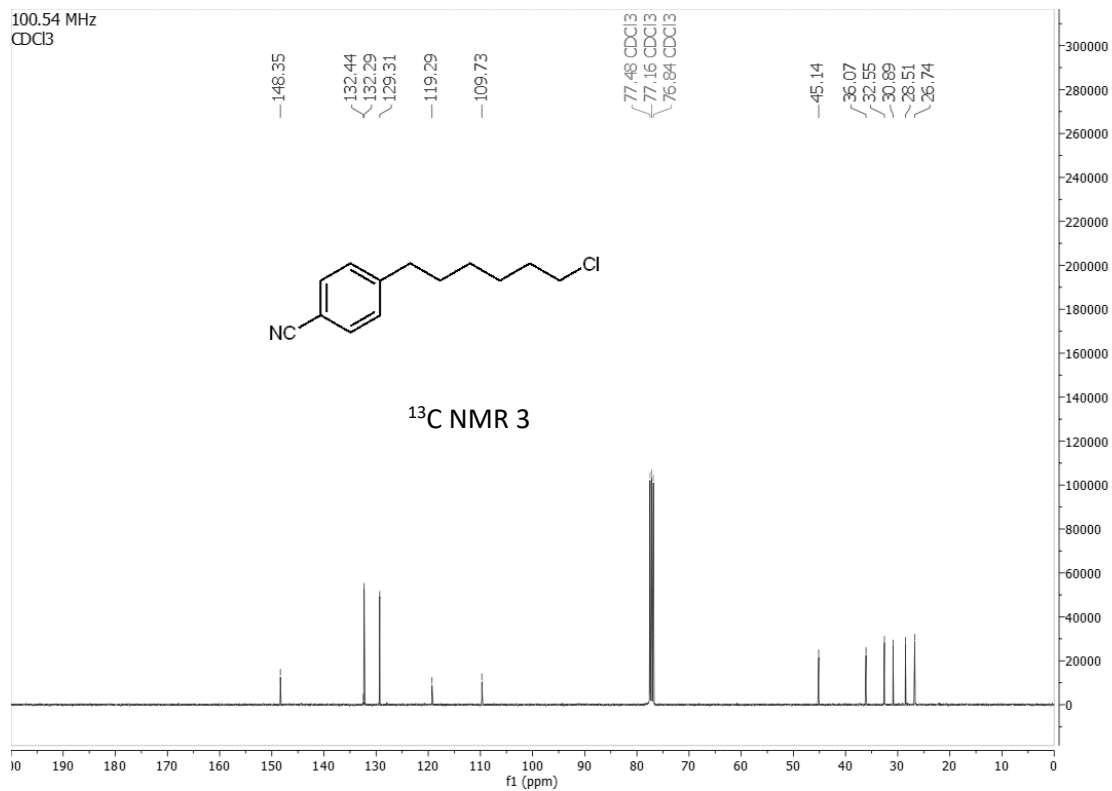




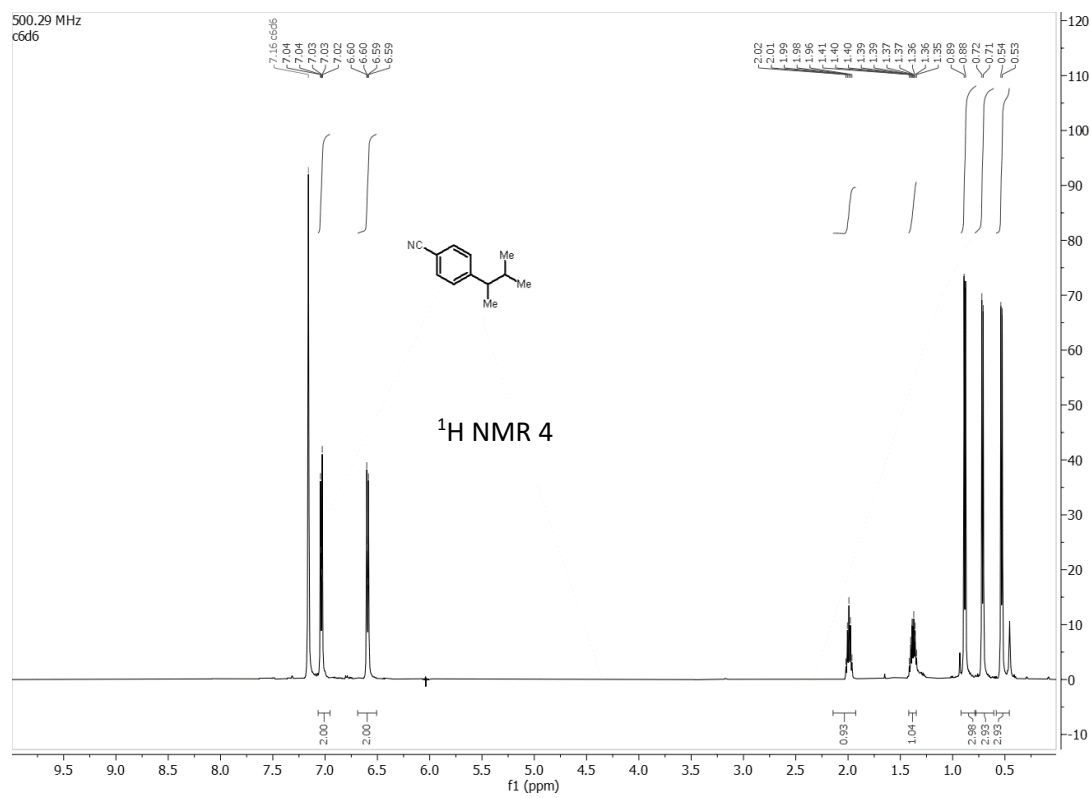
4-(4-hydroxybutyl)benzonitrile (2):

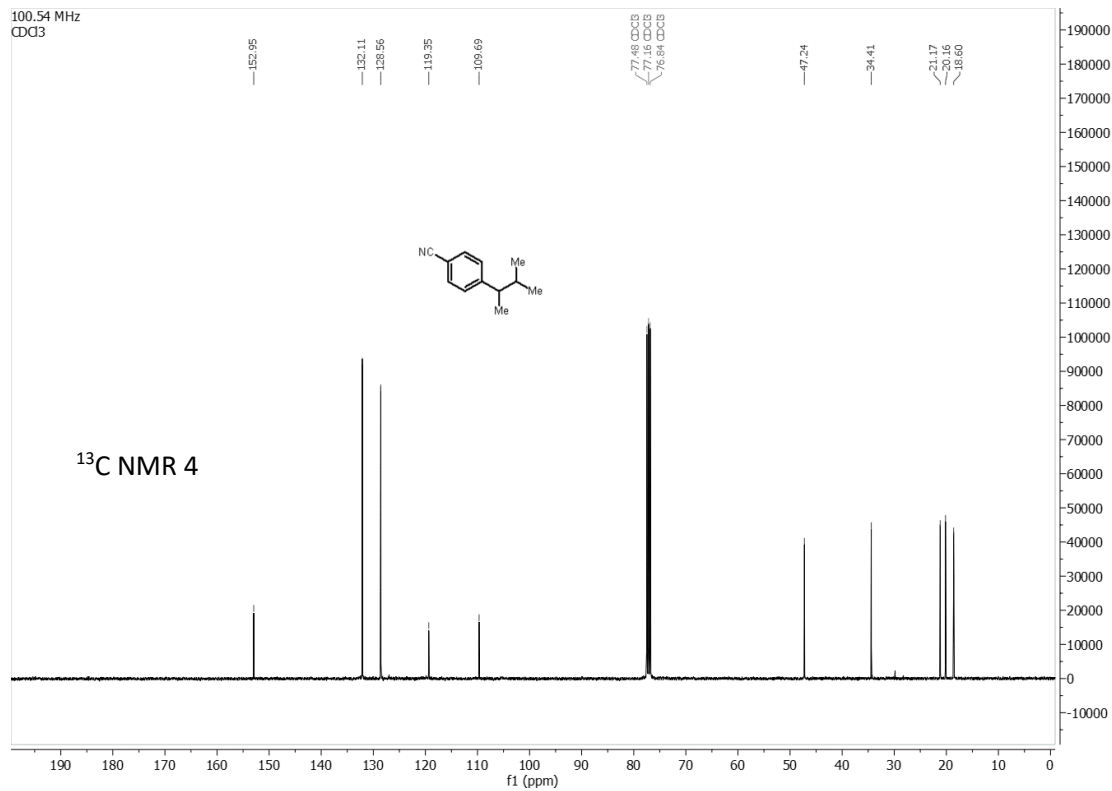


**4-(6-chlorohexyl)benzonitrile (3):**



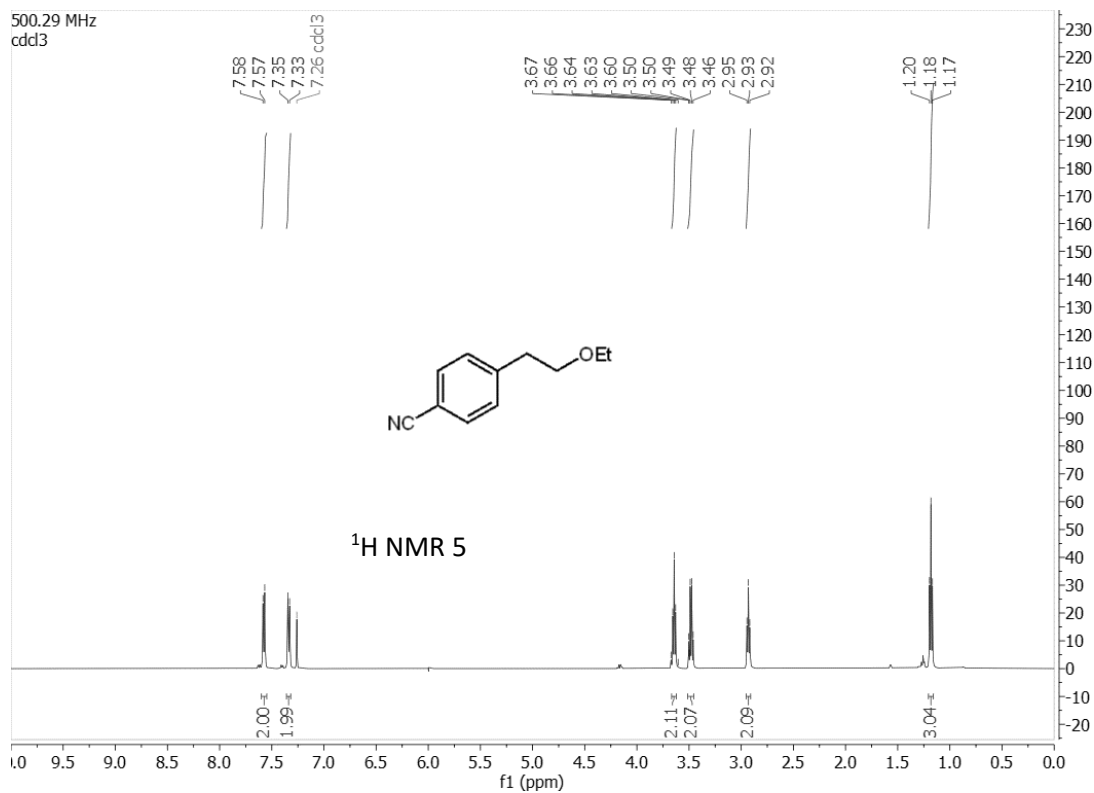
4-(3-methylbutan-2-yl)benzonitrile (4):

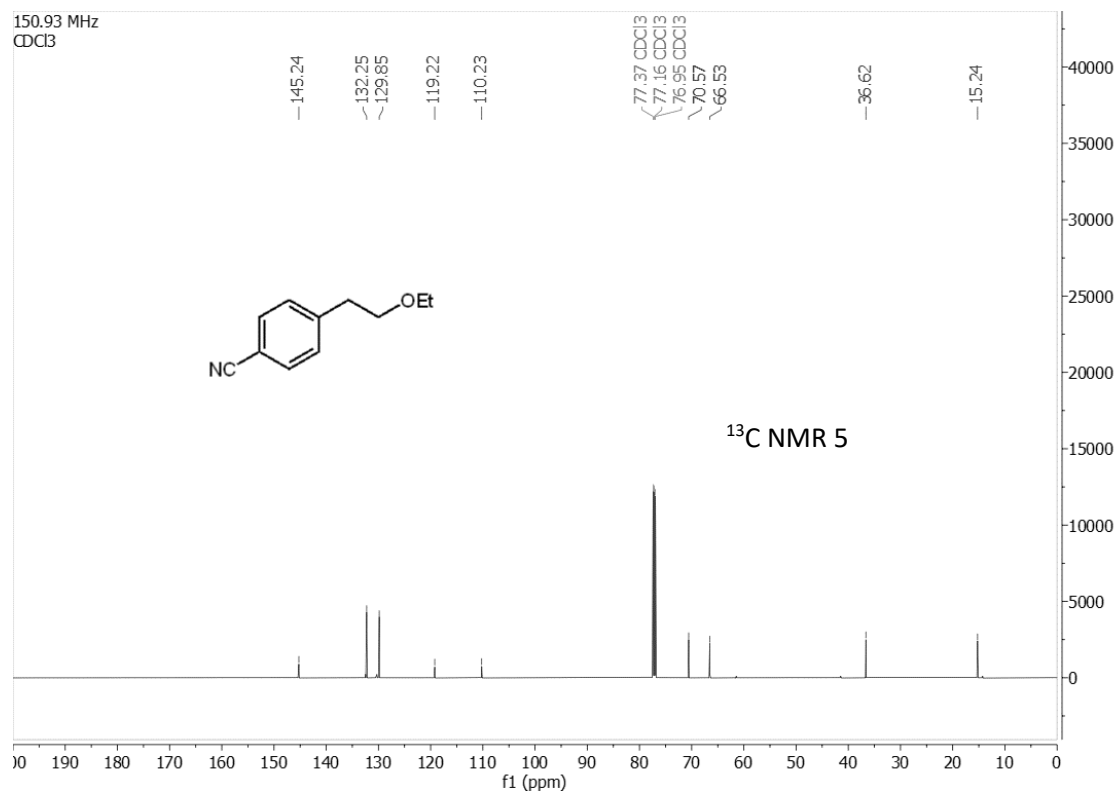




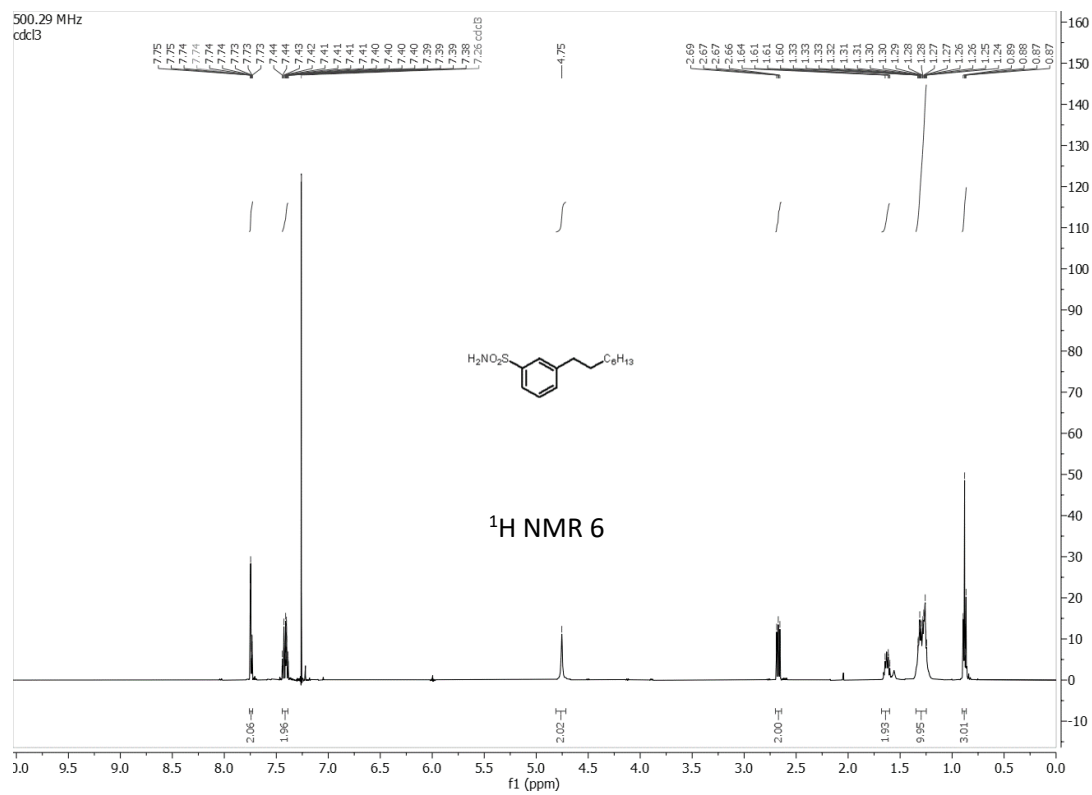
199

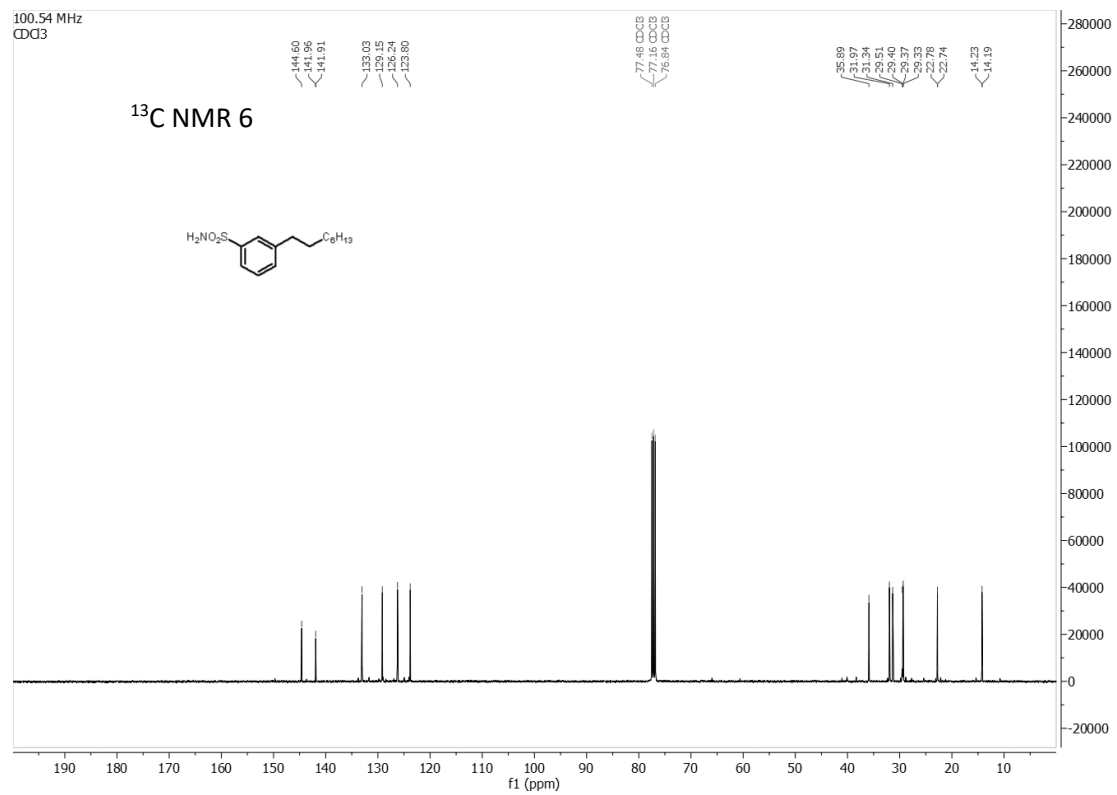
4-(2-ethoxyethyl)benzonitrile (5):



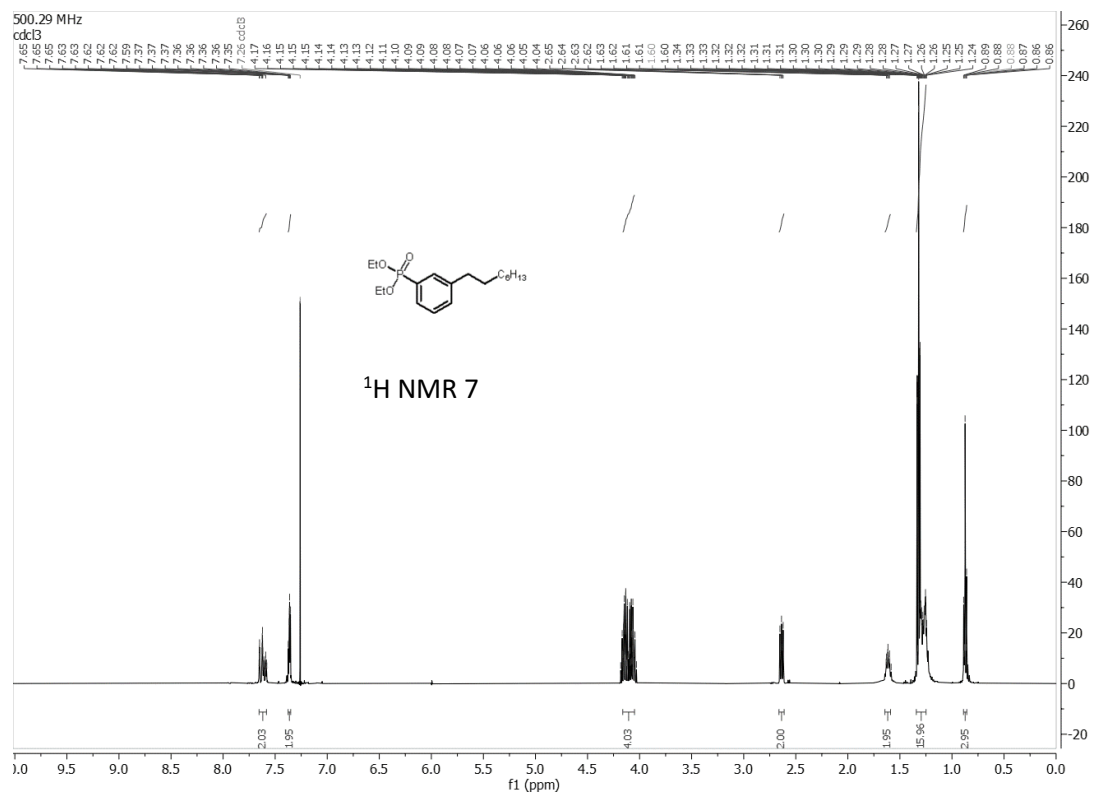


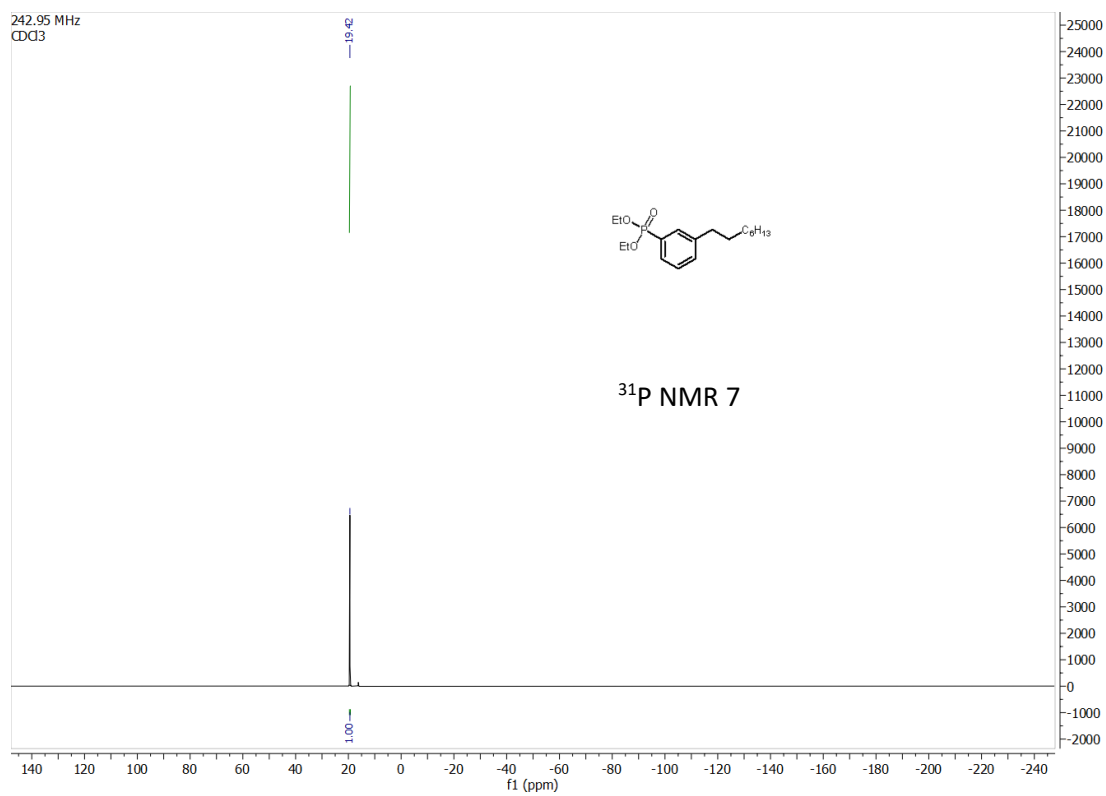
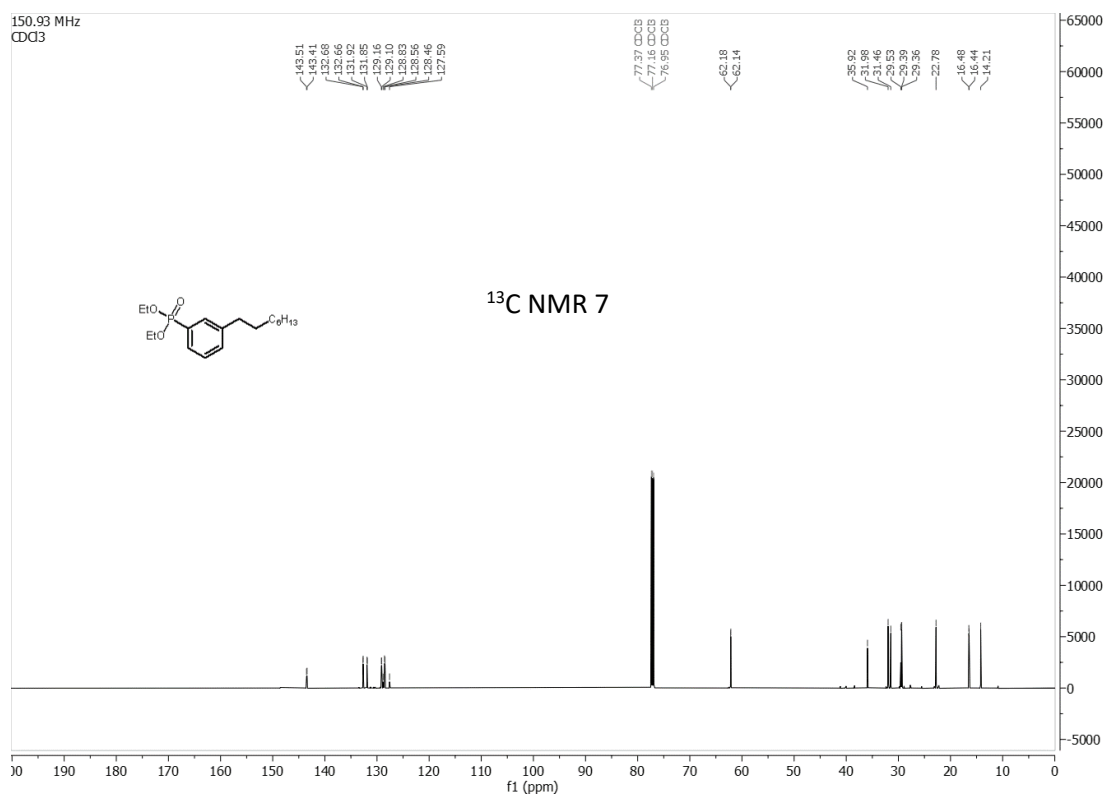
3-octylbenzenesulfonamide (6):

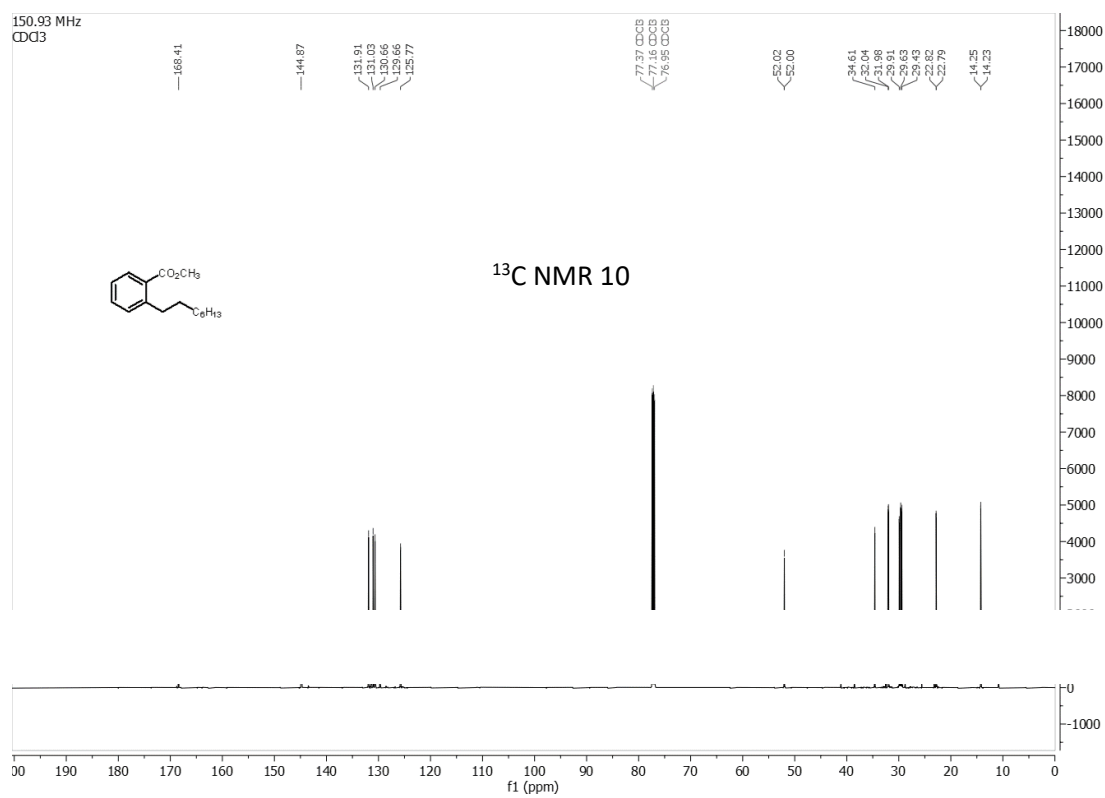
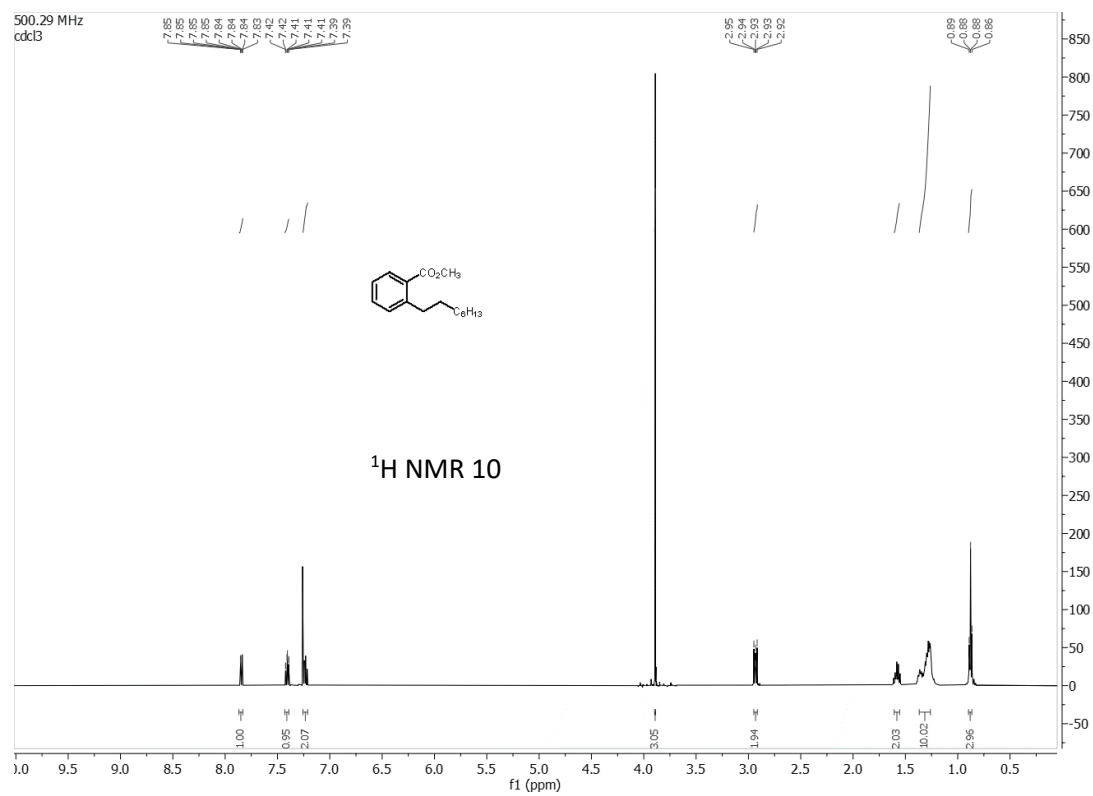


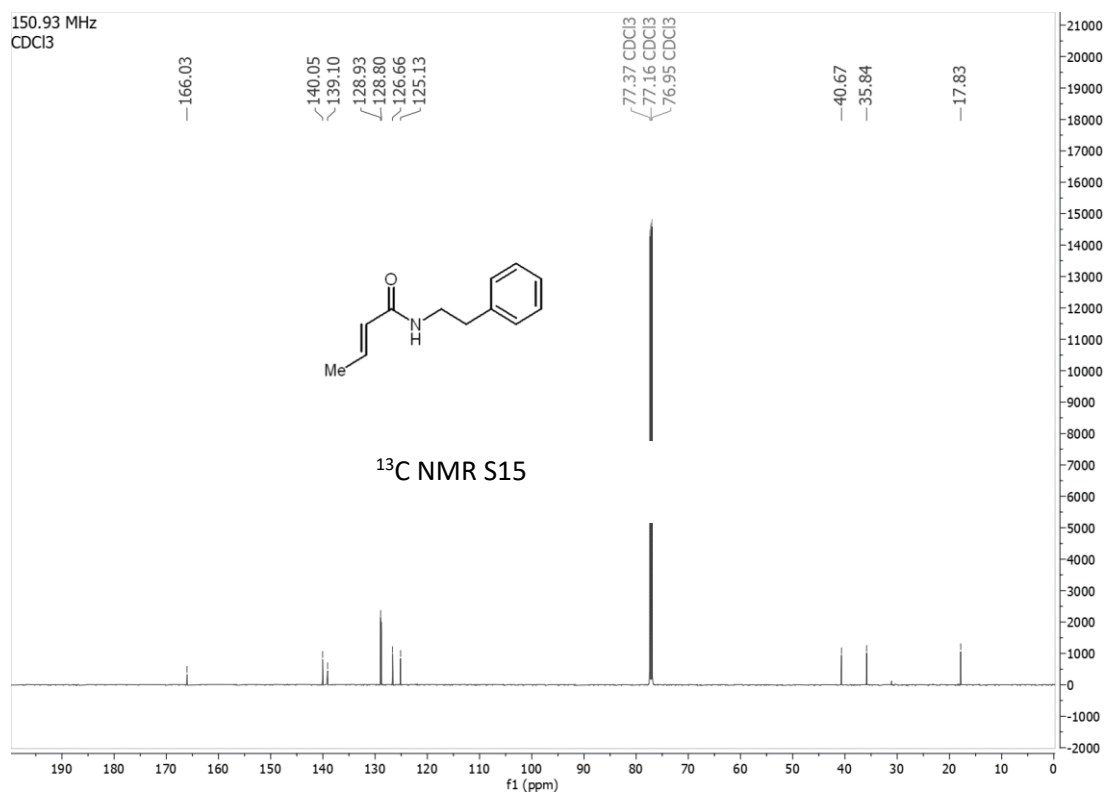
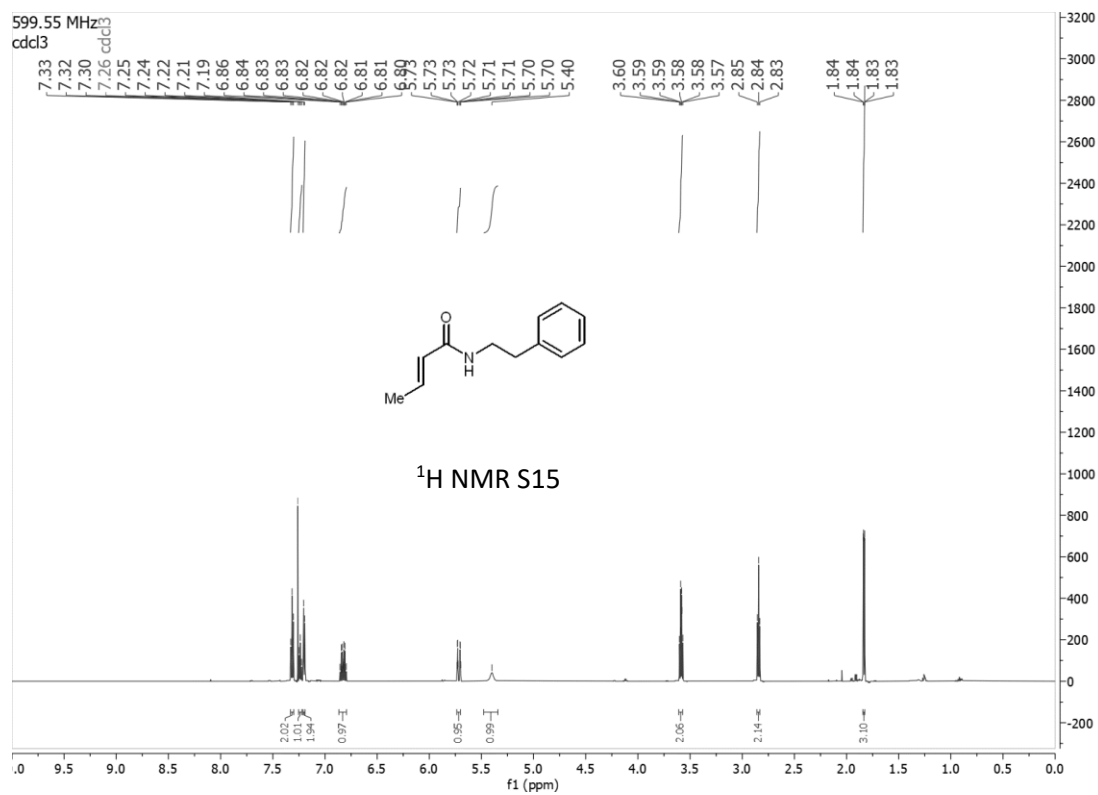


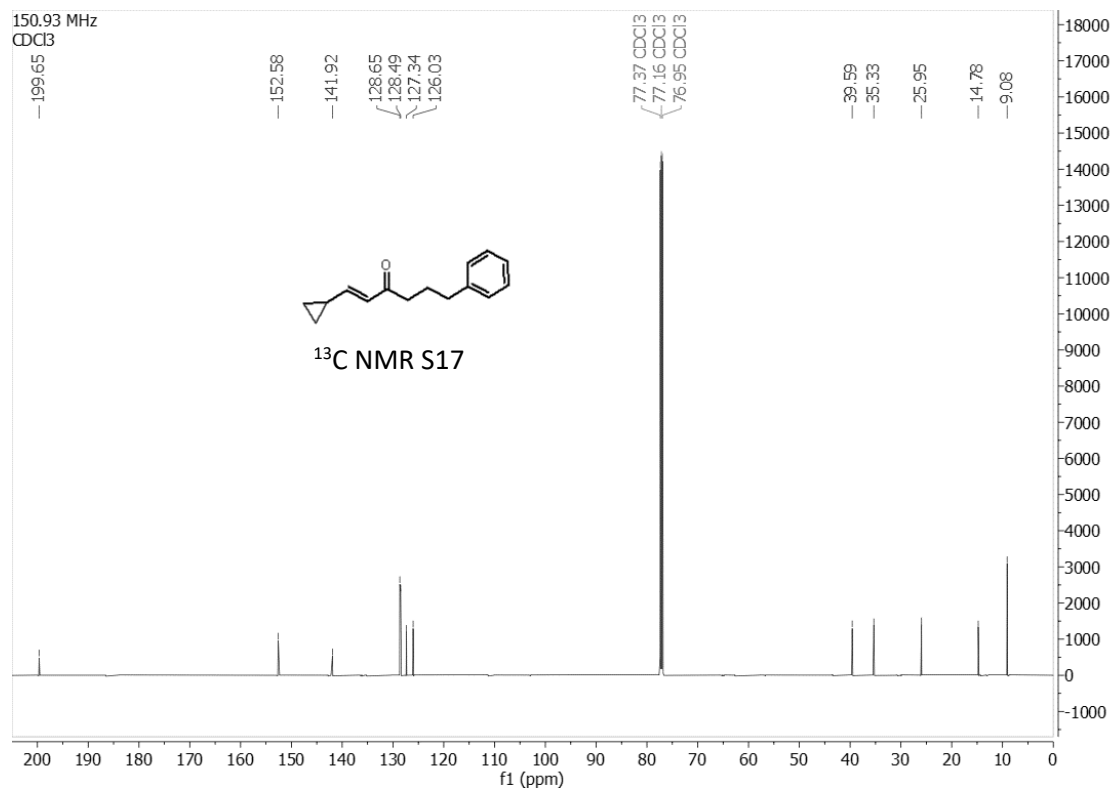
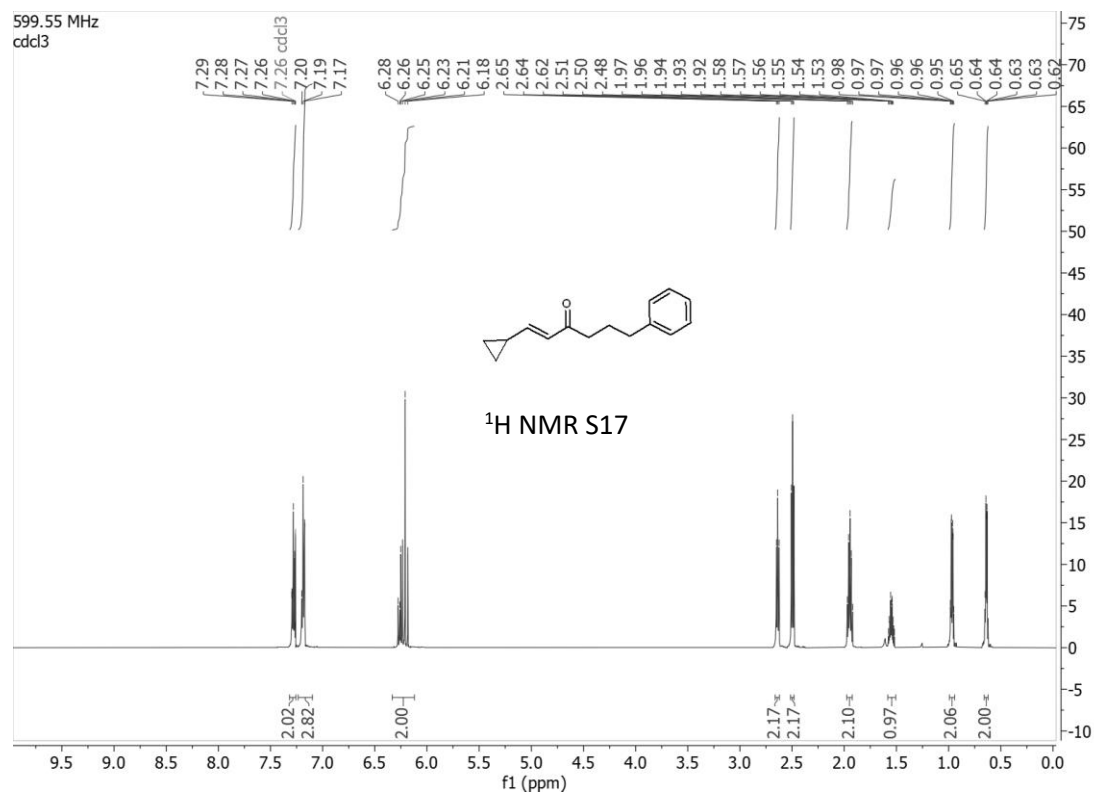
Diethyl (4-octylphenyl)phosphonate (7):

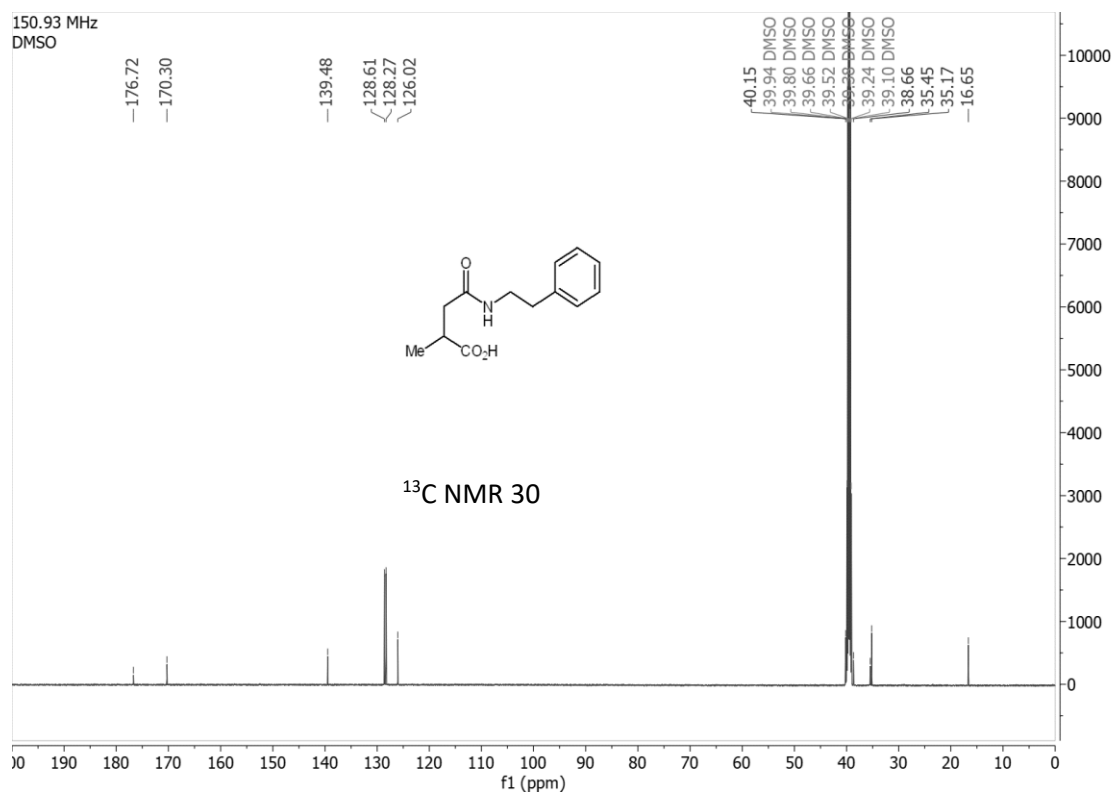
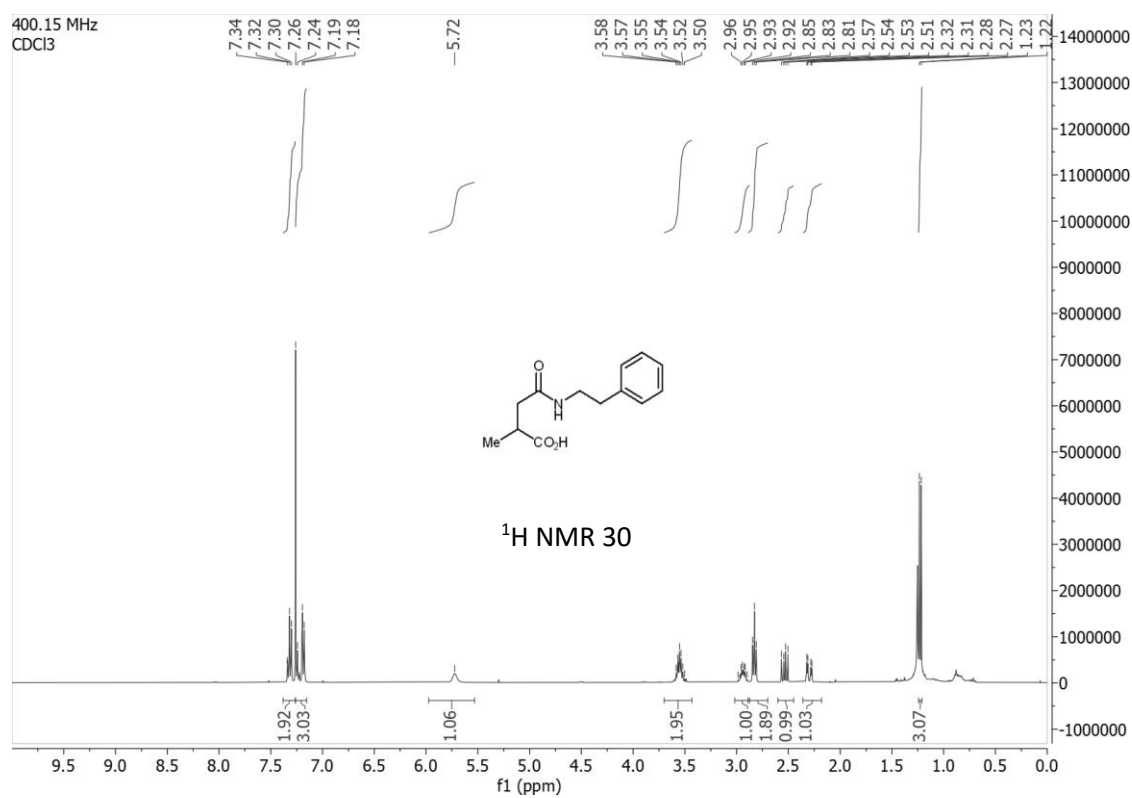


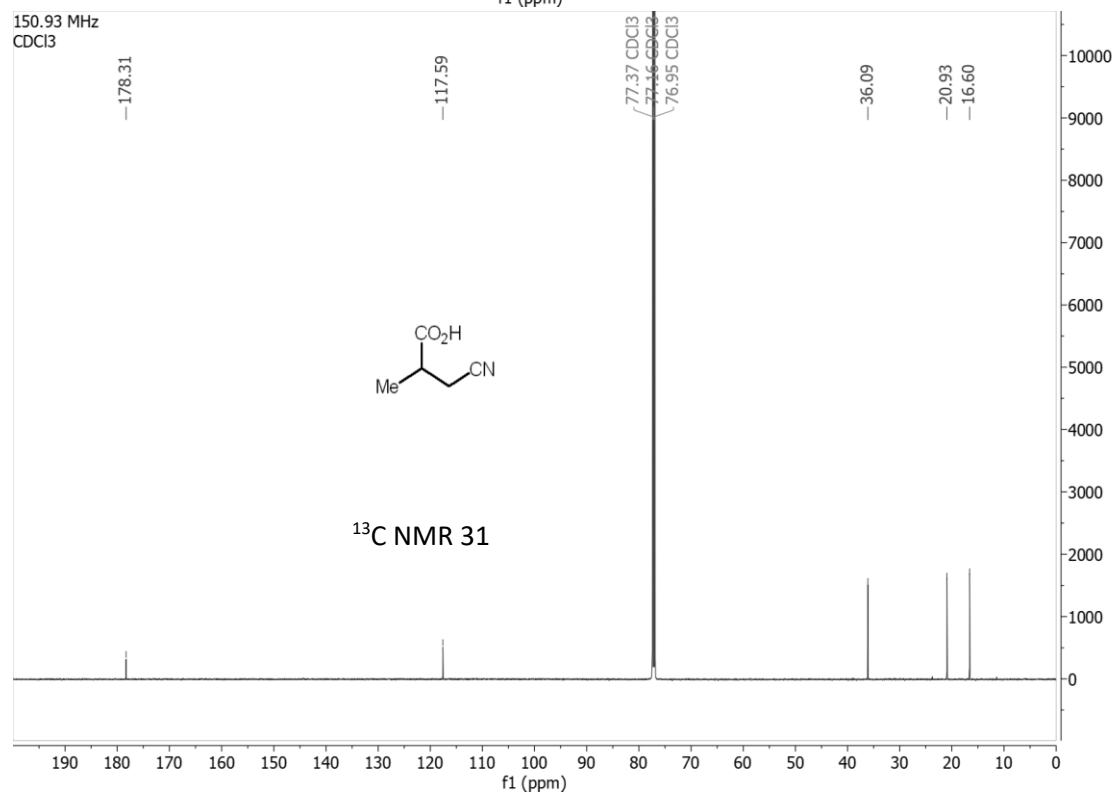
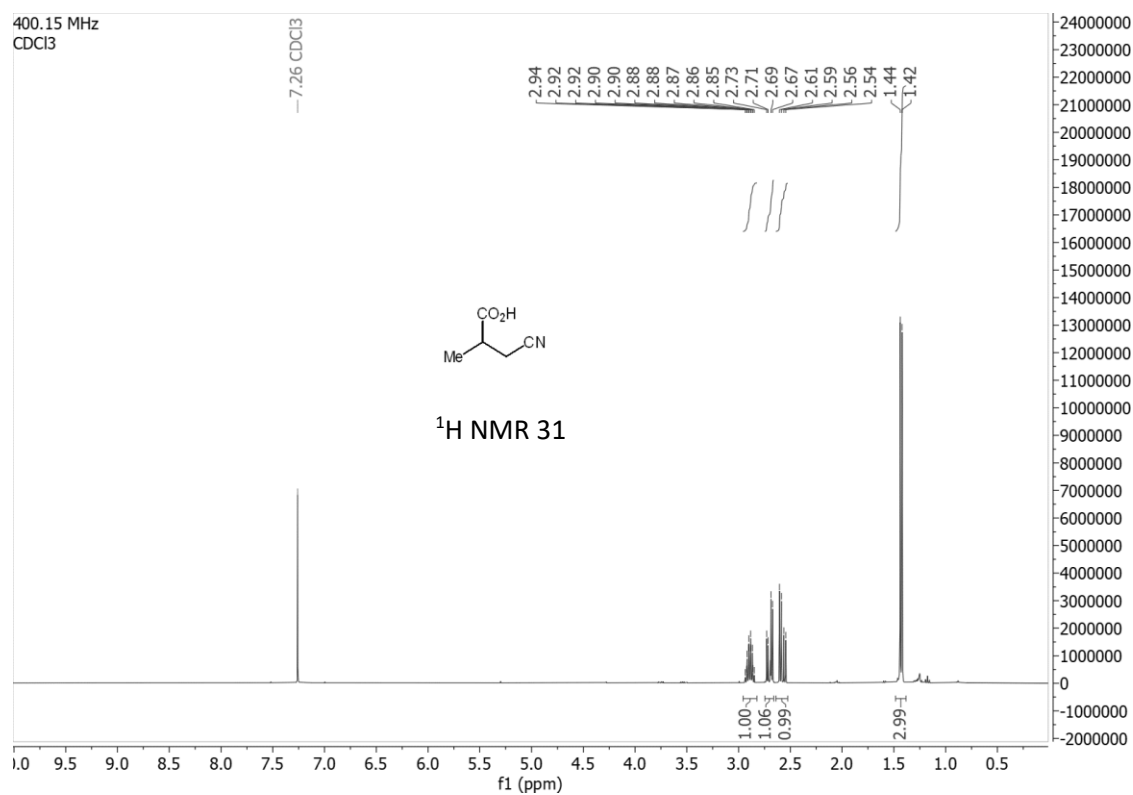


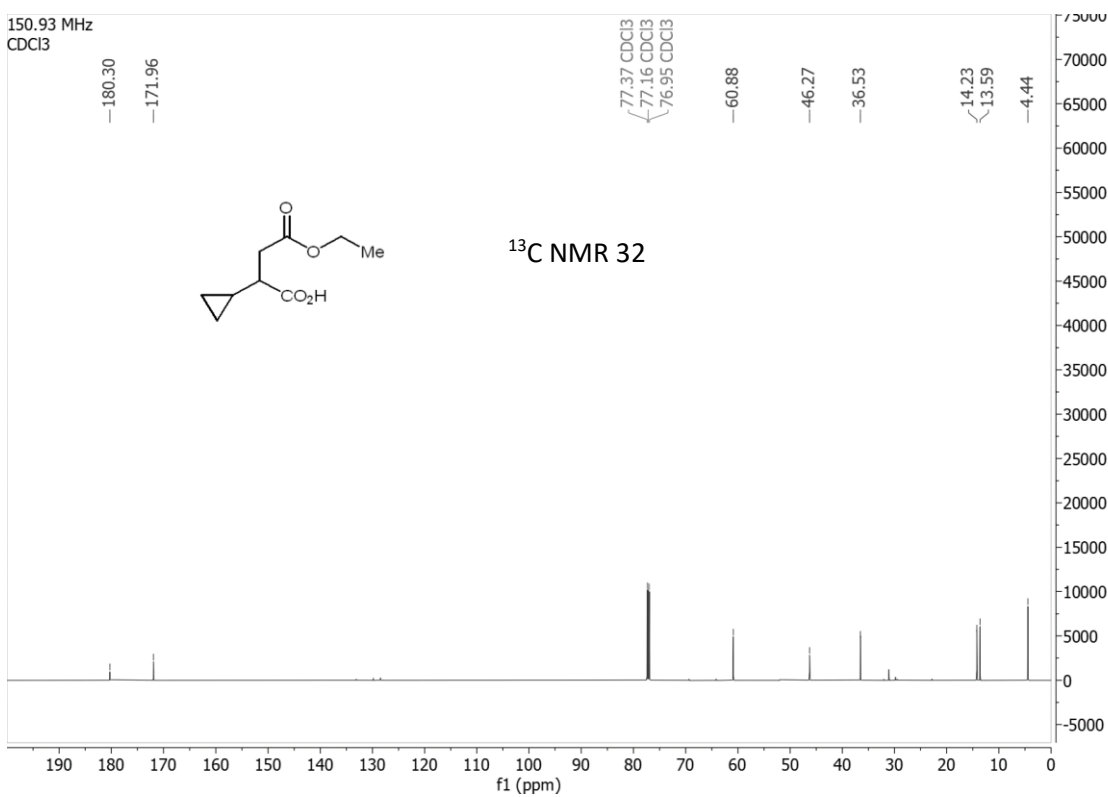
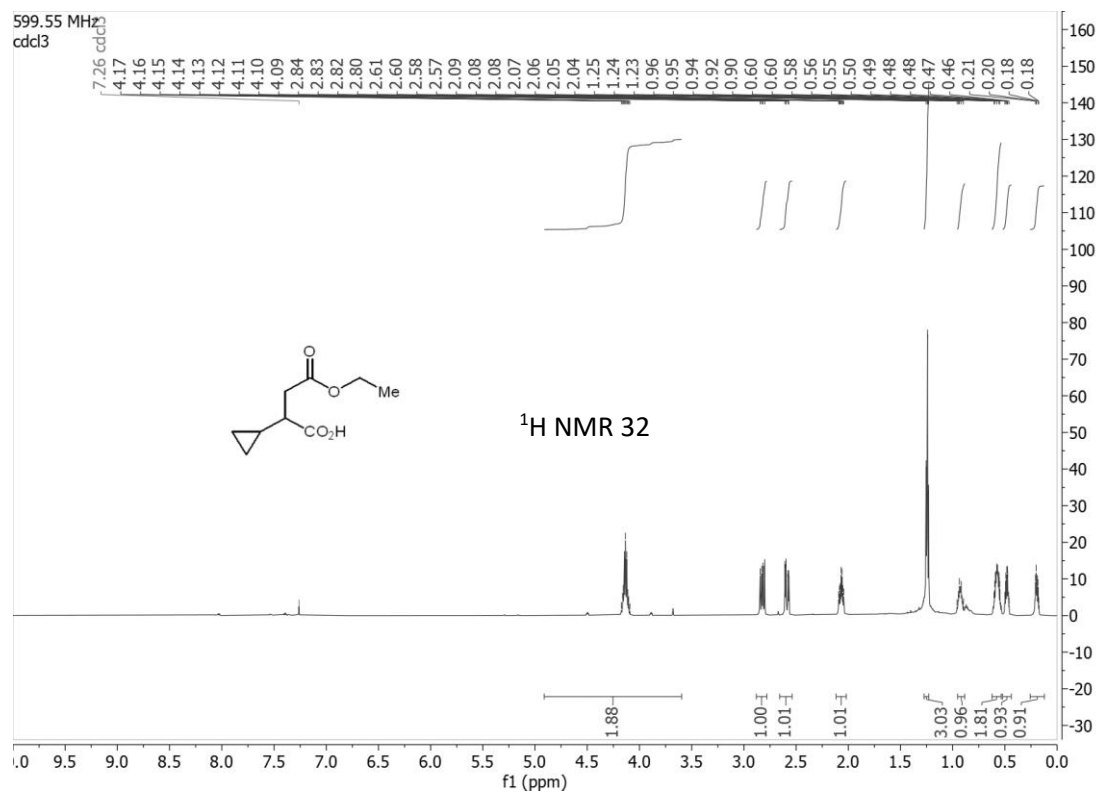
Methyl-2-octylbenzoate (10):

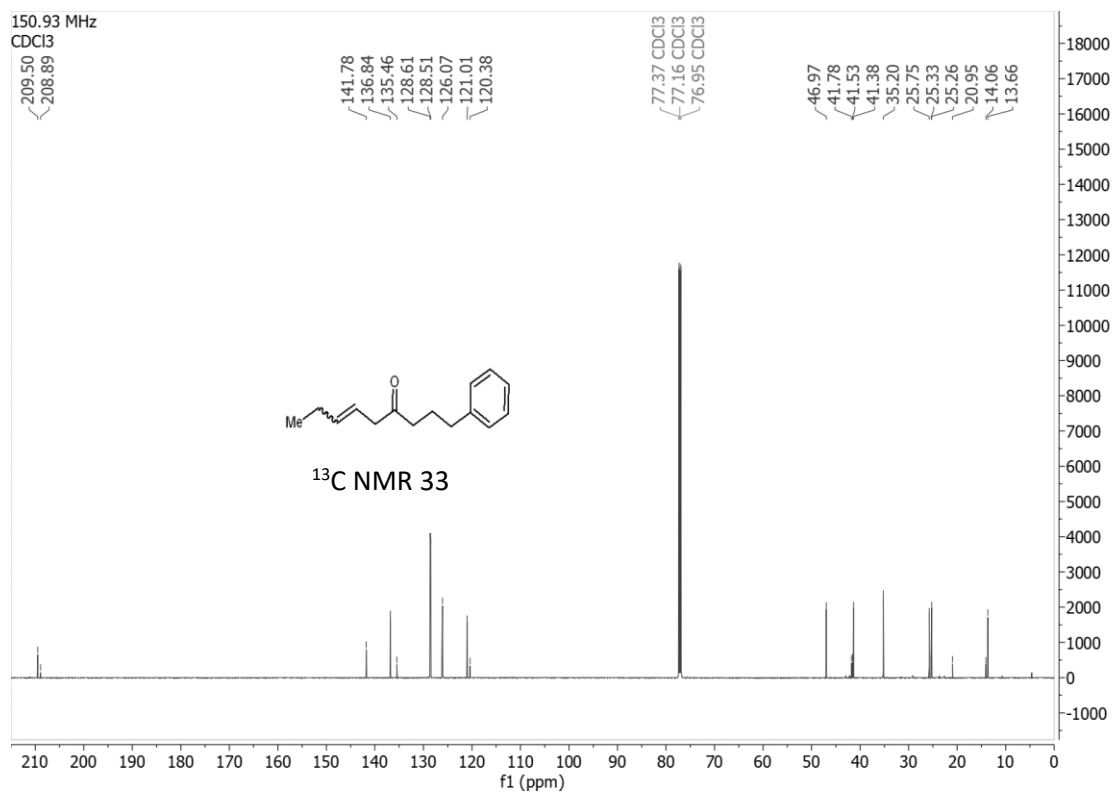
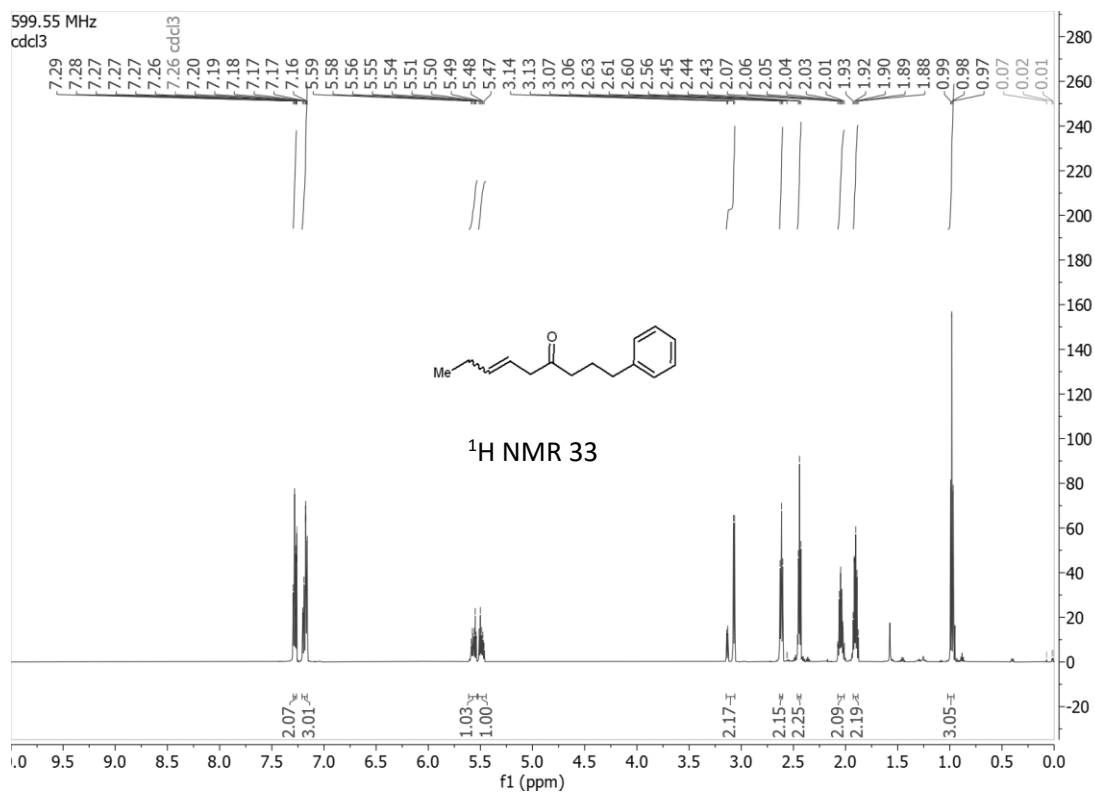
(E)-N-phenethylbut-2-enamide (S15):

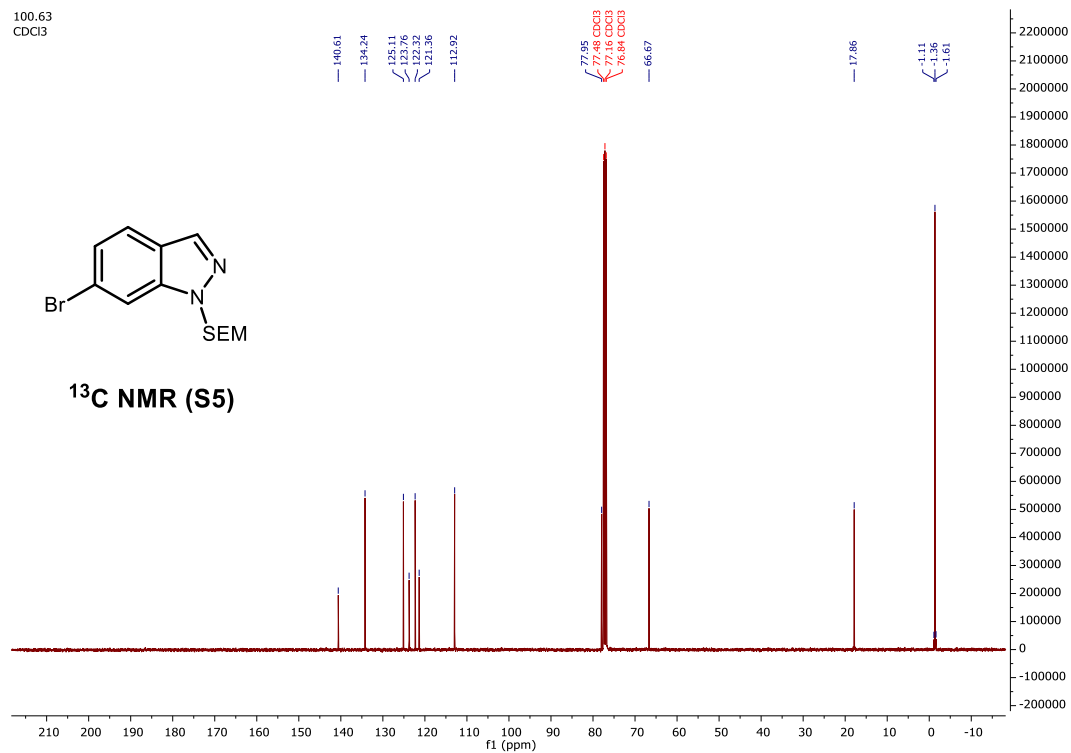
Ethyl (E)-3-cyclopropylacrylate (S16)

2-methyl-4-(phenethylamino)butanoic acid (30):

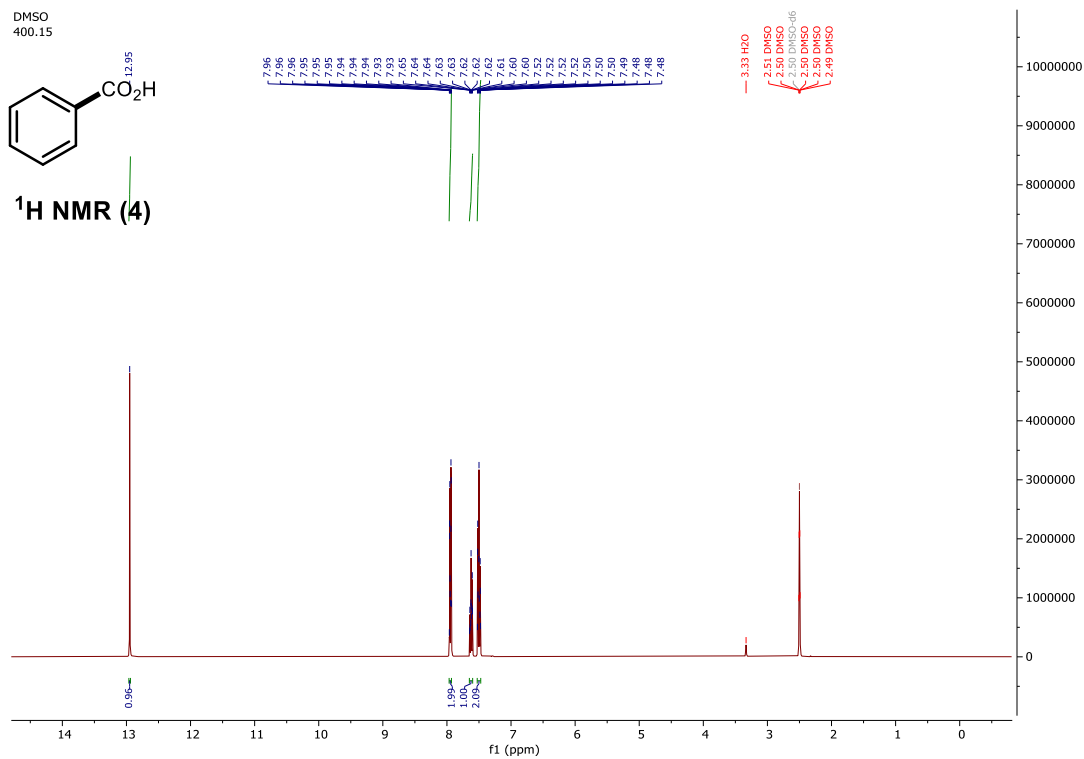
3-cyano-2-methylpropanoic acid (31):

2-cyclopropyl-4-ethoxy-4-oxobutanoic acid (32):

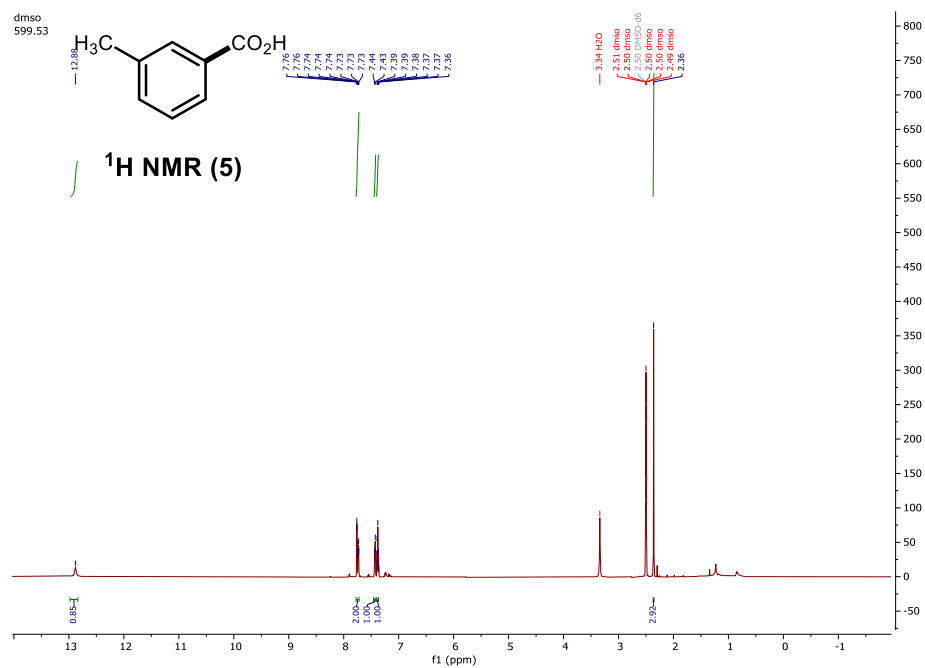
(E)-1-phenylnon-6-en-4-one (33):



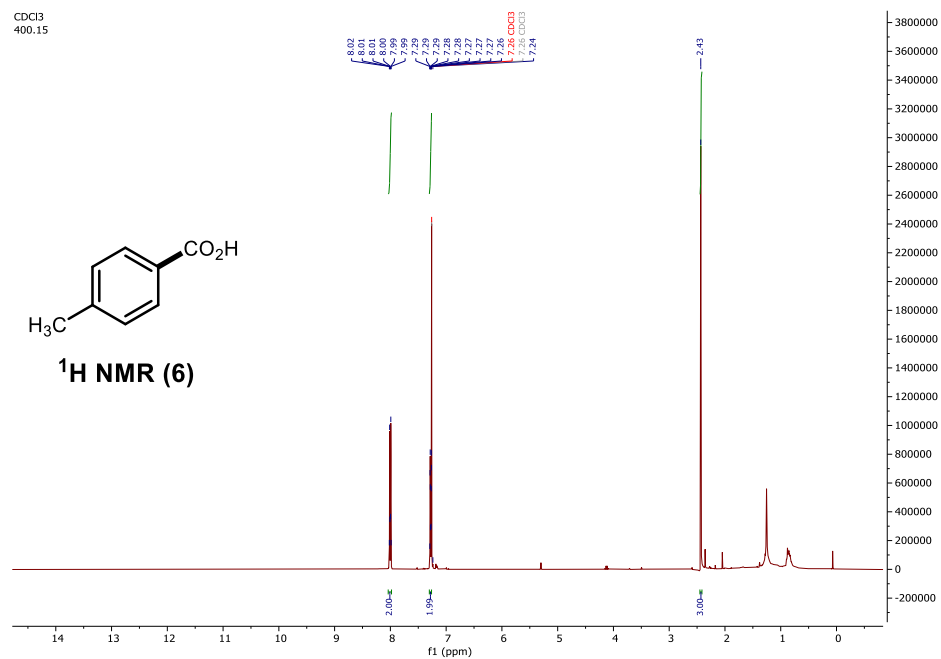
Benzoic acid (4):



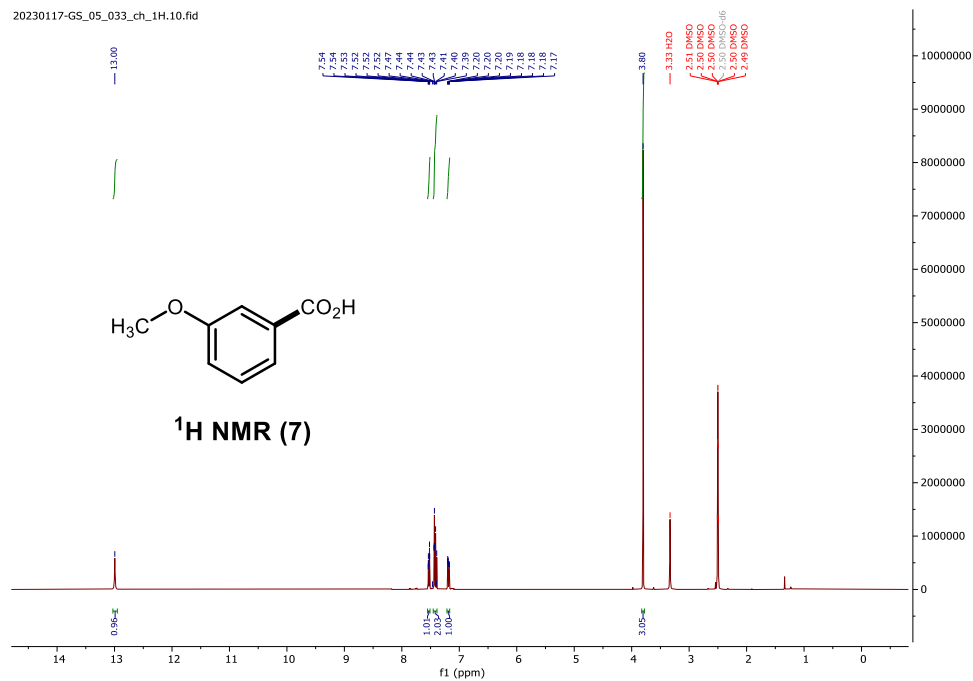
3-methylbenzoic acid (5)



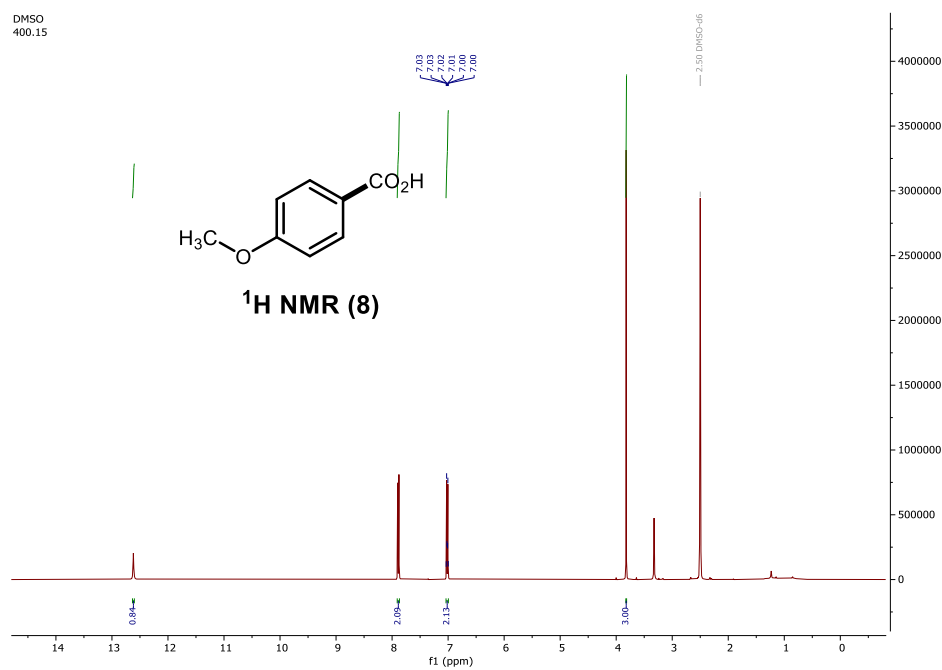
4-methylbenzoic acid (6)



3-methoxybenzoic acid (7)

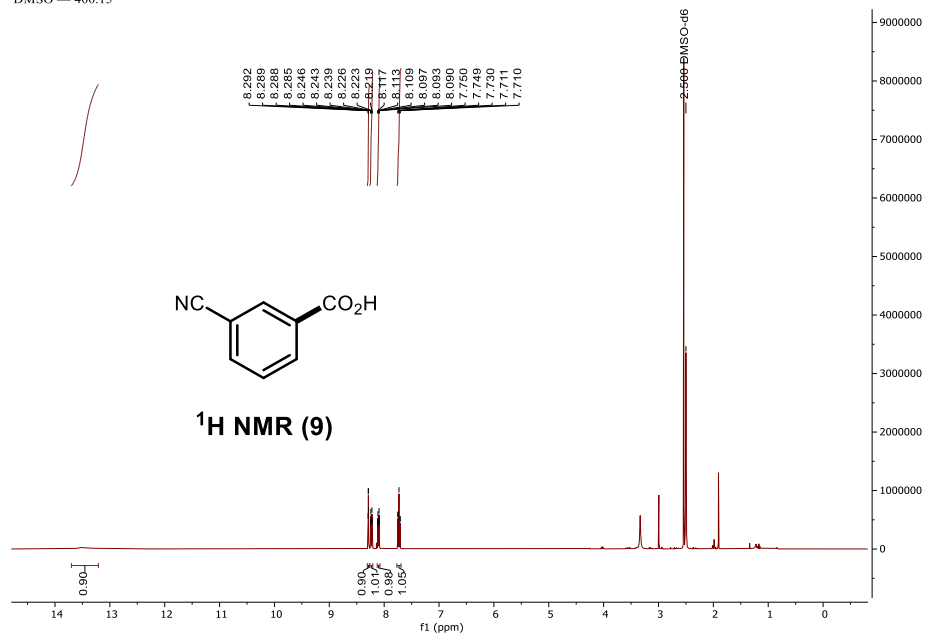


4-methoxybenzoic acid (8)

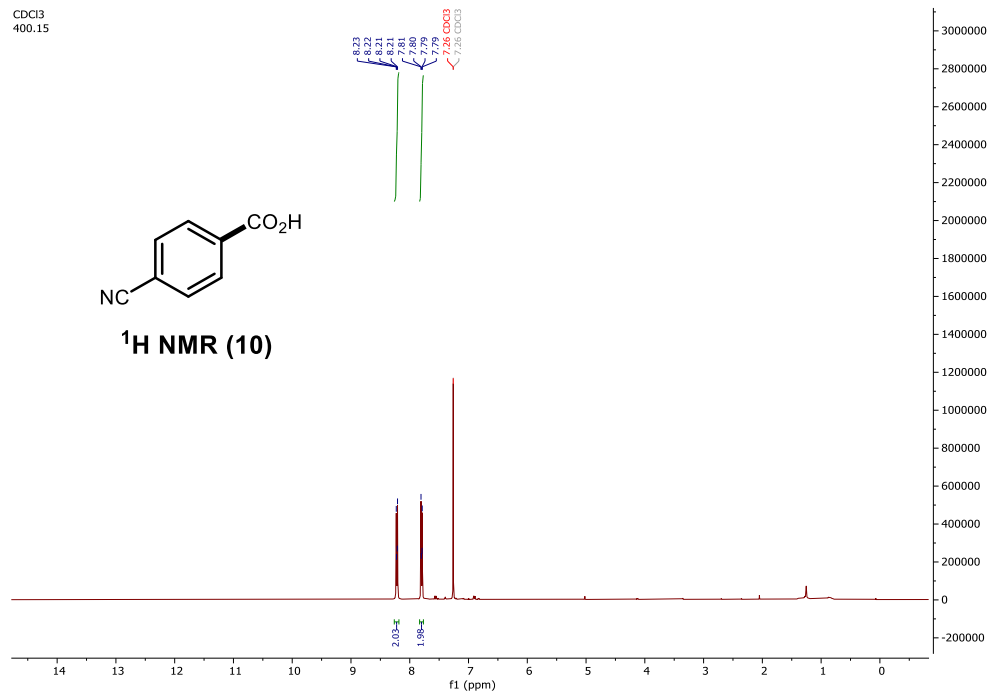


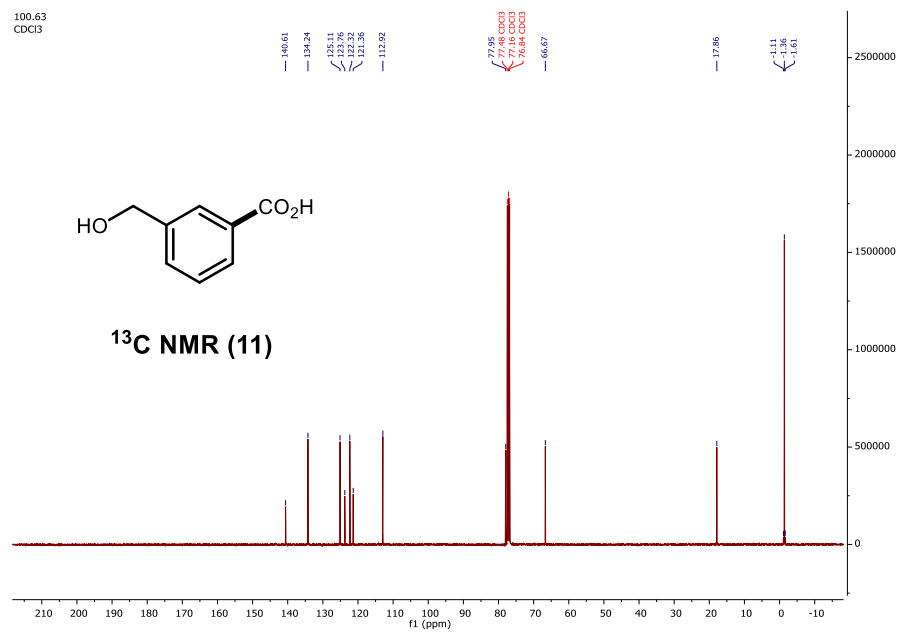
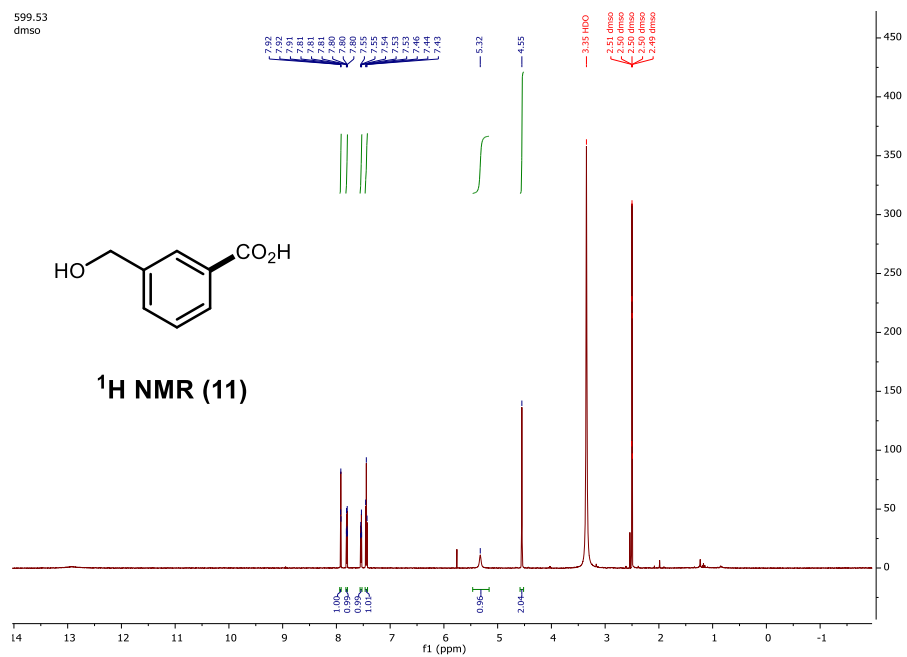
3-cyanobenzoic acid (9)

DMSO — 400.15

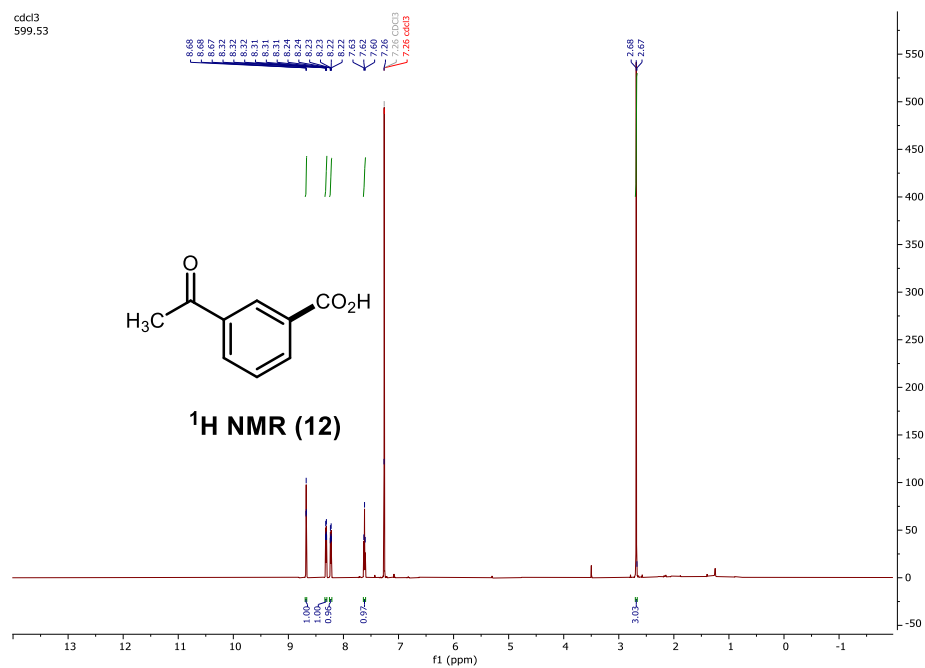


4-cyanobenzoic acid (10)

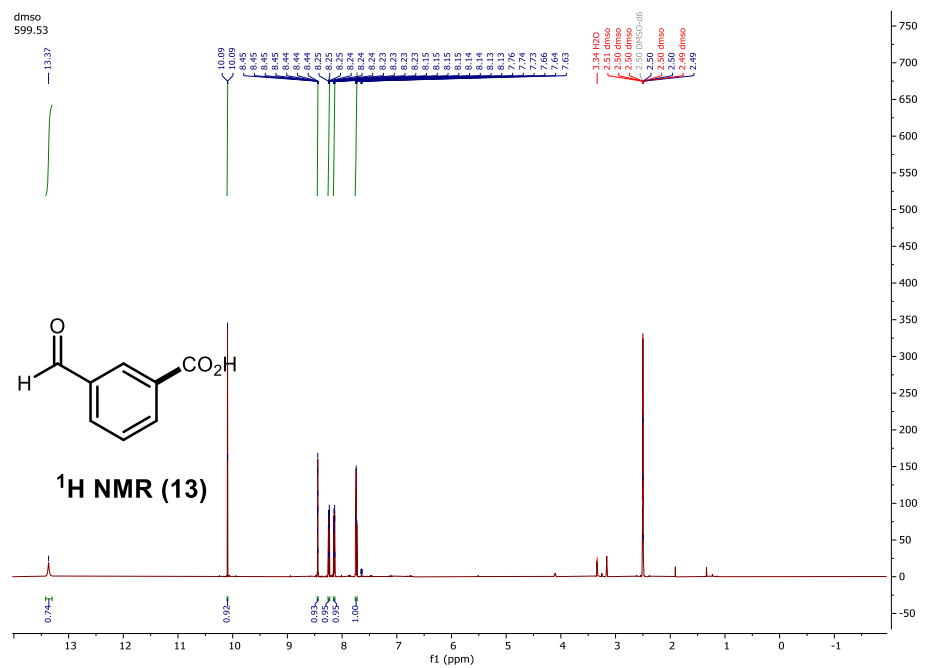
CDCl₃
400.15

3-(hydroxymethyl)benzoic acid (11)

3-acetylbenzoic acid (12):

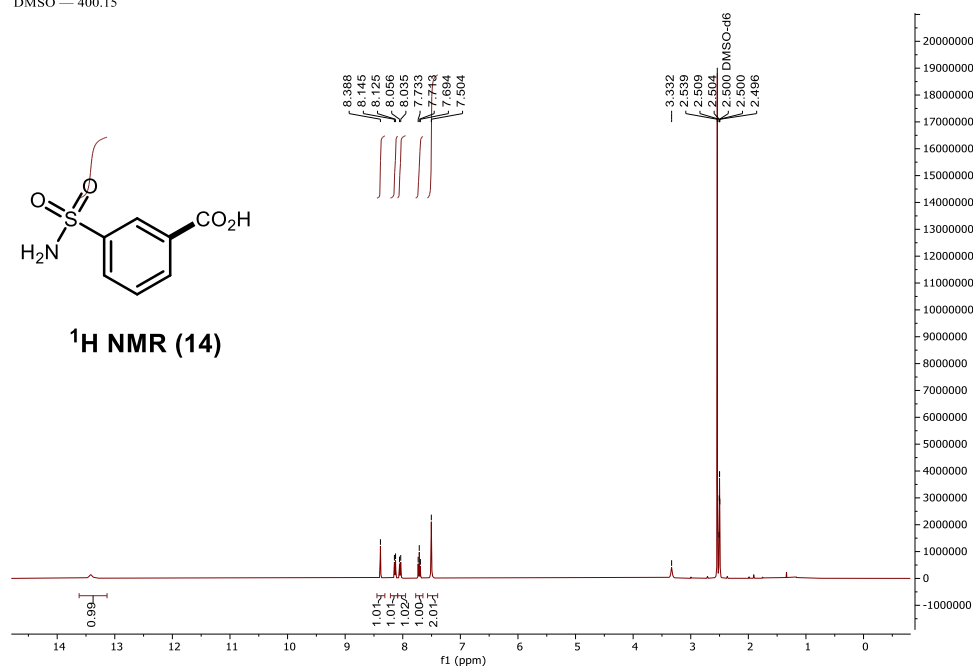


3-formylbenzoic acid (13)



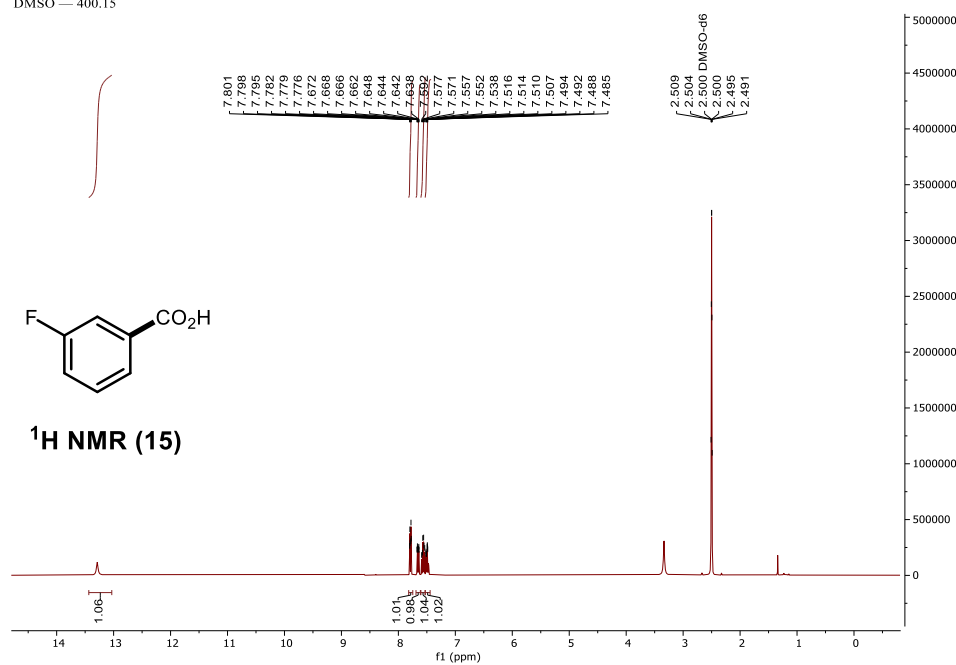
3-sulfamoylbenzoic acid (14):

DMSO — 400.15

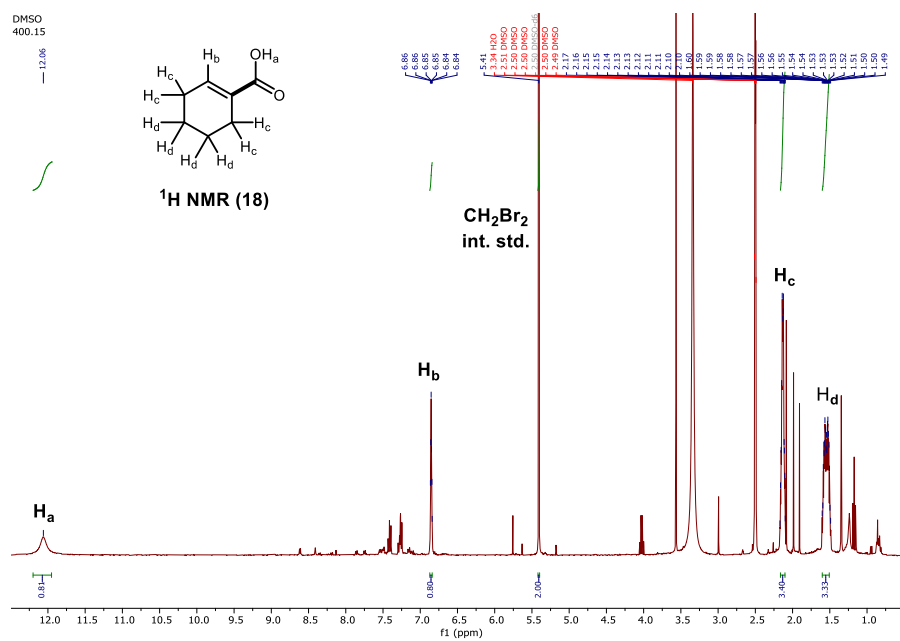


3-fluorobenzoic acid (15):

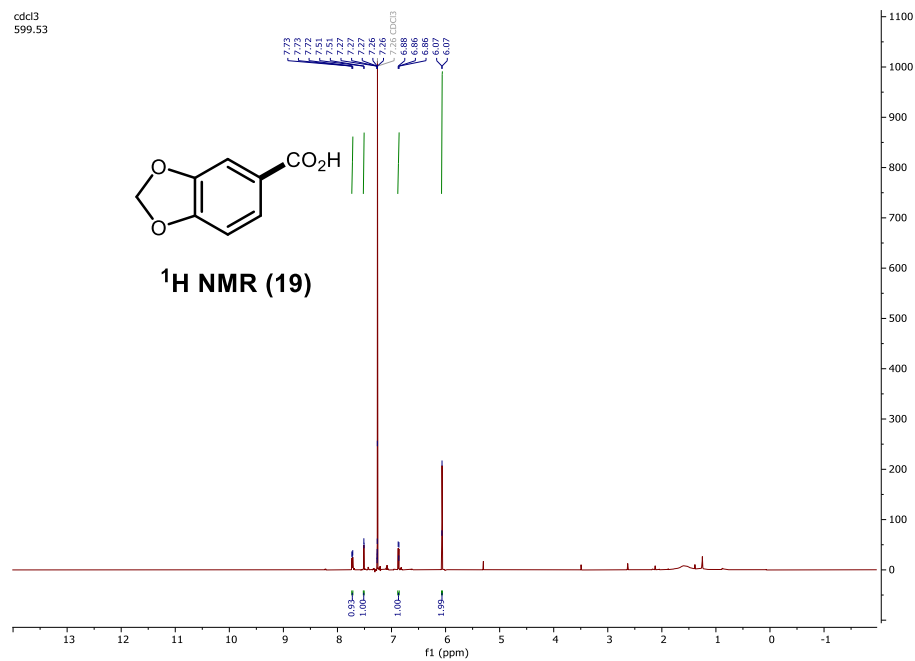
DMSO — 400.15



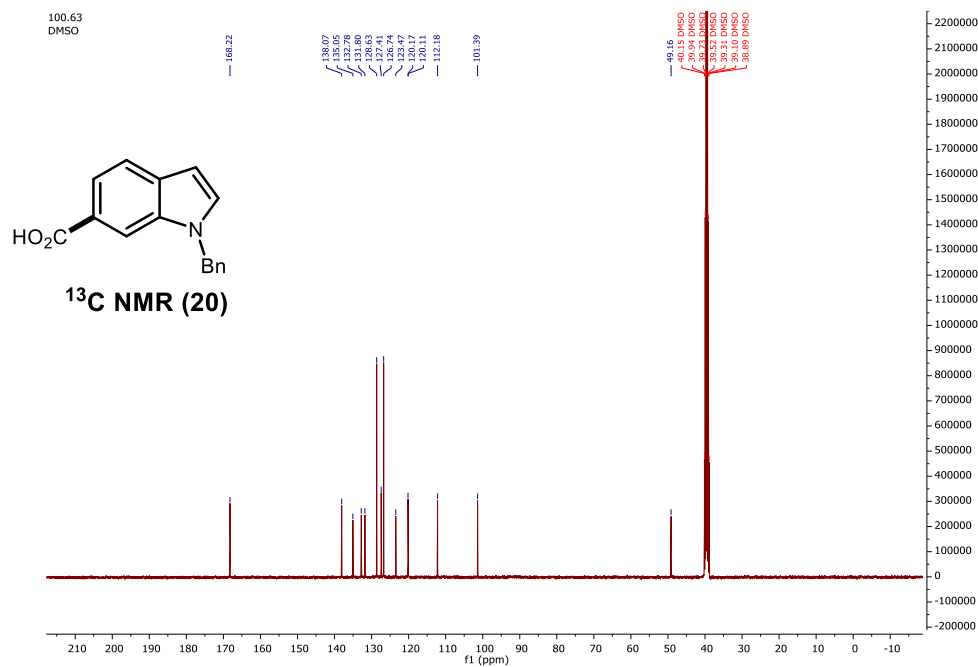
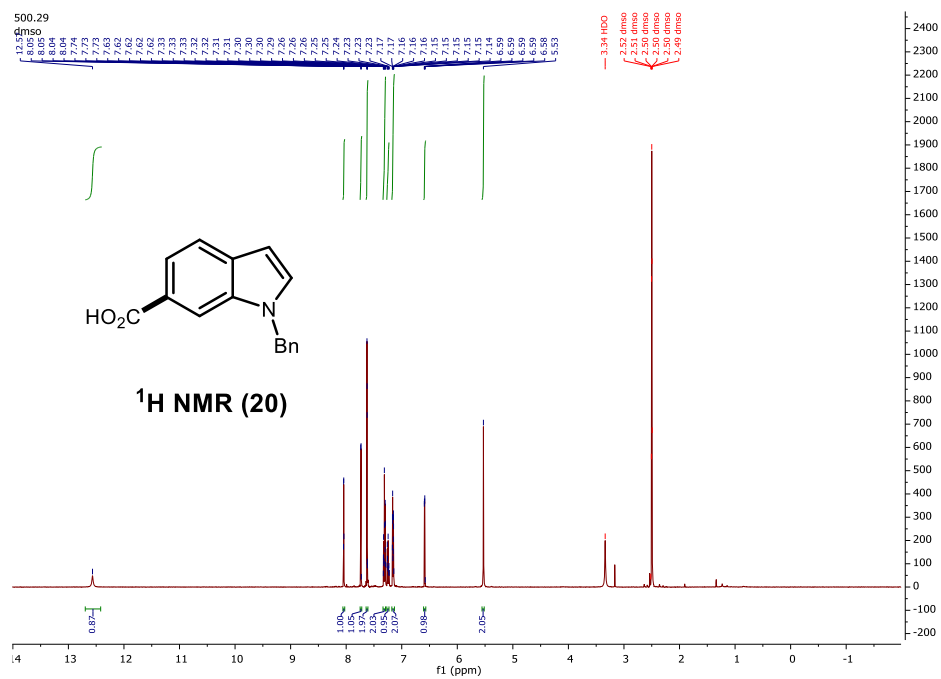
Cyclohex-1-ene-1-carboxylic acid (18)



Benzo[d][1,3]dioxole-5-carboxylic acid (19)



1-benzyl-1H-indole-6-carboxylic acid (20)



1-((2-(trimethylsilyl)ethoxy)methyl)-1*H*-indazole-6-carboxylic acid (21)

